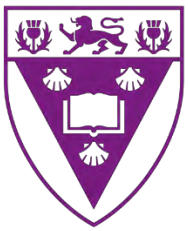

RHODES UNIVERSITY

Where leaders learn

Biochemical And Genetic Analysis of the *Mycobacterium smegmatis* CnoX Chaperedoxin.

A thesis submitted in fulfilment of the requirements for the degree of

MASTER OF SCIENCE

Microbiology

of

RHODES UNIVERSITY

Makhanda / Grahamstown

by

ARIANA H. J. WATKINS

ORCID ID:
https://orcid.org/0000-0002-1703-2178

July 2022

Abstract

Mycobacterium (M.) tuberculosis (Mtb) encounters numerous physical and chemical stresses associated with host immunity during infection. These include exposure to reactive oxygen, chlorine and nitrogen species, low pH, hypoxia, nutrient starvation, and metal toxicity. Cellular proteins are particularly susceptible to damage by these stresses, and the ability to prevent their irreversible damage is consequently crucial for bacterial growth and survival. Mtb employs a network of proteins that includes chaperones, disaggregases, and proteases to maintain the integrity of its proteome. The chaperedoxin, CnoX, is a recently identified stress-inducible chaperone that combines redox and holdase activities to prevent the over-oxidation and aggregation of proteins in *E. coli* and other proteobacterial species. In this study, we identified orthologs of the *E. coli* CnoX (*Ec*CnoX) in Mtb and *M. smegmatis* (Msm). Bioinformatics analysis of the Mtb and Msm CnoX orthologs (*Mt*CnoX and *Ms*CnoX, respectively) revealed that they possess similar domains, domain architectures and predicted tertiary structures as previously characterised CnoX enzymes, i.e. an N-terminal thioredoxin (Trx) domain fused to a C-terminal TPR-motif containing domain. The *Ec*CnoX, *Ms*CnoX, and *Mt*CnoX enzymes were expressed as recombinant, His-tagged proteins in *E. coli* and purified to near homogeneity. Biochemical analysis of the recombinant CnoX enzymes revealed that the *Ms*CnoX and *Mt*CnoX both lack thiol-disulphide oxidoreductase (thioredoxin) activity, as evidenced by their inability to catalyse the reduction of the disulphide bonds of insulin *in vitro*. Both mycobacterial CnoX enzymes displayed activity as chaperones (holdases) during thermal aggregation assays of the model substrate, malate dehydrogenase (MDH). In contrast to previously reported findings for *Ec*CnoX, the holdase activity of the mycobacterial CnoX enzymes was constitutive and did not require exposure to hypochlorous acid (HOCl) for activation. To establish the physiological role of CnoX in Msm, *cnoX* knockdown (KD) and knockout (KO) mutants were generated using CRISPRi-mediated gene silencing or homologous recombination, respectively. Consistent with previous findings, CnoX activity was not essential for the growth of Msm under conventional growth conditions. Reducing or eliminating CnoX activity in the Msm KD or KO mutants, respectively, did not confer increased sensitivity to HOCl as has been observed for an *E. coli* Δ*cnoX* mutant. Reduced CnoX activity in Msm did, however, confer sensitivity to the superoxide generator, plumbagin, and front-line antitubercular drugs rifampicin and isoniazid. The combination of biochemical and physiological data presented suggests that *Ms*CnoX may function as a holdase for substrates

following proteotoxic damage induced by certain types of oxidants, a line of investigation that will be pursued in future studies.

Table of Contents

List of Figures

List of Tables

List of Abbreviations

AES	Allelic Exchange Substrate
AGE	Agarose Gel Electrophoresis
Amp	Ampicillin
Amp^R	Ampicillin Resistant
ATc	Anhydrotetracycline
BCG	Bacille Calmette Guerin
CHP	Cumene Hydrogen Peroxide
Cip	Ciprofloxacin
CnoX	Chaperedoxin
CRISPR	Clustered Regularly Interspaced Short Palindromic Repeats
CRISPRi	CRISPR interference
CS	Citrate Synthase
$CuSO_4$	Copper Sulphate
dcas9	Deactivated *cas9*
ddH_2O	Double distilled water
dH_2O	Distilled water
DMSO	Dimethyl sulphoxide
dNTPs	Dinucleotide Triphosphates
DS	Downstream
DTT	Dithiothreitol
Emb	Ethambutol
Ec	*Escherichia coli*
FPLC	Fast Protein Liquid Chromatography
G+C	Guanine and Cytosine
FLP	Flippase
H_2O_2	Hydrogen Peroxide
HIV/AIDS	Human Immunodeficiency Virus/Acquired Immune Deficiency Syndrome
HOCl	Hypochlorous Acid
Hyg	Hygromycin
Hyg^R	Hygromycin Resistant
IDR	Intrinsically Disordered Region

IMAC	Immobilised Metal Affinity Chromatography
INH	Isoniazid
iNOS	Inducible Nitrous Oxide Synthase
IPTG	Isopropyl β-D-1-thiogalactopyranoside
Kan	Kanamycin
Kan^R	Kanamycin Resistant
KD	Knockdown
KO	Knockout
LA	Lysogeny (Broth) Agar
LB	Lysogeny Broth
LTBI	Latent Tuberculosis Infection
M9A	M9 Minimal Media Agar
M9B	M9 Minimal Media Broth
MCS	Multiple Cloning Site
MDR	Multidrug-Resistant
MPO	Myeloperoxidase
MSA	Multiple Sequence Alignment
Msm	*Mycobacterium smegmatis*
Mtb	*Mycobacterium tuberculosis*
MW	Molecular Weight
MWCO	Molecular Weight Cut Off
NaOCl	Sodium Hypochlorite
Ni-NTA	Nickel-Nitriloacetic Acid
OD_{600}	Optical Density at 600 nm
ORF	Open Reading Frame
PAM	Protospacer Adjacent Motif
PBS	Phosphate Buffered Saline
P_{lac}	*lac* Promoter
PMSF	Phenylmethylsulphonyl fluoride
P_{smyc}	Strong mycobacterial Promoter
qPCR	Quantitative Real-Time Polymerase Chain Reaction
RBS	Ribosomal Binding Site

RCS	Reactive Chlorine Species
RE	Restriction Endonuclease
Rif	Rifampicin
RNS	Reactive Nitrogen Species
ROS	Reactive Oxygen Species
RT	Reverse Transcriptase/Reverse Transcribed
RT-PCR	Reverse Transcription Polymerase Chain Reaction
SDS	Sodium Dodecyl Sulphate
SDS-PAGE	Sodium Dodecyl Sulphate Polyacrylamide Agarose Gel Electrophoresis
sgRNA	Single Guide RNA
SOE	Splice by Overlap Extension
*Sth*1 *dcas9*	*Streptococcus thermophilus* CRISPR1 inactivated *cas9*
TB	Tuberculosis
Tet	Tetracycline
Tet^R	Tetracycline Resistant
Tm	Melting Temperature
TPR	Tetratricopeptide Repeat
Trx/s	Thioredoxin/s
TrxR	Thioredoxin Reductase
US	Upstream
Van	Vancomycin
WT	Wild Type
XDR	Extensively Drug-Resistant
Zeo	Zeocin
Zeo^R	Zeocin Resistant/Zeocin Resistance Gene
Zeo^S	Zeocin Sensitive
ZOI	Zone of Inhibition

List of Units and Symbols

bp	Base Pairs
CFU	Colony Forming unit
cm	Centimetre
CV	Column Volume
°C	Degrees Celsius
Δ	Delta
g	Grams
h	Hour(s)
Kb	Kilobase
kDa	Kilodalton
kV	Kilovolt
M	Molar
min	Minute(s)
mg	Milligram
mL	Millilitre
mm	Millimetre
mM	Millimolar
ng	Nanogram
nM	Nanomolar
nt	Nucleotide
%	Percentage
pg	Picogram
Ω	Resistance
s	Second(s)
µF	Microfarad
µg	Microgram
µL	Microlitre
µM	Micromolar
V	Volt

Acknowledgements

Firstly, I would like to thank the National Research Foundation (NRF) for their funding of my research, without which, none of this would have been possible. Your funding allows new generations of scientists to emerge each year, and as one such individual, I can say just how much of a difference it has made. Thank you!

Secondly, to my favourite (and only) supervisor, Dr Garth L. Abrahams – there will never be enough words to thank you for your insights, guidance, assistance, training, and support. I have so much to be grateful for, and when I was accepted into your lab, I did not realize just how incredibly lucky I was. Your depth of knowledge, motivation, thinking, perfectionism, and humbleness are inspiring and if I am even half as brilliant as you are one day, I would consider myself fortunate. Thank you so much for all that you have done these last few years, I am so lucky to have started my scientific career with you.

To my Lab 309 lab mates: Thank you for all the support and help. A special mention to Claire McLaughlin, the self-proclaimed Queen of Trolls, and Gaby Jackson, thank you for all that you have done for me and still do. Most importantly, thanks for being the best bad influences.

To Professor C. Knox and Dr M. Jukes, thank you for your support in my research, for allowing me to come "shopping" when needed, and for contributing insights to my research. To Ronald Tonui, thank you for working with me and helping me with the biochemical assays. And a thank you to all of the others I worked with during my time at Rhodes, you have all taught me the immense value of collaboration across labs, and I will be forever appreciative.

And lastly, a big thank you to my friends and family who supported me through my research, despite not understanding half of the scientific jargon I rattled on about. I will never be able to express properly, just how much it means to me. To my mum and dad, who believed in me even when I didn't believe in myself, to Lia Cesler, who completed daily Pomodoro sessions with me while we both wrote our theses, and to Clayton Fletcher, for taking me on adventures so that I didn't spend the entire day, every day, inside working. Thank you all.

Chapter 1: Introduction

1.1 Introduction

Mycobacterium tuberculosis (Mtb) is an obligate bacterial pathogen and the etiological agent of tuberculosis (TB), an airborne disease responsible for significant morbidity and mortality worldwide each year. Prior to the emergence of SARS-CoV-2 and the COVID-19 pandemic in 2019, Mtb was the leading cause of infectious death worldwide, surpassing HIV/AIDS (World Health Organization, 2021). Mtb continues to pose a public health threat, however and was estimated to be responsible for 9.9 million new active TB cases and 1.3 million deaths in 2020 (World Health Organization, 2021). An additional 1.7 billion individuals, corresponding to a quarter of the world's population, are thought to have undetected, latent Mtb infections (LTBI) (Khabibullina *et al.*, 2022). Mtb reactivates and progresses to active disease in approximately 5-10 % of all LTBIs, which promotes the ongoing carriage and transmission of TB in humans. Individuals with compromised immune systems, such as those infected with HIV, diabetes mellitus or nutritional deficiencies, characteristics that are prevalent in low- to middle-income countries such as South Africa are at particularly high risk for developing active TB (Hogan *et al.*, 2020; World Health Organization, 2021). The global burden of Mtb is likely to increase even further in the next few years, with the COVID-19 pandemic projected to increase the overall number of TB cases and associated deaths by 20 % by 2025 (Hogan *et al.*, 2020).

Despite residing in only a single reservoir, the human host, prevention and control of Mtb has been hampered by several factors. Firstly, the diagnosis of active TB cases is often challenging in high-burden settings, resulting in delays in the implementation of antitubercular chemotherapy. Secondly, Mtb possesses a unique cell wall that is impermeable to many antibiotics, which limits available treatment options (Cook *et al.*, 2009; Hett and Rubin, 2008). Thirdly, while drug-sensitive forms of TB are treatable using existing antitubercular drugs, the chemotherapeutic regimen is complex, lengthy, and presents undesirable side effects, requiring the use of up to four different drugs for a minimum of six months. The antitubercular drug regimen is consequently often associated with poor patient adherence, which in conjunction with the limited availability of antitubercular drugs, has promoted the evolution and selection of drug-resistant Mtb strains (Singh and Chibale, 2021). Drug-resistant Mtb strains often require treatment with second-line drugs, which can be expensive, toxic, and require treatment periods of up to two years, which has resulted in a further lack of adherence, which compounds the growing drug resistance crisis (Migliori *et al.*, 2020). Lastly, while the Bacille Calmette

Guerin (BCG) vaccine exists, it was developed a century ago, and its effectiveness is limited to the prevention of disseminated forms of TB in children and provides no protection against primary infection or reactivation in adults (Colditz, 1994).

Newer antitubercular treatments have been developed and include bedaquiline, delamid, linezolid, and clofazimine, and provide some relief but their use is limited to cases of drug-resistant forms of TB. Despite their relatively recent approval, resistance to some of these drugs is already emerging (Perveen *et al.*, 2022). The development of new and more effective treatments that can shorten the duration of antitubercular treatment is therefore urgently required. An improved understanding of the mechanisms used by Mtb to resist the detrimental effects of host-imposed stresses on cellular components might facilitate the development of new approaches for controlling TB. In this study, we investigated the role of putative CnoX orthologs in protecting mycobacterial proteins from environmental stress, with a view to establishing the protein's utility as novel therapeutic targets.

1.2 The Family *Mycobacteriaceae*

The *Mycobacterial* genus is comprised of close to 200 species that are characterised by their aerobic to microaerophilic, non-motile, non-spore-forming, rod-shaped and acid-fast nature (Cirillo *et al.*, 2021; Lory, 2014; Tortoli, 2019). *Mycobacteria* is the only genus in the family *Mycobacteriaceae,* which is found within the order *Corynebacteriales* and phylum *Actinobacteria* (Goodfellow *et al.*, 2012). Similar to other phylum members, including *Corynebacteriaceae* and *Nocardiaceae,* mycobacteria possess a high genomic G + C content (62 to 70 %) and produce complex long-chain fatty acids (60–90 carbons) known as mycolic acids (Cook *et al.*, 2009). The mycolic acids together with various glycolipids constitute the inner and outer leaflets of the mycobacterial outer membrane, or "mycomembrane", respectively (reviewed by Vincent *et al.*, 2018). The mycolic acids present in the outer membrane's inner leaflet are covalently linked to an arabinogalactan-peptidoglycan cell wall, and together with the periplasm and inner (cytoplasmic) membrane constitute the mycobacterial cell envelope. The hydrophobic lipid-rich nature of the mycobacterial cell envelope makes it highly impermeable, allowing mycobacteria to resist acid-alcohol decolourisation following staining with phenol-based dyes thereby conferring mycobacteria with their "acid-fast" phenotype (Goren and Brokl, 1978). The relative impermeability of the cell envelope also provides mycobacteria with intrinsic resistance to many antibiotics and immune-generated antimicrobial molecules (Awuh and Flo, 2017; Cook *et al.*, 2009).

Mycobacterial species are diverse with respect to their ability to cause disease in humans and animals (Orgeur and Brosch, 2018; Saelens *et al.*, 2019). The majority are harmless, environmental species that exist as saprophytes or commensals in a variety of terrestrial or aquatic habitats and rarely, if ever, cause disease in humans or animals (Pereira *et al.*, 2020; Primm *et al.*, 2004). Included amongst these non-pathogenic mycobacterial species are *M. smegmatis* (Msm) and *M. gilvum* (Mgv) *and M. vanbaalenii* (Mvb) (Rahman *et al.*, 2014). Some environmental mycobacteria can cause occasional localised or disseminated infections in humans or animals, particularly in those with predisposing conditions or compromised immunity. These opportunistic species are typically acquired from environmental reservoirs and include members of the *M. avium* complex, such as *M. avium* (Mav) and *M. intracellulare* (Min). A relatively small number of mycobacterial species are obligate pathogens of animals and/or humans. These species typically have no environmental reservoir and are consequently dependent on their animal or humans hosts for survival and transmission. Included amongst these species are members of the *Mycobacterium tuberculosis* complex (MTBC), which can cause TB in humans or certain animal species, and *Mycobacterium leprae* (Mlp), the causative agent of leprosy. The MTBC is composed of several species, including Mtb, *M. africanum, M. bovis, M. canettii, M. caprae, M. microti, M. mungi, M. pinnipedii, M. orygis,* and *M. surricatae*. While Mtb and *M. africanum* are human-host adapted pathogens, the remaining members of the MTBC are adapted to animal hosts, with occasional zoonotic transmission to humans occurring.

Based on differences in their growth rate *in vitro*, mycobacteria can also be divided into fast- or slow-growing species (Bachmann *et al.*, 2020; Kim *et al.*, 2013). Fast-growing mycobacterial species typically take three to seven days to form visible colonies on solid growth media, while slow-growing species typically require more than seven days to do so (Kim *et al.*, 2013; Runyon, 1959). While several exceptions exist, the slow-growth phenotype has been associated with pathogenic mycobacterial species such as Mtb and Mlp, while fast-growing mycobacterial species are comprised of non-pathogenic or opportunistic pathogens (Cook *et al.*, 2009; Forrellad *et al.*, 2013). Given its relatively fast growth rate and lack of pathogenicity, Msm is often used as a model organism to elucidate specific aspects of mycobacterial physiology (Sundersingh *et al.*, 2020). All of the physiological studies conducted in this research project (**Chapter 4**) were consequently performed with Msm, as opposed to the slow-growing pathogenic Mtb.

1.3 *Mycobacterium tuberculosis*

1.3.1 The Infection Cycle

Mtb is an obligate pathogen with no external reservoirs or environmental niches, and whose pathogenicity, along with other pathogenic mycobacteria, is dependent on its ability to replicate within cells of its host, particularly macrophages (Berthet *et al.*, 1998; Camacho *et al.*, 1999; Ramakrishnan *et al.*, 2000). The life cycle of Mtb has consequently evolved around its ability to adapt to and survive within environments encountered within its human host (**Figure 1.1**). Mtb transmission occurs following the inhalation of aerosolised droplets containing infectious bacilli expelled by infected individuals while coughing, sneezing or vocalising. Once inhaled, the aerosolised droplets traverse the upper respiratory tract and reach the lungs, where they are deposited in the distal airways and alveoli. The initial recognition of Mtb in the alveoli is mediated by pattern recognition receptors (PRRs), such as C-type lectins and Toll-like receptors, which are found on the surface of tissue-resident alveolar macrophages (Ravesloot-Chávez *et al.*, 2021). The engagement of these receptors by Mtb pathogen-associated molecular patterns (PAMPs) triggers the phagocytic uptake of Mtb by alveolar macrophages, as well as the production and secretion of pro-inflammatory cytokines and chemokines that facilitate the recruitment of additional cellular and soluble innate immune effectors to the original site of infection (Bussi and Gutierrez, 2019; Cohen *et al.*, 2018; Ganbat *et al.*, 2016; Lovewell *et al.*, 2021; Wolf *et al.*, 2007). In some infected hosts, a robust innate immune response may be sufficient to clear the pathogen. In others, the infection may progress, with two possible outcomes: (i) the development of active disease, which is observed in 5 to 10 % of cases or (ii) the development of LTBI, which occurs in 90 to 95 % of infected individuals (Bhatt and Salgame, 2007). Individuals with LTBI have a ~10 % lifetime risk of developing active disease, which is increased to ~10 % per annum in individuals infected with HIV or other predisposing factors.

Following phagocytosis, Mtb-infected alveolar macrophages cross the alveolar epithelium to reach the lung interstitium (Cohen *et al.*, 2018). Within infected macrophages, Mtb can inhibit the conventional phagolysosomal maturation pathway, allowing the bacterium to evade the cell's oxygen- and non-oxygen-dependent killing mechanisms and replicate to high numbers (Carranza and Chavez-Galan, 2019). This process culminates in the lysis of infected host cells and the release of Mtb into the extracellular space. The released Mtb can infect other phagocytes such as interstitial and monocyte-derived macrophages, dendritic cells, and neutrophils that are recruited to the site of infection in response to ongoing cytokine signalling

(Armstrong and Hart, 1975; Davis *et al.*, 2002; Leemans *et al.*, 2001). The phagocytic uptake of Mtb by dendritic cells triggers their maturation to antigen-presenting cells, which migrate from the site of infection to adjacent draining lymph nodes. Here, the dendritic cells present Mtb-derived antigens to antigen-specific T cells, resulting in their activation and proliferation. These activated T cells migrate to the initial site of infection where they activate innate immune cells to restrict Mtb replication and limit inflammation (Kinsella *et al.*, 2021; Ravesloot-Chávez *et al.*, 2021). This promotes the formation and maturation of cellular aggregates around the infectious locus, leading to the formation of granulomas (Bouley *et al.*, 2001; Ramakrishnan, 2012). Depending on their structure and cellular composition, several different types of granulomas may develop during infection with Mtb, with each type associated with different levels of success in controlling Mtb infection (Kinsella *et al.*, 2021; Pagán and Ramakrishnan, 2015). The prototypical granulomas in TB are the caseous granulomas, which are comprised of epithelioid macrophages, neutrophils and dendritic cells surrounded by lymphocytes (B and CD4+ and CD8+ T cells) and fibroblasts. The central region of caseous granulomas is composed of an acellular, necrotic core consisting of dead phagocytes. Mtb infection is typically contained within this caseous and hypoxic environment. Under certain conditions, extensive necrosis of the inner caseous region can occur, resulting in the erosion of the granuloma, cavitation and release of Mtb into the airways (Urbanowski *et al.*, 2020). The resuscitation and replication of Mtb within this highly-oxygenated environment results in active TB disease and promotes onward transmission of the disease. In LTBIs, caseous granulomas often become calcified, with the calcification initiated from within the centre of the granuloma (Flynn *et al.*, 2011). These calcified granulomas generally represent a successful immune control and low bacterial burden. Other types of granulomas include fibrotic granulomas, which have a fibrotic centre and are collagenous throughout, and non-necrotising granulomas that consist primarily of macrophages with a few lymphocytes (Flynn *et al.*, 2011).

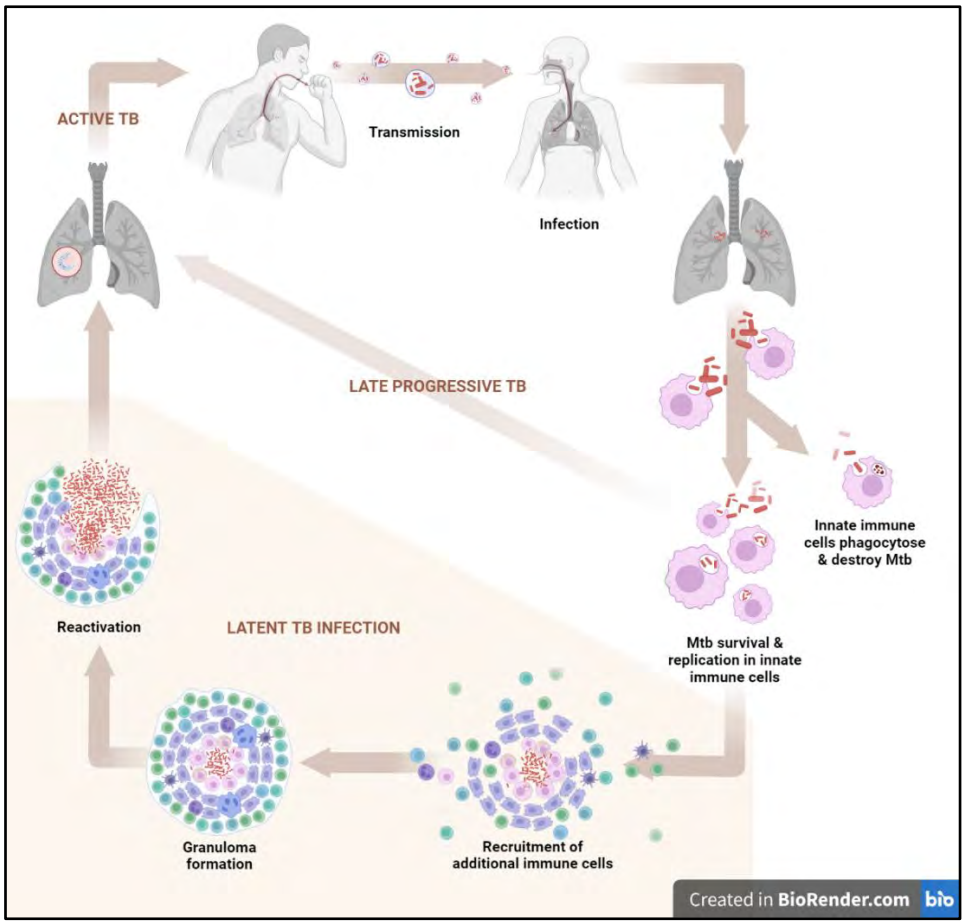

Figure 1.1 Schematic representation of the infection cycle of Mtb. The infection cycle is initiated following the expulsion of aerosolised droplets containing Mtb bacilli from an individual with active TB (**transmission**), and their inhalation by an uninfected individual (**infection**). Mtb is deposited within the lungs, where they are phagocytosed by alveolar macrophages. These cells act as their primary replication site and enable the recruitment of additional immune cells that help transport the Mtb deeper into the lung interstitium. This results in additional recruitment of innate and adaptive immune cells, whereupon the Mtb are either phagocytosed and destroyed by the activated immune cells or their growth is restricted in granuloma (**granuloma formation**), resulting in latent TB. In instances where the immune system fails to control bacterial replication, late progressive TB occurs either through the failure of the granuloma to contain the bacilli (**reactivation**) or by bypassing granuloma formation entirely in immunocompromised individuals. This causes active TB, where individuals are contagious and expel aerosolised droplets containing bacilli to other individuals (**transmission**).

1.3.2 Environmental stresses encountered by Mtb in the host

As discussed in the preceding section, Mtb resides in several micro-environments within the host during infection, which includes both phagocytic cells and granulomas. While these environments are often inhospitable for bacterial growth and survival, Mtb has developed a number of adaptations that allow it to resist bacterial killing and persist in infected hosts for extended periods of time. Following its uptake by macrophages, Mtb resides within a vacuolar compartment that is characterised by low pH, exposure to reactive oxygen and nitrogen species

(ROS and RNS, respectively), lysosomal hydrolases and antimicrobial proteins or peptides (Ravesloot-Chávez *et al.*, 2021). In non-activated macrophages, the vacuole is slightly acidified (~pH 6.4) and shows limited acquisition of lysosomal contents (Baker *et al.*, 2019). Activation with interferon-gamma (IFN-γ) enables the block in phagosomal maturation to be overcome, enabling the delivery of Mtb to a highly acidified phagolysosome (~pH 4.5) that is also enriched in proteins, peptides and chemicals with antimicrobial properties (Baek *et al.*, 2011; MacMicking *et al.*, 2003). Activated macrophages express two key enzymes, the phagocyte oxidase complex and inducible nitric oxide synthase (iNOS), which generate ROS and RNS in the phagosome, respectively (Piacenza *et al.*, 2019). Phagocyte oxidase transfers electrons from cytosolic NADPH across the phagosomal membrane to molecular oxygen (O_2), which results in the formation of superoxide ($O_2^{\bullet -}$), a toxic compound (Winterbourn, 2008; Winterbourn *et al.*, 2016). Superoxide is rapidly converted to hydrogen peroxide (H_2O_2), either spontaneously at low pH, or enzymatically by enzymes such as superoxide dismutase (SOD). Both superoxide and hydrogen peroxide can release iron from iron-sulphur clusters to generate hydroxyl radicals ($OH^{\bullet}$) via the Fenton reaction (Vásquez-Vivar *et al.*, 2000). These ROS can, collectively, damage a variety of cellular components including nucleic acids, lipids, carbohydrates and proteins, leading to growth inhibition or cell death.

In granulocytes, such as neutrophils, the enzyme myeloperoxidase (MPO) can catalyse the H_2O_2-mediated oxidation of chloride to form the reactive chlorine species (RCS) hypochlorous acid (HOCl; bleach), a powerful oxidant. While HOCl can react with and oxidise most cellular macromolecules, proteins, are thought to be its primary target (Winterbourn and Kettle, 2013; Gray et al, 2013). The primary targets oxidised by HOCl are sulphur-containing molecules, such as the amino acids cysteine and methionine (Gray *et al.*, 2013). HOCl can also react with primary and secondary amines, resulting in the formation of chloramines (-NHCl) that, in turn, can oxidise and chlorinate additional cellular components.

Like phagocyte oxidase, the activity of iNOS is induced in IFN-γ-activated phagocytic cells such as macrophages and neutrophils. The iNOS enzyme catalyses the oxidation of L-arginine to form L-citrulline and nitric oxide (NO) (Bogdan, 2015). The latter molecule can also be formed non-enzymatically from nitrite at low pHs, such as those encountered in the phagolysosome, under reducing conditions. NO can combine with superoxide to form peroxynitrite ($ONOO^-$), a strong oxidant that reacts with most biological molecules. In addition to peroxynitrite, nitric oxide can also form other RNS species such as nitroxyl (HNO), dinitrogen trioxide (N_2O_3), nitrite (NO_2^-), nitrogen dioxide (NO_2), nitronium cation (NO_2^+),

nitrosonium cation (NO^+) and S-nitrosothiols (RSNOs). Like ROS and RCS, many of these RNS can react with cellular components such as nucleic acids and proteins, perturbing their normal biological function, resulting in bacterial growth inhibition or death (Ehrt and Schnappinger, 2009).

Similar to the environment encountered in phagolysosomes, the pH in granulomas can vary from pH 5.0 to 7.2, with a median pH of 5.5 (Baker *et al.*, 2019). The necrotic core of caseous granulomas is also thought to be hypoxic, which limits the ability of Mtb to generate the energy needed to support active growth through aerobic respiration (Boshoff and Barry, 2005; Via *et al.*, 2008). Granulomas are, in addition, poorly vascularised, which limits the delivery of energy sources and other nutrients needed to support bacterial growth. In response to the combination of low pH, hypoxia and nutrient limitation, Mtb is thought to adapt to a state reduced replication that is associated with the initiation of Mtb dormancy, defined as a non-growing yet persistent state (Boshoff and Barry, 2005). Mtb may remain in this non-replicating, phenotypically drug-resistant, dormant state, until the immune system is sufficiently compromised and reactivation can occur (Cronan, 2022; Orme, 2014).

1.3.3 Effects of environmental stresses on cellular proteins

The three-dimensional (3D) structure of proteins is integral to their ability to perform their biological roles (Schramm *et al.*, 2020). The ability of proteins to fold into and maintain their 3D structure is therefore essential under both conventional growth conditions and during exposure to environmental stresses (Dobson *et al.*, 1998). Several environmental stresses are known to induce protein unfolding or misfolding, which promotes the interaction of exposed hydrophobic regions of polypeptide chains and subsequent aggregation (Schramm *et al.*, 2020). While some of these aggregates can be restored to their native conformations following unfolding or aggregation, others may accumulate in inactive or toxic forms that can be detrimental to bacterial growth and survival. This condition, referred to as proteotoxicity, can be induced by molecules that are endogenous to cells, or by exogenous factors. As discussed in the preceding section, Mtb encounters several physical and chemical stresses in the habitats it resides in during infection. These include, amongst others, exposure to ROS, RNS, RCS, acidic pHs, hypoxia, and nutrient starvation. While these stresses can affect a number of macromolecules within bacterial cells, proteins are particularly susceptible to damage that may result in proteotoxicity (Dahl *et al.*, 2015; Piacenza *et al.*, 2019; Winterbourn *et al.*, 2016).

One of the primary drivers of proteotoxicity in cells is oxidative damage caused by oxidants such as ROS, RCS and RNS. ROS and RCS induce the carbonylation (i.e. formation of aldehydes) and chlorination of amino acid residues, respectively, which can promote the reversible or irreversible unfolding, misfolding, aggregation and/or degradation of proteins (Dahl *et al.*, 2015; Gray *et al.*, 2013). The primary amino acids targeted by oxidative stress are the thiol-containing amino acids, cysteine and methionine. The oxidation of cysteine thiols by ROS results in the formation of sulphenic acid intermediates (R-SOH). The chlorination of thiol groups by RCS initially gives rise to sulphenyl chloride (R-SCl) intermediates that can subsequently attack other thiols or amines, or be further oxidised to yield sulphenic acid intermediates. Sulphenic acids are highly reactive and can be further oxidized to sulphinic (R-SO_2H) or sulphonic (R-SO_3H) acids, which are irreversible thiol oxidations that promote protein unfolding, misfolding, aggregation and/or degradation. Sulphenic acids can also react with proximal primary or secondary amino groups forming reversible sulphenamides that, upon further oxidation, form the irreversibly oxidised sulphonamides, (R-S[O2]-NH-R′), which likewise promotes the disruption of protein tertiary structure (Gray *et al.*, 2013). ROS and RCS can also oxidise methionine thiols, resulting in the formation of methionine sulphoxide (Met-SO), which can be further oxidised to methionine sulphone (Met-SO_2) (Aussel and Ezraty, 2021; Rosen *et al.*, 2009). While the formation of the methionine sulphoxide intermediate is reversible, methionine sulphone is not. The accumulation of over-oxidised methionine residues consequently promotes protein unfolding and irreversible aggregation. Besides sulphur-containing residues, ROS and RCS also react with the primary or secondary amines of histidine, tryptophan, lysine, tyrosine, arginine side and the residues found at the N-terminus of proteins. While the rates of oxidation with these amino acids are significantly lower than with thiol-containing amino acids, many of the reaction products are irreversible, increasing the tendency of proteins to unfold and aggregate. Like ROS and RCS, RNS can interact with cysteine thiols, converting them into S-nitrosothiol and subsequently sulphenic acid intermediates (Martínez and Andriantsitohaina, 2009). Peroxynitrite is a strong oxidant that can also induce the nitration of tyrosine residues to form nitrotyrosine, which may promote protein aggregation and inactivation (Radi, 2013).

Besides oxidative stress, the 3D structure of proteins is also dependent on other factors such as temperature (Hasday *et al.*, 2014; Santra *et al.*, 2017) and pH (Baker *et al.*, 2019). Shifts away from an organism's optimal growth range can, therefore, promote protein unfolding and aggregation. During infection, microbes are often exposed to elevated temperatures as a result of

inflammation and/or fever. This, together with the low pH encountered in the phagolysosome environment, can disrupt hydrogen bonds and other non-covalent interactions needed for proteins to fold into and subsequently maintain their secondary and tertiary structures, promoting their unfolding, misfolding and/or aggregation. Exposure to acid stress also increases the sensitivity of proteins to thiol-oxidative stress, exacerbating the damage induced by ROS, RCS and/or RNS (Coulson *et al.*, 2017).

1.4 Maintaining the Mycobacterial Proteostasis Network

The proteostasis network is critical for bacterial survival and is composed of over a hundred proteins that play a role in helping to fold and maintain protein structure (proteostasis), or degrade irreparably damaged proteins (proteolysis) (Lupoli *et al.*, 2018; Reichmann *et al.*, 2018). These proteins, often have redundant functions and either (1) detoxify or neutralise the source of proteotoxicity, preventing protein damage from occurring (preventative mechanisms), (2) reverse, repair or degrade damaged proteins in an ATP (energy)-dependent manner, reducing proteotoxicity, or (3) are specifically activated by stress condition and bind to oxidised or damaged proteins in an ATP (energy)-independent manner, preventing protein aggregation. Collectively, these mechanisms play an important role in protecting bacteria, including Mtb, from proteotoxic stresses (Lupoli *et al.*, 2018) and are discussed further in the following sections.

1.4.1 Preventative Mechanisms

Mechanisms capable of neutralising physical and chemical stresses before they damage proteins are the first line of defence against proteotoxicity. Mtb possesses several mechanisms to detoxify ROS and RNS to prevent oxidative damage to proteins and other macromolecules (Ehrt and Schnappinger, 2009). Mtb encodes two metal-dependent superoxide dismutase enzymes, a Mn/Fe-dependent SOD, SodA, and a Cu/Zn-dependent SOD, SodC, which catalyse the conversion of superoxide anions to form hydrogen peroxide (Dussurget *et al.*, 2001; Edwards *et al.*, 2001; Teixeira *et al.*, 1998; Wang *et al.*, 2018). SodC is required for resistance to superoxide and H_2O_2, and *sodC* mutants have increased susceptibility to these ROS relative to WT Mtb *in vitro* as well as in activated macrophages (Dussurget *et al.*, 2001). SodA is essential for bacterial growth *in vitro* and its reduced expression leads to increased sensitivity to H_2O_2 and diminished growth in a murine model of infection (Edwards *et al.*, 2001). Once formed, Mtb can detoxify H_20_2 generated by SOD or encountered in the environment via the action of a catalase-peroxidase enzyme, KatG, or alkyl hydroperoxide reductase protein, AhpC, which results in the formation of water and oxygen (Claiborne *et al.*, 1979; Diaz and Wayne,

1974; Wengenack *et al.*, 1999; Wong *et al.*, 2017). A Mtb *katG* mutant is sensitised to growth in the presence of H_2O_2 and also attenuated in a mouse model of chronic infection (Ng *et al.*, 2004). The AhpC enzyme, together with the peroxiredoxin AhpE, can also detoxify organic peroxides, peroxynitrite and fatty acid hydroperoxides into less reactive molecules such as alcohols (Shastri *et al.*, 2018). Mycobacterial mutants lacking AhpC activity are consequently sensitised to ROS and RNS such as cumene hydroperoxide and peroxynitrite, respectively (Master *et al.*, 2002; Springer *et al.*, 2001).

Disulphide bonds formed as a result of cysteine thiol oxidation by ROS and RCS can be reduced by members of the thioredoxin (Trx) and glutaredoxins (Grx) families (Baba and Bhatnagar, 2018; Ulrich and Jakob, 2019). Trxs are oxidoreductases capable of reducing oxidized thiols in disulphide bonds or sulphenic acid intermediates via direct thiol/disulphide exchange. Trxs are comprised of five β-strands sandwiched between four α-helices, with a conserved catalytic active site motif, CXXC (Holmgren, 1995, 1985). The first Cys within the CXXC motif serves as an attacking residue that initiates the reduction reaction by forming a mixed disulphide intermediate with oxidised thiols in protein substrates. The second Cys is then deprotonated, pre-empting a nucleophilic attack on the mixed disulphide intermediate resulting in the release of the reduced substrate protein and oxidation of the Trx protein. The Trx disulphide is subsequently reduced by the thioredoxin reductase, TrxR, using electrons obtained from NADPH (Collet and Messens, 2010; Williams, 1995). Protein disulphides can also be reduced by the Grx system, but the disulphide form of glutaredoxin is restored by the low molecular weight non-protein thiol, glutathione (GSH) (Ulrich and Jakob, 2019). The Mtb genome encodes three thioredoxins (TrxA, TrxB1, and TrxC) and one thioredoxin reductase (TrxB2, alternatively known as TrxR) that is essential (Attarian *et al.*, 2009; Lin *et al.*, 2016; Zhang *et al.*, 1999). The purified TrxB1 has been shown to reduce H_2O_2 and dinitrobenzene in biochemical assays and its activity is essential for bacterial growth *in vitro*, as well as during the acute and chronic phases of mouse infection (Lin *et al.*, 2016; Zhang *et al.*, 1999). Mtb also encodes two methionine sulfoxide reductases (Msrs), MsrA and MsrB, which function to convert methionine sulphoxide formed as a result of methionine thiol oxidation, back to methionine using thioredoxin reductase and NADPH as the reducing system (Lee *et al.*, 2009). Loss of Msr activity in Mtb conferred sensitivity to the strong oxidant HOCl and acidified nitrate, a source of the RNS nitric oxide, but not to H_2O_2 or cumene hydroperoxide (Lee *et al.*, 2009).

Unlike many other bacterial species, mycobacteria lack a glutathione system. Instead, they produce the low-molecular-weight compound, mycothiol (MSH) as a major non-protein antioxidant to protect against oxidative stressors (Newton *et al.*, 2008, 1996). The redox-active sulfhydryl group of MSH protects proteins from oxidants by reacting with exogenous or endogenous reactive intermediates. During this reaction MSH is oxidized to mycothiol disulphide (MSSM). The enzyme mycothiol disulphide reductase subsequently reduces the oxidised MSSM, regenerating MSH (Buchmeier *et al.*, 2003; Rawat *et al.*, 2007). In addition to MSH, Mtb also produces, ergothioneine, a sulphur-containing histidine derivative as a second, non-protein antioxidant (Saini *et al.*, 2016; Singh *et al.*, 2016). Msm and Mtb mutants with reduced levels of mycothiol and ergothioneine display sensitivity to several ROS, RNS, redox cycling agents and antibiotics that include, amongst other H_2O_2, cumene hydroperoxide, NO, menadione, plumbagin, rifampicin and isoniazid (Buchmeier *et al.*, 2003; Rawat *et al.*, 2007; Saini *et al.*, 2016; Singh *et al.*, 2016). Ergothioneine functions as an antioxidant, protecting against oxidative stress (Paul and Snyder, 2010; Rahman *et al.*, 2003), and together with mycothiol may also play a role in minimising the reductive damage caused by acid stress (Buchmeier *et al.*, 2006).

1.4.2 ATP-dependant machineries

In instances where the levels of oxidants cannot be fully neutralised by the mechanisms described above, bacterial proteins can unfold and aggregate, which can be fatal if not adequately managed. Aggregated proteins can be re-solubilised and rescued by disaggregases and foldases if reparable, or degraded by proteases if irreversibly damaged (see **Table 1.1**) (Lupoli *et al.*, 2018). Aggregated proteins are disaggregated (solubilised) by ClpB, an ATP-dependant disaggregase, which allows proteins that can be rescued to be refolded by ATP-dependent foldases. The DnaK/DnaJ/GrpE (DnaKJE) and GroEL/ES complexes are the primary cellular foldases, which function to fold or refold inactivated proteins, as well as folding nascent proteins (Fay and Glickman, 2014). In the DnaKJE complex, DnaK is required for native protein folding and is essential in mycobacteria (Fay and Glickman, 2014), DnaJ is a co-chaperone that helps regulate the refolding processes, while GrpE acts as a nucleotide (ATP/ADP) exchange factor (Pierpaoli *et al.*, 1997; Schröder *et al.*, 1993). In the GroEL/ES complex, GroEL functions as a chaperone, and GroES functions as a co-chaperone (Hartl and Hayer-Hartl, 2002). HtpG is an ATP-dependant chaperone that is required for protein folding following exposure to host cell stresses, particularly RNS (Genest *et al.*, 2011; Harnagel *et al.*, 2021). In the instances where proteins are irreversibly damaged or denatured, they require

degradation and are targeted to ATP-dependant proteases such as ClpP, Lon, and the proteasomal complex, which collectively facilitate this degradation (Frees *et al.*, 2014; Lupoli *et al.*, 2018; Raju *et al.*, 2012). These three classes of proteins effectively maintain the proteostasis network under normal and some proteotoxic stress conditions, when cellular ATP is still available.

Table 1.1 The ATP-dependent and -independent mechanisms involved in maintaining the bacterial proteostasis network.

Component	Role	Mtb Homolog	Msm Homolog	Reference
ATP-dependant mechanisms				
ClpB	Holdase/disaggregase	Rv0384c	MSMEG_0732	(Parsell *et al.*, 1994; Rosenzweig *et al.*, 2013; Weibezahn *et al.*, 2004)
ClpP	Protease	Rv2460c Rv2461c	MSMEG_4672 MSMEG_4673	(Frees *et al.*, 2014; Raju *et al.*, 2012)
DnaK	Foldase	Rv0350	MSMEG_0709	(Fay and Glickman, 2014)
DnaJ	Holdase	Rv0352	MSMEG_0711	(Pierpaoli *et al.*, 1997; Schröder *et al.*, 1993)
GroEL	Foldase	Rv3417c	MSMEG_1583	(Pierpaoli *et al.*, 1997; Schröder *et al.*, 1993)
GroES	Co-chaperone	Rv3418c	MSMEG_1582	(Hartl and Hayer-Hartl, 2002)
GrpE	Co-chaperone	Rv0351	MSMEG_0710	(Hartl and Hayer-Hartl, 2002)
HtpG	Foldase	Rv2299c	No known ortholog	(Genest *et al.*, 2011; Harnagel *et al.*, 2021)
Lon	Protease	No ortholog	MSMEG_3582	(Lupoli *et al.*, 2018)
ATP-independent, stress-induced molecular chaperones				
CnoX	HOCl-activated or constitutive holdase	Rv1324	MSMEG_4917	(Goemans *et al.*, 2018a; Meireles *et al.*, 2020)
Hsp33	HOCl-activated or H_2O_2+ heat-activated holdase	No mycobacterial orthologs		(Cremers *et al.*, 2014; Jakob *et al.*, 1999; Winter *et al.*, 2008)
Polyphosphate	Chemical holdase			(Dahl *et al.*, 2015)
RidA	HOCl-activated holdase	No mycobacterial orthologs		(Müller *et al.*, 2014)
Ruc	Redox-regulated holdase	Rv0991c	MSMEG_5479	(Becker *et al.*, 2020)

1.4.3 ATP-independent, stress-induced molecular chaperones

The ATP-dependent members of the proteostasis network are, like other proteins, susceptible to inactivation by physical and chemical stresses, which reduces their ability to maintain proteostasis during periods of severe stress (Khor *et al.*, 2004; Melkani *et al.*, 2004; Winter *et al.*, 2005). In addition, the exposure to strong oxidants, such as HOCl, results in a dramatic reduction in cellular ATP levels caused by, amongst others, the inhibition or cellular respiration, inactivation of ATP synthase, and the formation of polyphosphate from ATP, further reducing their activity (Barrette *et al.*, 1987; Winter *et al.*, 2005). Under these conditions, ATP-independent proteins known as stress-induced chaperones or holdases are activated, and compensate for the absence of ATP-dependent folding factors by binding to and preventing protein misfolding and aggregation until the stress abates. The holdases then transfer the damaged substrates to ATP-dependent foldases, such as DnaKJE or GroEL/S, which restore the proteins correct tertiary structure. These stress-induced chaperones include, amongst other examples, polyphosphate, Hsp33, RidA, and CnoX.

The chemical holdase, polyphosphate, is synthesised from inorganic phosphates (P_i) by the enzyme polyphosphate kinase (*ppk*) using cellular ATP, and reversibly degraded to P_i by exopolyphosphatases (*ppx*) (Akiyama *et al.*, 1993; Gray *et al.*, 2014; Zhang *et al.*, 2002). Exopolyphosphatases are inactivated by HOCl, acid, nutrient starvation, and osmotic or high-temperature stress, inhibiting polyphosphate degradation, thereby allowing its accumulation (Gray *et al.*, 2014). Polyphosphates then bind to unfolded proteins, preventing their aggregation, until normal conditions are restored. They then transfer the proteins to foldases such as DnaKJE and are subsequently degraded, providing an ATP supply for the ATP-dependant folding machinery (Gray *et al.*, 2014).

The Hsp33 holdase has a redox-sensing domain with four highly conserved cysteine residues and is activated by either HOCl, H_2O_2 or increased temperatures (Graumann *et al.*, 2001; Winter *et al.*, 2008). Normally, the cysteines present in Hsp33 are reduced and coordinate a Zn^{2+} ion, resulting in a tightly folded conformation. However, exposure to HOCl and ROS oxidises the cysteines in a reversible manner, forming two intramolecular disulphide bonds, releasing the Zn^{2+}. This results in a conformational change that expose the hydrophilic linker region of Hsp33, which binds to unfolded proteins, protecting them from stress-induced aggregation (Graumann *et al.*, 2001). Trxs or Grxs reduce Hsp33 after the stress abates, and once cellular ATP levels have increased, the substrates are transferred to DnaKJE system, inactivating Hsp33 in the process (Hoffmann *et al.*, 2004).

RidA is a dual-function protein that acts as an enamine/imine deaminase that prevents toxic metabolite accumulation under normal growth conditions. In the presence of HOCl, RidA is converted into an efficient holdase that protects oxidised proteins from aggregation (Müller *et al.*, 2014). The holdase activity of RidA is activated by chlorination of several positively charged residues within the protein, which increases its hydrophobicity thereby enabling it to bind to oxidised and unfolded substrate proteins and protecting them from misfolding and aggregation (Dahl *et al.*, 2015; Müller *et al.*, 2014). The CnoX protein has recently been identified as an additional example of a stress-induced chaperone in *E. coli* and other related bacterial species, and will be discussed further in the following section.

1.5 Chaperedoxin (CnoX) Proteins

The CnoX proteins are a family of highly conserved enzymes that prevents the irreversible oxidation and aggregation of proteins. They does so by combining the ability to reduce oxidised thiols in proteins with chaperone (holdase) activity (Dupuy *et al.*, 2022; Goemans *et al.*, 2018a). This allows it to transfer substrates to foldases such as DnaKJE or GroEL in a folding-competent (i.e. reduced) state prior to refolding (Goemans *et al.*, 2018a, 2018b). Given its ability to combine both chaperone and redox functions, the enzymes have been termed "chaperedoxins" (Goemans *et al.*, 2018a). CnoX family members are comprised of two domains: an N-terminal Trx-like domain with a variably conserved CXXC[N24]C active site motif, and a C-terminal tetratricopeptide repeat (TPR)-motif containing domain (Goemans *et al.*, 2018a; Lin and Wilson, 2011; Meireles *et al.*, 2020). The N-terminal Trx domain fold is comprised of a four-stranded β-sheet sandwiched by three α-helices (Atkinson and Babbitt, 2009) and is associated with the redox-related properties of CnoX enzymes (reviewed by Dupuy and Collet, 2021). This includes the ability of CnoX proteins to act as thiol-disulphide oxidoreductases (thioredoxins), together with their ability to rescue oxidised thiols via the formation of mixed-disulphides (Dupuy and Collet, 2021). The C-terminal TPR-motif containing domain, by contrast, has been shown to be associated with holdase activity of CnoX, which can be either constitutive or inducible (Goemans *et al.*, 2018a; Lin and Wilson, 2011; Meireles *et al.*, 2020). This activity is consistent with the known ability of TPR-motifs to mediate protein-protein interactions, and its common occurrence in holdases and other folding factors (Allan and Ratajczak, 2011). The TPR-domain of the CnoX of *E. coli* is composed of ten α-helices, which are divided into two similar sub-domains (TPR A and TPR B). Each sub-domain is comprised of five α-helices, which define a groove rich in charged residues to which CnoX client proteins are thought to bind (Lin and Wilson, 2011).

The ability of CnoX proteins to function as oxidoreductases is dependent on the presence of two conserved Cys residues located in the canonical CXXC catalytic motif of Trx-fold containing proteins. CnoXs ability to form mixed disulphide with oxidised substrates is, by contrast, mediated a Cys residue located 24 amino acid residues away from the Trx-folds CXXC catalytic motif. (Goemans *et al.*, 2018a, 2018b; Meireles *et al.*, 2020). Based on the presence of the three Cys residues within the Trx domains extended active site motif, CXXC[N24]C, CnoX enzymes have been divided into four functional groups (**Table 1.2**): Group A CnoX enzymes contain a CXXC catalytic motif, but no additional downstream Cys residue; Group B CnoX enzymes contain a complete CXXC catalytic motif and an additional downstream Cys; Group C CnoX enzymes contain an SXXC motif and an additional downstream Cys residue; and Group D CnoX enzymes contain an SXXS/C motif and no additional downstream Cys residue (Meireles *et al.*, 2020).

Table 1.2 Categories of Chaperedoxins.

Group	Motif	Bacterial Species Examples	Reference
A	CXXC[N24]X	*C. crescentus* *X. fastidiosa*	(Goemans *et al.*, 2018b) (Meireles *et al.*, 2020)
B	CXXC[N24]C	*P. aeruginosa*	(Meireles *et al.*, 2020)
C	SXXC[N24]C	*E. coli*	(Goemans *et al.*, 2018a)
D	SXXS[N24]X SXXC[N24]V SXXS[N24]V	*M. smegmatis* *M. tuberculosis*	

The CnoX enzyme from *E. coli* (*Ec*CnoX) has been most extensively studied to date (Dupuy *et al.*, 2022; Goemans *et al.*, 2018a; Lin and Wilson, 2011; Meireles *et al.*, 2020). The enzyme possesses an SXXC[N24]C motif within its Trx-domain ($S_{35}QHC_{38}[N24]C_{63}$), with two Cys residues located at amino acid 38 (C_{38}) and 63 (C_{63}) of the protein, and a Ser at residue 35 (S_{35}). Given the absence of the canonical CXXC catalytic motif, the *Ec*CnoX enzyme lacks thiol-disulphide oxidoreductase activity both *in vitro* and *in vivo* (Goemans *et al.*, 2018a). The *Ec*CnoX is, nevertheless, capable of forming mixed-disulphides with oxidised thiols in oxidised substrate proteins (Dupuy *et al.*, 2022; Goemans *et al.*, 2018a, 2018b). This activity is mediated by C_{63} and protects substrate proteins from irreversible oxidation, which can both promote aggregation and inhibit disaggregation and refolding by cellular ATP-dependent dissagregases and foldases (Dupuy *et al.*, 2022; Goemans *et al.*, 2018a, 2018b). The *Ec*CnoX proteins have also been shown to possess holdase activity. While the protein does not display

any holdase activity under conventional growth conditions, its activity is rapidly activated following exposure to HOCl (Goemans *et al.*, 2018a). Like RidA, the HOCl-mediated activation of *Ec*CnoX occurs in response to the chlorination of several residues in the protein's TPR domain, which increases its hydrophobicity and hence affinity for unfolded polypeptides (Goemans *et al.*, 2018a). In line with the protein's biochemical properties, *Ec*CnoX activity was shown to be essential for growth in the presence of HOCl, but not other physical or chemical stresses (Goemans *et al.*, 2018a; Meireles *et al.*, 2020). In contrast to *Ec*CnoX, the CnoX enzymes from *C. crescentus* (*Cc*CnoX; Goemans *et al.*, 2018b), *X. fastidiosa* (*Xf*CnoX; Meireles *et al.*, 2020), and *P. aeruginosa* (*Pa*CnoX; Meireles *et al.*, 2020) all possess canonical CXXC catalytic site motifs (See **Table 1.2**) and consequently all display thiol-disulphide oxidoreductase activity. Like *Ec*CnoX, the Group A *Xf*CnoX possesses holdase activity that is HOCl-inducible (Meireles *et al.,* 2020). The *Cc*CnoX, which is also classified in Group A, is constitutively active and does not require pre-activation with HOCl. This property was attributed to the enzyme's greater surface hydrophobicity relative to *Ec*CnoX, which is thought to confer the protein with a higher affinity for unfolded protein substrates even without HOCl-activation (Meireles *et al.*, 2020). While the *Pa*CnoX, which as a Group B CnoX contains all three active site Cys residues, displays oxidoreductase activity, it was found to lack both constitutive and HOCl-inducible holdase activity (Meireles *et al.,* 2020). The ability of C_{63} in the *Pa*CnoX to mediate mixed disulphide formation was not, however, investigated in this study (Meireles *et al.*, 2020). In contrast to the findings reported for *E. coli*, the loss of CnoX activity in *C. crescentus* and *P. aeruginosa* did not sensitise the encoding organism to HOCl or any other physical or chemical stress investigated *in vitro* or *in vivo* (Goemans *et al.*, 2018b; Meireles *et al.*, 2020). Taken together, these observations suggest that the biochemical properties, enzymatic activities, and biological roles of CnoX may have been tailored during the course of evolution to meet the physiological needs of each organism (Goemans *et al.*, 2018b; Meireles *et al.*, 2020).

The *Ec*CnoX and *Cc*CnoX proteins are capable of transferring substrates to both the DnaKJE and GroEL/ES chaperones (Dupuy *et al.*, 2022; Goemans *et al.*, 2018a, 2018b). The CnoX enzymes are, furthermore, the only holdases known to interact with the GroEL/ES folding machinery to date (Dupuy *et al.*, 2022; Goemans *et al.*, 2018a, 2018b; Meireles *et al.*, 2020). The *Ec*CoX has recently been shown to interact with GroEL via its C-terminal α-helix, which is highly conserved amongst all CnoX family members. The deletion of the last 10 amino acids of *Ec*CnoX consequently abolishes its interaction with the GroEL chaperone. Based on their

observations, Dupuy *et al.* (2022) proposed that CnoX acts as a "molecular plugin" that serves as a redox quality-control system for GroEL substrates. Based on this model, CnoX binds to the GroEL chaperone at a location that is distinct from GroEL substrates. If a GroEL substrate contains an oxidised thiol (e.g. sulphenic acid or disulphide bond), CnoX will reduce the oxidised thiol via its oxidoreductase activity, or form a mixed disulphide that can be reduced by alternative cytoplasmic reducing pathways (e.g. glutathione). This will release the substrate in a reduced form that can be refolded by GroEL. The binding of the GroES co-chaperone induces a conformational change in GroEL, which triggers the release of CnoX and entry of the reduced substrate into the GroEL chamber for folding (Dupuy *et al.*, 2022).

1.6 Rationale

Mtb is exposed to a number of physical and chemical stresses during the infection of its human host. The ability of the bacterium to latently infect or cause active infections in otherwise healthy individuals, nevertheless, suggests that it can circumvent many of the immune-imposed stresses designed to limit bacterial growth and/or survival. Many of the mechanisms used by Mtb to detoxify ROS, RCS, and RNS, or remove and repair damage caused by these effector molecules have been identified and characterised (Ehrt and Schnappinger, 2009; Lupoli *et al.*, 2018; Rankine-Wilson *et al.*, 2021). Recently, much attention has been focused on the protective role members of the proteostasis network provides in maintaining the integrity of the mycobacterial proteome during growth *in vitro* and *in vivo* (Becker *et al.*, 2020; Lupoli *et al.*, 2018). Included amongst members of this network are a number of ATP-dependent proteins such as DnaJKE, GroELS, ClpB and ClpP, which facilitate the solubilisation, refolding, and degradation of damaged or denatured proteins. When exposed to stress conditions, these proteins cooperate with holdases, which bind to denatured or misfolded proteins in an ATP-independent manner. Upon restoration of more favourable conditions, holdases transfer their substrates to their energy-dependent counterparts for efficient refolding. While the CnoX family of holdases has been extensively studied in *E. coli* and other proteobacterial species, very little is known about its presence and potential physiological role in mycobacterial species such as Mtb and Msm.

1.7 Aims and Objectives

The overall aim of the research project was to identify CnoX orthologs in Msm and/or Mtb and establish their potential role in conferring resistance to physical and chemical stresses using a combination of biochemical, genetic, and physiological studies.

The experimental objectives of this research project were to:

1) Identify orthologs of CnoX in Msm and Mtb.

2) Clone, express and purify the recombinant Msm and Mtb CnoX enzymes, together with the *E. coli* CnoX and Msm TrxC thioredoxin as controls for holdase and thioredoxin activity, respectively.

3) Determine whether the recombinant Msm and Mtb CnoX enzymes possess activity as thiol-disulphide oxidoreductases and/or holdases *in vitro.*

4) Generate Msm knockdown (KD) and knockout (KO) mutant strains to examine the effects of silencing or eliminating CnoX activity, respectively.

5) Determine the physiological role of CnoX in Msm by comparing the growth of the Msm WT and KD or KO mutants under both standard growth conditions and following exposure to physical and chemical stresses.

6) Determine the ability of the Msm and Mtb CnoX enzymes to genetically complement an *E. coli cnoX* mutant in the presence and absence of HOCl.

Chapter 2: Materials and Methods

2.1 Bacterial Strains

The bacterial strains used during this study are listed in **Table 2.1**. *E. coli* Mach1 and TOP10 cells were obtained from ThermoFisher Scientific and used for the routine cloning, isolation and/or maintenance of plasmids. *E. coli* XJa and XJb (DE3) Autolysis strains (Zymo Research) were used for small- and large-scale expression of recombinant proteins, respectively. The parental strain of the Keio collection, *E. coli* BW25113, and its isogenic, CnoX-deficient derivative (Δ*cnoX*::Kan^R) were obtained from Horizon Discovery and used for heterologous complementation studies (Baba *et al.*, 2006). The Kan^R cassette was removed by FLP recombinase-mediated recombination after transformation with the temperature-sensitive plasmid, pE-FLP, followed by selection on LA/Amp plates at 30 °C. Colonies that had lost the Kan^R cassette were identified by colony PCR using the oligonucleotide primers, EcCnoXCheckFor and EcCnoXCheckRev (**Table 2.3**). The strain was cured of pE-FLP by streaking on LA followed by incubation at 37 °C. The electroporation-proficient Msm mc^2155 strain (Snapper *et al.*, 1990) was used for all mycobacterial work, including the generation of KD and KO mutants.

2.2 Bacterial growth media and conditions

E. coli strains were routinely grown under aerobic conditions at 37 °C in Lysogeny Broth (LB) [1 % (w/v) tryptone, 0.5 % (w/v) yeast extract, and 1 % (w/v) NaCl] with shaking (180 rpm), or on solid LB Agar medium (LA) [LB broth, 1.5 % (w/v) agar], unless otherwise specified. For growth in chemically defined media, bacteria were grown in M9 minimal medium broth (M9B) (48 mM Na_2HPO_4, 22 mM NaH_2PO_4, 8.6 mM NaCl, 19 mM NH_4Cl, 2.0 mM $MgSO_4$, 0.1 mM $CaCl_2$) supplemented with 0.2 % (w/v) glucose or 0.2 % (v/v) glycerol as the sole carbon source, or on the surface of M9 minimal medium agar plates (M9A) [M9B supplemented with 1.5 % (w/v) agar)]. Where applicable, antibiotics were added to the following final concentrations: ampicillin at 100 μg/mL, kanamycin at 50 μg/mL, hygromycin at 200 μg/mL and zeocin at 100 μg/mL.

M. smegmatis mc^2155 (wild-type [WT]) and mutant strains were grown under aerobic conditions at 37 °C in Middlebrook 7H9 medium (BD Difco) supplemented with 0.2 % (v/v) glycerol, 0.2 % (w/v) glucose, 0.85 % (w/v) NaCl and 0.2 % (v/v) Tween 80 or on solid Middlebrook 7H10 or 7H11 agar supplemented with 0.5 % (v/v) glycerol, 0.2 % (w/v) glucose and 0.85 % (w/v) NaCl, unless otherwise specified. Where applicable, antibiotics were added

to the growth medium at the following final concentrations: hygromycin at 50 μg/mL, kanamycin at 25 μg/mL, zeocin at 12.5 μg/mL and ATc at either 100 ng/mL or 200 ng/mL.

For the long-term storage and maintenance of bacterial strains, cultures were grown to late exponential phase in either LB (for *E. coli*) or Middlebrook 7H9 medium (for Msm). The bacterial suspension was diluted 1:1 in 50 % (v/v) glycerol, which served as a cryopreservant. The cells were allowed to equilibrate in the glycerol at room temperature for 15 min, before being transferred to a -80 °C freezer for long-term storage. Working stocks of the strains were prepared by scraping the surface of the glycerol stock onto LA (*E. coli*) or Middlebrook 7H11 medium (Msm), followed by streaking for single colonies, incubation at 37 °C for 16 h, and short-term storage at 4 °C (for *E. coli*) or ambient temperatures (Msm). Plates were stored and used for up to 2 weeks (*E. coli*) or 4 weeks (Msm). Single bacterial colonies were used to start liquid cultures used in the bacterial growth assays described in **Section 2.3**.

Table 2.1 Bacterial strains and plasmids used and generated during this study.

Strains	Relevant Characteristics/Genotype	Source/Reference
E. coli		
Mach1	Δ*rec*A1*398 end*A1 *F- φ80(lacZ)ΔM15 ΔlacX74 hsd*R*(rK-mK+) ton*A	ThermoFisher Scientific
Top10	F- *mcr*A Δ(*mrr-hsd*RMS-*mcr*BC) Φ80*lacZ*ΔM15 Δ*lac*X74 *rec*A1 *ara*D139 Δ(*ara-leu*)7697 *gal*U *gal*K *rps*L (Str^R) *end*A1 *nup*G	ThermoFisher Scientific
BW25113 WT	Δ(*ara*D-*ara*B)567, Δ*lacZ*4787(::rrnB-3), λ, rph-1, Δ(*rha*D-*rha*B)568, *hsd*R514	CGSC 7636 Barry L. Wanner (Dharmacon)
BW25113 Δ*cnoX*::*Kan^R*	Δ(*araD-araB*)567, Δ*lacZ*4787(::*rrn*B-3), λ, rph-1, Δ(*rhaD-rhaB*)568, *hsd*R514 Δ*cnoX*, Kan^R	Dharmacon
BW25113 Δ*cnoX*	Δ(*araD-araB*)567, Δ*lacZ*4787(::rrnB-3), λ, rph-1, Δ(*rhaD-rhaB*)568, *hsd*R514 Δ*cnoX*	This Study
***XJa (*DE3) Autolysis**	*E. coli* K *rec*A1 *sup*E44 *end*A1 *hsd*R17 (r_k-, m_k+) *gyr*A96 *rel*A1 *thi mcr*A Δ(*lac-pro*AB) Δ*ara*B::λR, *cat* F'[*tra*D36 *pro*AB$^+$ *lac*I^q *lac*ZΔM15] λDE3	Zymo Research
***XJb (*DE3*)* Autolysis**	*E. coli* B F- *omp*T *hsd*S_B(r_B- m_B-) *gal dcm*$^+$ *ara*B::R, *cat* λDE3	Zymo Research
M. smegmatis		
mc^{2}155	A high-frequency transformation (electroporation-proficient) wild-type strain.	Albert Einstein College of Medicine (Snapper *et al.*, 1990)
mc^{2}155 Δ*cnoX*::*Zeo^R*	Marked c*noX* deletion mutant derived from mc^{2}155. Zeomycin-resistant (Zeo^R) ΔMSMEG_4917:: Zeo^R.	This Study
mc^{2}155 Δ*cnoX*	Unmarked c*noX* deletion mutant derived from mc^{2}155 Δ*cnoX*::*Zeo^R* ΔMSMEG_4917	This Study
mc^{2}155 Δ*cnoX*::pCnoX-CompX	Genetically complemented Δ*cnoX* deletion mutant. Expresses *cnoX* from the P_{smyc} promoter. Giles *attB*:pCnoX-CompX (P_{smyc}-*cnoX*)	This Study
mc^{2}155 Δ*cnoX*::pCnoX-CompP	Genetically complemented Δ*cnoX* deletion mutant. Expresses *cnoX* from the P_{cnoX} promoter. Giles *attB*:pCnoX-CompP (P_{cnoX}-*cnoX*)	This Study

Plasmids	Description	Source/Reference
Protein Expression Vectors		
pJET1.2/Blunt	High copy number vector with the lethal *eco47IR* gene for positive selection without IPTG induction, Amp^R.	ThermoFisher Scientific
pJET1.2::EcCX	High copy number vector with the *E. coli cnoX* gene cloned into the MCS of pJET1.2/Blunt.	This study
pJET1.2::MsCX	High copy number vector with the codon optimised *Msm cnoX* gene cloned into the MCS of pJET1.2/Blunt.	This study
pJET1.2::MtCX	High copy number vector with the codon optimised *Mtb cnoX* gene cloned into the MCS of pJET1.2/Blunt.	This study
pQE-80L	Protein expression vector that adds a 6 × His tag to the N-terminus of proteins expressed from the IPTG-regulatable T5 promoter, Amp^R.	Qiagen
pQE-80L::EcCX	Protein expression vector that adds a 6 × His tag to the N-terminus of the *Ec cnoX* gene expressed from the IPTG-regulatable T5 promoter, Amp^R.	This study
pQE-80L::MsCX	Protein expression vector that adds a 6 × His tag to the N-terminus of the codon optimised *Msm cnoX* gene expressed from the IPTG-regulatable T5 promoter, Amp^R.	This study
pQE-80L::MtCX	Protein expression vector that adds a 6 × His tag to the N-terminal of the codon optimised *Mtb cnoX* gene expressed from the IPTG-regulatable T5 promoter, Amp^R.	This study
CRISPRi Vectors		
pLJR962	Low copy, integrative (L5) vector that expresses a *Sth*1 *dCas9* enzyme from an anhydrotetracycline (ATc)-inducible promoter, L5 Integrase, Kan^R.	(Rock *et al.*, 2017)
pLJR962::*cnoX* sgRNA1	Low copy, integrative (L5) vector that expresses a *Sth*1 *dCas9* enzyme and Msm *cnoX*_sgRNA1 from ATc-inducible promoters, L5 Integrase, Kan^R.	This study
pLJR962::*cnoX* sgRNA2	Low copy, integrative (L5) vector that expresses a *Sth*1 *dCas9* enzyme and Msm *cnoX*_sgRNA2 from ATc-inducible promoters, L5 Integrase, Kan^R.	This study
pLJR962::*cnoX* sgRNA3	Low copy, integrative (L5) vector that expresses a *Sth*1 *dCas9* enzyme and Msm *cnoX*_sgRNA3 from ATc-inducible promoters, L5 Integrase, Kan^R.	This study
pLJR962::*mmpL3* sgRNA1	Low copy, integrative (L5) vector that expresses a *Sth*1 *dCas9* enzyme and Msm *mmpl3*_sgRNA from ATc-inducible promoters, L5 Integrase, Kan^R	This study
Generation of KO Vectors		
pJV53	High copy number vector that encodes Che9c 60-61 under the control of an acetamidase promoter for mycobacterial recombineering, Kan^R.	(van Kessel and Hatfull, 2007)
pML2714	Temperature-sensitive vector that expresses Cre recombinase for mycobacterial recombineering, Kan^R.	(Ofer *et al.*, 2012)
pMSG360Zeo	Low copy number vector that contains a Zeo^R cassette flanked by two *lox*P sites for mycobacterial recombineering, Zeo^R.	(Barkan *et al.*, 2010)
Generation of Complementation Vectors		
pGiles::P_{smyc}	Mycobacterial integrative vector. Bacteriophage Giles *attP.* P_{smyc}, upstream of MCS. Hyg^R.	(Kolbe *et al.*, 2020)
pCnoX-CompX	Msm *cnoX* gene cloned under the control of the P_{smyc} promoter of pGiles::P_{smyc}. Hyg^R.	This study
pCnoX-CompP	Msm *cnoX* gene and its native promoter cloned into pGiles::P_{smyc}, Hyg^R.	This study
pUC19 Giles Integrase	Suicide vector that expresses the Giles Integrase.	(Kolbe *et al.*, 2020)
Generation of Heterologous Complementation Vectors		
pE-FLP	A low copy number, temperature-sensitive vector that expresses the FLP-recombinase, Amp^R.	(St-Pierre *et al.*, 2013)

2.3 Growth Assays

2.3.1 Growth assays in liquid medium

For growth assays, single bacterial colonies grown on 7H11 agar plates were inoculated into 5 mL of 7H9 medium and grown at 37 °C until saturated. The saturated cultures were diluted 1:100 into 7H9 medium and grown at 37 °C overnight (~16 h) until the late-exponential phase. The OD_{600} of the cultures was measured at an absorbance of 600 nm (OD_{600}) and the cells were diluted into fresh, pre-warmed 7H9 medium to a starting OD_{600} of 0.05. The cultures were incubated at 37 °C and the OD_{600} values were determined at the time points indicated in the Results section (**Chapter 4**). All absorbance readings were measured using a Jenway 6200 spectrophotometer and 1 cm path length semi-micro cuvettes (Lasec). When required, cell suspensions were diluted in 7H9 medium to reduce the OD_{600} below 1.0 before measuring the absorbance. The growth assays were performed using three independent biological replicates, with two technical replicate measurements used for each sample.

2.3.2 Survival assays in liquid medium

Cultures of Msm WT or mutant strains were started from single colonies and grown to late exponential-phase as described above (**Section 2.3.1**) before being diluted into 7H9 medium to a starting OD_{600} of 0.05. The cultures were grown to the mid-exponential phase (OD_{600} of 0.4 to 0.6) and diluted to an OD_{600} of 0.1 in 7H9 medium. For heat-shock experiments, bacterial cultures were diluted to an OD_{600} of 0.1 in 7H9 medium and incubated at the indicated temperatures (45 and 53 °C) and bacterial survival was enumerated after 0, 15, 30, 45, 60, and 180 min and 0, 3, 6, 9, 12, and 24 hours, respectively. All strains were analysed using three biological and two technical replicates.

2.3.3 Spotting assays

Bacterial cultures were sampled in 100 µL aliquots and diluted using a ten-fold dilution series (10^0 - 10^{-7}). 5 µL of each dilution was spot-plated onto the surface of a 7H10 plate. The spots were allowed to dry on the surface of plates before they were inverted and incubated aerobically at 37 ºC for 48-72 h to allow for colony outgrowth. The number of viable cells in each spot was enumerated and bacterial survival was calculated relative to the number of bacteria present at the outset of the experiment (t = 0).

2.3.4 Disc Diffusion Assays

Msm WT or mutant strains were grown to mid-exponential phase (OD_{600} of 0.4 to 0.6) and diluted to an OD_{600} of 0.1 in 7H9 medium. 1 mL of the diluted cultures was added to 3 mL of

molten top agar solution [1 % (w/v) agar in water, cooled to 45 °C], gently mixed and poured on the surface of a 7H10 agar plate. Once the top agar solidified, sterile paper discs (Whatman #1, 6 mm) impregnated with 10 µL of each test compound (see **Table 2.2**) were placed on the surface of the agar overlay with sterile forceps. The plates were incubated at 37 °C for 24 to 48 h and the zone of inhibition (ZOI) surrounding each disc was measured to the nearest millimetre (mm). When required, the growth medium and assay plates were supplemented with ATc (100 ng/mL) to silence gene expression, as specified in the Results Section (**Chapter 4.1**). Two biological replicates were performed for each test compound, with each plate prepared in duplicate containing discs with each compound in triplicate.

2.3.5 Broth microdilution assays

Msm WT or mutant strains were grown to an early exponential phase (OD_{600} of 0.2 to 0.4) and diluted to a final OD_{600} of 0.002 in 7H9 medium. Test compounds (see **Table 2.2**) were prepared in 96-well microtiter plates using two-fold serial dilutions in a total volume of 50 µL. The diluted bacterial cultures were added to the test compounds (or controls) in a 1:1 ratio to yield a final volume of 100 µL, and mixed by aspiration. The microtiter plates were incubated at 37 °C for 1 to 3 days with the bacterial growth recorded every 24 h. For quantitative analysis, resazurin was added to each well to a final concentration of 30 µg/mL and the plates were allowed to incubate for an additional 12-24 h. Where required, ATc was added to the growth medium at a concentration of 200 ng/mL to silence gene expression.

Table 2.2 The concentrations of the antimicrobial compounds used for disc diffusion with mycobacterial strains.

Compound	Mechanism of Action	Concentration
Antibiotic Stress		
Ciprofloxacin	Bactericidal; inhibits DNA replication through the inhibition of the DNA topoisomerase and DNA gyrase (LeBel, 1988).	0.08 mg/mL
Ethambutol	Not fully elucidated; bacteriostatic that is suspected to inhibit arabinosyl transferase, a key enzyme in the formation of arabinogalactan, a cell wall component (Vilchèze, 2020).	0.25 mg/mL
Isoniazid	Bactericidal; activated by KatG, and inhibits InhA enoyl reductase, leading to cell death in actively growing cells (Vilchèze and Jacobs, 2019).	2 mg/mL
Rifampicin	Binds to the bacterial RNA polymerase and inhibits RNA elongation (Campbell *et al.*, 2001; Unissa and Hanna, 2017).	4 mg/mL
Oxidative Stress		
Cumene Hydrogen Peroxide	Induces lipid peroxidation that damages the cell membrane (Akaike *et al.*, 1992).	50 mM
Diamide	Form of oxidative stress; rapidly forms disulphide bonds in thiols through oxidation (Ezraty *et al.*, 2017).	0.5 M
Hydrogen Peroxide	A form of oxidative stress; produces hydroxyl radicals that target membrane lipids, DNA, and proteins (Linley *et al.*, 2012).	1 M
Plumbagin	Generates superoxide anions (ROS). Additionally, it targets the mycobacterial enzyme, thymidylate synthase (ThyX) that synthesises dTMP from dUMP (Sarkar *et al.*, 2020).	5 mM
Sodium Hypochlorite	Form of RCS. Reacts with water, generating HOCl that causes mass protein unfolding and aggregation through the oxidation of sulphur-containing amino acids and chlorination of several others (Gundlach and Winter, 2014; Nauseef, 2019). Additionally, it depletes cellular ATP levels (Drazic *et al.*, 2015; Müller *et al.*, 2014).	0.5 M
Reducing Stress		
DTT	A reducing agent that reduces disulphide bonds, interfering with potassium transport systems and other complexes (Kirakosyan *et al.*, 2004).	1.2 M

2.4 Nucleic Acid Isolation, Purification, and Quantification

2.4.1 DNA Isolation, Purification, and Quantification

DNA from *E. coli* was isolated and purified using commercial kits according to the manufacturer's instructions. Genomic DNA (gDNA) was purified using the GeneJET Genomic DNA Purification Kit (ThermoFisher Scientific). Plasmids were purified using the GeneJET Plasmid MiniPrep Kit (ThermoFisher Scientific) or E.Z.N.A. Plasmid DNA Mini Kit (Omega Bio-tek). PCR products and other linearised DNA fragments were purified using the GeneJET PCR Purification Kit (ThermoFisher Scientific). When required, DNA fragments were electrophoresed using agarose gel electrophoresis (AGE) and excised with a scalpel blade after visualisation with a blue light transilluminator (IORodeo; 470 nm). The DNA in the excised gel fragment was purified with the Silica Bead Gel Purification Kit (ThermoFisher Scientific).

2.4.2 RNA Isolation, Purification, and Quantification.

Msm was grown in Middlebrook 7H9 broth to mid-exponential phase (OD_{600} of ~0.6) and harvested at 2000 × g for 5 min at room temperature. The resulting cell pellet was resuspended in 1 mL TRIzol (ThermoFisher Scientific) or TRI Reagent (Zymo Research) and stored at -80 °C for later use. The cells were homogenised with 0.1 mm acid-washed glass beads (Sigma-Aldrich) in a BeadBug 3 Microtube Homogeniser (Benchmark Scientific) for 6000 rpm for 30 s (4 times with 30 s cooling intervals). The samples were centrifuged at 13 400 × g for 2 min at 4 °C and the supernatant was transferred into a clean tube containing an equal volume of 100 % ethanol. RNA present in the samples was purified using the Direct-zol RNA MiniPrep kit (Zymo Research) and DNA was removed by on-column treatment with DNase according to the manufacturer's recommendations. Residual gDNA in the eluted RNA samples was removed using the RapidOut DNA Removal Kit (ThermoFisher Scientific) and the absence of DNA contamination was confirmed by the absence of specific or non-specific amplicons in control semi-quantitative and/or quantitative PCR (qPCR) reactions.

2.4.3 Nucleic acid quantification

The purity and concentration of DNA samples were determined by measuring the sample absorbance at a wavelength of 260 nm using a Nanodrop ND-1000 Spectrophotometer (ThermoFisher Scientific) and a conversion factor of 50 ng and 33 ng for single and double-stranded nucleic acids, respectively. The purity of the samples was assessed by determining the absorbance ratios at 260/280 or 260/230 nm, which indicates contamination with RNA or organic salts, respectively. When required, the concentration of DNA samples was determined

by comparing the intensity of ethidium-bromide-stained DNA samples relative to that of known quantities of DNA present in DNA ladders following AGE and visualisation under UV light (**Section 2.7** below).

2.5 General Recombinant DNA Procedures

All recombinant DNA and molecular biology techniques were performed according to standard protocols (Ausubel *et al.*, 2003; Sambrook and Russell, 2001) unless otherwise specified. All restriction and modification enzymes, kits and reagents were used according to the manufacturer's instructions, unless otherwise specified.

2.5.1 Restriction Endonuclease Digestion of DNA

Restriction endonuclease (RE) digestion of DNA was performed with either FastDigest (ThermoFisher Scientific) or Anza (ThermoFisher Scientific) restriction endonucleases according to the manufacturer's recommendations. Analytical restriction enzyme digests were performed with 1 µg of plasmid DNA, 1 µL of each restriction enzyme (10 U/µL), 1 × restriction enzyme buffer and ultrapure, nuclease-free dH_2O (Gibco) to a final volume of 30 µL. Preparative restriction enzyme digests were performed with 1 to 3 µg of plasmid DNA or PCR product, 1 µL of each restriction enzyme (10 U/µL) per 1 µg DNA, 1 × restriction enzyme buffer and ultrapure, nuclease-free ddH_2O (ThermoFisher Scientific) to a final volume of 30 to 90 µL. The reactions were incubated for 1 to 16 h at 37 °C before analysis by AGE (**Section 2.7**) and/or purification (**Section 2.4.1**) for use in downstream applications.

2.5.2 Enzymatic Modification of DNA

All DNA modification reactions were performed according to the manufacturer's recommendations. To prevent the re-ligation of plasmids following restriction with blunt- or compatible sticky-ends, the plasmids were treated with FastAP Thermosensitive Alkaline Phosphatase (ThermoFisher Scientific). The reactions were performed by adding 1 × FastAP or RE buffer, 1 µL FastAP, 1 µg DNA, and ultrapure, nuclease-free dH_2O (ThermoFisher Scientific) to a final reaction volume of 20 µL, followed by incubation at 37 °C for 15 min. The dephosphorylated vector was purified as described in **Section 2.4.1** before use in ligation reactions.

DNA fragments with sticky ends were converted to blunt-ended fragments using the Anza DNA End Repair Kit (ThermoFisher Scientific). The reactions were performed by mixing 1 × Anza End Repair buffer, 1 µL Anza DNA End Repair Mix, 1 µg of DNA and ultrapure,

nuclease-free water to a final reaction volume of 20 µL, followed by incubation at 20 °C for 15 min. The reactions were then purified before use in ligation reactions.

PCR products lacking 5'-phosphate groups were phosphorylated before ligation into dephosphorylated vectors using the Anza T4 PNK 5' Phosphorylation kit (ThermoFisher Scientific). The reactions were performed by mixing 1 × Anza PNK buffer, 1 µL Anza T4 PNK enzyme, 1 µg DNA, and ultrapure, nuclease-free H_2O (ThermoFisher Scientific) to a final reaction volume of 20 µL. The reactions were incubated at 20 °C for 15 min followed by inactivation of PNK at 80 °C for 5 min. The phosphorylated vectors were used directly in ligation reactions.

2.5.3 Ligation Reactions

Sticky-end cloning reactions were performed at a 3:1 (insert:vector) molar ratio in 20 µL reaction volumes with either 2 µL T4 DNA ligase (ThermoFisher Scientific) and 2 µL T4 DNA ligase buffer or 10 µL Instant Sticky-End Ligase Master Mix (New England Biolabs), the appropriate volumes of vector and insert, and ultrapure, nuclease-free dH_2O to a final volume of 20 µL. Blunt-end cloning reactions were performed at a 3:1 (insert:vector) ratio in 20 µL reaction volumes with 100 ng vector and the corresponding amount of insert, 5 µL T4 DNA Ligase Master Mix and the remainder with nuclease-free dH_2O (ThermoFisher Scientific) to a final volume of 20 µL.

2.6 PCR Amplification Procedures

Oligonucleotides used for plasmid construction, PCR strain verification, and real-time quantitative PCR are listed in **Table 2.3**. Oligonucleotide sequences were designed using the genomic sequence of *E. coli* BW25113 (GenBank Accession Number CP009273.1), Msm mc^2155 (GenBank CP000480.1) or Mtb (GenBank AL123456) and manufactured by Inqaba Biotec or ThermoFisher Scientific. All PCR reactions were performed using the Applied Biosystems SimpliAmp (ThermoFisher Scientific) or MultiGene Mini Personal (Labnet International) thermal cyclers.

2.6.1 Preparative PCR Reactions

PCR amplification of DNA fragments used for the generation of recombinant plasmids or allelic exchange substrates (AES) was performed using the Phusion High-Fidelity PCR Kit (ThermoFisher Scientific) according to the manufacturer's instructions. PCR reactions were performed in 50 µL reaction volumes containing 10 µL 5 × HF buffer, 0.3 µM forward and reverse primers, 200 µM deoxynucleotide triphosphates (dNTPs), 10 to 100 ng of template

DNA, 0.5 µL of Phusion DNA polymerase, and the balance of the volume (to 50 µL) with nuclease-free ddH_2O (ThermoFisher Scientific). For the amplification of genes with a high G+C content (>55 %), the HF buffer was replaced with a 5 × GC buffer, and DMSO was added to a final concentration of 3 % (v/v). PCR was performed using the following thermocycling parameters: (i) initial denaturation at 98 °C for 3 min, (ii) denaturation at 98 °C for 20 s (30 cycles), (iii) annealing at the appropriate annealing temperature for the primer pair in use for 30 s, (iv) extension at 72 °C for 30 s/kb, and (v) a final extension at 72 °C for 7 min. The annealing temperatures were calculated based on the melting temperatures (Tm) of the forward and reverse primers, as per the manufacturer's instructions (see **Table 2.3**).

2.6.2 Analytical PCR Reactions

Analytical PCR reactions were performed using Taq DNA polymerase using pre-prepared 2 × PCR master mixes [Dream Taq Master Mix (ThermoFisher Scientific), KAPA Taq Ready Mix (Sigma), or Taq Master Mix (New England Biolabs)]. PCR amplification was performed in 25 µL reaction volumes containing 12.5 µL of the 2 × Taq Master Mix, 0.3 µM of the forward and reverse primers, 2.5 µL DNA-containing solution, and 7.5 µL nuclease-free ddH_2O. The following cycling conditions were used for amplification: initial denaturation at 95 °C for 4 min, followed by 30 cycles of denaturation (95 °C for 30 s), annealing (the appropriate annealing temperature for primer pair for 30 s), extension (72 °C for 60 s/kb) and a final extension at 72 °C for 7 min. The annealing temperature was calculated according to the Tm of the forward and reverse primers, as per the manufacturer's recommendations (see **Table 2.3**).

2.6.3 Colony PCR Reactions

The construction of recombinant plasmids and mutant strains was confirmed by colony PCR using cell lysates as previously described (Woodman *et al.*, 2016). For *E. coli*, bacteria were grown in micro-centrifuge tubes in 100 µL of LB supplemented with the appropriate antibiotics and incubated at 37 °C for 4 to 16 h. The cells were harvested by centrifugation at 13 400 × g for 1 min and the supernatant was discarded. The cell pellets were resuspended in 100 µL nuclease-free ddH_2O and lysed by boiling at 100 °C for 10 min. The boiled cells were centrifuged at 13 400 × g for 2 min to remove cell debris. The supernatant containing DNA was transferred to a sterile microfuge tube and 2.5 µL was used in 25 µL analytical PCR reactions as described above (**Section 2.6.2**). For Msm, bacterial colonies were resuspended in 200 µL nuclease-free water containing 5 % (v/v) Chelex 100 Resin (200-400 mesh, Bio-Rad) as previously described (Singer-Sam *et al.*, 1989). The resuspended cells were boiled at 100 °C

for 10 min, centrifuged at 13 400 × g for 2 min, and 2.5 µL used in 25 µL in analytical PCR reactions as described above (**Section 2.6.2**).

2.6.4 Reverse Transcriptase and Real-Time Quantitative PCR (qPCR)

First-strand cDNA was synthesised by reverse transcribing 250 ng of total RNA with the Superscript IV VILO Mastermix (ThermoFisher Scientific) or LunaScript RT Supermix (New England Biolabs) kits. Semi-quantitative PCR reactions were performed in 25 µL volumes as described above (**Section 2.6.2**) using gene-specific primers and 2 µL cDNA as a template. Real-time quantitative PCR (qPCR) reactions were performed in 10 µL volumes containing 5 µL 2 × PowerUp SYBR Green Master Mix (ThermoFisher Scientific), 0.3 µM gene-specific forward and reverse primers (1 µL each) and 3 µL cDNA as a template. qPCR reactions were performed in a Quant Studio 3 Real-Time PCR System (ThermoFisher Scientific) using the following cycling conditions: (i) activation of UDG at 50 °C for 2 min; (ii) initial denaturation at 95 °C for 2 min; (iii) 40 cycles of denaturation at 95 °C for 15 s followed by annealing and extension at 60 °C for 1 min. Where required, the melting curves of qPCR amplicons were determined after amplification using the following cycling conditions: (i) denaturation at 95 °C for 15 s, annealing at 60 °C for 1 min (iii) denaturation at 95 °C for 15 s. The efficiency of all primer pairs was validated (90 to 110 % efficiency) against a standard curve generated using 3 µL of a 10-fold dilution series of Msm gDNA (1 to 1 000 000 pg DNA) as a template in qPCR reactions. Gene expression levels were normalised relative to the Msm *sigA* gene and calculated by the Quant Studio Design & Analysis Software (ThermoFisher Scientific) using the 2-ΔCt or 2-ΔΔCt method (Livak and Schmittgen, 2001; Schmittgen and Livak, 2008).

Table 2.3 List of oligonucleotide primers used during this study.

Primer Name	Primer Sequence	Amplicon properties / Region Targeted
Generation and Confirmation of *Msm* KO Mutant [a, b, c, d]		
pKMZeo-For	GCATGGTGGCCCGGTATA	Forward primer for the amplification of the Zeo^R cassette from pMSG360Zeo.
pKMZeo-Rev	CCGAAATCCGGTACAGTTCGA	Reverse primer for the amplification of the Zeo^R cassette from pMSG360Zeo.
CnoX-US-For	TCCTGCGTCGCTGAGAGA	Forward primer for the amplification of the US fragment of the Msm *cnoX* gene.
CnoX-US-Rev	TATACCGGGCCACCATGCGTC ACGTCGTTTCCGGTG	Reverse SOE primer for the amplification of the US fragment of the Msm *cnoX* gene. 5-end is complementary to pKMZeo-For (underlined).
CnoX-DS-For	TCGAACTGTACCGGATTTCGG AATCTCGCGAACGCCCTG	Forward SOE primer for the amplification of the DS fragment of the Msm *cnoX* gene. 5-end is complementary to pKMZeo-Rev (underlined).
CnoX-DS-Rev	CCTCAACGCCATCTACCG	Reverse primer for the amplification of the DS fragment of the Msm *cnoX* gene.
CnoX-US2-For	GGCCAAGGTGAACGTCAA	Forward gene-specific primer for confirming allelic exchange in the Msm *cnoX* knockout mutant.
CnoX-DS2-Rev	TACGCCTACAGCGAGAACTA	Reverse gene-specific primer for confirming allelic exchange in the Msm *cnoX* knockout mutant.
Zeo-Check-For	CATGACCGAGATCGGCGA	Forward Zeo^R cassette specific primer for confirming allelic exchange in the Msm *cnoX* knockout mutant.
Zeo-Check-Rev	GTGTCAGTCCTGCTCCTC	Reverse Zeo^R cassette specific primer for confirming allelic exchange in the Msm *cnoX* knockout mutant.
CnoX-CompP-XbaI-For	ATA**TCTAGA**GGACACAATCA ACGACACGTTG	Forward primer used for amplifying the Msm *cnoX* gene and its native promoter. 5' XbaI RE site.
CnoX-CompX-SphI-For	TCC**GCATGC**TTAATTAAGGA GGTATCTCAT*ATG*ACTCGTCC ACGTCCTTCC	Forward primer used for amplifying the Msm *cnoX* gene without its native promoter. 5' SphI RE site, ribosome binding site and start codon.
CnoX-Comp-HindIII-Rev	ATA**AAGCTT**AGTACAGGGCG TTCGC	Reverse primer used for amplifying the Msm *cnoX* gene with or without its native promoter. 5' HindIII RE site.
Generation and Confirmation of KD Mutants using CRISPRi [e]		
pLJR-Seq-For	AAGCTCTCACCAACCGTG	Forward primer used to confirm successful cloning of sgRNAs into pLJR962.
pLJR-Seq-Rev	CTGATTCTGTGGATAACCGT	Reverse primer used to confirm successful cloning of sgRNAs into pLJR962.
CnoX-sgRNA1-For	GGGAGCACCGGCCAGCGCCG GACCG	Forward oligonucleotide used to generate Msm *cnoX*_sgRNA1.
CnoX-sgRNA1-Rev	AAACCGGTCCGGCGCTGGCC GGTGC	Reverse oligonucleotide used to generate Msm *cnoX*_sgRNA1.
CnoX-sgRNA2-For	GGGAGCCGCTGCGCGGTGGC GCGCTG	Forward oligonucleotide used to generate Msm *cnoX*_sgRNA2.
CnoX-sgRNA2-Rev	AAACCAGCGCGCCACCGCGC AGCGGC	Reverse oligonucleotide used to generate Msm *cnoX*_sgRNA2.
CnoX-sgRNA3-For	GGGAGGGGTGATTGGGCTGG GCTT	Forward oligonucleotide used to generate Msm *cnoX*_sgRNA3.
CnoX-sgRNA3-Rev	AAACAAGCCCAGCCCAATCA CCCC	Reverse oligonucleotide used to generate Msm *cnoX*_sgRNA3.
mmpL3-sgRNA1-For	GGGAGCGACAGACTGGCTGC CCTCGTC	Forward oligonucleotide used to generate Msm *mmpL3*_sgRNA
mmpL3-sgRNA1-Rev	AAACTCGGCATACTTCGTTAC CGAC	Reverse oligonucleotide used to generate Msm *mmpl3*_sgRNA.
RT-PCR and real-time qPCR		
Msm-SigA-RTF	TGTGGGACGAGGAAGAGTC	Forward primer used to amplify a 100 bp Msm *sigA (mysA/MSMEG_2758)*-specific amplicon.
Msm-SigA-RTR	CCGATCTGCTTGAGGTAGGC	Reverse primer used to amplify a 100 bp Msm *sigA (mysA/MSMEG_2758)*-specific amplicon.
CnoX-RTF	CTGTTGACCTCTCGGCACTC	Forward primer used to amplify a 90 bp, Msm *cnox*-specific amplicon.
CnoX-RTR	CTTCGGTGACCTCTGTGACG	Reverse primer used to amplify a 90 bp, Msm *cnoX*-specific amplicon.

Primer Name	Primer Sequence	Amplicon properties / Region Targeted
Generation of Recombinant Protein Expression Vectors [b]		
MsCnoX-For	ATA**GGATCC**ACACGTCCGCG TCCGAG	Forward primer used to amplify the Msm *cnoX* gene from pJET1.2. 5' BamHI RE site.
MsCnoX-Rev	ATA**CTGCAG**TTAATACAGTG CATTTGCCAGATTACGAC	Reverse primer used to amplify the Msm *cnoX* gene from pJET1.2. 5' PstI RE site.
MtCnoX-For	ATA**GGATCC**ACCCGTCCGCG TCCG	Forward primer used to amplify the Mtb *cnoX* gene from pJET1.2. 5' BamHI RE site.
MtCnoX-Rev	ATA**CTGCAG**TTAATACAGTG CATTTGCCAGATTACGAC	Reverse primer used to amplify the Mtb *cnoX* gene from pJET1.2. 5' PstI RE site.
EcCnoX-For	ATA**GGATCC**AGCGTGGAAAA CATTGTG	Forward primer used to amplify the *E. coli cnoX* gene from pJET1.2. 5' BamHI RE site.
EcCnoX-Rev	ATA**CTGCAG**TTAATACAGCA GTGCATACAG	Reverse primer used to amplify the *E. coli cnoX* gene from pJET1.2. 5' PstI RE site.
MsTrxC-For	ATA**GGATCC**AGTGAGGACAG CGCGACC	Forward primer used to amplify the Msm *trxC* from the Msm genome. 5' BamHI RE site.
MsTrxC-Rev	ATA**AAGCTT**TCAGAGGGCGT CGGAGAG	Reverse primer used to amplify the Msm *trxC* from the Msm genome. 5' HindIII RE site.
Generation of a Heterologous Complemented *E. coli* Strain		
EcCnoXCheckFor	AGCCGAAGATGCGCTATC	Forward primer for confirming the genotype of the *E. coli cnoX* knockout mutant.
EcCnoXCheckRev	TTCCGACGGTCGATTCAG	Reverse primer for confirming the genotype of the *E. coli cnoX* knockout mutant.

[a] Complementary regions are underlined with a dotted line.
[b] Restriction enzyme sites are bold and underlined.
[c] RBS sites are underlined with a wavy line.
[d] Start sites (ATG) are underlined with a wavy line and italicised.
[e] Sticky end tails compatible with the pLJR962 *BsmBI* cleavage are underlined.

Table 2.4 Expected PCR product sizes when amplifying plasmids and WT or mutant strains with indicated primer pairs.

Primer Pairs	Gene/Allele	Expected PCR Product
Generation and Confirmation of *Msm* KO Mutant		
pKMZeo-For **pKMZeo-Rev**	pMSG360Zeo Zeo^R gene flanked by two loxP sites cassette	740 bp (**Figure 4.6**)
CnoX-US-For **CnoX-US-Rev**	Msm WT *cnoX* US region	474 bp (**Figure 4.6**)
CnoX-DS-For **CnoX-DS-Rev**	Msm WT *cnoX* DS region	408 bp (**Figure 4.6**)
CnoX-US-For **CnoX-DS-Rev**	AES	1 582 bp (**Figure 4.7**)
CnoX-US2-For **CnoX-US2-Rev**	Msm WT *cnoX* Msm Δ*cnoX*::Zeo^R Msm Δ*cnoX*	2 158 bp (**Figure 4.8**, **Figure 4.9**) 2 018 bp (**Figure 4.8**) 1 348 bp (**Figure 4.8**)
CnoX-US2-For **Zeo-Check-Rev**	Msm WT *cnoX* Msm Δ*cnoX*::Zeo^R	Lacks ZeoR cassette binding site. No PCR product is expected. (**Figure 4.8**, **Figure 4.9**) 989 bp (**Figure 4.8**)
Zeo-Check-For **CnoX-DS2-Rev**	Msm WT *cnoX* Msm Δ*cnoX*::Zeo^R	Lacks ZeoR cassette binding site. No PCR product is expected (**Figure 4.8**, **Figure 4.9**) 865 bp (**Figure 4.8**)
CnoX-CompP-XbaI-For **CnoX-Comp-HindIII-Rev**	Msm WT *cnoX* with its natural promoter	1 339 bp (**Figure C4.1**)
CnoX-CompX-SphI-For **CnoX-Comp-HindIII-Rev**	Msm WT *cnoX*	914 bp (**Figure C4.1**)
Generation and Confirmation of KD Mutant using CRISPRi		
pLJR-Seq-For **pLJR-Seq-Rev**	Region of pLJR962 containing insertion site for sgRNAs	450 bp
CnoX-sgRNA1-For **pLJR-Seq-Rev**	Inserted MSMEG_4917 sgRNA 1 and portion of pLJR962	250 bp (**Figure C3.3**)
CnoX-sgRNA2-For **pLJR-Seq-Rev**	Inserted MSMEG_4917 sgRNA 2 and portion of pLJR962	250 bp (**Figure C3.3**)
CnoX-sgRNA3-For **pLJR-Seq-Rev**	Inserted MSMEG_4917 sgRNA 3 and portion of pLJR962	250 bp (**Figure C3.3**)
mmpL3-sgRNA1-For **pLJR-Seq-Rev**	Inserted MSMEG_mmpL3 sgRNA and portion of pLJR962	250 bp (**Figure C3.3**)
Generation of Recombinant Protein Expression Vectors		
MsCnoX-For **MsCnoX-Rev**	pQE-80L::*Msm_cnoX*	906 bp (**Figure C2.1**)
MtCnoX-For **MtCnoX-Rev**	pQE-80L::*Mtb_cnoX*	930 bp (**Figure C2.1**)
EcCnoX-For **EcCnoX-Rev**	pQE-80L::*Ec_cnoX*	870 bp (**Figure C2.1**)
MsTrxC-For **MsTrxC-Rev**	Msm WT *trxC*	329 bp (**Figure C2.1**)
Generation of a Heterologous Complemented *E. coli* Strain		
EcCnoXCheckFor **EcCnoXCheckRev**	*E. coli* BW25113 *E. coli* BW25113 Δ*cnoX*::Kan^R *E. coli* BW25113 Δ*cnoX*	1 311 bp (**Figure E1.1**, **Figure E1.2**) 1764 bp (**Figure E1.1**, **Figure E1.2**) 556 bp (**Figure E1.1**, **Figure E1.2**)

2.7 Agarose Gel Electrophoresis

Agarose gels (0.8 % or 2 % (w/v)) were prepared using TopVision Agarose Tablets (ThermoFisher Scientific, R2801) in 1 × TAE buffer (40 mM Tris, 20 mM acetic acid, 1 mM EDTA, pH 8.0). Ethidium bromide (0.5 µg/mL) was added to the agarose to facilitate the visualisation of DNA. Samples were loaded using 6 × TriTrack Loading Dye (ThermoFisher Scientific). The sizes of DNA fragments were estimated by comparing the migration of DNA fragments to that of DNA fragments contained in the 1 kb GeneRuler Plus DNA Ladder (ThermoFisher Scientific), GeneRuler 50 bp DNA Ladder (ThermoFisher Scientific), or Low Range DNA Ladder (AmplIqon) (**Appendix B, Figure B1.1**). Gels were electrophoresed at 80 to 100 V for 45 to 60 min using a Mini-Sub Cell GT horizontal Electrophoresis Chamber (Bio-Rad) and a Universal PowerPac Power Supply (Bio-Rad). Gels were viewed under UV light using a ChemiDoc XRS+ Imaging System (Bio-Rad) and digital images were acquired using the accompanying software (Image Lab, Bio-Rad).

2.8 Bacterial Transformation

DNA was introduced into *E. coli* through the preparation of chemically competent cells and appropriate transformation, whereas DNA was introduced into Msm through the preparation of electrocompetent cells and electroporation.

2.8.1 Preparation of Chemically Competent Cells

Large-scale preparation of chemically competent *E. coli* cells (>100 mL) was performed using a previously established protocol (Inoue *et al.*, 1990). Cultures were grown at 37 °C for 8 h with shaking at (250 rpm) and diluted 1:100 into 125 mL LB. The cultures were incubated at 18 °C with shaking (250 rpm) until an OD_{600} of ~0.55. Cultures were transferred onto ice for 10 min and centrifuged at 2 500 × g for 10 min at 4 °C (Megafuge 1.0R, Heraeus). The supernatant was discarded and the pellet resuspended in 40 mL ice-cold transformation buffer (55 mM $MnCl_2$, 15 mM $CaCl_2$, 250 mM KCl, 10 mM PIPES (pH 6.7). The cells were centrifuged at 2 500 × g for 10 min at 4 °C and the supernatant was discarded. The cell pellet was resuspended in 10 mL of ice-cold transformation buffer supplemented with 0.75 % (v/v) DMSO and stored on ice for an additional 10 min. The cells were used immediately or aliquoted into smaller volumes and stored at -80 °C for later use.

Small-scale preparation of chemically competent *E. coli* cells (10 to 50 mL) was performed using the Mix 'n Go! *E. coli* Transformation Kit (Zymo Research), according to the recommendations of the manufacturer. In brief, cultures were grown at 37 °C for 16 h with shaking (180 rpm) and diluted 1:100 in 10 mL ZymoBroth. The cultures were incubated with shaking (180 rpm) until OD_{600} of ~0.4 to 0.6. Cultures were transferred to ice for 10 min and centrifuged at 2 500 × g for 10 min at 4 °C (Megafuge 1.0R, Heraeus). The supernatant was discarded and the pellet was resuspended in 1 × ice-cold Wash Buffer. The cells were centrifuged at 2 500 × g for 10 min at 4 °C and the supernatant was discarded. The cell pellet was resuspended in 1 × ice-cold Competent Buffer and used immediately or aliquoted into smaller volumes and stored at -80 °C for later use.

2.8.2 Transformation of Chemically Competent Cells

DNA was introduced into chemically competent cells by adding ligation product (1 to 5 µL) or plasmid DNA (1 to 50 ng) to 50 µL of chemically competent cells in pre-chilled 1.5 mL microcentrifuge tubes. The samples were mixed by aspiration and incubated on ice for 10 min. The cells were transferred to 42 °C for 1 min and 950 µL LB was added. The cells were incubated at 37 °C for 1 h before being centrifuged at 13 400 × g for 1 min. The cell pellets were resuspended in 50 µL LB and streaked onto the appropriate selective medium. Plates were incubated overnight at 37 °C and antibiotic-resistant transformants were selected for further analysis.

The introduction of DNA into chemically competent cells prepared with the Mix 'n Go! *E. coli* Transformation Kit was performed according to the manufacturer's instructions. DNA was introduced into chemically competent cells by adding ligation reactions (1 to 5 µL) or plasmid DNA (1 to 50 ng) to 50 µL of chemically competent cells in pre-chilled 1.5 mL microcentrifuge tubes. The samples were mixed by aspiration and either plated immediately (for selection of bacteria transformed with plasmids conferring resistance to ampicillin) or incubated at 37 °C for 1 h following the addition of 950 µL LB (for selection of bacteria transformed with plasmids conferring resistance to antibiotics other than ampicillin). The cells were centrifuged at 13 400 × g for 1 min, resuspended in 50 µL LB and streaked onto the appropriate selective medium. Plates were incubated overnight at 37 °C and antibiotic-resistant transformants were selected for further analysis.

2.8.3 Preparation of Electrocompetent Msm Cells

Msm electrocompetent cells were prepared as previously described (Goude *et al.*, 2015). Msm was inoculated into 5 mL 7H9 medium and grown at 37 °C until saturated. The culture was diluted 1:100 into 100 mL pre-warmed 7H9 medium and grown at 37 °C until an OD_{600} of ~0.6 was reached. The culture was chilled on ice for 1.5 h and the cells were harvested by centrifugation at 4000 × g for 10 min. The supernatant was discarded and the resulting cell pellet was washed three times with 25 mL ice-cold 10 % (v/v) glycerol. Following the final wash step, the cell pellet was resuspended in 2 mL 10 % (v/v) glycerol, and either stored at -80 °C or used for electroporation immediately.

For the generation of Msm mutants by recombineering, electrocompetent Msm harbouring pJV53 were prepared as previously described (van Kessel and Hatfull, 2007). Msm (pJV53) was inoculated into 5 mL 7H9 medium and grown at 37 °C until saturated. The culture was diluted 1:100 into 100 mL pre-warmed 7H9 medium supplemented with 0.2 % (w/v) succinate, grown to OD_{600} of ~0.6 and acetamide added to a final concentration of 0.2 % (w/v) to induce expression of the pJV53-encoded Che9c 60-61 proteins. The culture was grown at 37 °C for an additional 3 h, harvested, and washed three times with 25 mL ice-cold 10 % (v/v) glycerol. Following the final wash step, the cell pellet was resuspended in 2 mL 10 % (v/v) glycerol and either stored at -80 °C or used for electroporation immediately.

2.8.4 Electroporation of Electrocompetent Msm cells

Plasmid DNA (100 to 800 ng) was combined with 400 µL electrocompetent Msm cells and incubated on ice for 10 min before being transferred to a pre-chilled electroporation cuvette (0.2 cm, ThermoFisher Scientific). The cuvettes were placed in a GenePulser Xcell Electroporator (Bio-Rad) and pulsed using the following parameters: 2.5 kV, 25 µF, 1000 Ω. The cell suspension was mixed with 1 mL pre-warmed 7H9 medium and incubated at 37 °C for 3 to 16 h to allow for the expression of the antibiotic resistance genes. The cells were harvested by centrifugation at 13 400 × g for 1 min, resuspended in 100 µL 7H9 medium and plated on 7H10 or 7H11 medium supplemented with the appropriate antibiotics. The plates were incubated at 37 °C for 3 to 7 days and antibiotic-resistant transformants were selected for further analysis. Cells transformed with plasmids containing temperature-sensitive replicons were incubated at 30 °C to prevent plasmid loss under non-permissive conditions.

2.9 DNA Sequencing and Bioinformatic Analyses

A complete list of the bioinformatics tools, algorithms and software programs used during this study is included in **Table 2.5** below. The DNA inserts of recombinant plasmids were sequenced to verify the absence of mutations introduced during PCR. Sequencing was performed by Inqaba Biotec using Sanger sequencing with the BigDye Terminator v3.1 Cycle Sequencing kit. Chromatograms and DNA sequences were viewed, edited and analysed using SnapGene (GSL Biotech; https://www.snapgene.com). Sequence similarities between nucleotide or protein sequences present in reference databases were identified using the BLASTN and BLASTP search tools available at the National Center for Biotechnology Information (NCBI), respectively. Pairwise alignments between proteins were performed using the BLAST Global Alignment Tool. The domain boundaries and structural organisation of proteins were identified using the NCBI's Conserved Domain Database. Multiple sequence alignments (MSA) were constructed using Clustal Omega or MUSCLE. MSAs were viewed using SnapGene Viewer and secondary structure elements in MSAs were rendered using the ESPript 3.0 algorithm. The physicochemical properties of proteins were predicted using the ProtParam tool. The 3D modelling of the tertiary structures of proteins was performed using the C-I-TASSER server with the structure of the *S. enterica* YbbN protein as a template (3QDN; (unpublished research). The models were visualised and rendered using ChimeraX. Identification of CnoX homologues was performed using the AnnoTree online tool using KEGG K05838 as a search query, and subsequent MSAs were performed as above.

Table 2.5 Bioinformatic software and analysis tools used in this study.

Software	URL	Reference
AnnoTree	http://annotree.uwaterloo.ca/	(Mendler *et al.*, 2019)
BLASTN	https://blast.ncbi.nlm.nih.gov/Blast.cgi	(Altschul *et al.*, 1990)
BLASTP	https://blast.ncbi.nlm.nih.gov/Blast.cgi	(Altschul *et al.*, 1990)
BLAST Global Alignment Tool	https://blast.ncbi.nlm.nih.gov/Blast.cgi	(Needleman and Wunsch, 1970)
ChimeraX	https://www.rbvi.ucsf.edu/chimerax	(Goddard *et al.*, 2018; Pettersen *et al.*, 2021)
C-I-TASSER	https://seq2fun.dcmb.med.umich.edu/C-I-TASSER/	(Zheng *et al.*, 2021)
Clustal Omega	http://www.clustal.org/omega	(Sievers and Higgins, 2018)
Conserved Domain Database	https://www.ncbi.nlm.nih.gov/Structure/cdd/	(Lu *et al.*, 2020; Marchler-Bauer *et al.*, 2007)
ESPript 3	http://espript.ibcp.fr/ESPript/ESPript/	(Robert and Gouet, 2014)
Graphpad Prism 9.0	https://www.graphpad.com/scientific-software/prism/	GraphPad Software
Illustrator for Biological Science	http://ibs.biocuckoo.org	(Liu *et al*., 2015)
ImageJ	https://imagej.nih.gov/	National Institutes of Health
Mega11	https://www.megasoftware.net/	(Tamura *et al.*, 2021)
MUSCLE	https://drive5.com/muscle	(Edgar, 2004)
ProtParam tool	https://web.expasy.org/protparam	(Gasteiger *et al.*, 2005)
SnapGene	https://www.snapgene.com	GSL Biotech
SnapGene Viewer	https://www.snapgene.com	GSL Biotech
Tm Align	https://zhanggroup.org/TM-align/	(Zhang and Skolnick, 2005)
WebLogo	https://weblogo.berkeley.edu/	(Crooks *et al.*, 2004)

2.10 Protein Expression and Purification

2.10.1 Generation of expression constructs

For the recombinant expression of proteins in *E. coli,* the *cnoX* genes from Msm, and Mtb (*MscnoX*, and *MtcnoX*, respectively) (**Appendix A**, **Table A2**) were codon optimised and purchased as synthetic DNA fragments, together with the *E. coli cnoX* gene *(EccnoX)* (ThermoFisher Scientific, Gene Art Strings). The DNA fragments were ligated into pJET1.2 using the CloneJET PCR Cloning Kit (ThermoFisher Scientific) and introduced into *E. coli* Mach1 chemically competent cells. Transformants were selected on LA/Amp medium following overnight incubation at 37 °C and recombinant plasmids were identified by restriction enzyme digestion and DNA sequencing.

For cloning into the pQE-80L expression vector (Qiagen), the *E. coli,* Msm *and* Mtb *cnoX* genes in pJET1.2 (pJET1.2::*EccnoX*, pJET1.2::*MscnoX*, pJET1.2::*MtcnoX,* respectively) were PCR amplified using primer pairs EcCnoX-For/EcCnoX-Rev, MsCnoX-For/MsCnoX-Rev, and MtCnoX-For/MtCnoX-Rev (**Table 2.3**), which contain the recognition sequences for BamHI and PstI at the 5'-ends of the forward and reverse primers, respectively. Following PCR

generating blunt ends, the amplicons were purified and digested with BamHI and ligated into pQE-80L digested with BamHI and SmaI to obtain pQE-80L::*EccnoX*, pQE-80L::*MscnoX*, pQE-80L::*MtcnoX*. The ligations were introduced into *E. coli* TOP10 chemically competent cells, and transformants selected for on LA/Amp plates. Transformants were selected on LA/Amp medium following incubation overnight at 37 °C and recombinant plasmids were identified by restriction enzyme digestion and DNA sequencing.

The coding sequence of the Msm *trxC* gene was PCR amplified from Msm genomic DNA using primer pair MsTrxC-For/MsTrxC-Rev, respectively. Following purification, the amplified products were digested with BamHI and HindIII and ligated into the corresponding sites of pQE-80L to obtain pQE-80L::MsTrxC. The ligations were transformed into *E. coli* TOP10 competent cells, and transformants selected for on LA/Amp plates. Recombinant plasmids harbouring the *trxC* gene were identified by colony PCR of selected Amp^R transformants and confirmed by restriction enzyme digestion and DNA sequencing of plasmids isolated from positive clones.

2.10.2 Recombinant Protein Expression

Expression plasmids for the recombinant expression of either *Ec*CnoX, *Ms*CnoX, *Mt*CnoX, or *Ms*TrxC genes were introduced into chemically competent *E. coli* XJa or XJb (DE3) cells and plated on LA/Amp selective medium. Following overnight incubation at 37 °C, transformants were inoculated into 5 mL LB/Amp and grown at 37 °C for 16 h. The cultures were diluted 1:100 in pre-warmed LB/Amp supplemented with 3 mM L-arabinose and 1 mM $MgCl_2$ to induce the expression of the host-encoded λ endolysin gene. The cultures were incubated at 37 °C until an OD_{600} of ~0.6. and recombinant protein expression induced by the addition of isopropyl-D-1-thiogalactopyranoside (IPTG) to a final concentration of 0.1 mM. The cultures were incubated for an additional 3 h at 37 °C and cells were harvested by centrifugation at 4000 × g for 10 min at 4 °C. The supernatant was discarded and the cell pellet was frozen at -80 °C to facilitate cell lysis following the release of the λ endolysin. The cell pellet was resuspended in a twentieth culture volume Lysis Buffer [Na_2HPO_4 (50 mM), NaCl (300 mM), Imidazole (10 mM, pH 8.0)] supplemented with 0.1 % (v/v) Triton X-100, and 1 × Pierce Protease Inhibitor (ThermoFisher Scientific). The cells were placed in an ice-water bath and lysed by ultrasonic disruption for 15 s with 15 s cooling intervals (4 × 1 min total cycle time) using a VC-50 Vibra Cell Ultrasonic Processor (Sonics & Materials Inc.) set to an amplitude of 50 %. The lysed cells were centrifuged at 20 000 × g for 30 min at 4 °C to separate the supernatant containing soluble proteins (soluble fraction) from the cell pellet containing any

unlysed cells, cell debris, and/or aggregated proteins (insoluble fraction). The expression of recombinant proteins in the soluble and/or insoluble fractions of IPTG-induced and uninduced samples were analysed by SDS-PAGE (**Section 2.10.5**). *E. coli* harbouring the parental pQE-80L vector was included as a negative control in all studies.

2.10.3 Protein Purification

All recombinant proteins were purified by affinity chromatography on 1 mL HisPur Ni-NTA chromatography columns (ThermoFisher Scientific) using an KTA purifier FPLC system (Cytiva). The Ni-NTA columns were pre-equilibrated with 10 column volumes (CV) wash buffer [Na_2HPO_4 (50 mM), NaCl (300 mM), Imidazole (20 mM, pH 8.0)]. Supernatants from whole-cell lysates were loaded onto the columns following clarification through a cellulose acetate syringe filter (0.22 µM) to remove any residual precipitated or insoluble material. The columns were washed with 20 CV wash buffer and the proteins eluted from the column using a linear gradient ranging from 100 % Buffer A [50 mM NaH_2PO_4, 300 mM NaCl, 10 mM imidazole, pH 8.0)] / 0 % Buffer B [50 mM NaH_2PO_4, 300 mM NaCl, 500 mM imidazole, (pH 8.0)] to 70 % Buffer A / 30 % Buffer B over 20 CV. Fractions isolated over this concentration gradient (10 to 150 mM imidazole) were collected in 1 mL volumes using a KTA Fraction collector 900 (Cytiva). Fractions were analysed by SDS-PAGE and those containing recombinant proteins were pooled and dialysed against 1 L dialysis buffer [Na_2HPO_4 (50 mM), NaCl (300 mM), pH 8.0)] using SnakeSkin Dialysis Tubing (10K MWCO, 35 mm; ThermoFisher Scientific) to remove imidazole. The dialysis was performed at 4 °C for 16 h with constant stirring and three buffer changes. The recombinant proteins were concentrated using a Pierce Protein Concentrator, 10 kDa MWCO (ThermoFisher Scientific) as per the manufacturer's instructions. The proteins were aliquoted and snap frozen at −80 °C for further storage. The purity of the recombinant proteins, relative to the clarified lysate and wash and flow-through fractions were determined by SDS-PAGE analysis.

2.10.4 Protein Quantification

The protein concentration of samples was determined using the Pierce Coomassie or BCA Protein Assay Kits (both ThermoFisher Scientific) according to the manufacturer's instructions. Bovine Serum Albumin (BSA) was used to generate a standard curve for the assay. The BSA was diluted in sterile water (0, 25, 125, 250, 500, 750, 1000, 1500 and 2000 µg/mL) and samples combined with Bradford or BCA reagent in triplicate, as per the manufacturer's instructions. Following incubation, the absorbance of each sample was measured at 595 or 562 nm, respectively. The mean absorbance values of the standards were

determined and used to construct a standard curve of the absorbance (OD_{595} or OD_{562}, respectively) vs. concentration (µg/mL). The protein extracts were diluted 10 × before measuring the absorbance values, which were used to determine the extract concentrations by extrapolating from the standard curve. The absorbance of unknown samples was similarly determined and used to interpolate the protein concentrations from the generated standard curve.

2.10.5 SDS–PAGE analysis

Proteins were resolved by denaturing SDS-PAGE performed according to previous methods (Laemmli, 1970) using the Mini Gel Tank System (ThermoFisher Scientific) and 12 % (w/v) resolving and 4 % (w/v) stacking gels. The acrylamide gels were prepared with a 12 % resolving gel [12 % (v/v) acrylamide, 375 mM Tris (pH 8.8), 0.1 % (w/v) ammonium persulphate (APS), 0.1 % (w/v) SDS, 0.01 % (v/v) TEMED] and a 4 % stacking gel [4 % (v/v) acrylamide, 50 mM Tris (pH 6.8), 0.1 % (w/v) ammonium persulphate (APS), 0.1 % (w/v) SDS, 0.01 % (v/v) TEMED] using the SureCast hand casting system as per the manufacturer's instructions. Equivalent amounts of protein samples were mixed with SDS-PAGE Loading Dye [62.5 mM Tris-HCl (pH 6.8), 2 % (w/v) SDS, 25 % (v/v) glycerol, 0.01 % (w/v) bromophenol blue, 5 % (v/v) β-mercaptoethanol]. The samples were heated at 95 °C for 10 min to denature proteins and reduce disulphide bonds. The samples were loaded on the gels and run in 1 × SDS PAGE Running Buffer [25 mM Tris, 192 mM glycine, 0.1 % (w/v) SDS] and electrophoresed at 125 V for 120 min using a PowerPac HC (Bio-Rad). The Pierce Unstained Protein Ladder (ThermoFisher Scientific) or PageRuler Prestained Protein Ladder (ThermoFisher Scientific) (**Appendix B, Figure B1.2**) was used as a molecular weight marker for all experiments. After electrophoresis, the gels were stained with a Coomassie Blue R-250 Staining Solution [0.1 % (w/v) Coomassie Blue R-250, 40 % (v/v) methanol, 10 % (v/v) acetic acid] for 16 h, followed by destaining with Coomassie Blue R-250 Destaining Solution [40 % (v/v) methanol, 10 % (v/v) acetic acid]. The gels were visualised using a ChemiDoc XRS+ Imaging System (Bio-Rad) and digital images acquired using the accompanying software (Image Lab, Bio-Rad).

2.11 Biochemical Assays

2.11.1 Malate Dehydrogenase (MDH) Aggregation Suppression Assay

Protein holdase activity was completed as previously described (Burger *et al.*, 2014; Hartman *et al.*, 1993). The substrate protein, malate dehydrogenase (MDH), was prepared in assay buffer [100 mM NaCl and 50 mM Tris-Cl (pH 7.4)] at a concentration of 0.72 µM and combined with

an equal volume of various concentrations of the recombinant *Ms*CnoX, *Mt*CnoX or *Ec*CnoX proteins (0.72 µM, 0.18 µM, 0.045 µM, 0.0113 µM, and 0.0028 µM), prepared in the same buffer. The reactions were gently mixed before incubation at 48 °C for 90 min. The heat-induced aggregation of the MDH and/or CnoX proteins was monitored by recording the absorbance at 360 nm every 30 min using a Spectramax M3 with the SoftMax® Pro 7.0 Software (Molecular Device, USA). The experiments were carried out in triplicate with three technical replicates each.

2.11.2 Thioredoxin-Catalysed Insulin Reduction by DTT Assays

Protein oxidoreductase was examined as previously described assays (Arnér and Holmgren, 2005; Goemans *et al.*, 2018a; Holmgren, 1979). Briefly, 150 µM insulin (Sigma-Aldrich) and 1.25 µM of either *Ms*CnoX, *Mt*CnoX, *Ec*CnoX and *Ms*TrxC were mixed in 100 mM potassium phosphate buffer (pH 6.5) and 1 mM EDTA. *Ms*TrxC at a final concentration of 1.25 µM, replaced the CnoX proteins and acted as a positive control. DTT at a final concentration of 0.8 mM initiated the reaction. The increase in turbidity was monitored at 650 nm using a SpectraMax M3 with the SoftMax® Pro 7.0 Software (Molecular Device, USA). The experiments were carried out in duplicate with three technical replicates each.

2.12 Generation of mutant strains

2.12.1 Generation of an Msm *cnoX* KD strain

To conditionally silence the expression of the Msm *cnoX* gene, a CRISPRi-based approach was employed (Rock *et al.,* 2017). To facilitate the expression of sgRNA molecules complementary to the *cnoX* gene, we identified dCas9 PAM sequences (5-NNRGVAN-3) on the non-coding strand of the Msm *cnoX* gene. Complementary oligonucleotides with 18-22 bp homology to the DNA sequence on the 5'-end of each PAM sequence were synthesised (Inqaba Biotec). To facilitate cloning into BsmBI-digested pLJR962, GGGA and AAAC sequences were incorporated at the 5'-end of the oligonucleotides corresponding to the coding and non-coding strands of the *cnoX* gene, respectively.

The non-phosphorylated sgRNA primers were diluted in nuclease-free water to 100 µM before use in phosphorylation and annealing reactions. 1 µL of each primer was combined with 6.5 µL nuclease-free water, 1 µL T4 ligase buffer and 0.5 µL polynucleotide kinase (PNK). Phosphorylation reactions were performed at 37 °C for 30 min in a thermocycler. The reaction was incubated at 95 °C for 5 min to inactivate PNK and denature the primers. The phosphorylated primers were then annealed by cooling to 25 °C at a rate of 0.1 °C/min. The

PCR tubes were centrifuged and the oligos diluted 1:200 into nuclease-free water. The efficiency of annealing was monitored by subjecting 5 µL of the diluted double-stranded, annealed oligo alongside an equivalent amount of single-stranded primers on a 2.0 % (w/v) agarose gel.

The annealed oligos were cloned into BsmBI-digested pLJR962 using Golden Gate Cloning, as described by McNeil and Cook (2019). The reactions were performed by combining 2.5 µL annealed sgRNA oligo, 4.25 µL nuclease-free water, 1.25 µL uncut pJR962 (20 ng/µL), 0.5 µL T4 DNA Ligase, 1 µL 10 × T4 Ligase Buffer, and 0.5 µL BsmBI. The reactions were placed in a thermocycler and incubated for 30 cycles of (i) restriction enzyme digestion with BsmBI at 42 °C for 5 min followed by (ii) ligation at 16 °C for 5 min. Any remaining uncut vector was digested by incubation at 55 °C for a further 30 min. The reactions were inactivated at 80 °C for 10 min and 2.5 µL was introduced into *E. coli* Mach1 chemically competent cells. Transformants were selected on LA/Amp plates after 16 h of growth at 37 °C. Plasmids were isolated for each of the CRISPRi constructs and the inserts were amplified with primers pLJR962-Seq-For and pLJR962-Seq-Rev, which anneal to regions on either side of the BsmBI site used for cloning into pLJR962. The amplicons were submitted for Sanger sequencing to confirm the successful cloning of the ~30 bp oligos.

Once confirmed by sequencing, the CRISPRi plasmids (pLJR962::CnoX sgRNA1, pLJR962::CnoX sgRNA2, pLJR962::CnoX sgRNA3, pLJR962::mmpL3 sgRNA) were transformed into electrocompetent Msm cells as described in **Section 2.8.4** and selected on 7H10/Kan plates. Msm cells transformed with the pLJR962 vector lacking an insert, or targeting the essential Msm *mmpL3* gene were included as CRISPRi growth controls. The plates were incubated at 37 °C for 3 days and Kan^R transformants were selected for further genotypic and/or phenotypic analysis.

2.12.2 Generation of an Msm cnoX KO mutant

The allelic exchange substrate (AES) for recombineering was generated by splice-by-overlap extension PCR (SOE-PCR) as previously described (Judd *et al.*, 2021) and shown in **Figure 2.1**. DNA fragments of 474 and 408 bp upstream (US) and downstream (DS), respectively, of the Msm *cnoX* (MSMEG_4917) gene were amplified by preparative PCR (**Section 2.6.1**) using cnoX-US-For/cnoX-US-Rev, and cnoX-DS-For/cnoX-DS-Rev as primer pairs, respectively. The 740 bp loxP-flanked Zeocin-resistance cassette was amplified from plasmid pMSG350Zeo (Barkan *et al.*, 2010) using primers pKMZeo-For and pKMZeo-Rev, which were designed to

contain 22-bp regions of complementarity to the 5'-ends of the cnoX-US-Rev and cnoX-DS-For primers, respectively. Following the first round of PCR amplification, the PCR reactions were treated with 1 µL DpnI and incubated at 37 °C for 1 h to remove any methylated template DNA. The amplicons from the first round of PCR were purified, mixed in equimolar amounts (10 pM) and 5 µL used as a template in the PCR reactions with the cnox-US-For and cnoX-DS-Rev as the forward and reverse primers. The 1582 bp, full-length AES was gel purified following AGE and electroporated into electrocompetent Msm::pJV53 cells.

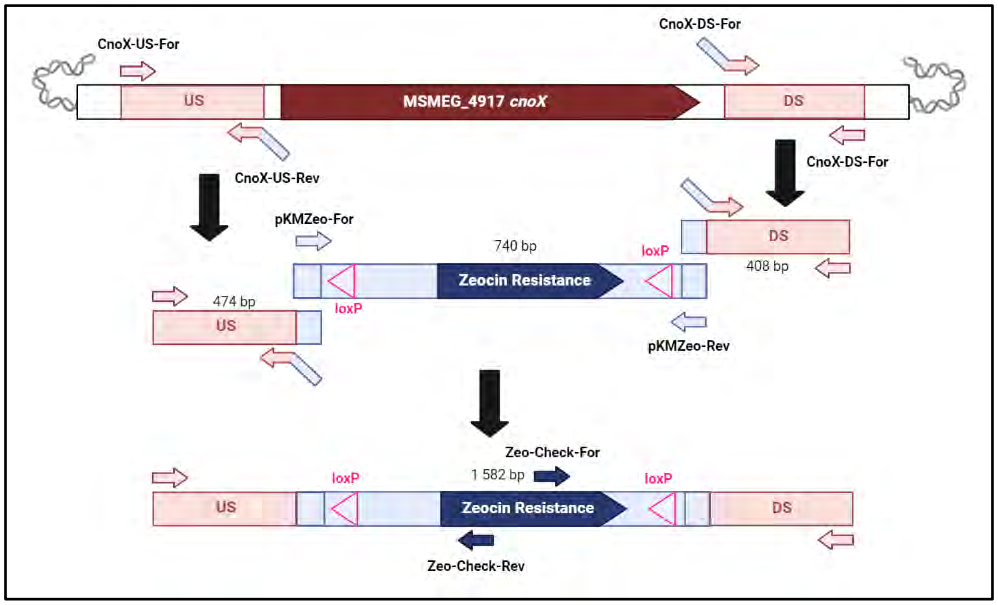

Figure 2.1 Schematic for the generation of the MSMEG _4917 allelic exchange substrate. DNA regions of 474 bp and 408 bp upstream (US) or downstream (DS) of the *cnoX* gene were PCR amplified (pink shading) using primer pairs cnoX-US-For/cnoX-US-Rev and cnoX-DS-For/cnoX-DS-Rev, respectively. The 740 bp loxP-flanked Zeocin-resistance cassette from pMSG360Zeo (light and dark blue shading) was amplified using primers pKMZeo-For and pKMZeo-Rev. The three amplicons were purified, combined and amplified using cnoX-US-For and cnoX-DS-Rev to generate an allelic exchange substrate (AES) of 1582 bp. All primers used are indicated as arrows. The sizes of the fragments are indicated.

2.12.3 Generation of Complementation Vectors for Genetic Complementation

Plasmids for the genetic complementation of the *cnoX* mutant were constructed by PCR amplification of coding sequences of the Msm *cnoX* gene, either with or without its native promoter. The coding sequence of *cnoX* without its native promoter was amplified using the CnoX-CompX-SphI-For and CnoX-Comp-HindIII-Rev primers, which were designed to contain the recognition sites for SphI and HindIII to facilitate subsequent cloning, respectively. Following amplification, the PCR products were restricted with SphI and HindIII and ligated into the 3 kb pGiles::P_{smyc} vector (Kolbe *et al.*, 2020) that had been restricted with the

corresponding enzymes. This places the expression of the *cnoX* gene under the control of the vector-provided P_{smyc} promoter and *tttrpA+* terminator (Ehrt *et al.*, 2005; Huff *et al.*, 2010). The amplification of the coding sequence of the *cnoX* gene together with its native promoter was performed using CnoX-CompX-XbaI-For and CnoX-Comp-HindIII-Rev primers, which were designed to contain the recognition sites for XbaI and HindIII, respectively. Following amplification, the PCR product was purified, restricted with XbaI and HindIII and ligated into the 2.7 kb fragment of pGiles::P_{smyc} (Kolbe *et al.*, 2020) which was gel-purified after restriction with the same enzymes to remove the ~0.3 kb constitutive smyc promoter. The ligation reactions were introduced into *E. coli* TOP10 chemically competent cells and transformants selected on LA/Hyg medium. Selected hygromycin-resistant transformants were analysed by colony PCR with gene-specific primers, as well as plasmid purification and restriction enzyme digestion to verify the successful construction of recombinant plasmids. The PCR amplified regions of recombinant plasmids were verified via Sanger sequencing as described in **Section 2.9**. The confirmed constructs for genetic complementation were co-electroporated with pUC19 Giles Integrase (Kolbe *et al.*, 2020) into the *cnoX* mutant for subsequent phenotypic analysis *in vitro.*

Chapter 3: Identification and Characterisation of the *Msm* and *Mtb* CnoX proteins

3.1 Identification of the Mycobacterial Orthologs of the CnoX proteins

To identify orthologs of the *Ec*CnoX protein in representative fast and slow-growing mycobacterial species, a BLASTP sequence similarity search was performed against the completed genomes of Msm and Mtb, respectively. Using this approach, the MSMEG_4917- and MSMEG_6934-encoded proteins were identified as the only ORFs in the genome of Msm with sequence similarity to the *Ec*CnoX (BLASTP E-values = $1E^{-20}$ and $2E^{-13}$, respectively). The Rv1324- and Rv3914-encoded proteins were likewise identified as the only orthologs of *Ec*CnoX in the genome of Mtb (BLASTP E-values = $1E^{-17}$ and $2E^{-13}$, respectively). The MSMEG_6934 and Rv3914-encoded proteins have been functionally characterised as the TrxC enzymes of Msm and Mtb, respectively, and were not studied further (Akif *et al.*, 2008; Danelishvili *et al.*, 2017). The MSMEG_4917 and Rv1324 ORFs, by contrast, are predicted to encode 296 and 304 amino acid proteins with 26 % (38 %) and 22 % (37 %) identity (similarity) to the *Ec*CnoX, respectively. Evaluation of the domain architecture of the MSMEG_4917 and Rv1324 gene products using the Conserved Domain Database showed that they belong to a cluster of orthologous groups of proteins, COG3118, the sole COG within the YbbN superfamily (Cl34555). The YbbN (CnoX) superfamily of proteins contains an N-terminal Trx domain linked to a C-terminal domain comprised of several TPR motifs (**Figure 3.1**). The predicted Trx domain is present within the N-terminal halves of the Msm (**Figure 3.1 B**; amino acids 39-143) and Mtb (**Figure 3.1 C**, amino acids 45-149) CnoX orthologs. Both proteins are predicted to contain three TPR motifs in their C-terminal half, in contrast with the four TPR motifs predicted in the *Ec*CnoX protein (**Figure 3.1 A, B, C**). The Trx domains of the mycobacterial proteins are preceded by an N-terminal extension (NTE) of 38 and 44 amino acids, respectively, which is absent from the *Ec*CnoX (**Figure 3.1 A, B, C**). Bioinformatic analysis suggests that the NTEs of both mycobacterial proteins are intrinsically disordered. The functional significance of the NTE, which is absent from all CnoX enzymes biochemically characterised to date, is not known. Based on their sequence similarity to the *Ec*CnoX and classification within the YbbN superfamily, we will refer to the CnoX orthologs encoded MSMEG_4917 and Rv1324 as *Ms*CnoX and *Mt*CnoX for the remainder of this study, respectively.

As discussed in **Section 1.5,** the CnoX family of proteins can be divided into four groups (Groups A-D) based on the presence or absence of three conserved Cys residues in the Trx domain of the protein**.** An alignment of the amino acid sequence of the *Ms*CnoX and *Mt*CnoX proteins with that of the characterised CnoX enzymes of *E. coli (Ec*CnoX; Group C), *C. crescentus* (*Cc*CnoX; Group B), *P. aeruginosa* (*Pa*CnoX; Group B) and *X. fastidiosa* (*Xf*CnoX; Group A) revealed that the mycobacterial CnoX proteins lack the $C_{35}XXC_{38}$ catalytic motif (*Ec*CnoX numbering) required for the thiol-disulphide oxidoreductase activity of certain CnoX members (**Figure 3.2**). Instead, the *Ms*CnoX and *Mt*CnoX have an $S_{35}XXS_{38}$ and $S_{35}XXC_{38}$ motif in the corresponding position of their polypeptides, respectively. The mycobacterial CnoX proteins similarly lack the C_{63} residue previously shown to be required for the formation of mixed disulphides by the *Ec*CnoX. As such, *Ms*CnoX and *Mt*CnoX possess an $S_{35}XXS_{38}[N24]X_{63}$ and an $S_{35}XXC_{38}[N24]X_{63}$ motif, respectively, which is characteristic of the Group D CnoX proteins (**Figures 3.1 and 3.2**).

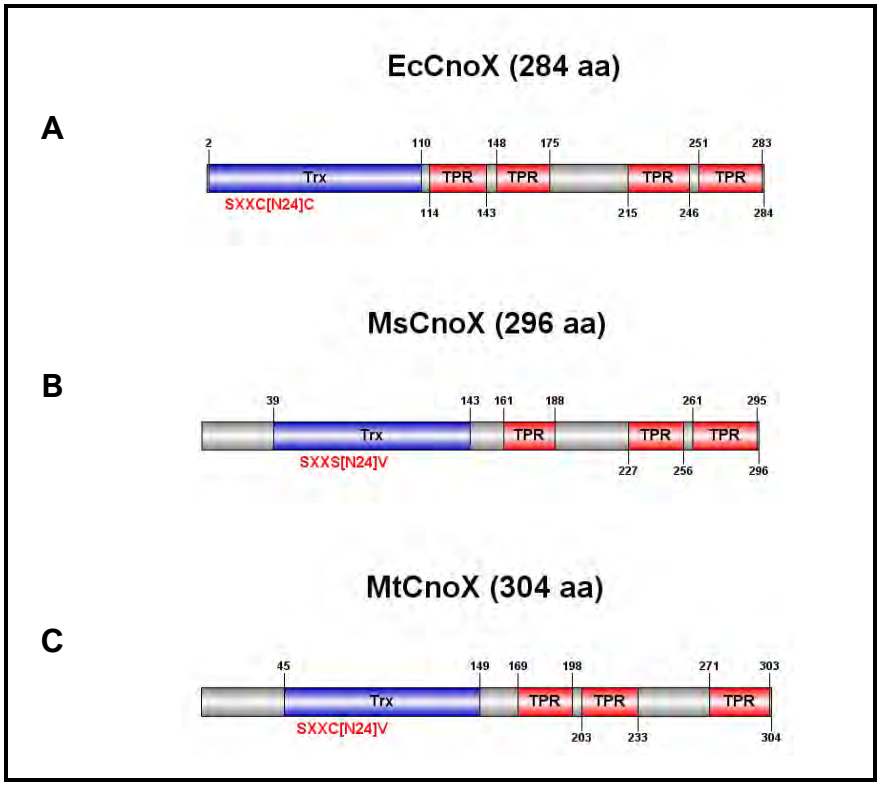

Figure 3.1 Schematic representation of the domain architecture of the (A) *Ec*CnoX, (B) *Ms*CnoX and (C) *Mt*CnoX. The proteins consist of two domains: (i) an N-terminal Trx domain (blue boxes) and (ii) a C-terminal domain comprised of several TPR motifs (red boxes). The *Ms*CnoX and *Mt*CnoX contain an extended N-terminal region (amino acids 1-38 and 1-44 respectively) unlike the *Ec*CnoX. The locations of the domains or motifs are indicated by the numbering above and below each sequence. The specific sequence of the **S/C$_{35}$XXS/C$_{38}$[N$_{24}$]X$_{63}$** motif present in the Trx domain of CnoX is indicated. Images were generated using Illustrator for Biological Sequences (IBS).

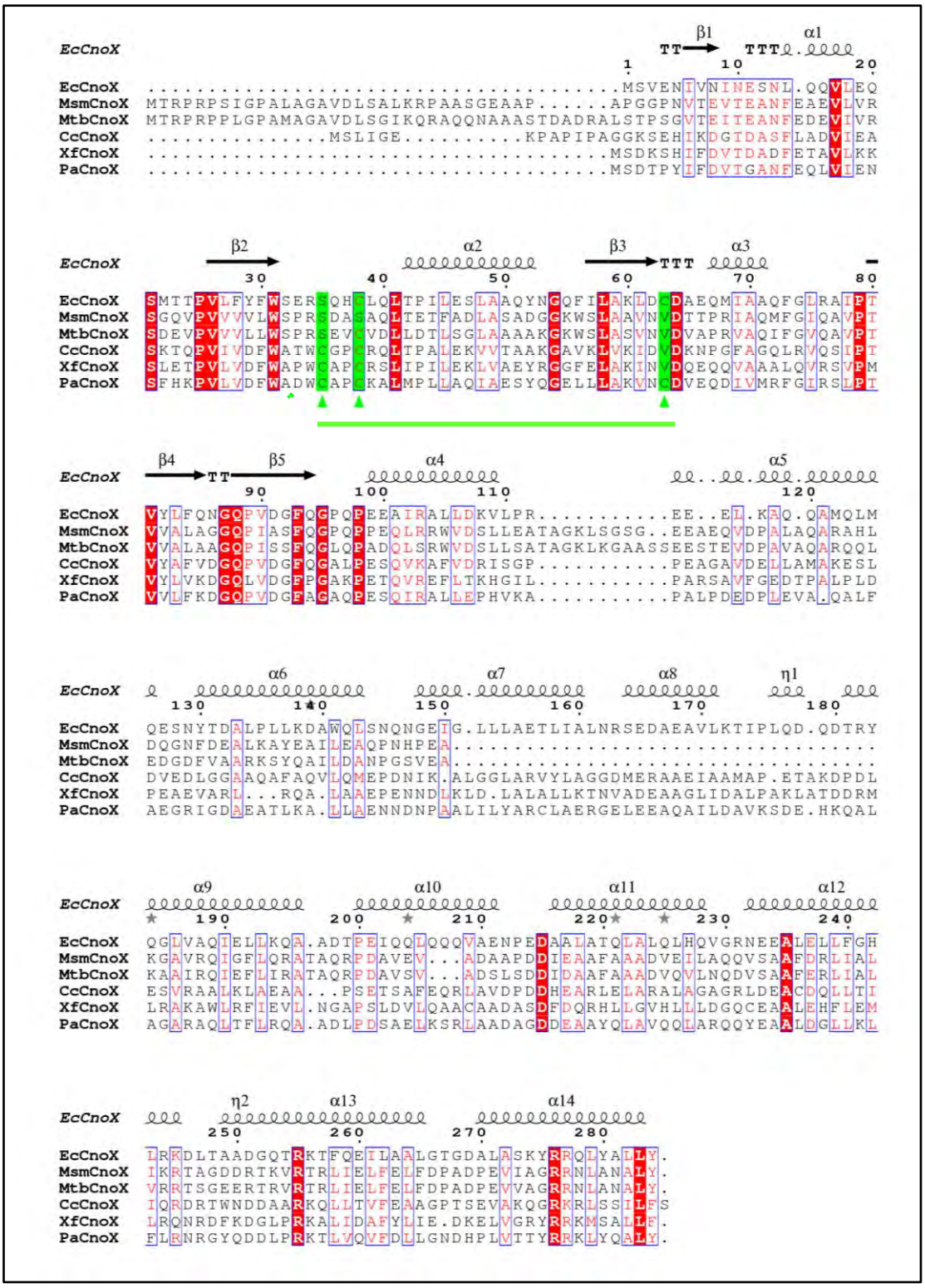

Figure 3.2 Amino acid sequence alignment of the CnoX proteins from *Ec*CnoX, *Ms*CnoX, *Mt*CnoX, *Cc*CnoX, *Xf*CnoX, and *Pa*CnoX. The amino acid numbering is based on the sequence of the *Ec*CnoX protein (1 - 284). The location of the secondary structure elements (α-helices and β-sheets) in the *Ec*CnoX protein is shown above the alignment. Identical and similar amino acids are boxed using white and red typeface, respectively. The sequence and position of the semi-conserved residues in the Trx domain's $S/C_{35}XXS/C_{38}[N24]X_{63}$ motif are highlighted and underlined in green.

To confirm the presence of the Trx and TPR domains in the mycobacterial CnoX proteins, we used the C-I-TASSER and TM-align online tools to model the tertiary structure of Msm and Mtb CnoX proteins based on their similarity to proteins contained in the Protein Data Bank (PDB) (Zhang and Skolnick, 2005; Zheng *et al.*, 2021). Using this approach, the Msm and Mtb proteins were shown to possess the greatest structural similarity to the *Salmonella enterica* serovar Typhimurium CnoX (*St*CnoX; PDB 3QDN), which possesses 95 % (98 %) identity (similarity) to the *Ec*CnoX from its close phylogenetic relative, *E. coli.* The *Ms*CnoX and *Mt*CnoX were subsequently modelled using the *St*Cnox protein as a template (**Figure 3.3, A**). Overall, 83 and 86 % of the amino acid residues in *Ms*CnoX and *Mt*CnoX could be structurally aligned to those in the *St*Cnox, with a root-mean-square deviation (RMSD) value of 0.98 and 0.91 Å, respectively. The TM-score (Zhang and Skolnick, 2005), a measure of the topological similarity of two protein structures, was calculated as 0.81 and 0.84 for the *St*CnoX and predicted *Ms*CnoX and *Mt*CnoX proteins, respectively. TM-scores are assigned values ranging from 0 to 1, with values greater than 0.5 indicating the presence of the same fold or domains in two protein structures, and a score of 1 indicating a perfect match (Xu and Zhang, 2010).

Based on their modelled structures, the mycobacterial CnoX proteins are predicted to contain an N-terminal domain with a thioredoxin-fold, comprised of a four-stranded antiparallel β-sheet (β2, β3, β4, β5) surrounded by three α-helices (α2, α3, α4) (**Figure 3.3 C and D**) (Holmgren *et al.*, 1975; Martin, 1995; Martin *et al.*, 1993). The active site $S_{35}XXS_{38}/C_{38}$ motif is located at the N-terminus of the first α-helix (α2) of the thioredoxin fold of each CnoX protein (**Figure 3.3 A-D**). The Trx domain of the *St*CnoX differs from that of the mycobacterial proteins, however, in that it contains an additional β-sheet (β1) at its N-terminus (**Figure 3.3; A**), which is replaced by the disordered NTE in the mycobacterial proteins. The C-terminal, TPR-motif containing the domain of the *Ec*CnoX and *St*CnoX proteins possess two similar sub-domains (TPR A and TPR B; **Figure 3.3 A**) each comprised of five α-helices (α5, α6, α7, α8, α9 and α10, α11, α12, α13, α14, respectively) (Lin and Wilson, 2011). The structures of the Mtb and Msm proteins are predicted to contain both TPR A and B subdomains. While the mycobacterial proteins contain each of the 5 α-helices in the TPR B sub-domain, they lack two of the five α-helices (α7 and α8) present in the TPR A subdomain present in the enterobacterial CnoX proteins. The topology of the remaining three α-helices (α 5, 6 and 9) in the TPR A sub-domain are, furthermore, predicted to differ between the *Ms*CnoX and *Mt*CnoX proteins (**Figure 3.3; C and D**). The significance of these differences, if any, is currently not known but may reflect unique functional adaptations of each of the mycobacterial CnoX proteins. The

last ten C-terminal amino acids of all putative CnoX proteins are highly conserved (YRRQLYALLY), which allows binding to GroEL (Dupuy *et al.*, 2022). In the mycobacterial CnoX proteins, this region was also highly conserved (GRRNLANALY) (**Figure 3.5 B**). The overall similarity between the predicted mycobacterial and enterobacterial CnoX proteins, nevertheless, indicates that both the Trx and TPR domains are structurally conserved in the proteins and that they may consequently fulfil similar biological roles.

Figure 3.3 (Overleaf) The predicted tertiary structures of the Msm and Mtb CnoX enzymes. The Msm and Mtb CnoX proteins tertiary structures were modelled using C-I-TASSER with the **(A)** *St*CnoX (PDB ID: 3QDN) as a template. **(B)** The *Ec*CnoX (PDB ID: 3QOU)(B) is displayed for reference. The predicted tertiary structures of the **(C)** *Ms*CnoX and **(D)** and *Mt*CnoX are shown. The CnoX thioredoxin-like domain (blue) is comprised of 4 to 5 β-strands (dark blue) while the TPR domain (red) is comprised of the TPR A and TPR B subdomains. The α-helices (α1-14) and β-strands (β1-5) are numbered according to those present in the *Ec*CnoX and the N- and C-termini are indicated. The mycobacterial CnoX proteins **(C and D)** possess a disordered N-terminal extension (purple) that replaces the β1-strand present in the *St*CNoX and *Ec*CnoX proteins. The **S/C$_{35}$XXS/C$_{38}$**[N$_{24}$]**V/C$_{63}$** residues are coloured and indicated according to the *Ec*CnoX numbering: Cysteines (lime green), serines (yellow), and valines (cyan). **(E and H)** The *St*CnoX (coral) was superimposed with either the **(F)** *Ms*CnoX (blue) or **(I)** *Mt*CnoX (red) to produce the superimpositions shown in **(G)** and **(J)**. For clarity, the NTE present in the mycobacterial CnoX proteins has been hidden in **F-J.**

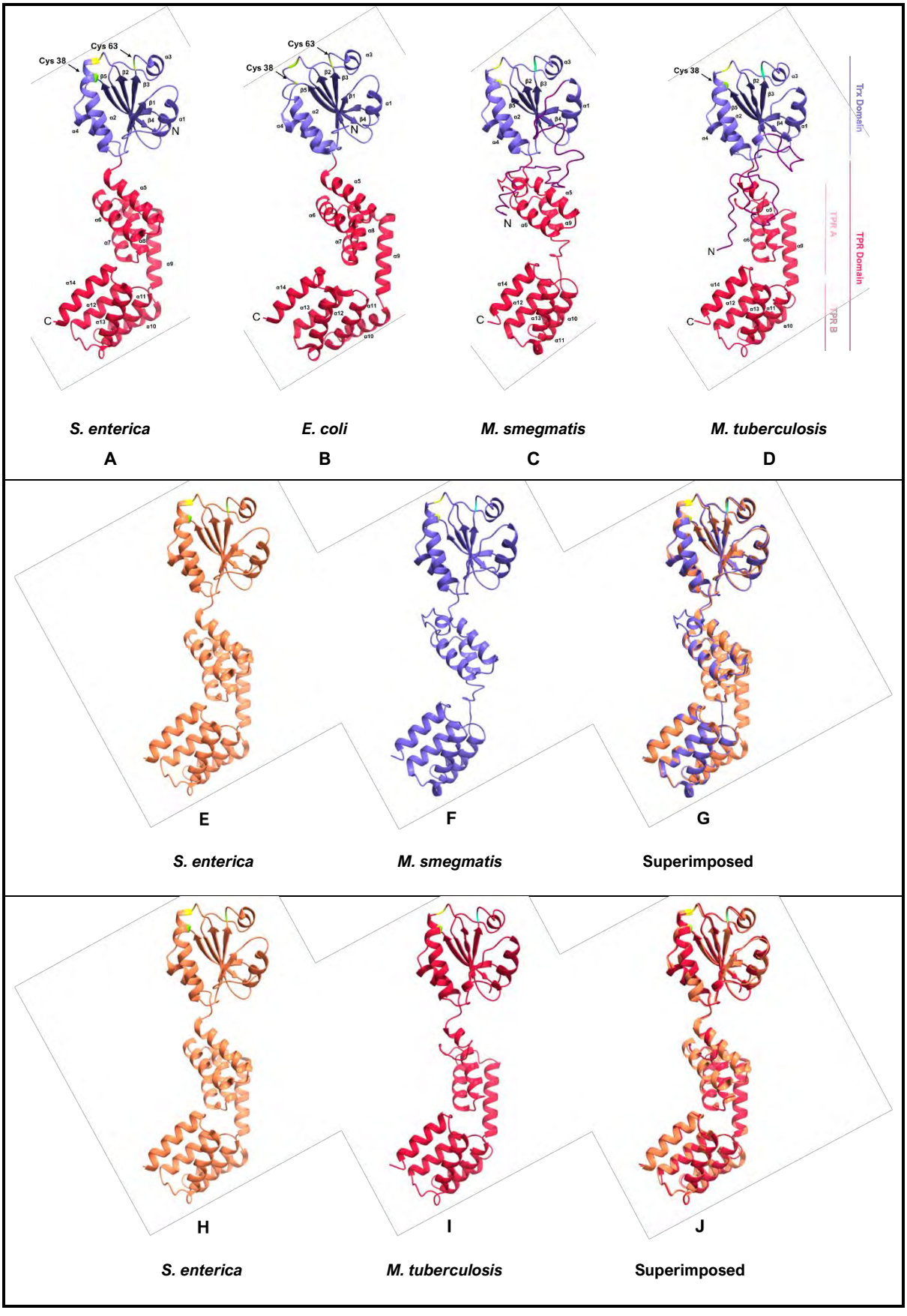
Cys 63
Cys 38
N
C
Trx Domain
TPR Domain
TPR A
TPR B
S. enterica
A
E. coli
B
M. smegmatis
C
M. tuberculosis
D
E
S. enterica
F
M. smegmatis
G
Superimposed
H
S. enterica
I
M. tuberculosis
J
Superimposed

Having identified CnoX homologs in Mtb and Msm, we were interested in examining the distribution of CnoX amongst other mycobacterial species. For this, we initially used the online phylogenetic tool, Annotree, which contains uniform protein-function annotations of bacterial and archaeal genomes derived from the Genome Taxonomy DataBase (GTDB) (Mendler *et al.*, 2019). Of the 30,238 representative bacterial genomes in GTDB, CnoX orthologs (KEGG Orthology Identifier KO5838) were identified in 11109 species (36.7 %), distributed across 45 phyla. No CnoX representatives were identified in the remaining 63.3 % of bacterial species or in 1672 archaeal species genomes present in GTDB (**Figure 3.4 and data not shown**). The vast majority (94.6 %) of the bacterial CnoX homologs were contained within two bacterial phyla, the Proteobacteria (61.99 %) and Actinobacteria (32.65 %).

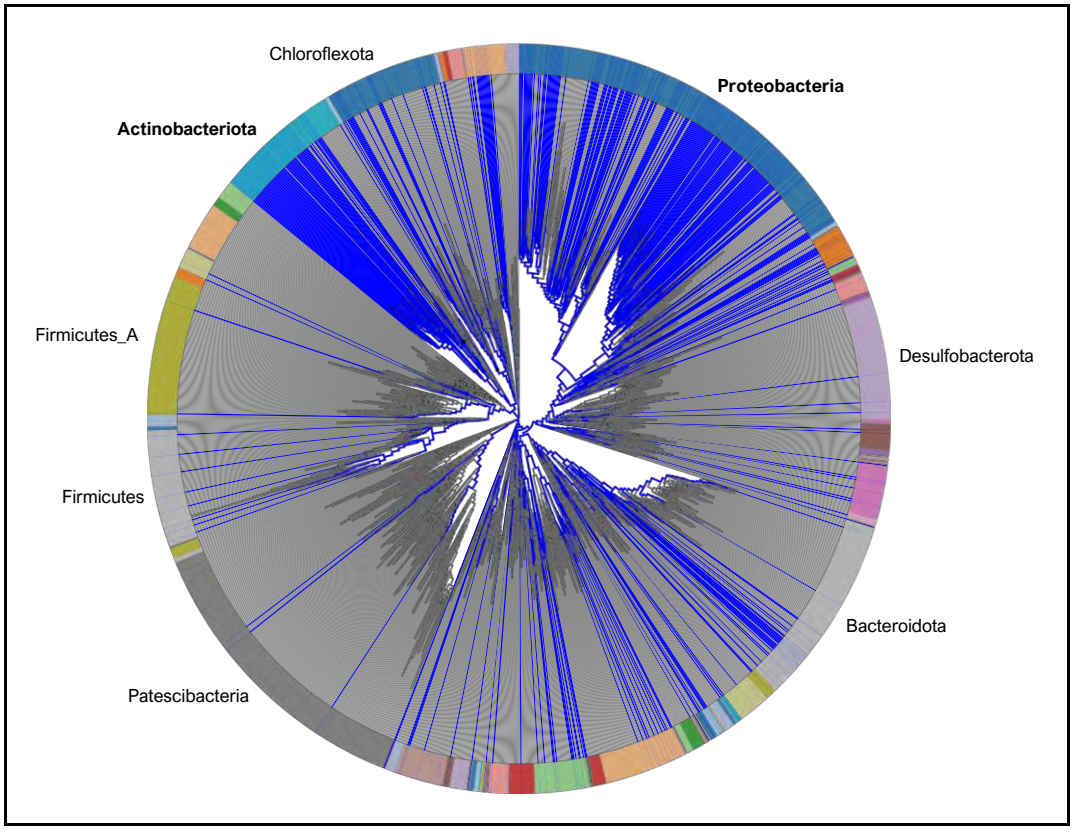

Figure 3.4 Distribution of CnoX orthologs amongst bacterial phyla. CnoX orthologs were identified using the Annotree phylogenetic tool and the KEGG orthology (KO) identifiers for CnoX (YbbN; K05838). Blue lines represent species that contain a CnoX homolog (≥ 30 % amino acid identity between query and KEGG ortholog group subject, ≥ 70 % subject alignment, ≥ 70 % query alignment, E value ≤ 0.00001) within each phylum. The name of the phylum to which the indicated species belongs is listed along the perimeter of the tree. Grey lines represent the absence of CnoX orthologs in the indicated phyla.

While the *Proteobacterial* phylum collectively accounted for the largest number of CnoX homologs present in the GTDB, the *Mycobacteriaceae* contained 5.9 % of all such sequences at the family level, ranking behind only the *Rhodobacteraceae* and *Burkholderiaceae* proteobacterial families (**Table 3.1**). The *Enterobacteriaceae*, by comparison, accounted for only 4.5 % of all CnoX sequences, which includes the *Ec*CnoX and *St*CnoX. The distribution and biological roles of CnoX from diverse proteobacterial species have been described in several previous studies (Dupuy and Collet, 2021; Goemans and Collet, 2019; Lin and Wilson, 2011). The conservation of CnoX amongst a broad range of actinobacterial species, however, suggests that the protein has retained an important biological role in this group of microorganisms as well.

Table 3.1 Distribution of CnoX orthologs amongst bacterial families. The percentage of CnoX orthologs in each family was calculated relative to the total number of CnoX orthologs identified in unique, representative species genomes contained in the GTDB**.** The thirty families with the greatest number of CnoX orthologs amongst its constituent species are shown. The phylum and class to which each family belongs are indicated.

	Family	Phylum	Class	% Total
1	*Rhodobacteraceae*	*Proteobacteria*	*Alphaproteobacteria*	6.4
2	*Burkholderiaceae*	*Proteobacteria*	*Betaproteobacteria*	6.2
3	*Mycobacteriaceae*	*Actinobacteria*	*Actinomycetes*	5.9
4	*Streptomycetaceae*	*Actinobacteria*	*Actinomycetes*	5.6
5	*Pseudomonadaceae*	*Proteobacteria*	*Gammaproteobacteria*	5.3
6	*Rhizobiaceae*	*Proteobacteria*	*Alphaproteobacteria*	4.9
7	*Enterobacteriaceae*	*Proteobacteria*	*Gammaproteobacteria*	4.5
8	*Sphingomonadaceae*	*Proteobacteria*	*Alphaproteobacteria*	4.4
9	*Microbacteriaceae*	*Proteobacteria*	*Actinomycetes*	4.2
10	*Alteromonadaceae*	*Proteobacteria*	*Gammaproteobacteria*	2.4
11	*Micrococcaceae*	*Proteobacteria*	*Actinomycetes*	2.2
12	*Xanthomonadaceae*	*Proteobacteria*	*Gammaproteobacteria*	2.0
13	*Vibrionaceae*	*Proteobacteria*	*Gammaproteobacteria*	2.0
14	*Xanthobacteraceae*	*Proteobacteria*	*Xanthobacteraceae*	1.8
15	*Pseudonocardiaceae*	*Actinobacteria*	*Actinomycetes*	1.7
16	*Beijerinckiaceae*	*Proteobacteria*	*Beijerinckiaceae*	1.5
17	*Micromonosporaceae*	*Proteobacteria*	*Alphaproteobacteria*	1.4
18	*Streptosporangiaceae*	*Actinobacteria*	*Actinomycetes*	1.3
19	*Halomonadaceae*	*Proteobacteria*	*Gammaproteobacteria*	1.3
20	*Acetobacteraceae*	*Proteobacteria*	*Alphaproteobacteria*	1.2
21	*Caulobacteraceae*	*Proteobacteria*	*Alphaproteobacteria*	1.2
22	*Actinomycetaceae*	*Actinobacteria*	*Actinomycetes*	1.1
23	*Nocardioidaceae*	*Actinobacteria*	*Actinomycetes*	1.0
24	*Pasteurellaceae*	*Proteobacteria*	*Gammaproteobacteria*	1.0
25	*Bifidobacteriaceae*	*Proteobacteria*	*Actinomycetes*	1.0
26	*Dermatophilaceae*	*Actinobacteria*	*Actinomycetes*	0.8
27	*Rhodanobacteraceae*	*Proteobacteria*	*Gammaproteobacteria*	0.8
28	*Cellulomonadaceae*	*Actinobacteria*	*Actinomycetes*	0.8
29	*Oleiphilaceae*	*Proteobacteria*	*Gammaproteobacteria*	0.7
30	*Shewanellaceae*	*Proteobacteria*	*Gammaproteobacteria*	0.7

We next compared the amino acid sequence of the CnoX orthologs identified in Mycobacteria with that of the *Mt*CnoX. Alignment of the amino acid sequence of 14 representative mycobacterial species, revealed a high level of conservation amongst these proteins (**Figure 3.5; See Appendix F for complete list**). All of the mycobacterial orthologs possess the bipartite CnoX structure described above, with Trx and TPR domains present at the N- and C-termini, respectively. Similar to Msm and Mtb, the CnoX orthologs identified in other mycobacterial species all contained an NTE of ~40 to 50 amino acid residues, relative to the proteobacterial CnoX enzymes (**Figure 3.5 A and Appendix F**). Some variation in the length of the NTE that was observed may be attributable to the close proximity of several potential in-frame start codons (ATG or GTG), however, resulting in differences in the N-termini predicted for the coding sequences used in the alignment. The C-terminal α-helix of CnoX proteins has recently been shown to be required for CnoXs interaction with the GroEL chaperonin (Dupuy *et al.,* 2022). The last ten amino acids of the *Ec*CnoX is essential for this interaction and several residues within this sequence is highly conserved amongst previously identified CnoX family members (**Figure 3.5 B**; YRRQLYALLY). Comparison of the corresponding region of the mycobacterial CnoX proteins revealed that the sequence GRRNLANALY is highly conserved amongst mycobacterial species (**Figure 3.5 B**).

Similar to the CnoX proteins from Mtb and Msm, the remaining mycobacterial orthologs all lack a $C_{35}XXC_{38}$ catalytic motif in the active site of the Trx domain, possessing instead the $S_{35}XXS_{38}$, $S_{35}XXC_{38}$, or in two cases, a $S_{35}XXA_{38}$ motif that typifies Category D CnoX proteins (see **Appendix F**). A phylogenetic analysis of the distribution of these CnoX orthologues showed that the slow-growing, pathogenic mycobacterial species were predominantly associated with the $S_{35}XXC_{38}$ motif, whereas the fast-growing species possessed the $S_{35}XXS_{38}$ motif (**Figure 3.5 A and 3.6**).

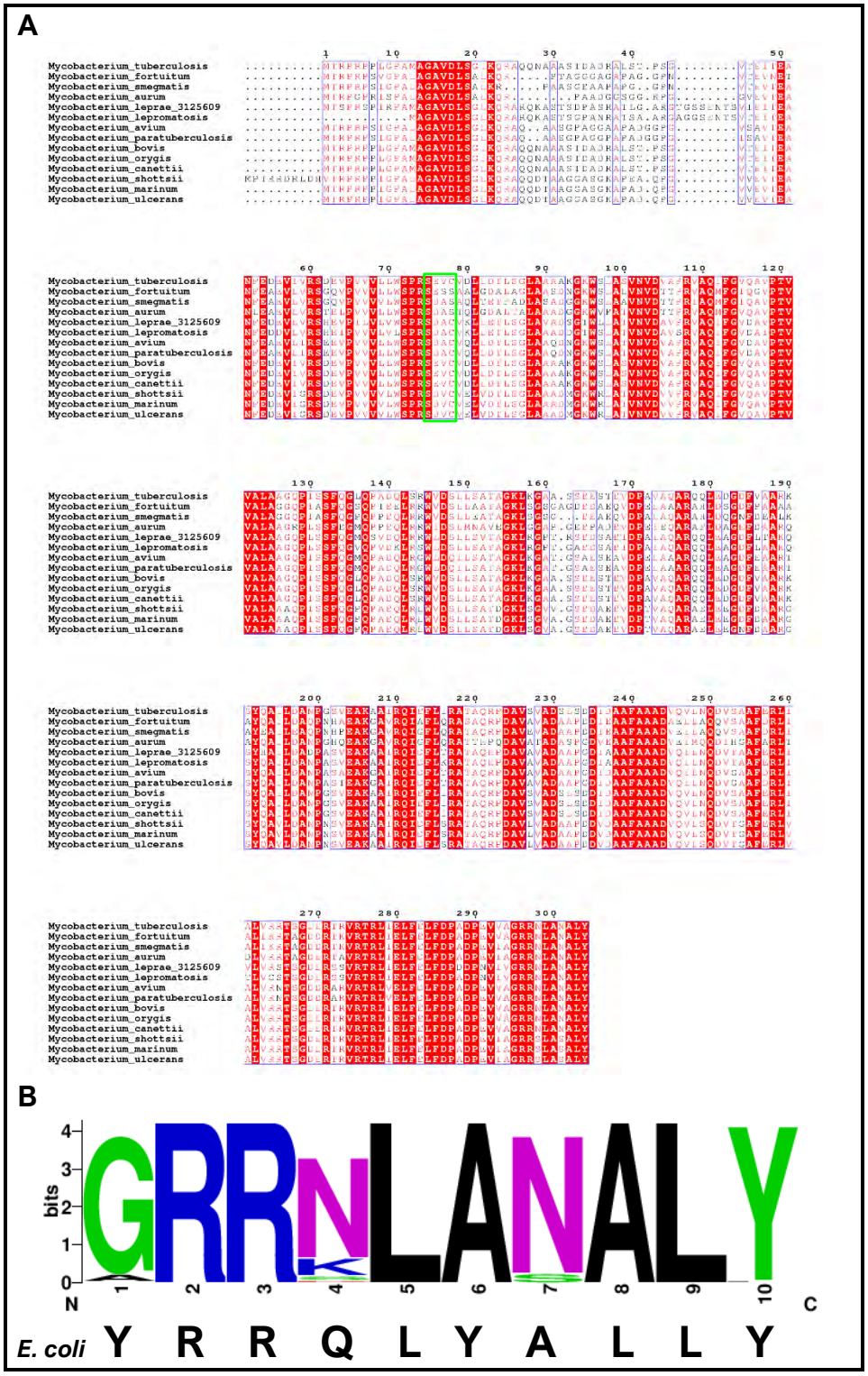

Figure 3.5 A) Amino acid sequence alignment of mycobacterial CnoX orthologs from representative species and B) Amino acid logo of the conservation of the mycobacterial C-terminal amino acids. A) The amino acid numbering is based on the sequence of the *Mtb*CnoX protein (1 - 304). Identical and similar amino acids are boxed using white and red typeface, respectively. The position of the **S/C$_{35}$XXS/C$_{38}$** motifs are indicated in the green box. B) The logo conservation of the C-terminal amino acids of mycobacterial CnoX proteins with the reference *E. coli* C-terminal sequence below generated using WebLogo.

Figure 3.6 (Overleaf). Phylogenetic tree showing the conservation of CnoX orthologs in the genus *Mycobacterium*. Mycobacterial *cnoX* ortholog sequences were obtained from UniProt using the *Mt*CnoX as a query and aligned using MUSCLE. Phylogenetic reconstruction was created using Maximum Likelihood statistical analysis with 1000 Bootstrap replicates and the Dayhoff model with Freqs. with Gamma Distributed With Invariant Sites and a site coverage cut-off of 95 %. The scale bar indicates estimated sequence divergence. The circles indicate fast-growing (blue), intermediate-growing (yellow), slow-growing (orange), pathogenic (red), opportunistic pathogens (pink), non-pathogenic (green) species. The right-hand bar indicates the Trx motif: SXXS (blue bar), SXXC (green bar), or SXXA (pink bar). The Mtb Complex is indicated by an asterisk.

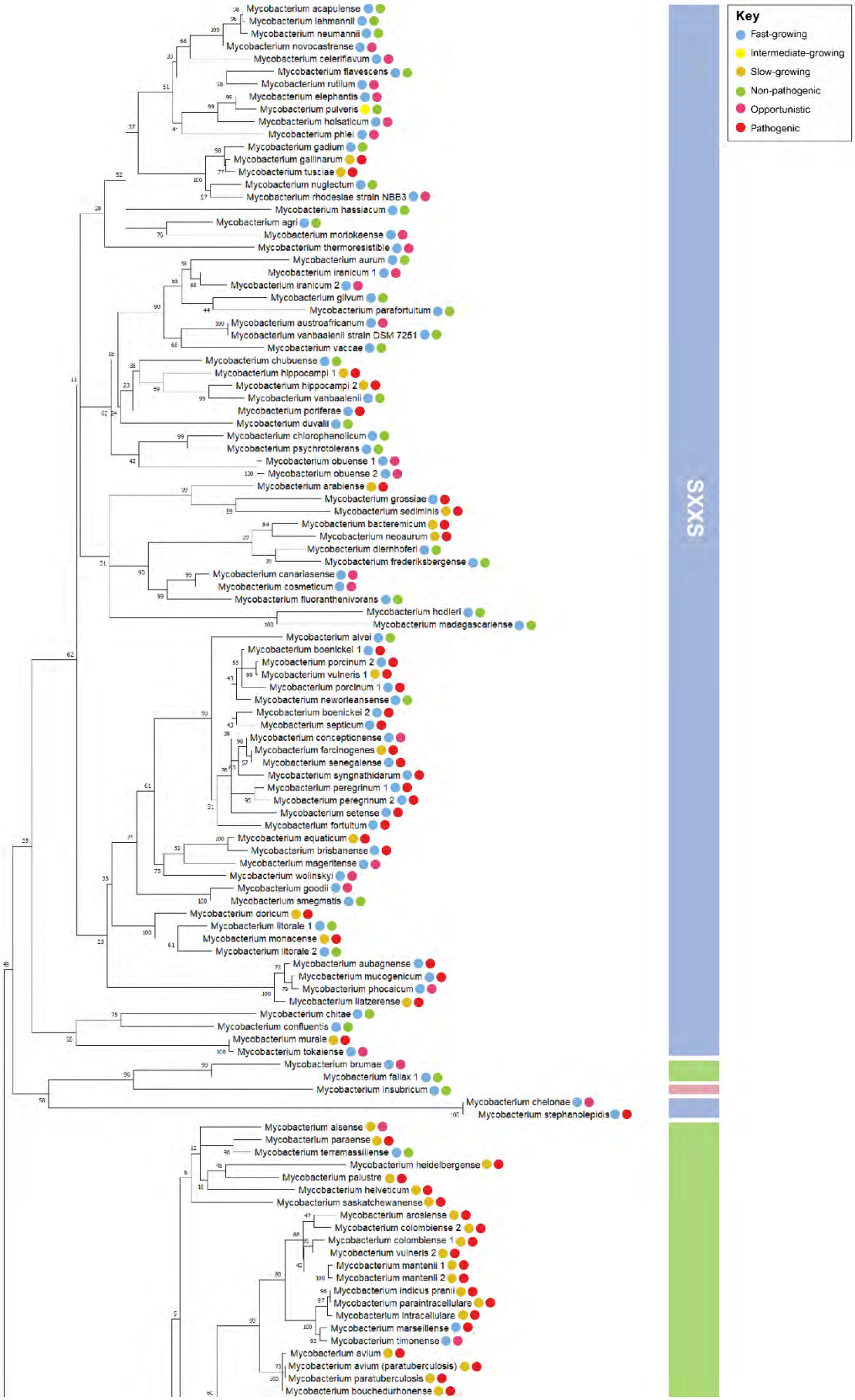
Key
Fast-growing
Intermediate-growing
Slow-growing
Non-pathogenic
Opportunistic
Pathogenic
SXXS
Mycobacterium acapulense
Mycobacterium lehmannii
Mycobacterium neumannii
Mycobacterium novocastrense
Mycobacterium celeriflavum
Mycobacterium flavescens
Mycobacterium rutilum
Mycobacterium elephantis
Mycobacterium pulveris
Mycobacterium holsaticum
Mycobacterium phlei
Mycobacterium gadium
Mycobacterium gallinarum
Mycobacterium tusciae
Mycobacterium nuglectum
Mycobacterium rhodesiae strain NBB3
Mycobacterium hassiacum
Mycobacterium agri
Mycobacterium moriokaense
Mycobacterium thermoresistibile
Mycobacterium aurum
Mycobacterium iranicum 1
Mycobacterium iranicum 2
Mycobacterium gilvum
Mycobacterium parafortuitum
Mycobacterium austroafricanum
Mycobacterium vanbaalenii strain DSM 7251
Mycobacterium vaccae
Mycobacterium chubuense
Mycobacterium hippocampi 1
Mycobacterium hippocampi 2
Mycobacterium vanbaalenii
Mycobacterium poriferae
Mycobacterium duvalii
Mycobacterium chlorophenolicum
Mycobacterium psychrotolerans
Mycobacterium obuense 1
Mycobacterium obuense 2
Mycobacterium arabiense
Mycobacterium grossiae
Mycobacterium sediminis
Mycobacterium bacteremicum
Mycobacterium neoaurum
Mycobacterium diernhoferi
Mycobacterium frederiksbergense
Mycobacterium canariasense
Mycobacterium cosmeticum
Mycobacterium fluoranthenivorans
Mycobacterium hodleri
Mycobacterium madagascariense
Mycobacterium alvei
Mycobacterium boenickei 1
Mycobacterium porcinum 2
Mycobacterium vulneris 1
Mycobacterium porcinum 1
Mycobacterium neworleansense
Mycobacterium boenickei 2
Mycobacterium septicum
Mycobacterium conceptionense
Mycobacterium farcinogenes
Mycobacterium senegalense
Mycobacterium syngnathidarum
Mycobacterium peregrinum 1
Mycobacterium peregrinum 2
Mycobacterium setense
Mycobacterium fortuitum
Mycobacterium aquaticum
Mycobacterium brisbanense
Mycobacterium mageritense
Mycobacterium wolinskyi
Mycobacterium goodii
Mycobacterium smegmatis
Mycobacterium doricum
Mycobacterium litorale 1
Mycobacterium monacense
Mycobacterium litorale 2
Mycobacterium aubagnense
Mycobacterium mucogenicum
Mycobacterium phocaicum
Mycobacterium llatzerense
Mycobacterium chitae
Mycobacterium confluentis
Mycobacterium murale
Mycobacterium tokaiense
Mycobacterium brumae
Mycobacterium fallax 1
Mycobacterium insubricum
Mycobacterium chelonae
Mycobacterium stephanolepidis
Mycobacterium alsense
Mycobacterium paraense
Mycobacterium terramassiliense
Mycobacterium heidelbergense
Mycobacterium palustre
Mycobacterium helveticum
Mycobacterium saskatchewanense
Mycobacterium arosiense
Mycobacterium colombiense 2
Mycobacterium colombiense 1
Mycobacterium vulneris 2
Mycobacterium mantenii 1
Mycobacterium mantenii 2
Mycobacterium indicus pranii
Mycobacterium paraintracellulare
Mycobacterium intracellulare
Mycobacterium marseillense
Mycobacterium timonense
Mycobacterium avium
Mycobacterium avium (paratuberculosis)
Mycobacterium paratuberculosis
Mycobacterium bouchedurhonense

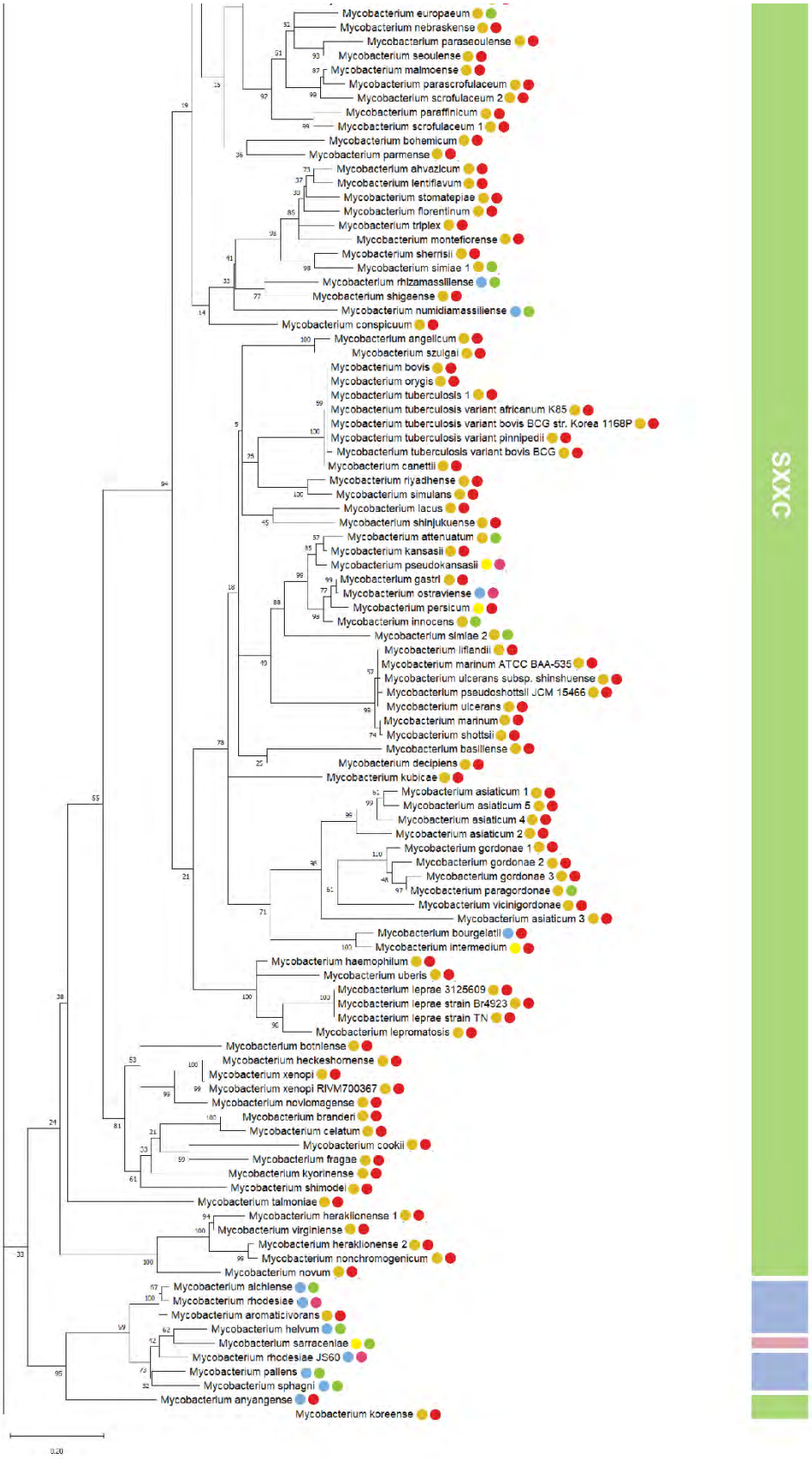
Mycobacterium europaeum
Mycobacterium nebraskense
Mycobacterium parascrofulaceum
Mycobacterium seoulense
Mycobacterium malmoense
Mycobacterium parascrofulaceum
Mycobacterium scrofulaceum 2
Mycobacterium paraffinicum
Mycobacterium scrofulaceum 1
Mycobacterium bohemicum
Mycobacterium parmense
Mycobacterium ahvazicum
Mycobacterium lentiflavum
Mycobacterium stomatepiae
Mycobacterium florentinum
Mycobacterium triplex
Mycobacterium monteficrense
Mycobacterium sherrisii
Mycobacterium simiae 1
Mycobacterium rhizamassiliense
Mycobacterium shigaense
Mycobacterium numidiamassiliense
Mycobacterium conspicuum
Mycobacterium angelicum
Mycobacterium szulgai
Mycobacterium bovis
Mycobacterium orygis
Mycobacterium tuberculosis 1
Mycobacterium tuberculosis variant africanum K85
Mycobacterium tuberculosis variant bovis BCG str. Korea 1168P
Mycobacterium tuberculosis variant pinnipedii
Mycobacterium tuberculosis variant bovis BCG
Mycobacterium canettii
Mycobacterium riyadhense
Mycobacterium simulans
Mycobacterium lacus
Mycobacterium shinjukuense
Mycobacterium attenuatum
Mycobacterium kansasii
Mycobacterium pseudokansasii
Mycobacterium gastri
Mycobacterium ostraviense
Mycobacterium persicum
Mycobacterium innocens
Mycobacterium simiae 2
Mycobacterium lirandii
Mycobacterium marinum ATCC BAA-535
Mycobacterium ulcerans subsp. shinshuense
Mycobacterium pseudoshottsii JCM 15466
Mycobacterium ulcerans
Mycobacterium marinum
Mycobacterium shottsii
Mycobacterium basiliense
Mycobacterium decipiens
Mycobacterium kubicae
Mycobacterium asiaticum 1
Mycobacterium asiaticum 5
Mycobacterium asiaticum 4
Mycobacterium asiaticum 2
Mycobacterium gordonae 1
Mycobacterium gordonae 2
Mycobacterium gordonae 3
Mycobacterium paragordonae
Mycobacterium vicinigordonae
Mycobacterium asiaticum 3
Mycobacterium bourgelatii
Mycobacterium intermedium
Mycobacterium haemophilum
Mycobacterium uberis
Mycobacterium leprae 3125609
Mycobacterium leprae strain Br4923
Mycobacterium leprae strain TN
Mycobacterium lepromatosis
Mycobacterium botniense
Mycobacterium heckeshornense
Mycobacterium xenopi
Mycobacterium xenopi RIVM700367
Mycobacterium novilmagense
Mycobacterium branderi
Mycobacterium celatum
Mycobacterium cookii
Mycobacterium fragae
Mycobacterium kyorinense
Mycobacterium shimodei
Mycobacterium talmoniae
Mycobacterium heraklionense 1
Mycobacterium virginiense
Mycobacterium heraklionense 2
Mycobacterium nonchromogenicum
Mycobacterium novum
Mycobacterium alcihlense
Mycobacterium rhodesiae
Mycobacterium aromaticivorans
Mycobacterium helvum
Mycobacterium sarraceniae
Mycobacterium rhodesiae JS60
Mycobacterium pallens
Mycobacterium sphagni
Mycobacterium anyangense
Mycobacterium koreense
0.20
SXXG

3.2 Cloning, Expression, and Purification of Recombinant Proteins

3.2.1 Construction of expression vectors for production of recombinant proteins

To investigate the biochemical properties of the mycobacterial CnoX homologs, the coding sequences of *Ms*CnoX and *Mt*CnoX were PCR amplified and ligated into pQE-80L for expression in *E. coli* as N-terminal His-tagged proteins. Following confirmation of the successful generation of the recombinant plasmids by restriction endonuclease digestion and DNA sequencing (**Appendix C1 and C2**), the plasmids designated as pQE-80L::*Ms*CnoX, and pQE-80L::*Mt*CnoX respectively, were introduced into *E. coli* XJb for recombinant protein expression, as described below (**Section 3.2.2**). For use as control proteins that possess either holdase and disulphide oxidoreductase activities, the coding sequences of the *Ec*CnoX and *Msm* TrxC (*Ms*TrxC) enzymes were cloned into pQE-80L in an identical manner yielding pQE-80L::*Ec*CnoX and pQE-80L::*Ms*TrxC, respectively. The control proteins were subsequently purified and analysed in parallel with the two mycobacterial CnoX enzymes.

3.2.2 Expression analysis of recombinant proteins in *E. coli*

To establish whether the recombinant CnoX and TrxC enzymes were expressed in soluble form following induction from the IPTG-inducible promoter on pQE-80L, protein supernatants were isolated from cells grown in either the presence (+ IPTG) or absence (- IPTG) of inducer and subjected to SDS-PAGE analysis followed by Coomassie brilliant blue staining. As shown in **Figure 3.7,** no difference in the protein expression profile of control *E. coli* cells harbouring the parental pQE-80L vector was observed when cells were grown in either the absence or presence of the IPTG (**Figure 3.7; Lanes 10 and 11**, respectively). The protein supernatants prepared from *E. coli* harbouring pQE-80L::*Ms*CnoX (**Figure 3.7; Lanes 2 and 3**), pQE-80L::*Mt*CnoX (**Figure 3.7; Lanes 4 and 5**), pQE-80L::*Ec*CnoX (**Figure 3.7; Lanes 6 and 7**) and pQE-80L::*Ms*TrxC (**Figure 3.7; Lanes 8 and 9**), by contrast, contained recombinant proteins with measured molecular weights of ~38 kDa, ~40 kDa, ~32 kDa, and ~15 kDa, respectively, when cells were grown in the presence (**Lanes 3, 5, 7 and 9**) but not the absence of IPTG (**Lanes 2, 4, 6 and 8**).

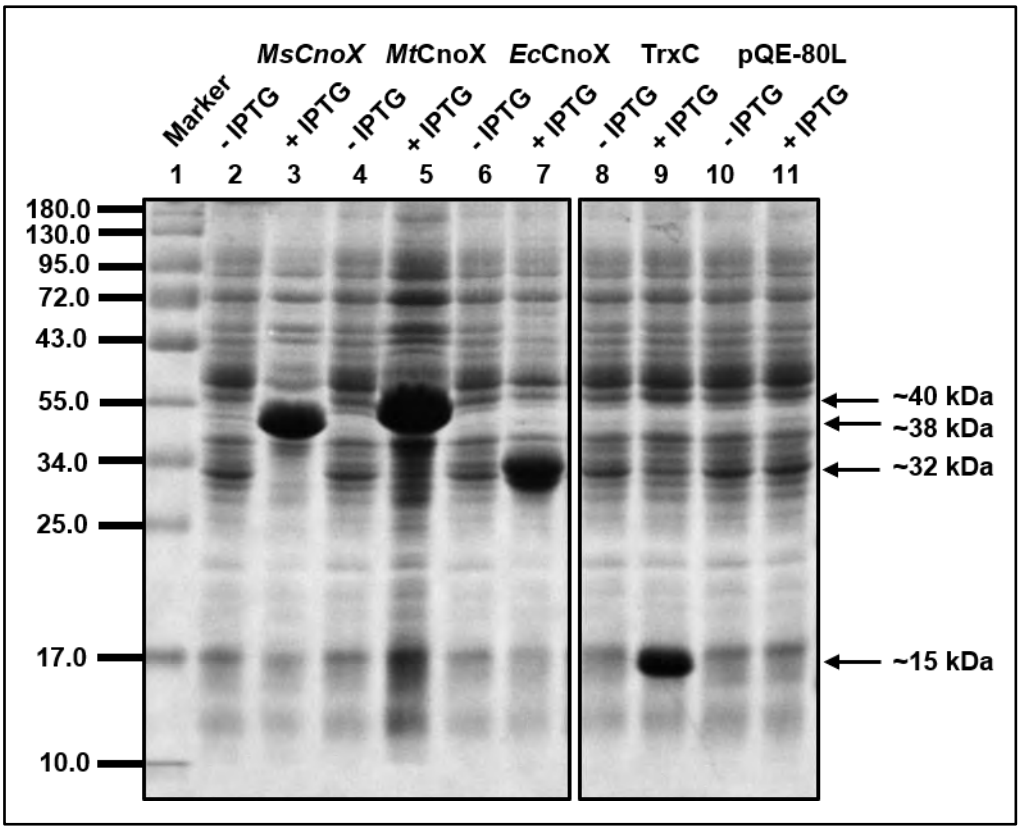

Figure 3.7 SDS-PAGE analysis of the soluble fraction containing the expressed *Ms*CnoX, *Mt*CnoX, *Ec*CnoX, and *Ms*TrxC recombinant proteins. *E. coli* XJb cells were transformed with the pQE-80L encoding the *Ms*CnoX, *Mt*CnoX, *Ec*CnoX, *Ms*TrxC. *E. coli* XJb transformed with the parental pQE-80L vector was included as a negative control. **Lane 1**: Molecular Weight Marker; **Lane 2:** uninduced pQE-80L::*Ms*CnoX culture; **Lane 3:** induced pQE-80L::*Ms*CnoX culture; **Lane 4:** uninduced pQE-80L::*Mt*CnoX culture; **Lane 5:** induced pQE-80L::*Mt*CnoX culture; **Lane 6:** uninduced pQE-80L::*Ec*CnoX culture; **Lane 7:** induced pQE-80L::*Ec*CnoX culture; **Lane 8:** uninduced pQE-80L::*Ms*TrxC culture; **Lane 9:** induced pQE-80L::*Ms*TrxC culture; **Lane 10:** uninduced pQE-80L vector only culture; **Lane 11:** induced pQE-80L vector only culture. Black arrows indicate the molecular weights of each of recombinant protein.

While the His-tagged *Ec*CnoX and *Ms*TrxC proteins migrated with molecular weights that were in close agreement with those calculated from their deduced primary sequence (i.e. 33.2 kDa and 13.9, respectively), the recombinant *Ms*CnoX and *Mt*CnoX proteins both displayed molecular weights greater than that predicted by their amino acid sequences, inclusive of the His-tag (i.e. 32.5 and 33.5 kDa respectively). The reason(s) for this discrepancy is currently not clear, although it may potentially be attributable to the presence of the disordered NTE in the mycobacterial CnoX proteins (see **Section 3.1** above) and/or the predicted non-globular, extended nature of the CnoX proteins, which has been shown to contribute to the anomalous migration of these proteins during SDS-PAGE (Lin and Wilson, 2011; Receveur-Bréchot *et al.*, 2005). The observation that the recombinant CnoX and TrxC proteins were predominantly

present in the soluble supernatant fraction of cell lysates (**Figure 3.7**; see **Figure D1.1** for corresponding insoluble fraction), nevertheless, suggested that they may be amenable to purification by immobilised metal affinity chromatography (IMAC), described in the following section.

3.2.3 Purification of the recombinant production of enzymes

The *Ms*CnoX, *Mt*CnoX, *Ec*CnoX and *Ms*TrxC recombinant proteins were purified by IMAC using Ni-NTA cartridges on an ÄKTA FPLC system. Bacterial supernatants containing the recombinant His-tagged proteins were prepared as described in **Section 2.10** before being applied to Ni-NTA columns. The non-specific binding of the His-tagged proteins to the columns was minimised by the inclusion of imidazole in the equilibration and lysis buffers and unbound proteins were removed by extensive washing of the columns with wash buffer. The His-tagged proteins were eluted with a linear gradient of imidazole that was subsequently removed by dialysis. The successful expression and purification of each recombinant protein was evaluated by SDS-PAGE analysis of the supernatants from both uninduced and induced cultures, together with the flow-through, wash and pooled eluted fractions (**Figure 3.8 A - D**). As observed in **Section 3.2.2**, the *Ms*CnoX, *Mt*CnoX, *Ec*CnoX and *Ms*TrxC proteins were all expressed in soluble form following their induction with IPTG during growth at 37 °C for 3 h (**Figure 3.8 A - D,** "Uninduced" vs "Induced Soluble" and "Induced Insoluble"). Following their separation from other cellular proteins on the Ni-NTA columns (**Figure 3.8 A - D**, "Flowthrough" and "Wash"), the recombinant proteins were purified to near homogeneity (≥ 90 % purity) as assessed by SDS-PAGE. While the MsCnoX displayed the highest purity level (~98.5 %) following IMAC, the *Mt*CnoX, *Ec*CnoX and *Ms*TrxC proteins co-eluted with several contaminant bands (92.1 %, 90 %, 90 % final purity, respectively). While multiple attempts were made to optimise the purification condition, the number of contaminants present in the protein preparations could not be removed by IMAC purification alone (data not shown).

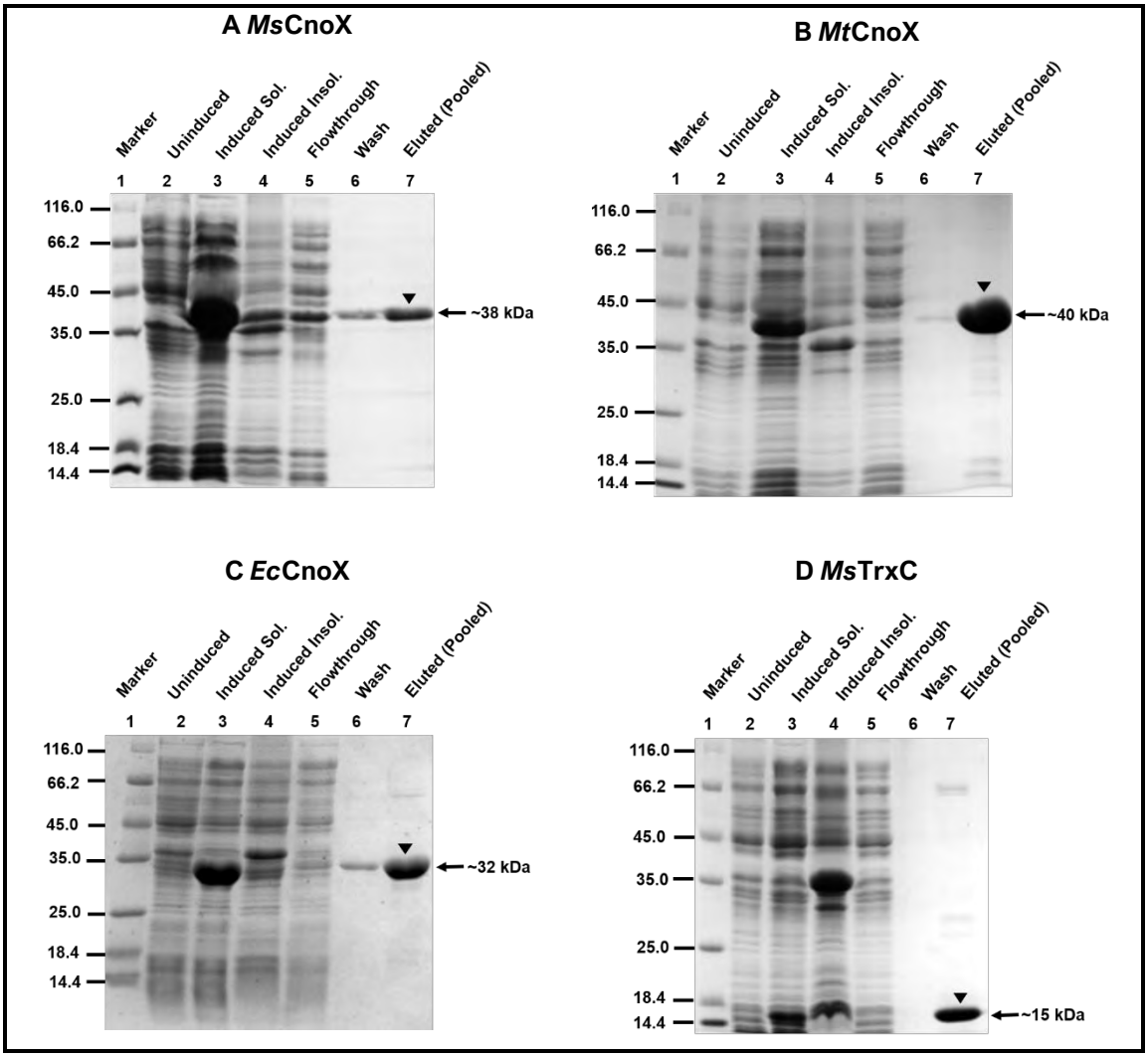

Figure 3.8 SDS-PAGE analysis of the purity of the recombinant (A) *Ms*CnoX, (B) *Mt*CnoX, (C) *Ec*CnoX, and (D) *Ms*TrxC. The recombinant proteins were expressed in *E. coli* and purified from supernatants by IMAC. Protein samples were subjected to SDS-PAGE analysis followed by staining with Coomassie Brilliant blue. **Lane 1:** Molecular Weight Marker; **Lane 2:** Supernatant (soluble) from the bacterial culture before protein induction; **Lane 3:** Supernatant (soluble) from bacterial culture following induction with IPTG for 3 h at 37 °C; **Lane 4**: Insoluble, pellet fraction from bacterial culture following induction of expression with IPTG for 3 h at 37 °C; **Lane 5**: Flow-through fraction; **Lane 6:** Wash fraction; **Lane 7:** Eluted fraction containing pooled recombinant protein following dialysis. The sizes of the molecular weight markers are indicated on the left in kDa. The arrow indicates the position of the His-tagged protein.

3.3 Biochemical Characterisation of the Mycobacterial CnoX enzymes

3.3.1 MDH Suppression of Aggregation Assays

The CnoX enzymes from several bacterial species, including the *Ec*Cnox, have recently been shown to possess either constitutive or inducible holdase activity (Goemans *et al.*, 2018a, 2018b; Meireles *et al.*, 2020). To examine whether the *Ms*CnoX and *Mt*CnoX proteins are capable of functioning in a similar capacity, we analysed their ability to inhibit the aggregation of the model substrate protein, malate dehydrogenase (MDH) (Bentley and Boshoff, 2019; Burger *et al.*, 2014; Hartman *et al.*, 1993). MDH is thermolabile and susceptible to heat-induced unfolding and aggregation following exposure to elevated temperatures (e.g. 45 to 48 °C). In the presence of proteins with holdase activity, MDH aggregation can be suppressed, which can be measured spectrophotometrically by monitoring the degree of light scattering caused by protein aggregation at 360 nm. The stability of the recombinant CnoX proteins under the assay conditions was first examined. Following exposure to thermal stress (i.e. 48 °C), the MDH substrate protein displayed significant aggregation after 90 min, which was allocated an arbitrary reference value of 100 % aggregation. The *Ms*CnoX, *Mt*CnoX, and *Ec*CnoX proteins displayed greater thermal stability under identical conditions, with aggregation levels ~60 % lower than that observed for MDH (**Figure 3.9**, aggregation levels of 39 %, 37.6 %, and 38.3 %, respectively).

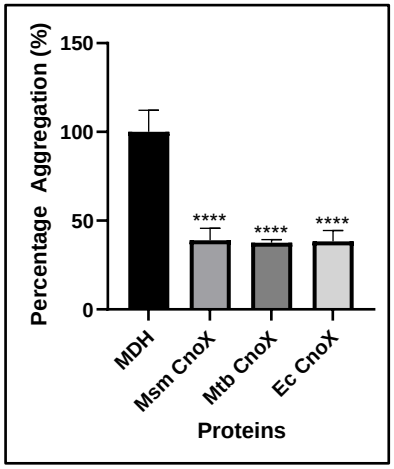

Figure 3.9 Examination of the thermal stability of the *Ms*CnoX, *Mt*CnoX, and *Ec*CnoX proteins. Malate dehydrogenase (MDH) and the purified *Ms*CnoX, *Mt*CnoX, and *Ec*CnoX proteins (0.72 μM) were exposed to heating at 48 °C, with a final absorbance reading (A_{360}) taken at 90 min to show the degree of aggregation. The aggregation of the CnoX proteins was determined relative to that of MDH, which was allocated an arbitrary reference value of 100 % aggregation. The results are representative of two independent experiments with three technical replicates each. Statistical analysis was calculated using Student's t-test; **** denotes $p < 0.0001$.

Once the baseline levels of CnoX aggregation had been established, the proteins' ability to suppress the aggregation of MDH was examined (**Figure 3.10**)**.** As previously observed, MDH displayed significant aggregation following heat treatment (**Figure 3.10**). The addition of either *Ms*CnoX or *Mt*CnoX to MDH before exposure to heating suppressed the latter's protein aggregation in a concentration-dependant manner (**Figure 3.10 A and B**). While the *Ec*CnoX could also suppress the aggregation of MDH, it could only do so effectively at the highest protein concentration used i.e. 0.72 μM. This is consistent with previous observations showing that the *Ec*CnoX protein possessed minimal activity as a holdase without prior HOCl-activation (Goemans *et al.*, 2018a), and is only able to prevent aggregation at high concentrations (Avelange-Macherel *et al.*, 2019).

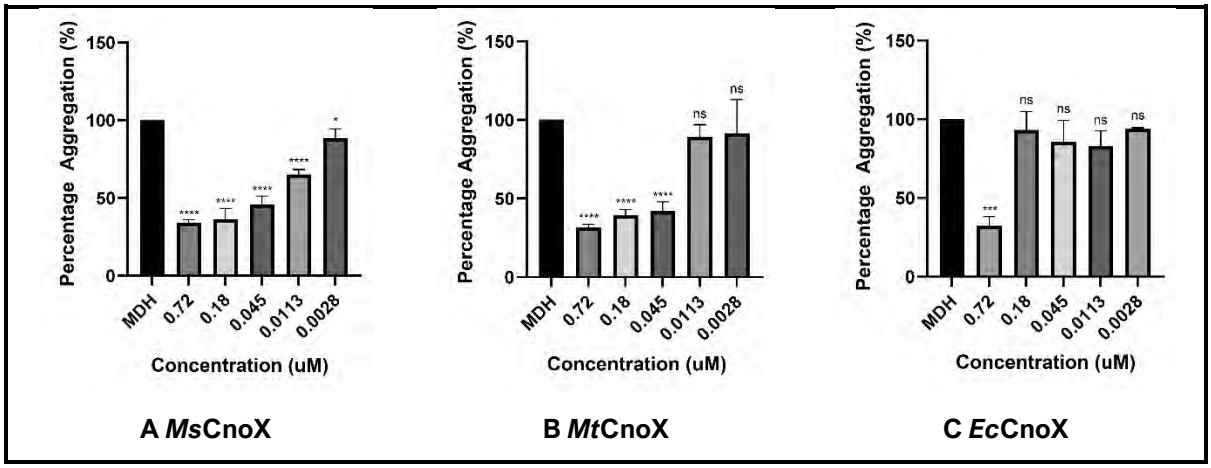

Figure 3.10. Aggregation of malate dehydrogenase (MDH) in the presence and absence of holdase enzymes. MDH was incubated in either the absence (MDH) or presence of the **A)** *Ms*CnoX, **B)** *Mt*CnoX, and **C)** *Ec*CnoX enzymes at the indicated concentrations (0.72 μM, 0.18 μM, 0.045 μM, 0.0113 μM and 0.0028 μM) and expose to heat stress at 48 °C. The degree of light scattering, indicative of MDH aggregation, was determined at 360 nm after 90 min. The percentage aggregation of the CnoX and MDH samples was normalised against CnoX only relative aggregation and calculated relative to that observed MDH aggregation in the absence of CnoX. The error bars represent the standard deviation from three technical replicates. The results are representative of two independent experiments. Statistical analysis was calculated using Students t-test; **** denotes $p < 0.0001$, *** denotes $p < 0.003$, * denotes $p < 0.0468$, and ns denotes 'not significant'.

3.3.2 Thioredoxin-Catalysed Insulin Reduction Assays.

The catalytic CXXC motif within the Trx domain is required for the thiol-disulphide oxidoreductase activity displayed by certain members of the CnoX family (Meireles *et al.*, 2020). The *Ms*CnoX and *Mt*CnoX proteins lack this CXXC motif (**Section 3.1**) and are, therefore, unlikely to possess thiol-oxidoreductase activity. To validate this experimentally, we measured the ability of the mycobacterial CnoX proteins to reduce the disulphide bonds of the

model substrate, insulin, using DTT as an electron donor (Holmgren, 1979). As expected, the recombinant *Ms*TrxC protein, which contains a catalytic CXXC motif, mediated the rapid reduction of insulin as revealed by the increase in turbidity due to the precipitation of insulins β-chain during the assay (**Figure 3.11**; blue line). By contrast, no significant precipitation was observed when TrxC was replaced with *Ms*CnoX (**Figure 3.10 A**), *Mt*CnoX (**Figure 3.11 B**) or *Ec*CnoX (**Figure 3.11 C**). This observation suggests that the mycobacterial CnoX proteins lack thiol-disulphide oxidoreductase activity, similar to the SXXC motif-containing *Ec*CnoX protein (Goemans *et al.*, 2018a). Taken together, our results suggest that the *Ms*CnoX and *Mt*CnoX proteins possess holdase activity to prevent protein aggregation of client proteins, but lack the thiol-disulphide oxidoreductase activity required to reduce oxidised thiols formed following exposure to oxidative stress.

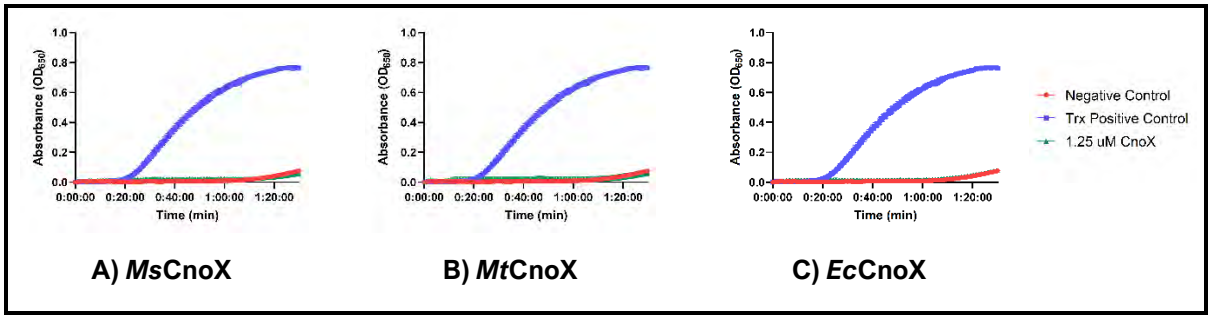

Figure 3.11 Examination of the oxidoreductase capabilities of the A) *Ms*CnoX, B) *Mt*CnoX, and C) *Ec*CnoX proteins. The purified Msm CnoX, Mtb CnoX, and *E. coli* CnoX protein (1.25 µM) (green line) were mixed with insulin (150 µM), and the reaction was initiated with the addition of DTT (0.8 mM). The change in turbidity was monitored at A_{650}. TrxC was included as a positive control (blue line). The results are representative of two independent experiments and standard deviations are indicated.

Chapter 4: Generation and Characterisation of Msm Mutant Strains

4.1 Generation and Characterisation of an Msm KD Mutant Strain

4.1.1 Construction of Msm CnoX KD mutant strains

To gain additional insights into the physiological role of the CnoX protein in mycobacteria, the effect of silencing *cnoX* gene expression on the growth of Msm was examined using CRISPR-interference (CRISPRi) (Rock *et al.*, 2017). The CRISPRi system used relies on the co-expression of dCas9 and a sgRNA targeting sequence from two ATc-inducible promoters located on the CRISPRi plasmid, pLJR962. In the presence of ATc, both dCas9 and the sgRNA targeting sequence are expressed, resulting in the silencing of target gene expression.

To generate CRISPRi vectors capable of silencing *cnoX* expression in Msm, sgRNAs that target the non-template strand of the gene were designed and cloned into pLJR962 (see **Appendix C3** for details). Following verification of their successful generation by restriction enzyme digestion and sequencing (**Appendix C3**) the recombinant plasmids, designated pLJR962::*cnoX*_sgRNA1, pLJR962::*cnoX*_sgRNA2 and pLJR962::*cnoX*_sgRNA3 were introduced into Msm WT to generate three *cnoX* KD mutant strains Msm *cnoX* KD1, *cnoX* KD2 and *cnoX* KD3, respectively. To generate strains that could serve as negative and positive growth controls, Msm was also transformed with the parental pLJR962 and pLJR962::mmpL3_sgRNA plasmids (see **Appendix C2** for details), to generate the Msm WT (pLJR962) and *mmpL3* KD strains, respectively. pLJR962 lacks a sgRNA targeting sequence and the growth of the WT (pLJR962 only) strain should, as a result, not be affected by the availability of ATc in the growth medium. The sgRNA in pLJR962::*mmpL3* sgRNA1, by contrast, targets the expression of the essential *mmpL3* gene, which is required for the transport of trehalose monomycolate across the mycobacterial membrane (Tahlan *et al.*, 2012). The growth of the Msm *mmpL3* KD strain should consequently be inhibited in the presence, but not absence, of ATc (McNeil and Cook, 2019; Rock *et al.*, 2017).

4.1.2 Genotypic and Phenotypic characterisation of the Msm *cnoX* KD mutant

Genome-wide essentiality studies have suggested that the *cnoX* gene is not required for the growth of Msm or Mtb in a rich medium under standard laboratory conditions (de Wet *et al.*, 2018; DeJesus *et al.*, 2017; Dragset *et al.*, 2019; Minato *et al.*, 2019; Sassetti *et al.*, 2001). The ATc-mediated silencing of *cnoX* expression is consequently not expected to affect the growth of the *cnoX* KD mutant strain under these conditions. To test this directly, the growth of the three *cnoX* KD mutants was compared on solid 7H11 medium in either the absence or presence of ATc (0 and 200 ng/mL, respectively) using an agar spotting assay (**Figure 4.1**). The growth of the WT Msm (pLJR962) strain was similar in both the presence (+ATc) and absence (-ATc) of ATc in the growth medium. As expected, the growth of the Msm *mmpL3* KD strain was similar to the WT (pLJR962) strain in the absence of ATc but was significantly reduced following the silencing of the essential *mmpL3* gene with ATc. The growth of the Msm *cnoX* KD1, *cnoX* KD2 and *cnoX* KD3 strains was, by contrast, similar to that of the Msm (pLJR962) strain and not affected by ATc. Since no significant differences in the growth of the Msm *cnoX* KD1, *cnoX* KD2 and *cnoX* KD3 were observed in these studies, further analysis was conducted with the Msm *cnoX* KD1 strain, whose sgRNA targeting sequence had the greatest predicted PAM strength based on the nucleotide sequences recognised by dCas9 (See **Appendix C2**).

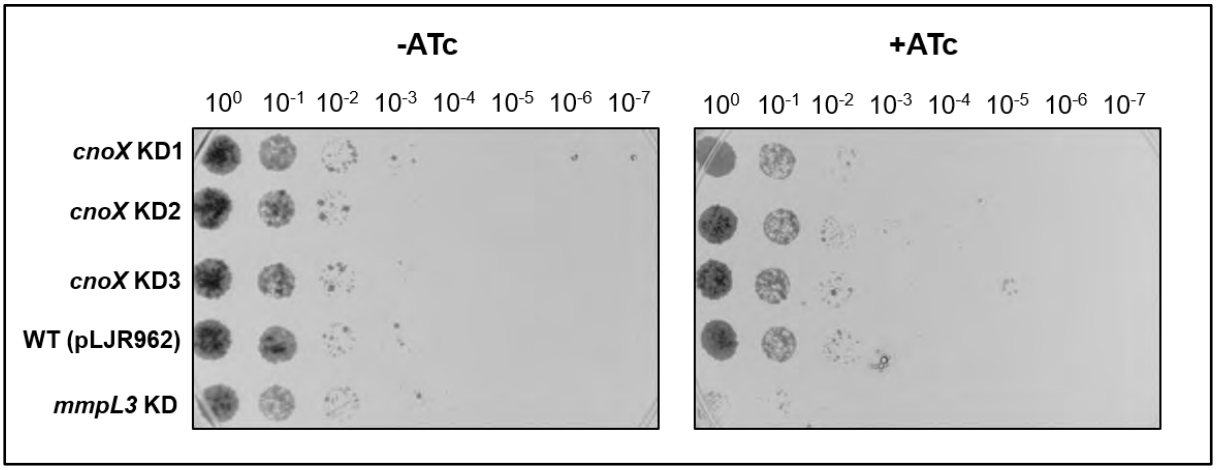

Figure 4.1 Survival of the Msm WT (pLJR962 only), and CRISPRi KD mutants in the presence and absence of ATc. The Msm WT (pLJR962), Δ*cnoX* KD1, KD2, and KD3, and Δ*mmpL3* KD strains were diluted to an OD_{600} of 0.1, serially diluted ten-fold, and spotted on 7H11 plates in the presence (+ATC; 200 ng/mL) or absence (-ATc; 0 ng/mL) ATc to induce gene silencing. The plates were incubated at 37 °C for 48 h before imaging. These images are representative of the three experimental replicates.

To confirm that silencing of the *cnoX* gene occurs following the induction of sgRNA expression by ATc in the KD mutant, the relative levels of *cnoX* expression in the Msm WT (pLJR962) and *cnoX* KD1 strain were compared following growth in the presence and absence of ATc. The expression level under each condition was determined by qRT-PCR and normalised relative to the Msm *sigA* (MSMEG_2758) housekeeping gene, as described in **Section 2.6.4**. Initial analyses revealed the *cnoX* gene was constitutively expressed at similar levels in both the WT (pLJR962) and *cnoX* KD strains under standard laboratory growth conditions in the absence of ATc (data not shown). While the expression of *cnoX* was not significantly altered in the presence of ATc in the WT (pLJR962) strain, an approximate ~100-fold reduction in gene expression was observed following induction of sgRNA expression in the *cnoX* KD mutant strain (**Figure 4.2)**. This finding indicates that efficient gene silencing is achieved in the *cnoX* KD1 mutant strain, making it suitable for assessing the function of CnoX in Msm. The lack of growth inhibition observed for the KD strain on solid growth media in the presence of ATc (**Figure 4.1**) is, therefore, unlikely to be due to a lack of effective gene silencing in the presence of ATc.

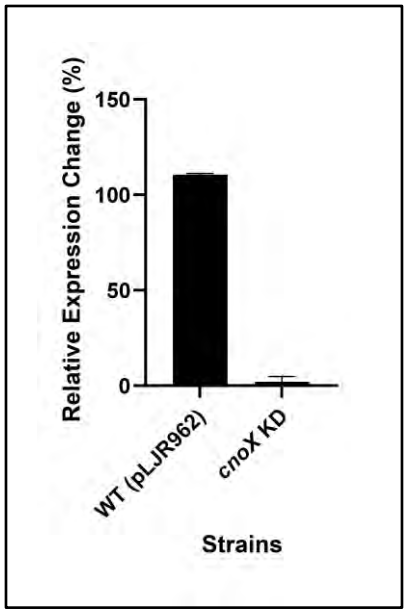

Figure 4.2 Relative expression levels of *cnoX* in the Msm WT (pLJR962) and cnoX KD mutant strains. Msm cultures were diluted to an OD_{600} of 0.1 and grown to mid-exponential phase (OD_{600} ~0.8) in either the absence (0 ng/mL) or presence of ATc (200 ng/mL) and total RNA isolated. Equivalent amounts of RNA were converted to cDNA and the relative expression levels of *cnoX* in the presence and absence of ATc were determined using the $2^{-\Delta\Delta Ct}$ method. Expression levels were normalised to the *sigA* gene and the values depicted represent the percentage of *cnoX* transcripts present in cells grown in the presence relative to the absence of ATc.

To determine the effect of silencing the expression of *cnoX* during growth in liquid medium, we compared the growth of the Msm *cnoX* KD strain in the presence of increasing concentrations of ATc (0 to 3200 ng/mL) using the broth microdilution method. In line with the results observed following growth on solid medium, no significant differences in the growth of the WT (pLJR962) or Msm *cnoX* KD were observed in the presence of ATc concentrations up to 400 ng/mL (see **Appendix D2**, **Figure D2.1**). No growth was observed for either strain at the remaining ATc concentrations used (≥ 800 ng/mL), however, due to the growth inhibitory (antibiotic) properties of the chemical when used at elevated concentrations. To maximise the reduction of the cellular levels of CnoX, we also examined the effect of sub-culturing the Msm KD strain in ATc before setting up the microdilution assays as described above. Reducing the expression levels of *cnoX* in this manner did not, however, sensitise the strain to subsequent ATc-mediated growth inhibition (see **Appendix D2**, **Figure D2.1; pre-depleted**).

We next compared the growth kinetics of the WT (pLJR962) and *cnoX* KD strains in 7H9 medium in the presence and absence of ATc. As shown in **Figure 4.3**, the growth of the WT and *cnoX* KD strains was similar during lag and early exponential phase (<18 h). Thereafter, the WT strain displayed a more rapid growth rate and reached a higher final OD than the corresponding *cnoX* KD mutant in the absence of ATc (**Figure 4.3)**. The growth of both WT and *cnoX* KD strains was reduced in the presence of 200 ng/mL ATc, however, suggesting that ATc may have a slight inhibitory effect on bacterial growth when used at this concentration. The difference in growth rates and final cell densities attained in the presence and absence of ATc did not, however, reach the level of statistical significance for either WT or KD mutant strain. (i.e. +ATc vs -ATc) The results obtained on solid media for the KD mutant, coupled with our subsequent findings that a Msm *cnoX* null mutant is not compromised for growth in liquid medium (**Section 4.2.4**), suggest that the *cnoX* gene is not essential for Msm growth under standard laboratory conditions. This finding would also be consistent with the results of several recent genome-wide essentiality studies that have found the *cnoX* gene to be dispensable for the growth of Msm under similar growth conditions (Bosch *et al.*, 2021; de Wet *et al.*, 2020).

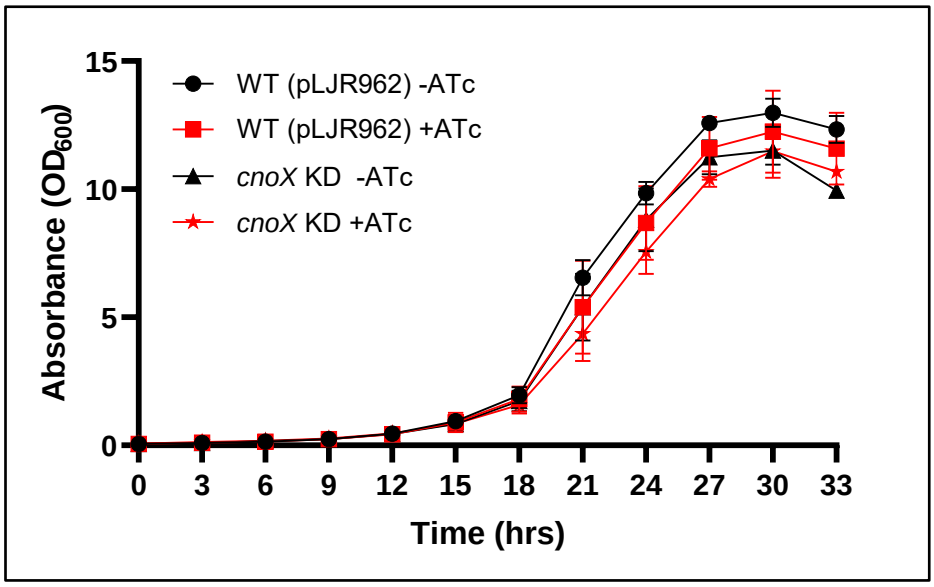

Figure 4.3 Growth kinetics of the Msm CRISPRi KD mutant. The Msm *cnoX* KD mutant and WT (pLJR962) control strains were diluted to an OD_{600} of 0.05 in the presence (200 ng/mL) and absence (0 ng/mL) ATc to induce gene knockdown, and their growth was measured over 33 h with OD_{600} measurements taken at 3 h intervals. The average of two biological replicates with two experimental replicates is indicated with ± SD.

The CnoX enzyme from *E. coli* has been shown to possess HOCl-activated holdase *in vitro* (Goemans *et al.*, 2018a; Meireles *et al.*, 2020). The role of CnoX in conferring protection against HOCl-mediated killing is, nevertheless, equivocal. While the studies of Goemans *et al.* (2018) demonstrated a role for CnoX in promoting bacterial survival in the presence of HOCl, these findings could not be recapitulated by others (Meireles *et al.*, 2020) (see **Section 4.3**). To determine whether CnoX is required for Msm growth and/or survival in the presence of HOCl, we examined the organism's susceptibility to this oxidant on solid growth medium using a disc diffusion assay. As shown in **Figure 4.4,** no significant difference in the sensitivity of the WT or *cnoX* KD Msm strains to HOCl was observed in either the presence or absence of ATc. Silencing *cnoX* gene expression, similarly, did not affect the strain's sensitivity to oxidative stress caused by either hydrogen peroxide (H_2O_2) or cumene hydroperoxide (CHP), an organic peroxide. Both strains produced similar inhibition profiles following exposure to the thiol-specific reducing and oxidising agents, DTT and diamide, respectively (**Figure 4.4)**. The KD mutant, however, displayed increased sensitivity to plumbagin in the presence of ATc, a compound that generates superoxide anions and is known to target the mycobacterial thymidylate synthase protein (Sarkar *et al.*, 2020) (**Figure 4.4**).

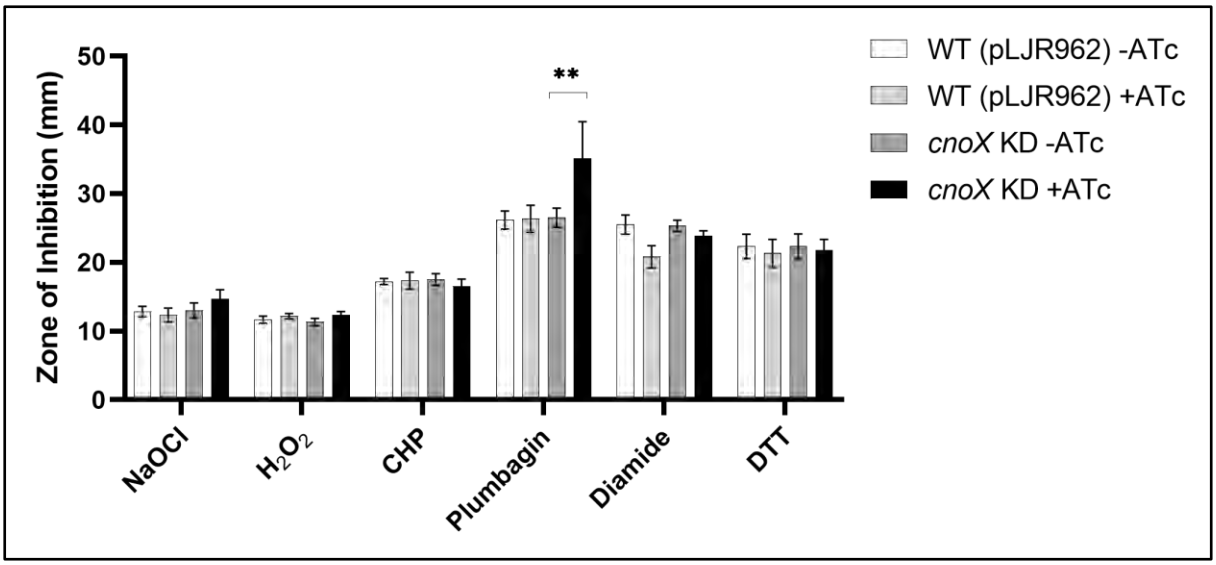

Figure 4.4 Disc diffusion assays assessing the susceptibility of the Msm *cnoX* KD mutant to oxidative and reductive stress. The Msm CRISPRi cnoX KD mutant and WT (pLJR962) control strains were cultured in the presence (200 ng/mL) and absence (0 ng/mL) of ATc to mid-log phase, followed by dilution to a final OD_{600} of 0.025 in 1 % (w/v) molten agar to prepare agar overlay plates. Sodium hypochlorite (NaOCl), hydrogen peroxide (H2O2), cumene hydroperoxide (CHP), plumbagin, diamide, and dithiothreitol (DTT) were aliquoted onto discs and plated on the agar overlay plate. The zones of inhibition (ZOI) were measured after 48 h. The average of 2 to 4 biological replicates each with three experimental replicates with ±SD is indicated. Statistical analysis was calculated using multiple unpaired T-tests; ** denotes $p < 0.01$ between the cnoX KD +ATc and -ATc strains. Unless otherwise indicated, all of the strains show no significant difference.

To determine whether CnoX depletion sensitises Msm to growth inhibition by antimicrobial compounds, we compared the growth of the WT and KD strain in the presence of the first-line drugs isoniazid, rifampicin and ethambutol, as well as the second-line drug ciprofloxacin. No significant difference in the sensitivity of the *cnoX* KD mutant to ciprofloxacin or ethambutol was observed. Increased susceptibility to isoniazid and rifampicin was, however, observed when the *cnoX* KD mutant was grown in the presence, but not the absence of ATc (**Figure 4.5**).

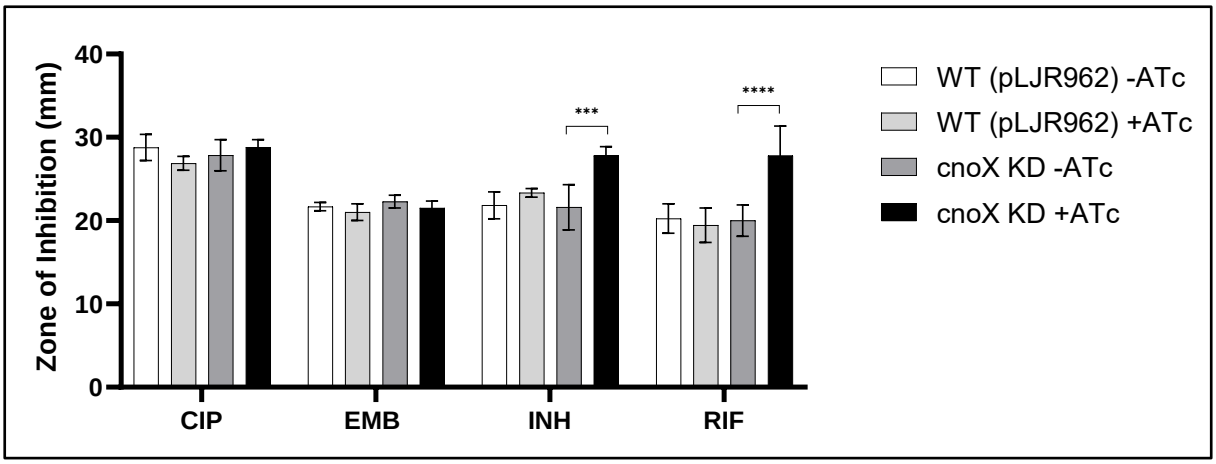

Figure 4.5 Disc diffusion assays assessing the susceptibility of the Msm *cnoX* KD mutant to antibiotic stress. The Msm CRISPRi cnoX KD mutant and WT (pLJR962) control strains were cultured in the presence and absence of 200 ng/mL ATc to mid-log phase, followed by dilution to a final OD600 of 0.025 in 1 % (w/v) molten agar to prepare agar overlay plates. Ciprofloxacin (CIP), ethambutol (EMB), isoniazid (INH), and rifampicin (RIF) were aliquoted onto discs and plated on the agar overlay plate. The zones of inhibition (ZOI) were measured after 48 h. The average of 2 to 4 biological replicates each with three experimental replicates with ±SD is indicated. Statistical analysis was calculated using multiple unpaired T-tests; **** denotes $p < 0.0001$, *** denotes $p < 0.001$ between the cnoX KD +ATc and -ATc strains. Unless otherwise indicated, all of the strains show no significant difference.

4.2 Construction of an Msm CnoX KO mutant

4.2.1 Generation of Allelic Exchange Substrate for Splice by Overlap Extension

While ATc-mediated transcriptional silencing has been used to confirm the essentiality of numerous mycobacterial genes, it has several shortcomings that may limit its usefulness when determining gene function (Evans and Mizrahi, 2015; Schnappinger and Ehrt, 2014). Firstly, transcriptional repression is often incomplete resulting in the production of residual levels of proteins that may be sufficient to rescue bacterial growth, even after ATc-induced gene silencing. Secondly, transcriptional repression is relatively slow when compared to methods that induce the degradation of target proteins directly, complicating the analysis of proteins with either long-half lives or present and required in low abundance in WT cells (Schnappinger and Ehrt, 2014; Wei *et al.*, 2011). To overcome some of these limitations, we generated an Msm deletion mutant in which the endogenous copy of *cnoX* was replaced with a zeomycin-resistance (Zeo^R) cassette. This was accomplished by homologous recombination using a linear allelic exchange substrate (AES), generated as described in the Materials and Methods (**Section 2.12.2**).

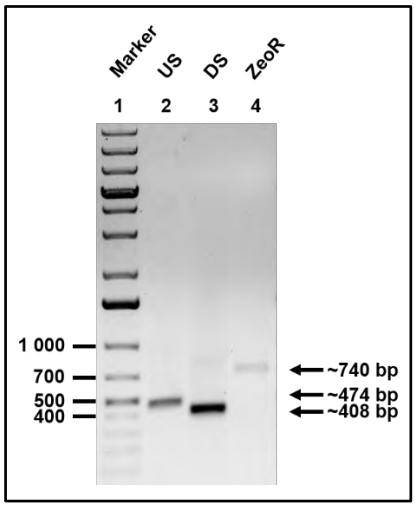

Figure 4.6 Agarose gel electrophoresis confirmation of the successful amplification of the upstream (US), downstream (DS) and zeomycin resistance cassette (Zeo^R) fragments. PCR reactions were performed using genomic DNA isolated from a WT strain (US and DS) or plasmid DNA from pMSG360Zeo (Zeo^R) and primers cnoX-US-For and cnoX-US-Rev (US), cnoX-DS-For and cnoX-DS-Rev (DS), and pKMZeo-For and pKMZeo-Rev (Zeo^R). The products of the PCR reactions were electrophoresed on a 0.8 % (w/v) agarose gel at 80 V for 50 mins. **Lane 1**: Molecular Weight Marker; **Lane 2**: upstream (US) region of the *cnoX* gene; **Lane 3**: downstream (DS) region of the *cnoX* gene; **Lane 4**: Zeo^R cassette amplified from pMSG360Zeo. Black arrows indicate the sizes of the predicted PCR amplicons.

As shown in **Figure 4.6**, the upstream (US) and downstream (DS) homology arms of the AES were obtained by PCR amplification of 474 (**Lane 2),** and 408 **(Lane 3)** bp fragments located at the 5'- or 3'-ends of the *cnoX* gene, respectively. Following gel purification, the US and DS fragments were spliced to the 740 bp loxP-flanked Zeo^R cassette (**Figure 4.6, Lane 4**), which had been PCR amplified from pMSG360-Zeo (Barkan *et al.*, 2010), using overlap-extension PCR. This resulted in the generation of the 1582 bp linear AES, as indicated by the presence of an amplicon of the corresponding size following agarose gel electrophoresis (**Figure 4.7, Lanes 2 and 3**).

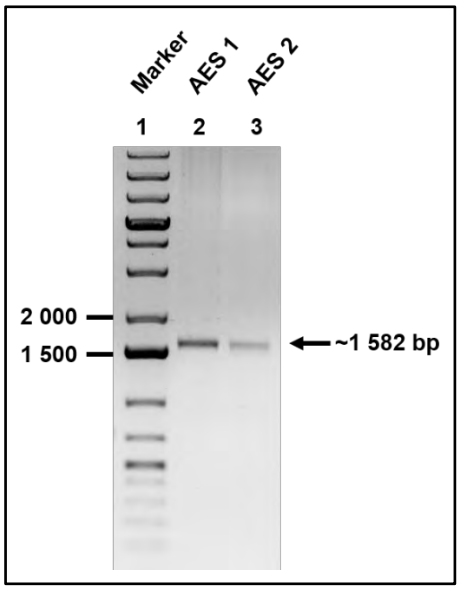

Figure 4.7 Agarose gel electrophoresis confirmation of the successful generation of an allelic exchange substrate (AES). PCR reactions were performed using PCR-purified US, DS, and Zeo^R DNA and primers cnoX-US-For and cnoX-DS-Rev were added after 10 cycles. The products of the PCR reactions were electrophoresed on a 0.8 % (w/v) agarose gel at 80 V for 50 mins. **Lane 1**: Molecular Weight Marker; **Lanes 2-3**: Allelic Exchange Substrate (AES) in duplicate. Black arrows indicate the sizes of the predicted PCR amplicons.

4.2.2 Generation of a marked Δ*cnoX* mutant

Following gel purification, the AES was introduced into Msm (pJV53) and transformants were selected on solid medium supplemented with zeomycin. The genotype of two randomly selected Zeo^R transformants was determined by PCR amplification using gDNA and the primer pairs cnoX-US2-For/cnoX-DS2-Rev, cnoX-US2-For/Zeo-Check-Rev, and Zeo-Check-For/cnoX-DS-2-Rev. Importantly, the flanking cnoX-US2-For and cnoX-DS2-Rev primers anneal to regions located upstream (5') of the primers used to generate the *cnoX* AES (**Figure 2.1**), enabling legitimate recombinants to be discriminated from illegitimate ones. Following agarose gel electrophoresis, PCR products of 2018, 989 and 865 bp were identified for each of

the Δ*cnoX*::Zeo^R mutant strains (**Figure 4.14, Lanes 5, 6, 7** and **8, 9, 10** for Mutant 1 and 2 respectively), which corresponds to the sizes predicted for a marked Δ*cnoX*::Zeo^R mutant. By contrast, a single band of ~2158 bp was identified for WT Msm when using the CnoX-US2-For and CnoX-DS2-Rev primers (**Lane 2**). No amplicons were visible in Lanes 3 and 4 of **Figure 4.8,** given the lack of binding sites for the Zeo^R-specific primers in the WT Msm strain, or samples lacking DNA templates (**Figure 4.8, Lanes 11-13**). Taken together, these results confirm the successful generation of the marked Msm Δ*cnoX*::Zeo^R mutant strain.

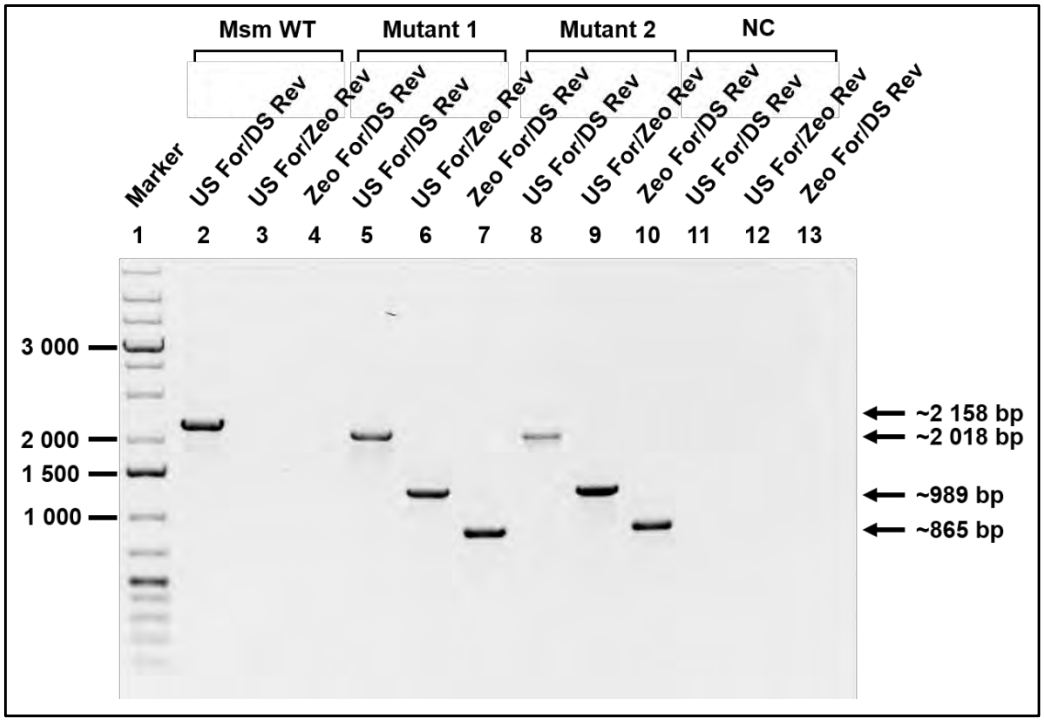

Figure 4.8 PCR confirmation of the genotype of the putative Msm cnoX::Zeo^R mutants. PCR reactions were performed using genomic DNA isolated from Msm WT or two putative *cnoX*::Zeo^R mutants (Mutant 1 and Mutant 2) using primers cnoX-US2-For and cnoX-DS2-Rev (US-For/DS-Rev), cnoX-US2-For and Zeo-Check-Rev (US-For/Zeo^R-Rev), and Zeo-Check-For and cnoX-DS2-Rev (Zeo^R-For/DS-Rev). The products of the PCR reactions were electrophoresed on a 0.8 % (w/v) agarose gel at 80 V for 50 mins. The gDNA used as a template in the PCR reactions were as follows: **Lanes 2-4**: Msm WT gDNA, **Lanes 5-7**: *cnoX*::Zeo^R mutant 1 gDNA, **Lane 8-10**: *cnoX*::Zeo^R Mutant 2 gDNA, **Lane 11-13**: No DNA, negative controls. Black arrows indicate the sizes of the predicted PCR amplicons.

4.2.3 Generation of an unmarked Δ*cnoX* mutant

To generate an unmarked Δ*cnoX* mutant, we next introduced the temperature-sensitive plasmid, pML2714, which encodes Cre-recombinase responsible for the excision of the loxP-flanked Zeo^R cassette into the marked Δ*cnoX*::Zeo^R mutant as described in **Section 2.1.13**. Following the selection of kanamycin-resistant transformants harbouring pML2714, the strains were confirmed to be sensitive to zeomycin (Zeo^S) by replica plating. The loss of the Zeo^R cassette was subsequently confirmed by colony PCR analysis of two independent Zeo^S mutants using the cnoX-US-2-For and cnoX-DS-2-Rev primers. An amplicon of 2158 bp was obtained for the WT Msm strain (**Figure 4.9, Lanes 2**), as expected. The two putative unmarked mutants yielded amplicons of 1348 bp (**Figure 4.9, Lanes 3-4**), by contrast, which is consistent with the expected size of the Δ*cnoX* allele following removal of the Zeo^R cassette. These observations demonstrate the successful removal of the Zeo^R cassette from the marked Δ*cnoX*::Zeo^R mutant to yield an unmarked Δ*cnoX* mutant, which was used in subsequent experiments.

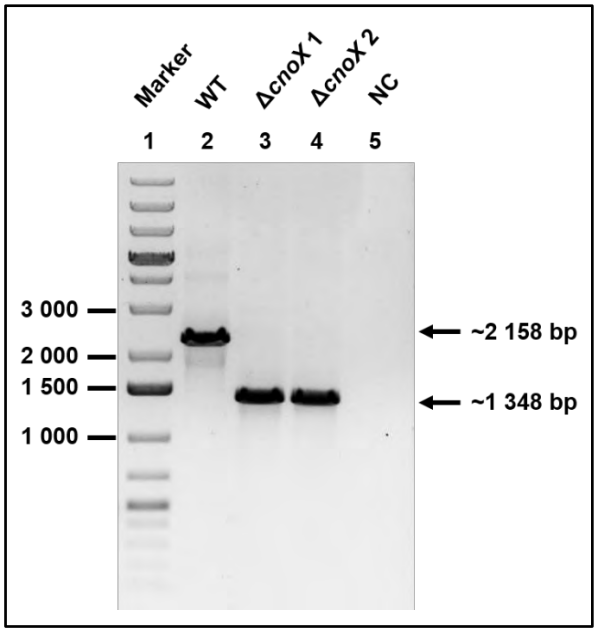

Figure 4.9 PCR confirmation of the putative unmarked Msm *cnoX* mutants. PCR reactions were performed using genomic DNA isolated from WT or two putative *cnoX* mutants (Δ*cnoX* 1 and Δ*cnoX* 2) using primers CnoX-US2-For and CnoX-DS2-Rev. The products of the PCR reactions were electrophoresed on a 0.8 % (w/v) agarose gel at 80 V for 50 mins. The gDNA used as a template in the PCR reactions were as follows: **Lanes 2**: Msm WT gDNA, **Lanes 3**: *cnoX* mutant 1 gDNA, **Lane 4**: *cnoX* mutant 2 gDNA, **Lane 5**: No DNA, negative control. Black arrows indicate the sizes of the predicted PCR amplicons.

To confirm that the expression of *cnoX* was eliminated in the unmarked mutant, its levels of expression were initially examined in the Msm WT Msm and Δ*cnoX* strain using semi-quantitative RT-PCR (**Figure 4.10**). When grown under standard laboratory conditions, an amplicon corresponding to the predicted size of the Msm *sigA* housekeeping gene (~100 bp) was identified for both the WT and mutant strains (**Figure 4.10 A**, **Lane 2**). A *cnoX*-specific amplicon of ~90 bp was similarly produced when using cDNA obtained from the WT strain (**Figure 4.10 B**, **Lane 2**), which is consistent with the constitutive expression previously observed for the gene under these conditions. No *cnoX*-specific amplicon was, however, produced when cDNA prepared from the Δ*cnoX* mutant was used, (**Figure 4.10 B, Lane 3**), confirming that the gene had been successfully disrupted thereby eliminating expression of the gene.

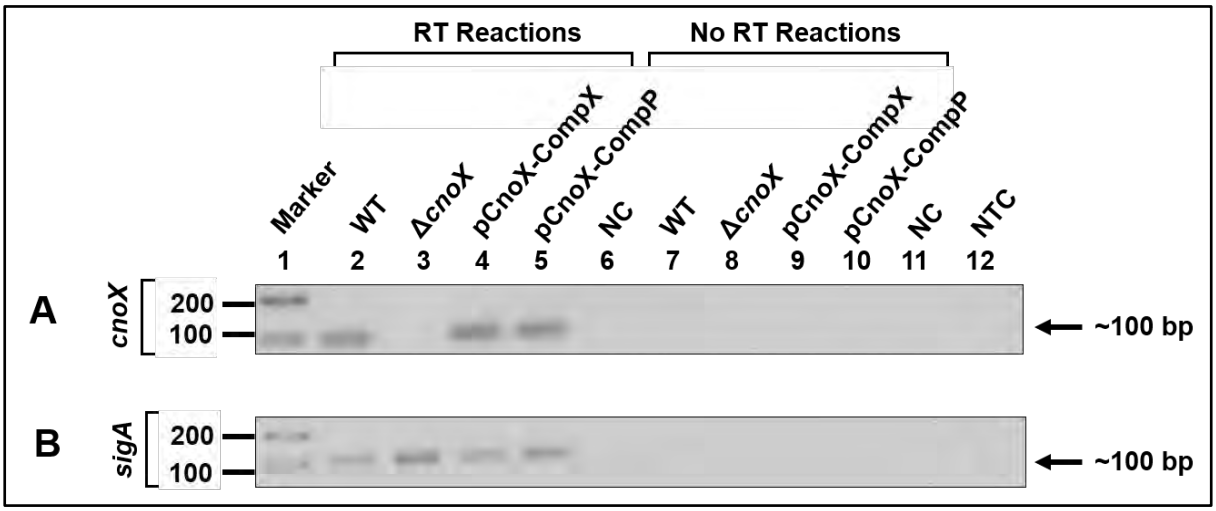

Figure 4.10 Semi-quantitative RT-PCR analysis of *cnoX* and *sigA* expression in Msm wildtype (WT), Δ*cnoX* mutant, and Δ*cnoX*::pCnoX-CompX and Δ*cnoX*::pCnoX-CompP complemented strains. RNA obtained from each strain was reverse transcribed (RT) into cDNA and PCR amplified using either *cnoX* (**A**) or housekeeping gene, *sigA* (**B**)-specific primers. 'No RT reactions' were included to confirm the absence of gDNA contamination. The products of the RT-PCR were electrophoresed on a 2 % (w/v) agarose gel at 80 V for 50 min. The cDNA used as a template in each reaction was as follows: **Lane 2**: Msm WT RT reaction; **Lane 3**: Msm Δ*cnoX* RT reaction; **Lane 4**: Msm Δ*cnoX*::pCnoX-CompX RT reaction; **Lane 5**: Msm Δ*cnoX*::pCnoX-CompP RT reaction; **Lane 6**: Negative Control (NC) RT reaction; **Lane 7**: Msm WT No RT control reaction; **Lane 8**: Msm Δ*cnoX* No RT control reaction; **Lane 9**: Msm Δ*cnoX*::pCnoX-CompX No RT control reaction; **Lane 10**: Msm Δ*cnoX*::pCnoX-CompP No RT control reaction; **Lane 11**: Negative Control (NC) RT reaction; **Lane 12**: No Template Control (NTC). Black arrows indicate the DNA fragments.

The lack of *cnoX* expression in the deletion mutant was subsequently confirmed by qRT-PCR**,** where the expression of the gene was observed to be undetectable relative to that present in the WT strain (**Figure 4.11,** see WT vs Δ*cnoX* mutant).

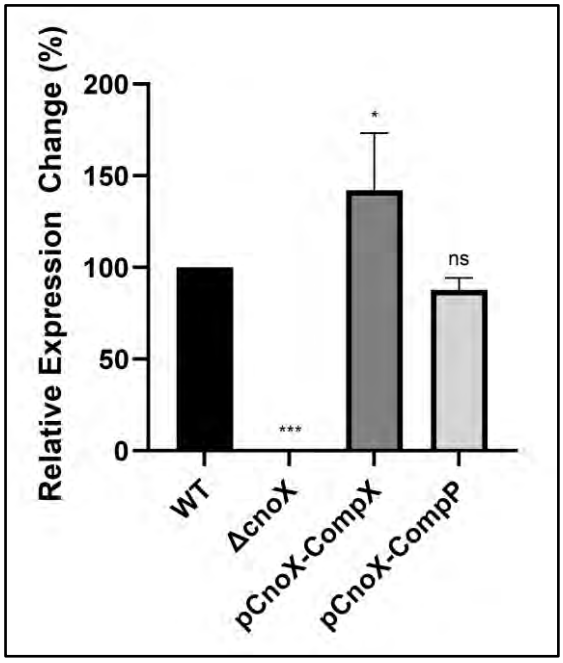

Figure 4.11 Relative expression levels of *cnoX* in the Msm WT, *cnoX* deletion mutant, and the genetically complemented strains. Msm cultures were diluted to an OD_{600} of 0.1 and grown to the mid-exponential phase (OD_{600} ~0.8) before the isolation of total RNA. Equivalent amounts of RNA were converted to cDNA and the relative expression levels of *cnoX* were determined using the 2-ΔΔCt method. Expression levels were normalised to *sigA* and the values depicted represent the percentage of *cnoX* transcripts. Statistical analysis was calculated using an ordinary one-way ANOVA test; *** denotes $p < 0.0002$, * denotes $p < 0.0301$, and ns denotes 'not significant'.

To generate vectors capable of genetically complementing the Δ*cnoX* mutant in subsequent physiological studies, the *cnoX* gene was cloned into the integrative plasmid pGiles::P_{smyc} (Kolbe *et al.*, 2020) under the control of either its natural promoter or the heterologous P_{smyc} promoter (Ehrt *et al.,* 2005). Following their generation, (see **Appendix C4** for more additional details) the plasmids, designated as pCnoX-CompP or pCnoX-CompX, were introduced into the Δ*cnoX* mutant to yield the complemented Msm Δ*cnoX*::pCnoX-CompP and Δ*cnoX*::pCnoX-CompX strains, respectively. As shown in **Figures 4.10 A and B**, expression of the *cnoX* gene in the Δ*cnoX* mutants was restored following the introduction of both the pCnoX-CompP or pCnoX-CompX plasmids (**Lanes 4 and 5**). qRT-PCR analysis indicated that the relative expression of *cnoX* from its native promoter on the integrating pCnoX-CompP (**Figure 4.11**) was similar to that found in WT Msm. An ~1.5-fold increase in *cnoX* expression

was, however, observed when complementation was accomplished using the pCnoX-CompX vector (**Figure 4.11**). This may potentially be due to the higher levels of expression obtained from the P_{smyc} promoter, which has previously been shown to promote high-level expression of genes under its control (Ehrt *et al.*, 2005; Kolbe *et al.*, 2020). Taken together, the results indicate that the *cnoX* deletion strain and genetically complemented strains are suitable for assessing the function of CnoX in Msm.

4.2.4 Phenotypic characterisation of the *cnoX* deletion mutant and genetically complemented strains.

Our previous experiments conducted with the *cnoX* KD strain suggested that the CnoX activity is not essential for bacterial growth under standard laboratory conditions. To validate this finding, the growth kinetics of the Msm WT and Msm Δ*cnoX* deletion mutant were monitored during growth in liquid media. As shown in **Figure 4.12,** the growth of the WT and *cnoX* mutant were similar during the lag and exponential phase, with no significant differences being observed up to 24 h. Our data supports our previous conclusions that CnoX activity is dispensable for bacterial growth *in vitro*.

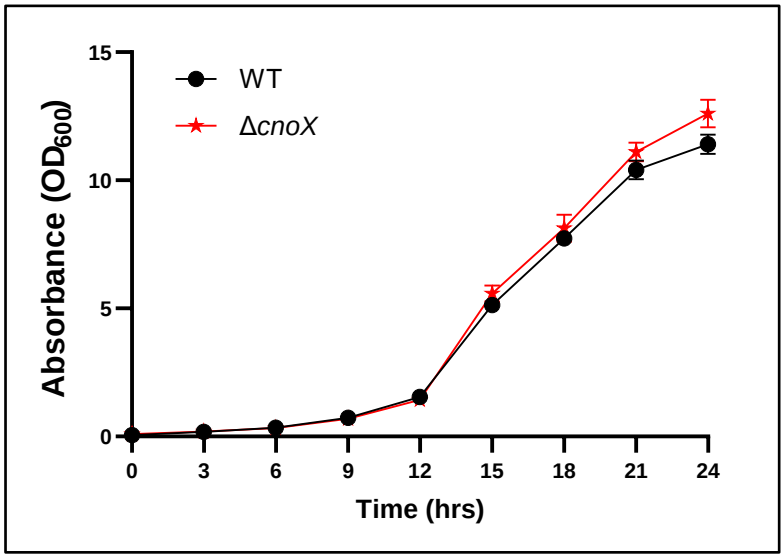

Figure 4.12 Growth kinetics of the Msm *cnoX* deletion mutant. Msm WT and *cnoX* deletion mutant cultures were diluted to an OD_{600} of 0.05 and their growth was measured over 24 h with OD_{600} measurements taken at 3 h intervals. The average of three biological replicates with two experimental replicates is indicated with ± SD.

Our previous results demonstrated that the *cnoX* KD mutant displays increased sensitivity to growth inhibition by plumbagin, isoniazid, and rifampicin. To validate these findings, the growth of the WT, Δ*cnoX* mutant and genetically complemented strains was compared under similar conditions. The results for shown in **Figure. 4.13** shows that loss of CnoX activity gene

did not confer increased susceptibility of the deletion mutant to growth inhibition by HOCl, as determined by disc diffusion assays. The WT and the Δ*cnoX* mutant also displayed identical MIC values for HOCl (8 mM) when assayed by the broth microdilution method (data not shown). In line with the growth phenotypes observed for the *cnoX* KD in **Figure 4.4**, the Δ*cnoX* mutant also displayed similar sensitivities as the WT to H_2O_2, CHP, diamide or DTT (**Figure. 4.13**). Like the *cnoX* KD, the deletion mutant's growth was more significantly inhibited by plumbagin than the WT strain. Ectopic expression of CnoX in the deletion mutant from the pCnoX complementation plasmid, moreover, restored the growth of the mutant strain to WT levels in the presence of this compound.

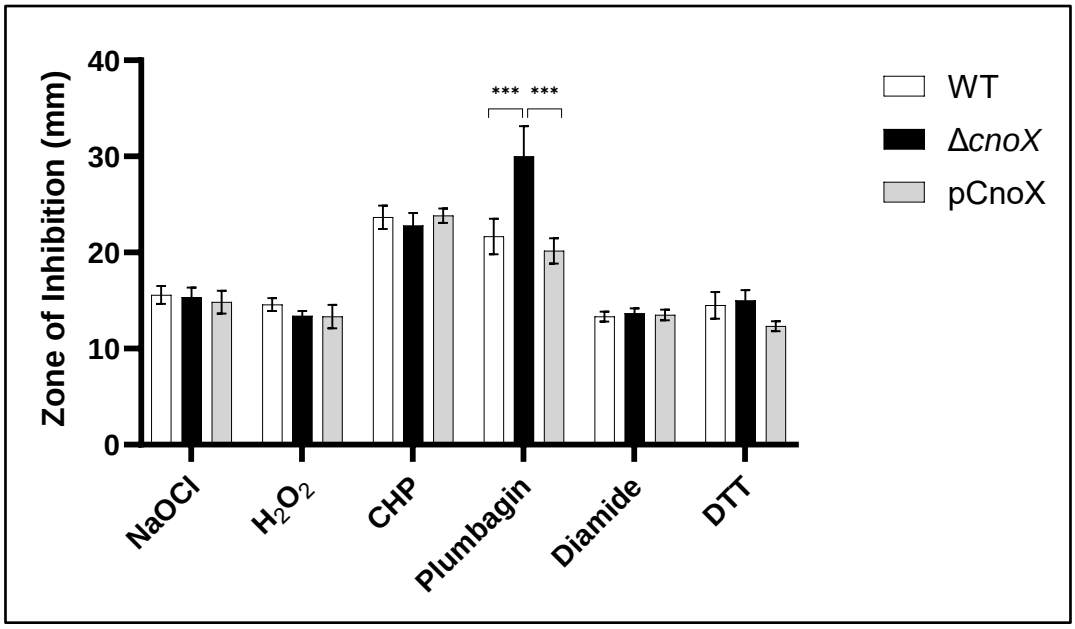

Figure 4.13 Susceptibility of the Msm Δ*cnoX* mutant to oxidative stress. The Msm WT, Δ*cnoX* KO, and genetically complemented (pCnoX) strains were cultured to an OD_{600} to mid-log phase, followed by dilution to a final OD_{600} of 0.025 in 1 % (w/v) molten agar to prepare agar overlay plates. Sodium hypochlorite (NaOCl), hydrogen peroxide (H_2O_2), cumene hydroperoxide (CHP), plumbagin, diamide, and dithiothreitol (DTT) were aliquoted onto discs and plated on the agar overlay plate. The zones of inhibition (ZOI) were measured after 48 h. The average of 2 to 4 biological replicates each with three experimental replicates with ±SD is indicated. Statistical analysis was calculated using multiple unpaired T-tests; *** denotes $p < 0.001$ between the ΔcnoX KO strain and either the WT or pCnoX strain. Unless otherwise indicated, all of the strains show no significant difference.

Assessment of the CnoX protein's role in preventing antibiotic-mediated killing using disc diffusion assays yielded similar results to those found in the *cnoX* KD mutant strain (**Figure 4.5**). We observed that the Δ*cnoX* KO mutant displayed increased sensitivity to the first-line antitubercular drugs, isoniazid and rifampicin, when compared with the WT and genetically complemented Δ*cnoX* pCnoX strain, which possessed similar resistance profiles (**Figure 4.14**). Interestingly, we observed that in the presence of ethambutol, the *cnoX* KO mutant, but not the WT or genetically complemented strain, displayed an increase in resistance to the antibiotic (**Figure 4.14**). In contrast to isoniazid and rifampicin, this phenotype was not observed following silencing of *cnoX* in the KD mutant strain (**Figure 4.5**). The significance of this observation is therefore inconclusive and will need to be validated in future studies.

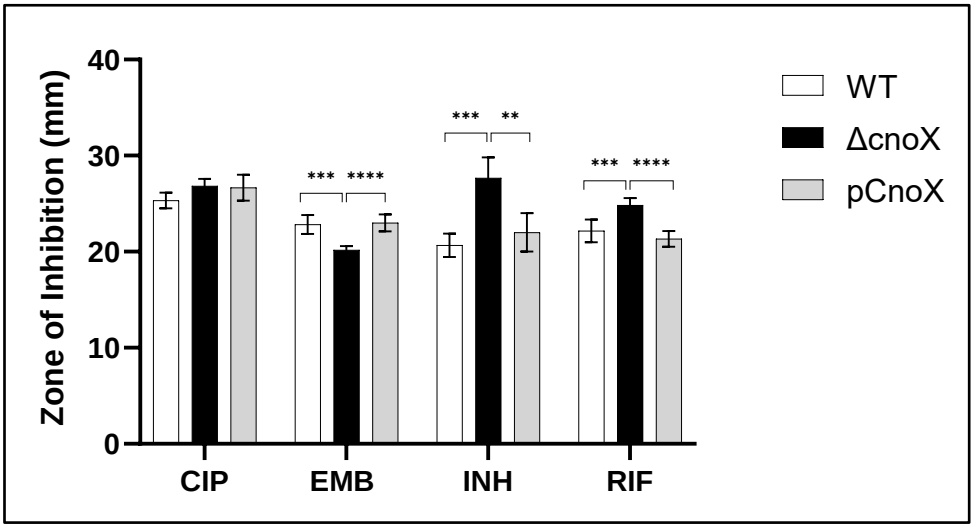

Figure 4.14 Susceptibility of the Msm *cnoX* KD mutant to antibiotic stress. The Msm WT, Δ*cnoX* KO mutant and complemented pCnoX strains were cultured to mid-log phase, followed by dilution to a final OD_{600} of 0.025 in 1 % (w/v) molten agar to prepare agar overlay plates. Ciprofloxacin (CIP), ethambutol (EMB), isoniazid (INH), and rifampicin (RIF) were aliquoted onto discs and plated on the agar overlay plate. The zones of inhibition (ZOI) were measured after 48 h. The average of 2 to 4 biological replicates each with three experimental replicates with ±SD is indicated. Statistical analysis was calculated using multiple unpaired T-tests; **** denotes $p < 0.0001$, *** denotes $p < 0.001$, ** denotes $p < 0.01$ between the Δ*cnoX* KO strain and either the WT or pCnoX strain. Unless otherwise indicated, all of the strains show no significant difference.

Several holdases function to protect proteins from irreversible unfolding and aggregation following exposure to elevated temperatures. To examine whether CnoX activity is required for supporting Msm growth during exposure to heat stress, the survival of the WT, deletion mutant, and genetically complemented strains was compared following exposure to 53 °C and 45 °C over a period of 3 and 24 hrs, respectively. As shown in **Figure 4.15 A and B,** the loss

of CnoX activity was not associated with decreased survival at either of the temperatures examined.

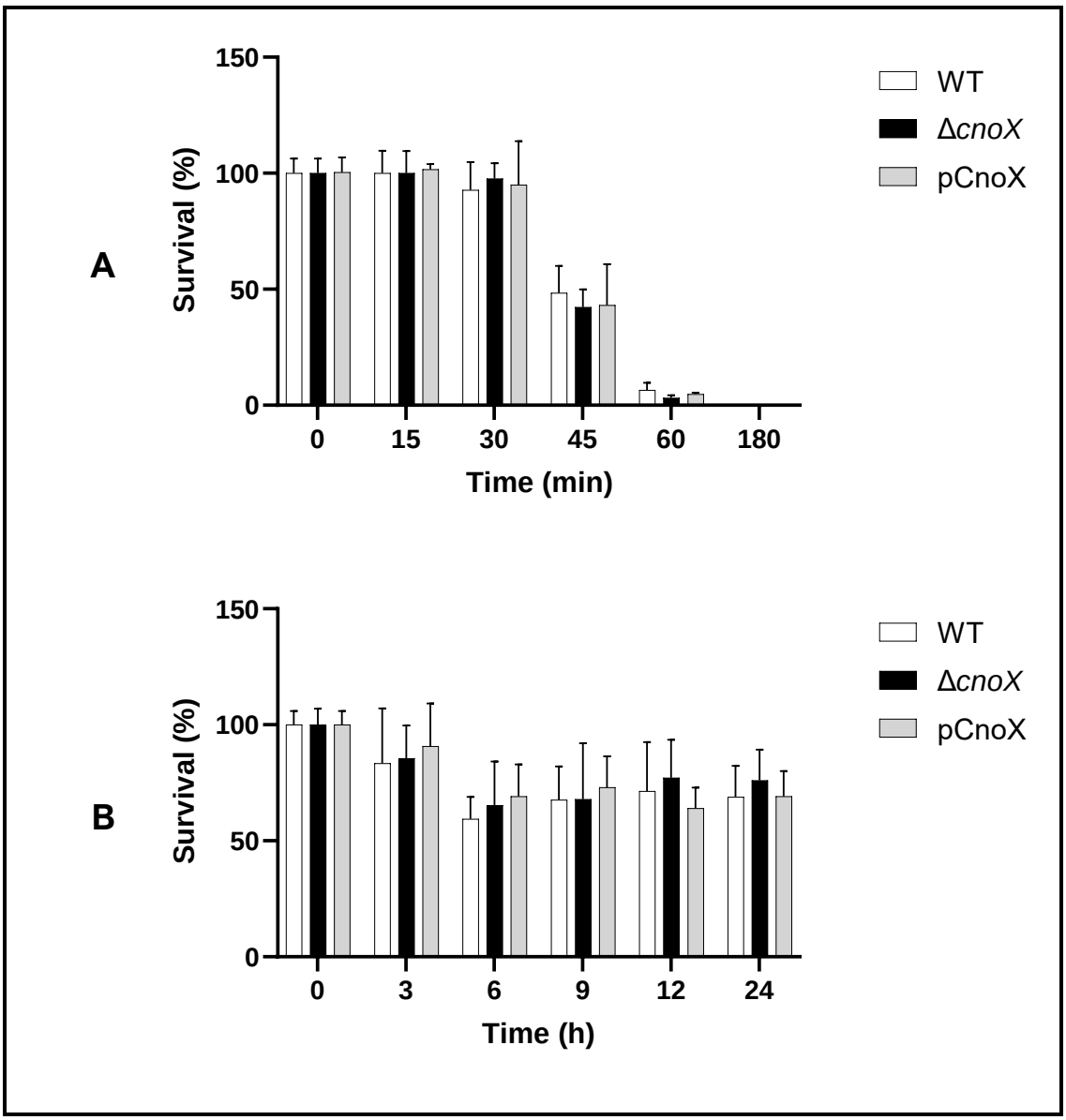

Figure 4.15 Susceptibility of the Msm *cnoX* KD mutant to A) 53 °C and B) 45 °C heat stress. The Msm WT, Δ*cnoX* KO mutant and complemented pCnoX strains were cultured to the mid-log phase, followed by dilution to a final OD_{600} of 0.1. The cultures were grown in 7H9 media at either 45 °C or 53 °C for the indicated time periods. Samples were removed and spotted at the indicated time points to determine the CFU/mL. The survival (%) was determined by comparing the CFU/mL of the samples to the CFU/mL at time 0. The average of 3 biological replicates each with 2 experimental replicates with ±SD is indicated.

4.3 Heterologous Complementation Analysis in *E . coli*

An *E. coli* Δ*cnoX* mutant has previously been reported to be sensitised to HOCl relative to its isogenic progenitor (Goemans *et al.*, 2018a). To examine the ability of the *Ms*CnoX and *Mt*CnoX proteins to function as chaperedoxins, we attempted to genetically complement an *E. coli* Δ*cnoX* mutant, which was obtained from the Keio Collection of *E. coli* marked, single-gene knockouts together with its isogenic progenitor, *E. coli* BW25113 (Baba *et al.*, 2006; Datsenko and Wanner, 2000). Following removal of the Kan^R cassette from the marked Δ*cnoX* mutant, the genotypes of the WT and unmarked Δ*cnoX* mutant was confirmed by PCR (see **Appendix E1**). The strains susceptibility to NaOCl was subsequently examined using survival, disk diffusion, and broth microdilution assays (**Appendix E2**). No significant differences in the HOCl susceptibility of the WT and Δ*cnoX* mutant were, however, observed under any of these assay conditions(**Appendix E2**). The reasons for the lack of sensitivity of the Δ*cnoX* mutant, as reported by Goemans *et al.* (2018a) is not currently clear. Our findings are, nevertheless, consistent with those of Meireles *et al.*, (2020) who were similarly unable to replicate the HOCl-sensitivity phenotype of an *E. coli* Δ*cnoX* null mutant in both the BW25113 and MG1655 genetic backgrounds. Despite extensive attempts at assay optimisation, we were unable to recapitulate the HOCl-sensitivity phenotype of the *E. coli* Δ*cnoX* mutant. This particular project objective was therefore discontinued.

Chapter 5: Discussion

Mycobacteria are exposed to various physical and chemical stress conditions within their natural environments. These include shifts in temperature, pH, oxygen tension and osmolarity, together with exposure to antibiotics or reactive oxygen, nitrogen or chlorine species (Gagneux, 2018; Pereira *et al.*, 2020). Many of these stresses can damage or denature proteins, resulting in their accumulation in unfolded, misfolded and/or aggregated forms that are often inactive or toxic. Microbes have consequently developed a variety of mechanisms to repair or remove damaged proteins, which may otherwise be detrimental to cellular growth and survival (Lupoli *et al.*, 2018; Schramm *et al.*, 2020). In addition to the well-established roles played by ATP-dependent chaperones, disaggregases and proteases such as DnaK, ClpB and ClpP, ATP-independent holdases such as CnoX have recently been shown to play an important role in maintaining the integrity of proteins following exposure to various physical and/or chemical stresses (reviewed by Goemans and Collet, 2019). Despite the high level of conservation of CnoX amongst mycobacterial species (**Figure 3.6**), including in *M. leprae*, *M. lepromatosis*, and *M. ulcerans*, whose genomes have undergone extensive genome decay (Avni *et al.*, 2018; Singh and Cole, 2011; Stinear *et al.*, 2007), the role(s) of the enzyme amongst slow- and fast-growing members of the genus has not been examined to date. To overcome this limitation, we identified the genes encoding orthologs of CnoX in the genomes of both Msm and Mtb and characterised their biochemical properties and physiological roles.

The CnoX enzymes characterised to date contain a Trx and a TPR domain at their N- and C-termini, respectively, and possess one or more of the following activities: (i) thiol-disulphide oxidoreductase activity, (ii) mixed-disulphide bond formation that prevents irreversible thiol oxidation or (iii) holdase activity. While the ability of CnoX family members to act as an oxidoreductase and form mixed disulphides is associated with their Trx domains, holdase activity depends on the proteins TPR domains (Dupuy and Collet, 2021). Our bioinformatics analysis of the Msm and Mtb CnoX orthologs (**Section 3.1**) demonstrated that both proteins possess similar domains and domain architecture to previously studied CnoX proteins (**Figure 3.1**) with the exception of an N-terminal extension (NTE), which appears to be restricted to the CnoX proteins of *Mycobacteria* and other actinobacterial species (**Appendix F**). The NTE is predicted to be intrinsically disordered, a feature that has been shown to facilitate the formation

of oligomers, recruitment and scaffolding of interaction partners, and formation of post-translational modifications in other proteins (van der Lee *et al.*, 2014). When present in small heat shock proteins or holdases, intrinsically disordered regions have been shown to promote proper substrate selection, binding, unfolding and solubilisation, amongst other factors (Bardwell and Jakob, 2012; Sudnitsyna *et al.*, 2012; van der Lee *et al.*, 2014). Additional work will be required to define whether the NTE of the mycobacterial CnoX enzymes posess any of these, or other, properties.

Biochemical analysis of the recombinant mycobacterial CnoX proteins revealed that while both proteins display holdase activity (**Section 3.3.1**), they lack the thiol-disulphide oxidoreductase associated with some CnoX family members (**Section 3.3.2**). The ability of proteins with Trx-domains to function as oxidoreductases depends on the presence of a conserved catalytic motif, CXXC, located at the N-terminus of the second alpha-helix in the domain's Trx-fold (**Section 3.1**). While the first Cys residue of the CXXC motif is essential for oxidoreductase activity, the second Cys can, in certain instances, be replaced with a Ser residue without apparent loss of activity (Fomenko and Gladyshev, 2009). The lack of oxidoreductase activity observed for the Msm and Mtb CnoX proteins is, therefore, likely to be attributable to the absence of the N-terminal Cys (C_{35}) from each protein's catalytic motif ($S_{35}DAS_{38}$ and $S_{35}EVC_{38}$ in Msm and Mtb, respectively). This view is supported by the site-directed mutagenesis studies of Meireles *et al.* (2020), which revealed that substituting S_{35} of the *Ec*CnoX $S_{35}QHC_{38}$ catalytic motif with C_{35} (*Ec*CnoX$_{S35C}$) was sufficient to confer the protein with thiol-disulphide oxidoreductase activity that was absent from the WT protein. Similarly, substituting C_{35} of the *Xf*CnoXs catalytic motif ($C_{35}APC_{38}$) with an A_{35} (*Xf*CnoX$_{C35A}$) abolished the WT protein's thiol-disulphide oxidoreductase activity. Interestingly, while the *Ec*CnoX$_{S35C}$ mutation resulted in the gain of oxidoreductase activity, it simultaneously abolished the protein's holdase activity. The *Xf*CnoX$_{C35A}$ mutant, by contrast, retained its holdase activity following introduction of the C35A mutation, despite losing oxidoreductase activity. Taken together, these observations suggest that the biochemical properties of CnoX enzymes are connected, with the number of redox-active Cys residues in the protein's Trx domain influencing both oxidoreductase and holdase activities, albeit in a species-specific manner (Meireles *et al.*, 2020). In future it would be of interest to determine the effects of replacing one or both of the Ser residues in the catalytic

motifs of the *Mt*CnoX and *Ms*CnoX proteins with Cys to confirm the association between the absence of C_{35} and lack of oxidoreductase activity, and to establish whether the proteins holdase activity is also affected (i.e. unchanged, enhanced, or inhibited). These studies may provide insights into why the catalytically active $C_{35}XXC_{38}$ motif is absent from the CnoX proteins of mycobacterial species, as well as for the selective retention of the $S_{35}XXS_{38}$ or $S_{35}XXC_{38}$ amongst fast- and slow-growing mycobacterial species, respectively (see below).

In addition to the two Cys residues found in the catalytic motif of the protein's Trx-folds, the *Ec*CnoX and XfCnoX contain a third redox-active Cys residue, positioned at amino acid 63. In *Ec*CnoX, C_{63} mediates the formation of mixed-disulphides with oxidised thiol groups in protein substrates, thereby protecting them from irreversible oxidation and promoting their refolding by the GroEL chaperonin (Dupuy *et al.*, 2022; Goemans *et al.*, 2018a). Given the absence of C_{63} from both *Ms*CnoX and *Mt*CnoX, we did not examine the ability of the recombinant enzymes to form mixed-disulphides with other substrate proteins during this study. While *Ms*CnoX lacks any Cys residues, the *Mt*CnoX harbours a single Cys residue equivalent to C_{38} of the *Ec*CnoX. The introduction of a C63A mutation in *Ec*CnoX, however, abolishes the protein's ability to form mixed-disulphides with oxidised substrates despite its retention of C_{38}. Unlike C_{63}, which is located on the protein's surface, C_{38} is buried within the enzyme's active site and is therefore unable to form mixed-disulphides with oxidised substrates (Goemans *et al.,* 2018a). The predicted model of *Mt*CnoX (**Figure 3.3**) suggests that the corresponding C_{38} is equally inaccessible in the *Mt*CnoX protein, which would make its involvement in mixed-disulphide formation unlikely. This assertion would have to be validated via experimental means in future studies, however.

Although the *Ms*CnoX and *Mt*CnoX do not display oxidoreductase activity, our results revealed that they can both function as efficient holdases (**Section 3.3**). In contrast to *Ec*CnoX (Goemans *et al.*, 2018a, 2018b), the holdase activity of the mycobacterial CnoX orthologs does not require pre-activation with HOCl to suppress the heat-induced aggregation of the model substrate, MDH (**Figure 3.10**). In this regard, the Msm and Mtb CnoX proteins resemble that of *C. crescentus* (*Cc*CnoX), which also displays holdase activity in the absence of HOCl. The constitutive activity of the *Cc*CnoX was attributed to the greater surface hydrophobicity of the protein under standard (i.e. non-oxidative) growth conditions, which confers the *Cc*CnoX with

a high affinity for substrate proteins, even without HOCl activation. Since *C. crescentus* inhabits aquatic environments where HOCl is unlikely to be encountered, it was speculated that the biochemical properties of the *Cc*CnoX has been tailored to play a more generalised role in the proteostasis network of the organism, such as protection against heat shock (Meireles *et al.*, 2020). The holdase activity of *Ec*CnoX has, by contrast, been shown to be activated in HOCl-containing environments following chlorination of amino acid residues present in the protein's TPR domain (Goemans *et al.*, 2018a; Meireles *et al.*, 2020). This induces a conformational change in the protein that increases its surface hydrophobicity and affinity for oxidised substrate proteins. The HOCl-dependent activation of the *Ec*CnoX has been proposed to be advantageous to pathogenic organisms such as *E. coli,* which may encounter HOCl produced by phagocytic cells during infection (Goemans *et al.*, 2018a, 2018b). We did not examine the effects of HOCl-activation on the mycobacterial CnoX enzymes during this study, since our attempts to demonstrate HOCl-activated activity for *Ec*CnoX were unsuccessful (data not shown). While holdase activity was observed for the protein without HOCl-activation at high *Ec*CnoX:MDH ratios (**Figure 3.10**), in our hands the activity was neither dose-dependent nor enhanced by pre-exposure to HOCl (data not shown). While the reason for this discrepancy is not clear, it may be related to the differences in the strategies used for the cloning, expression, purification and/or storage of the recombinant *Ec*Cnox protein compared with that used in previous studies. Alternatively, differences in the reagents or methodology used to activate and assay the recombinant *Ec*CnoX may have contributed to our inability to observe holdase activity following HOCl-activation. The MIC values established for HOCl against *E. coli* were, nevertheless, consistent with those previously reported (6 mM; Chen et al., 2021; Gundlach and Winter, 2014) and altering the source of HOCl did not alter the results of our assays. Previous studies demonstrating *Ec*CnoX's ability to suppress protein aggregation following HOCl-activation have also used citrate synthase (CS), as opposed to MDH, as a model substrate. Although some holdases, such as Hsp33, possess a broad substrate-specificity against several proteins that include both CS and MDH (Xu *et al.*, 2010), the substrate-specificity of the *Ec*CnoX may be more limited, thereby impeding our ability to observe holdase activity. The effect(s) of altering this variable, together with others, on *Ec*CnoX's HOCl-dependent holdase activity will have to be determined in future studies. Once established, it would be of interest to also examine the effects of HOCl on the holdase activities of *Ms*CnoX and *Mt*CnoX.

While the *Cc*CnoX displays holdase activity in the absence of HOCl, for instance, its activity is enhanced following HOCl-activation. The physiological significance of this finding is, however, not clear since the WT and *CccnoX* deletion mutant display equal sensitivities to HOCl *in vitro* (Goemans *et al.*, 2018b). The response of the *Ms*CnoX and *Mt*CnoX enzymes to HOCl may be of interest as well, however, given the different environments the two organisms typically inhabit. Our phylogenetic analysis indicated that similar to *Ms*CnoX and *Mt*CnoX, almost all of the mycobacterial CnoX orthologs possess an $S_{35}XXS_{38}[N24]V_{63}$ or $S_{35}XXC_{38}[N24]V_{63}$ motif and consequently belong to Group D CnoX enzymes, for which there are currently no known characterised examples (**Figure 3.6 and Appendix F**). Interestingly, the $S_{35}XXC_{38}[N24]V_{63}$ motif found in the *Mt*CnoX was highly conserved amongst the CnoX proteins from other slow-growing, pathogenic species. The $S_{35}XXS_{38}[N24]V_{63}$ motif found in the *Ms*CnoX was similarly conserved amongst the CnoX proteins from other fast-growing, saprophytic mycobacterial species (**Figure 3.6**). The retention of the $S_{35}XXC_{38}[N24]V_{63}$ motif in the CnoX enzymes from slow- but not fast-growing mycobacterial species, suggests that the C_{38} residue may possess functional significance related to the physiology of the former group of organisms, or the environments in which they reside. Given the differences in the biochemical properties of CnoX enzymes from different species identified to date, it would not be surprising if the activities of the *Ms*CnoX and *Mt*CnoX enzymes have been tailored to meet the unique metabolic, physiological and/or environmental needs of each species.

The holdase activity of the *Ec*CnoX enzymes is associated with its C-terminal, TPR motif-containing domain. An *Ec*CnoX$_{\Delta TPR}$ mutant consequently lacks holdase activity and its expression is unable to reverse the sensitivity of an Δ*Ec*CnoX mutant to HOCl (Goemans *et al.*, 2018a). TPR-motifs present in proteins typically form a solenoid-like structure comprised of two anti-parallel α-helices of approximately equivalent length (Main *et al.*, 2003). Arrays of 3 to 16 such TPR motifs can form a right-handed, super-helical structure with an amphipathic channel that can accommodate the binding of protein interaction partners (Cerveny *et al.*, 2013). Structural studies have shown that *Ec*CnoX contains two similar subdomains, TPR A and TPR B, with each subdomain composed of five α-helices (α-helix 5, 6, 7, 8, 9 and α-helix 10, 11, 12, 13, 14, respectively) (Lin and Wilson, 2011). The first four α-helices (α-helix 5, 6, 7 and 8) of the TPR A sub-domain form two of the four TPR-motifs present in the *Ec*CnoX

enzyme, while the last four α-helices (α-helix 11, 12, 13 and 14) of the TPR B sub-domain form the remaining two TPR-motifs. The remaining two α-helices (α-helix 9 and 10) form an extended two-helix region connecting the TPR A and B subdomains (Lin and Wilson, 2011). Our analysis of the secondary and tertiary structures of the mycobacterial CnoX proteins (**Figures 3.1 and 3.3**) revealed that they contain only three predicted TPR motifs due to the absence of the amino acid residues that comprise α-helix 7 and 8, which comprise the second TPR motif in *Ec*CnoX (**Figure 3.3**). The mycobacterial CnoX enzymes, nevertheless, still display holdase activity, indicating that its presence is not critical for this particular function of the enzymes. Whether other biochemical properties of the proteins, such as their substrate specificity or range, are affected by the absence of this TPR motif, remains to be established.

While the *Ec*CnoX and *Cc*Cnox have been shown to interact with the DnaKJE and/or GroEL chaperones after binding to their oxidised substrates, which promotes their reduction and refolding (Cerveny *et al.*, 2013; Goemans *et al.*, 2018a, 2018b), the interaction partners of the mycobacterial CnoX proteins remains to be determined. In this regard, it is noteworthy that the CnoX enzymes from Msm and Mtb both contain the TPR domain's highly conserved C-terminal α-helix (i.e. α-helix 14), which has been shown to mediate the interaction of *Ec*CnoX with the GroEL chaperone (Dupuy *et al.*, 2022). In contrast to *E. coli,* mycobacterial species contain multiple GroEL-encoding genes (Goyal *et al.*, 2006; Kong *et al.*, 1993; Rao and Lund, 2010). The GroEL1-encoding gene is typically arranged in an operon with that encoding GroES, whereas GroEL2 is encoded separately on the genome. While GroEL2 is retained in all Actinobacterial species, GroEL1 is often absent (Goyal *et al.*, 2006). Consistent with this observation, GroEL2 activity is essential for the growth of both Msm and Mtb, while GroEL1 is dispensable (Hu *et al.*, 2008; Ojha *et al.*, 2005). In contrast to most other mycobacterial species, Msm also contains a third GroEL, whose function has not yet established (Ojha *et al.*, 2005). In line with its observed essentiality, GroEL2 has been proposed to function as the main housekeeping chaperonin in Mycobacteria, where it is responsible for folding substrate proteins both under normal growth conditions and following exposure to stresses such as heat shock (Rao and Lund, 2010). GroEL1, by contrast may have evolved to have more specialised functions, which while not essential for viability may be required following exposure to specific stress conditions (Henderson *et al.*, 2013; Rao and Lund, 2010). In future, it would be

of interest to determine whether the Msm and Mtb CnoX enzymes interact with any of the mycobacterial GroEL proteins, and if so, the role of the C-terminal α-helix in mediating this interaction. Addressing the question of whether the mycobacterial CnoX proteins interact with GroEL may also facilitate the identification of substrates that the proteins transfer to the chaperonin for subsequent folding. While *Ec*CnoX forms mixed-disulphides with oxidised substrates before transferring them to GroEL (Goemans *et al.*, 2018a), the constitutive *Cc*CnoX recognises substrates refolded by GroEL following exposure to thermal stress (Goemans *et al.*, 2018b). The substrates recognised by the mycobacterial CnoX enzymes may differ, however, given the differences in the biochemical properties and enzymatic activities of the proteins compared to *Ec*Cnox and *Cc*CnoX, as discussed above.

While the biochemical properties and enzymatic activities of several CnoX enzymes have been characterised to date, the primary physiological role associated with CnoX activity is the increased survival the proteins confers to *E. coli* during growth in HOCl-containing environments (Goemans *et al.*, 2018a). This particular phenotype could, however, not be reproduced by us during this study. Meireles and co-workers (2020) were similarly unable to observe increased HOCl-sensitivity for an *E. coli cnoX* mutant when compared to the WT strain. The reason for this discrepancy is not clear but may relate to the use of different bacterial strains and/or methodologies during each of these studies. CnoX activity was, by contrast, found to be dispensable for the growth of *C. crescentus* and *P. aeruginosa* under standard growth conditions, as well as after exposure to a variety of physical and chemical stresses (Goemans *et al.*, 2018b; Meireles *et al.*, 2020). In this study, silencing or inactivation of the *MscnoX* gene did not significantly alter the growth or survival of Msm under standard conditions. While *Ms*CnoX was found to be dispensable for bacterial survival at elevated temperatures (**Figure 4.15**) and exposure to several oxidants (HOCl, H_20_2, cumene hydroperoxide, diamide) (**Figures 4.4** and **4.13**), cells with reduced levels or lacking CnoX were sensitised to plumbagin (**Figure 4.4** and **4.13**). Restoring the expression of the *MscnoX* gene in the respective mutants was found to rescue bacterial survival, indicating that this sensitivity was a consequence of the loss of CnoX activity. Naphthoquinones such as plumbagin are redox cycling agents that can undergo a one electron reduction following their uptake into cells, yielding the corresponding semiquinone radical (Bolton *et al.*, 2000; Hassan

and Fridovich, 1979). Under aerobic conditions, the semiquinone radical can react with dioxygen to generate superoxide and subsequently H_20_2, regenerating the oxidised form of the naphthoquinones in the process. Some quinones are also potent electrophiles, which can react with the thiol groups of proteins and non-protein antioxidants or nucleophilic amino groups on proteins and DNA (Bolton *et al.*, 2000). It is therefore conceivable that exposure to plumbagin induces protein damage, either directly by modifying protein functional groups or indirectly by generating ROS, which may contribute to increased proteotoxicity in the Msm mutants with reduced levels of CnoX activity. The Msm *cnoX* KD and KO mutants were, however, not sensitised to other oxidants used in this study, many of which are known to induce similar types of damage to proteins. This observation suggests that CnoX may confer resistance to superoxide and not to redox stress in general. Due to time limitations, we were unable to verify whether the Msm KD and KO mutants are sensitised to other superoxide-generating compounds, such as menadione, pyrogallol, or nitrofurantoin, or exclude that the growth inhibition caused by plumbagin was due to a non-redox-related property of the compound. This will, however, be examined in future studies, together with those designed to examine the effects of various oxidants on the expression levels of CnoX in Msm.

Interestingly, Msm also displayed increased sensitivity to the frontline antibiotics isoniazid and rifampicin following depletion or loss of CnoX in the Msm KD and KO, respectively (**Figures 4.5** and **4.14**). These two antibiotics inhibit bacterial growth via mechanisms that are distinct from each other, as well as plumbagin. Isoniazid is a pro-drug that is activated by the KatG enzyme to form an isonicotinic acyl-NADH complex that inhibits the InhA enoyl reductase enzymes, thereby interfering with mycolic acid biosynthesis (Shoeb *et al.*, 1985; Vilchèze and Jacobs, 2019; Zhang and Yew, 2009). In contrast, rifampicin targets bacteria by binding to the DNA-dependent RNA polymerase β-subunit and inhibiting RNA elongation (Campbell *et al.*, 2001; Unissa and Hanna, 2017). Some mycobacterial antioxidants and members of the proteostasis network, such as mycothiol (Rawat *et al.*, 2002), TrxC (Lin *et al.*, 2016) and ClpB (Harnagel *et al.*, 2021), have been shown to provide protection against various, seemingly unrelated compounds and it is possible that CnoX functions in a similar manner. Recently, it has been suggested that, despite having different cellular targets, bactericidal antibiotics induce cell death via a common mechanism (Belenky *et al.*, 2015; Dwyer *et al.*, 2014; Kohanski *et al.*,

2007). This involves the accumulation of ROS as a result of altered metabolism or respiration in bacterial strains following antibiotic exposure, leading to oxidative damage of proteins and nucleic acids and cell death (Belenky *et al.*, 2015; Dwyer *et al.*, 2014; Kohanski *et al.*, 2007). Several structurally different antibiotics, including isoniazid and rifampicin, have been shown to promote the formation of superoxide and other types of ROS in both Msm and Mtb, which are thought to contribute to the antibiotics bactericidal phenotypes (Fan *et al.*, 2018; McBee *et al.*, 2017; Piccaro *et al.*, 2014; Zeng *et al.*, 2019). CnoX activity may, consequently, be required to protect proteins from oxidative damage caused by elevated ROS levels induced by antibiotic treatment. Direct evidence for this theory is currently lacking, however, and it would have to be confirmed in future studies.

Concluding remarks

A central feature of the virulence of Mtb is its ability to grow and survive within the hostile environments encountered within phagocytic cells and granulomas during infection. An improved understanding of the mechanisms used by Mtb to resist the detrimental effects of host-imposed stresses on cellular components might facilitate the development of new approaches for controlling TB. The results obtained during this study provides initial insights into the potential role of CnoX orthologs in protecting mycobacterial proteins against physical or chemical stresses. The data from our biochemical studies suggest that the Mtb and Msm CnoX enzymes function as constitutive holdases. In Msm, CnoX activity was found to confer protection against small molecules known to generate ROS within the intracellular environment. The Msm CnoX may, consequently, play a role in protecting cellular proteins against oxidative damage and/or denaturation caused by these ROS. This hypothesis will, however, have to be confirmed in future studies. The generation and analysis of Mtb mutants, coupled with additional biochemical studies, will provide greater insights into the physiological role of these enzymes in both slow- and fast- growing mycobacterial species. The findings presented here will serve as a foundation for additional studies that are likely to contribute to a greater understanding of how Mtb and Msm maintain the integrity of their proteomes following exposure to environmental stresses.

Chapter 6: References

Akaike, T., Sato, K., Ijiri, S., Miyamoto, Y., Kohno, M., Ando, M., Maeda, H., 1992. Bactericidal activity of alkyl peroxyl radicals generated by heme-iron-catalyzed decomposition of organic peroxides. *Archives of Biochemistry and Biophysics* 294, 55–63. https://doi.org/10.1016/0003-9861(92)90136-K

Akif, M., Khare, G., Tyagi, A.K., Mande, S.C., Sardesai, A.A., 2008. Functional Studies of Multiple Thioredoxins from *Mycobacterium tuberculosis*. *Journal of Bacteriology* 190, 7087–7095. https://doi.org/10.1128/JB.00159-08

Akiyama, M., Crooke, E., Kornberg, A., 1993. An exopolyphosphatase of *Escherichia coli*. The enzyme and its *ppx* gene in a polyphosphate operon. *Journal of Biological Chemistry* 268, 633–639. https://doi.org/10.1016/S0021-9258(18)54198-3

Allan, R.K., Ratajczak, T., 2011. Versatile TPR domains accommodate different modes of target protein recognition and function. *Cell Stress and Chaperones* 16, 353–367. https://doi.org/10.1007/s12192-010-0248-0

Altschul, S.F., Gish, W., Miller, W., Myers, E.W., Lipman, D.J., 1990. Basic Local Alignment Search Tool. *Journal of Molecular Biology*. 215(3):403-10. https://doi.org/10.1016/S0022-2836(05)80360-2

Armstrong, J.A., Hart, P.D., 1975. Phagosome-lysosome interactions in cultured macrophages infected with virulent tubercle bacilli. Reversal of the usual nonfusion pattern and observations on bacterial survival. *Journal of Experimental Medicine* 142, 1–16. https://doi.org/10.1084/jem.142.1.1

Arnér, E.S.J., Holmgren, A., 2005. Measurement of Thioredoxin and Thioredoxin Reductase. *Current Protocols in Toxicology* 24. https://doi.org/10.1002/0471140856.tx0704s05

Atkinson, H.J., Babbitt, P.C., 2009. An Atlas of the Thioredoxin Fold Class Reveals the Complexity of Function-Enabling Adaptations. *PLoS Computational Biology* 5, e1000541. https://doi.org/10.1371/journal.pcbi.1000541

Attarian, R., Bennie, C., Bach, H., Av-Gay, Y., 2009. Glutathione disulfide and S-nitrosoglutathione detoxification by *Mycobacterium tuberculosis* thioredoxin system. *FEBS Letters* 583, 3215–3220. https://doi.org/10.1016/j.febslet.2009.09.007

Aussel, L., Ezraty, B., 2021. Methionine Redox Homeostasis in Protein Quality Control. *Frontiers in Molecular Biosciences*. 8, 665492. https://doi.org/10.3389/fmolb.2021.665492

Ausubel, F.M., Brent, R., Kingston, R.E., Moore, D.D., Seidman, J.G., Smith, J.A., Struhl, K., 2003. *Current protocols in molecular biology*. Greene Pub. Associates ; J. Wiley, order fulfillment, Brooklyn, N.Y. : Media, Pa.

Avelange-Macherel, M.-H., Rolland, A., Hinault, M.-P., Tolleter, D., Macherel, D., 2019. The Mitochondrial Small Heat Shock Protein HSP22 from Pea is a Thermosoluble Chaperone Prone to Co-Precipitate with Unfolding Client Proteins. *International Journal of Molecular Sciences* 21, 97. https://doi.org/10.3390/ijms21010097

Avni, E., Montoya, D., Lopez, D., Modlin, R., Pellegrini, M., Snir, S., 2018. A phylogenomic study quantifies competing mechanisms for pseudogenization in prokaryotes—The *Mycobacterium leprae* case. *PLoS ONE* 13, e0204322. https://doi.org/10.1371/journal.pone.0204322

Awuh, J.A., Flo, T.H., 2017. Molecular basis of mycobacterial survival in macrophages. *Cellular Molecular Life Sciences*. 74, 1625–1648. https://doi.org/10.1007/s00018-016-2422-8

Baba, S.P., Bhatnagar, A., 2018. Role of thiols in oxidative stress. *Current Opinion in Toxicology* 7, 133–139. https://doi.org/10.1016/j.cotox.2018.03.005

Baba, T., Ara, T., Hasegawa, M., Takai, Y., Okumura, Y., Baba, M., Datsenko, K.A., Tomita, M., Wanner, B.L., Mori, H., 2006. Construction of *Escherichia coli* K-12 in-frame, single-gene knockout mutants: the Keio collection. *Molecular Systems Biology* 2. https://doi.org/10.1038/msb4100050

Bachmann, N.L., Salamzade, R., Manson, A.L., Whittington, R., Sintchenko, V., Earl, A.M., Marais, B.J., 2020. Key Transitions in the Evolution of Rapid and Slow Growing Mycobacteria Identified by Comparative Genomics. *Frontiers in Microbiology* 10, 3019. https://doi.org/10.3389/fmicb.2019.03019

Baek, S.-H., Li, A.H., Sassetti, C.M., 2011. Metabolic Regulation of Mycobacterial Growth and Antibiotic Sensitivity. *PLoS Biology* 9, e1001065. https://doi.org/10.1371/journal.pbio.1001065

Baker, J.J., Dechow, S.J., Abramovitch, R.B., 2019. Acid Fasting: Modulation of *Mycobacterium tuberculosis* Metabolism at Acidic pH. *Trends in Microbiology* 12. https://doi.org/10.1016/j.tim.2019.06.005

Bardwell, J.C.A., Jakob, U., 2012. Conditional disorder in chaperone action 37, 9. *Trends in Biochemical Sciences* 37(12), 517-525. http://dx.doi.org/10.1016/j.tibs.2012.08.006

Barkan, D., Rao, V., Sukenick, G.D., Glickman, M.S., 2010. Redundant Function of *cmaA2* and *mmaA2* in *Mycobacterium tuberculosis* cis Cyclopropanation of Oxygenated Mycolates. *Journal of Bacteriology* 192, 3661–3668. https://doi.org/10.1128/JB.00312-10

Barrette, W.C., Albrich, J.M., Hurst, J.K., 1987. Hypochlorous acid-promoted loss of metabolic energy in *Escherichia coli*. *Infection and Immunity* 55, 2518–2525. https://doi.org/10.1128/iai.55.10.2518-2525.1987

Becker, S.H., Ulrich, K., Dhabaria, A., Ueberheide, B., Beavers, W., Skaar, E.P., Iyer, L.M., Aravind, L., Jakob, U., Darwin, K.H., 2020. *Mycobacterium tuberculosis* Rv0991c Is a Redox-Regulated Molecular Chaperone. *mBio* 11, 18. https://doi.org/10.1128/*mBio*.01545-20

Belenky, P., Ye, J.D., Porter, C.B.M., Cohen, N.R., Lobritz, M.A., Ferrante, T., Jain, S., Korry, B.J., Schwarz, E.G., Walker, G.C., Collins, J.J., 2015. Bactericidal Antibiotics Induce Toxic Metabolic Perturbations that Lead to Cellular Damage. *Cell Reports* 13, 968–980. https://doi.org/10.1016/j.celrep.2015.09.059

Bentley, S.J., Boshoff, A., 2019. *Trypanosoma brucei* J-Protein 2 Functionally Co-Operates with the Cytosolic Hsp70 and Hsp70.4 Proteins. *International Journal of Molecular Sciences* 20, 5843. https://doi.org/10.3390/ijms20235843

Berthet, F.-X., Lagranderie, M., Gounon, P., Laurent-Winter, C., Ensergueix, D., Chavarot, P., Thouron, F., Maranghi, E., Pelicic, V., Portnoï, D., Marchal, G., Gicquel, B., 1998. Attenuation of Virulence by Disruption of the *Mycobacterium tuberculosis erp* Gene. *Science* 282, 759–762. https://doi.org/10.1126/science.282.5389.759

Bhatt, K., Salgame, P., 2007. Host Innate Immune Response to *Mycobacterium tuberculosis*. *Journal of Clinical Immunology* 27, 347–362. https://doi.org/10.1007/s10875-007-9084-0

Bogdan, C., 2015. Nitric oxide synthase in innate and adaptive immunity: an update. *Trends in Immunology* 36, 161–178. https://doi.org/10.1016/j.it.2015.01.003

Bolton, J.L., Trush, M.A., Penning, T.M., Dryhurst, G., Monks, T.J., 2000. Role of Quinones in Toxicology. *Chemical Research in Toxicology* 13, 135–160. https://doi.org/10.1021/tx9902082

Bosch, B., DeJesus, M.A., Poulton, N.C., Zhang, W., Engelhart, C.A., Zaveri, A., Lavalette, S., Ruecker, N., Trujillo, C., Wallach, J.B., Li, S., Ehrt, S., Chait, B.T., Schnappinger, D., Rock, J.M., 2021. Genome-wide gene expression tuning reveals diverse vulnerabilities of *M. tuberculosis*. *Cell* 184, 4579-4592.e24. https://doi.org/10.1016/j.cell.2021.06.033

Boshoff, H.I.M., Barry, C.E., 2005. Tuberculosis — metabolism and respiration in the absence of growth. *Nature Reviews Microbiology* 3, 70–80. https://doi.org/10.1038/nrmicro1065

Bouley, D.M., Ghori, N., Mercer, K.L., Falkow, S., Ramakrishnan, L., 2001. Dynamic Nature of Host-Pathogen Interactions in *Mycobacterium marinum* Granulomas. *Infection and Immunity* 69, 7820–7831. https://doi.org/10.1128/IAI.69.12.7820-7831.2001

Buchmeier, N.A., Newton, G.L., Fahey, R.C., 2006. A Mycothiol Synthase Mutant of *Mycobacterium tuberculosis* Has an Altered Thiol-Disulfide Content and Limited Tolerance to Stress. *Journal of Bacteriology* 188, 6245–6252. https://doi.org/10.1128/JB.00393-06

Buchmeier, N.A., Newton, G.L., Koledin, T., Fahey, R.C., 2003. Association of mycothiol with protection of *Mycobacterium tuberculosis* from toxic oxidants and antibiotics: Mycothiol protection of *Mycobacterium tuberculosis*. *Molecular Microbiology* 47, 1723–1732. https://doi.org/10.1046/j.1365-2958.2003.03416.x

Burger, A., Ludewig, M.H., Boshoff, A., 2014. Investigating the Chaperone Properties of a Novel Heat Shock Protein, Hsp70.c, from *Trypanosoma brucei*. *Journal of Parasitology Research* 2014, 1–12. https://doi.org/10.1155/2014/172582

Bussi, C., Gutierrez, M.G., 2019. *Mycobacterium tuberculosis* infection of host cells in space and time. *FEMS Microbiology Reviews* 43, 341–361. https://doi.org/10.1093/femsre/fuz006

Camacho, L.R., Ensergueix, D., Perez, E., Gicquel, B., Guilhot, C., 1999. Identification of a virulence gene cluster of *Mycobacterium tuberculosis* by signature-tagged transposon mutagenesis. *Molecular Microbiology* 34, 257–267. https://doi.org/10.1046/j.1365-2958.1999.01593.x

Campbell, E.A., Korzheva, N., Mustaev, A., Murakami, K., Nair, S., Goldfarb, A., Darst, S.A., 2001. Structural Mechanism for Rifampicin Inhibition of Bacterial RNA Polymerase. *Cell* 104, 901–912. https://doi.org/10.1016/S0092-8674(01)00286-0

Carranza, C., Chavez-Galan, L., 2019. Several Routes to the Same Destination: Inhibition of Phagosome-Lysosome Fusion by *Mycobacterium tuberculosis*. *The American Journal of the Medical Sciences* 357, 184–194. https://doi.org/10.1016/j.amjms.2018.12.003

Cerveny, L., Straskova, A., Dankova, V., Hartlova, A., Ceckova, M., Staud, F., Stulik, J., 2013. Tetratricopeptide Repeat Motifs in the World of Bacterial Pathogens: Role in Virulence Mechanisms. *Infection and Immunity* 81, 629–635. https://doi.org/10.1128/IAI.01035-12

Chen, H., Wilson, J., Ercanbrack, C., Smith, H., Gan, Q., Fan, C., 2021. Genome-Wide Screening of Oxidizing Agent Resistance Genes in *Escherichia coli*. *Antioxidants* 10, 861. https://doi.org/10.3390/antiox10060861

Cirillo, D.M., Ghodousi, A., Tortoli, E., 2021. *Mycobacterium tuberculosis*: The Organism's Genomics and Evolution, in: Migliori, G.B., Raviglione, M.C. (Eds.), Essential Tuberculosis. Springer International Publishing, Cham, pp. 11–17. https://doi.org/10.1007/978-3-030-66703-0_2

Claiborne, A., Malinowski, D.P., Fridovich, I., 1979. Purification and characterization of hydroperoxidase II of *Escherichia coli* B. *Journal of Biological Chemistry* 254, 11664–11668. https://doi.org/10.1016/S0021-9258(19)86535-3

Cohen, S.B., Gern, B.H., Delahaye, J.L., Adams, K.N., Plumlee, C.R., Winkler, J.K., Sherman, D.R., Gerner, M.Y., Urdahl, K.B., 2018. Alveolar Macrophages Provide an Early *Mycobacterium tuberculosis* Niche and Initiate Dissemination. *Cell Host & Microbe* 24, 439-446.e4. https://doi.org/10.1016/j.chom.2018.08.001

Colditz, G.A., 1994. Efficacy of BCG Vaccine in the Prevention of Tuberculosis: Meta-analysis of the Published Literature. *JAMA* 271, 698. https://doi.org/10.1001/jama.1994.03510330076038

Collet, J.-F., Messens, J., 2010. Structure, Function, and Mechanism of Thioredoxin Proteins. *Antioxidants & Redox Signaling* 13, 1205–1216. https://doi.org/10.1089/ars.2010.3114

Cook, G.M., Berney, M., Gebhard, S., Heinemann, M., Cox, R.A., Danilchanka, O., Niederweis, M., 2009. Physiology of Mycobacteria, in: Advances in Microbial Physiology. *Elsevier*, pp. 81–319. https://doi.org/10.1016/S0065-2911(09)05502-7

Coulson, G.B., Johnson, B.K., Zheng, H., Colvin, C.J., Fillinger, R.J., Haiderer, E.R., Hammer, N.D., Abramovitch, R.B., 2017. Targeting *Mycobacterium tuberculosis* Sensitivity to Thiol Stress at Acidic pH Kills the Bacterium and Potentiates Antibiotics. *Cell Chemical Biology* 24, 993-1004.e4. https://doi.org/10.1016/j.chemBiol.2017.06.018

Cremers, C.M., Knoefler, D., Vitvitsky, V., Banerjee, R., Jakob, U., 2014. Bile salts act as effective protein-unfolding agents and instigators of disulfide stress in vivo. *Proceedings of the National Academy of Sciences* 111, E1610–E1619. https://doi.org/10.1073/pnas.1401941111

Cronan, M.R., 2022. In the Thick of It: Formation of the Tuberculous Granuloma and Its Effects on Host and Therapeutic Responses. *Frontiers in Immunology* 13, 820134. https://doi.org/10.3389/fimmu.2022.820134

Crooks, G.E., Hon, G., Chandonia, J.-M., Brenner, S.E., 2004. WebLogo: A Sequence Logo Generator 3. *Genome Research* 14(6), 1188-1190. http://genome.cshlp.org/lookup/doi/10.1101/gr.849004

Dahl, J.-U., Gray, M.J., Jakob, U., 2015. Protein Quality Control under Oxidative Stress Conditions. *Journal of Molecular Biology* 427, 1549–1563. https://doi.org/10.1016/j.jmb.2015.02.014

Danelishvili, L., Shulzhenko, N., Chinison, J.J.J., Babrak, L., Hu, J., Morgun, A., Burrows, G., Bermudez, L.E., 2017. *Mycobacterium tuberculosis* Proteome Response to Antituberculosis Compounds Reveals Metabolic

"Escape" Pathways That Prolong Bacterial Survival. *Antimicrobial Agents and Chemotherapy* 61. https://doi.org/10.1128/AAC.00430-17

Davis, J.M., Clay, H., Lewis, J.L., Ghori, N., Herbomel, P., Ramakrishnan, L., 2002. Real-Time Visualization of Mycobacterium-Macrophage Interactions Leading to Initiation of Granuloma Formation in Zebrafish Embryos. *Immunity* 17, 693–702. https://doi.org/10.1016/S1074-7613(02)00475-2

de Wet, T.J., Gobe, I., Mhlanga, M.M., Warner, D.F., 2018. CRISPRi-Seq for the Identification and Characterisation of Essential Mycobacterial Genes and Transcriptional Units (preprint). *Microbiology*. https://doi.org/10.1101/358275

de Wet, T.J., Winkler, K.R., Mhlanga, M.M., Mizrahi, V., Warner, D.F., 2020. Arrayed CRISPRi and Quantitative Imaging Describe the Morphotypic Landscape of Essential Mycobacterial Genes (preprint). *Microbiology.* https://doi.org/10.1101/2020.03.20.000372

DeJesus, M.A., Gerrick, E.R., Xu, W., Park, S.W., Long, J.E., Boutte, C.C., Rubin, E.J., Schnappinger, D., Ehrt, S., Fortune, S.M., Sassetti, C.M., Ioerger, T.R., 2017. Comprehensive Essentiality Analysis of the *Mycobacterium tuberculosis* Genome via Saturating Transposon Mutagenesis. *mBio* 8, e02133-16. https://doi.org/10.1128/*mBio*.02133-16

Diaz, G.A., Wayne, L.G., 1974. Isolation and Characterization of Catalase Produced by *Mycobacterium tuberculosis* 1. *American Review of Respiratory Disease* 110, 312–319. https://doi.org/10.1164/arrd.1974.110.3.312

Dobson, C.M., Šali, A., Karplus, M., 1998. Protein Folding: A Perspective from Theory and Experiment. *Angewandte Chemie International Edition* 37, 868–893. https://doi.org/10.1002/(SICI)1521-3773(19980420)37:7<868::AID-ANIE868>3.0.CO;2-H

Dragset, M.S., Ioerger, T.R., Zhang, Y.J., Mærk, M., Ginbot, Z., Sacchettini, J.C., Flo, T.H., Rubin, E.J., Steigedal, M., 2019. Genome-wide Phenotypic Profiling Identifies and Categorizes Genes Required for Mycobacterial Low Iron Fitness. *Scientific Reports* 9, 11394. https://doi.org/10.1038/s41598-019-47905-y

Drazic, A., Kutzner, E., Winter, J., Eisenreich, W., 2015. Metabolic Response of *Escherichia coli* upon Treatment with Hypochlorite at Sub-Lethal Concentrations. *PLoS ONE* 10, e0125823. https://doi.org/10.1371/journal.pone.0125823

Dupuy, E., Collet, J.-F., 2021. Fort CnoX: Protecting Bacterial Proteins From Misfolding and Oxidative Damage. *Frontiers in Molecular Biosciences* 8, 681932. https://doi.org/10.3389/fmolb.2021.681932

Dupuy, E., Van der Verren, S.E., Lin, J., Wilson, M.A., Dachsbeck, A., Viela, F., Latour, E., Gennaris, A., Vertommen, D., Dufrêne, Y.F., Iorga, B.I., Goemans, C.V., Remaut, H., Collet, J.-F., 2022. A molecular plugin rescues GroEL/ES substrates from pre-folding oxidation (preprint). *Biochemistry*. https://doi.org/10.1101/2022.05.03.490446

Dussurget, O., Stewart, G., Neyrolles, O., Pescher, P., Young, D., Marchal, G., 2001. Role of *Mycobacterium tuberculosis* Copper-Zinc Superoxide Dismutase. *Infection and Immunity* 69, 529–533. https://doi.org/10.1128/IAI.69.1.529-533.2001

Dwyer, D.J., Belenky, P.A., Yang, J.H., MacDonald, I.C., Martell, J.D., Takahashi, N., Chan, C.T.Y., Lobritz, M.A., Braff, D., Schwarz, E.G., Ye, J.D., Pati, M., Vercruysse, M., Ralifo, P.S., Allison, K.R., Khalil, A.S., Ting, A.Y., Walker, G.C., Collins, J.J., 2014. Antibiotics induce redox-related physiological alterations as part of their lethality. *Proceedings of the National Academy of Sciences*. 111. https://doi.org/10.1073/pnas.1401876111

Edgar, R.C., 2004. MUSCLE: multiple sequence alignment with high accuracy and high throughput. *Nucleic Acids Research* 32, 1792–1797. https://doi.org/10.1093/nar/gkh340

Edwards, K.M., Cynamon, M.H., Voladri, R.K.R., Hager, C.C., DeSTEFANO, M.S., Tham, K.T., Lakey, D.L., Bochan, M.R., Kernodle, D.S., 2001. Iron-cofactored Superoxide Dismutase Inhibits Host Responses to *Mycobacterium tuberculosis*. *American Journal of Respiratory and Critical Care Medicine* 164, 2213–2219. https://doi.org/10.1164/ajrccm.164.12.2106093

Ehrt, S., Guo, X.V., Hickey, C.M., Ryou, M., Monteleone, M., Riley, L.W., Schnappinger, 2005. Controlling gene expression in mycobacteria with anhydrotetracycline and Tet repressor. *Nucleic Acids Research* 33, e21–e21. https://doi.org/10.1093/nar/gni013

Ehrt, S., Schnappinger, D., 2009. Mycobacterial survival strategies in the phagosome: defence against host stresses. *Cellular Microbiology* 11, 1170–1178. https://doi.org/10.1111/j.1462-5822.2009.01335.x

Evans, J.C., Mizrahi, V., 2015. The application of tetracycline regulated gene expression systems in the validation of novel drug targets in *Mycobacterium tuberculosis*. *Frontiers in Microbiology* 6. https://doi.org/10.3389/fmicb.2015.00812

Ezraty, B., Gennaris, A., Barras, F., Collet, J.-F., 2017. Oxidative stress, protein damage and repair in bacteria. *Nature Reviews Microbiology* 15, 385–396. https://doi.org/10.1038/nrmicro.2017.26

Fan, X.-Y., Tang, B.-K., Xu, Y.-Y., Han, A.-X., Shi, K.-X., Wu, Y.-K., Ye, Y., Wei, M., Niu, C., Wong, K.-W., Zhao, G.-P., Lyu, L.-D., 2018. Oxidation of dCTP contributes to antibiotic lethality in stationary-phase mycobacteria. *Proceedings of the National Academy of Sciences*. 115, 2210–2215. https://doi.org/10.1073/pnas.1719627115

Fay, A., Glickman, M.S., 2014. An Essential Nonredundant Role for Mycobacterial DnaK in Native Protein Folding. *PLoS Genetics* 10, e1004516. https://doi.org/10.1371/journal.pgen.1004516

Flynn, J.L., Chan, J., Lin, P.L., 2011. Macrophages and control of granulomatous inflammation in tuberculosis. *Mucosal Immunology* 4, 271–278. https://doi.org/10.1038/mi.2011.14

Fomenko, D.E., Gladyshev, V.N., 2009. CxxS: Fold-independent redox motif revealed by genome-wide searches for thiol/disulfide oxidoreductase function. *Protein Science* 11, 2285–2296. https://doi.org/10.1110/ps.0218302

Forrellad, M.A., Klepp, L.I., Gioffré, A., Sabio y García, J., Morbidoni, H.R., Santangelo, M. de la P., Cataldi, A.A., Bigi, F., 2013. Virulence factors of the *Mycobacterium tuberculosis* complex. *Virulence* 4, 3–66. https://doi.org/10.4161/viru.22329

Frees, D., Gerth, U., Ingmer, H., 2014. Clp chaperones and proteases are central in stress survival, virulence and antibiotic resistance of *Staphylococcus aureus*. *International Journal of Medical Microbiology* 304, 142–149. https://doi.org/10.1016/j.ijmm.2013.11.009

Gagneux, S., 2018. Ecology and evolution of *Mycobacterium tuberculosis*. *Nature Reviews Microbiology* 16, 202–213. https://doi.org/10.1038/nrmicro.2018.8

Ganbat, D., Seehase, S., Richter, E., Vollmer, E., Reiling, N., Fellenberg, K., Gaede, K.I., Kugler, C., Goldmann, T., 2016. Mycobacteria infect different cell types in the human lung and cause species dependent cellular changes in infected cells. *BMC Pulmonary Medicine* 16, 19. https://doi.org/10.1186/s12890-016-0185-5

Gasteiger, E., Hoogland, C., Gattiker, A., Duvaud, S., Wilkins, M.R., Appel, R.D., Bairoch, A., 2005. Protein Identification and Analysis Tools on the ExPASy Server, in: Walker, J.M. (Ed.), The Proteomics Protocols Handbook. Humana Press, Totowa, NJ, pp. 571–607. https://doi.org/10.1385/1-59259-890-0:571

Genest, O., Hoskins, J.R., Camberg, J.L., Doyle, S.M., Wickner, S., 2011. Heat shock protein 90 from *Escherichia coli* collaborates with the DnaK chaperone system in client protein remodeling. *Proceedings of the National Academy of Sciences*. 108, 8206–8211. https://doi.org/10.1073/pnas.1104703108

Goddard, T.D., Huang, C.C., Meng, E.C., Pettersen, E.F., Couch, G.S., Morris, J.H., Ferrin, T.E., 2018. UCSF ChimeraX: Meeting modern challenges in visualization and analysis: UCSF ChimeraX Visualization System. *Protein Science* 27, 14–25. https://doi.org/10.1002/pro.3235

Goemans, C.V., Beaufay, F., Arts, I.S., Agrebi, R., Vertommen, D., Collet, J.-F., 2018b. The Chaperone and Redox Properties of CnoX Chaperedoxins Are Tailored to the Proteostatic Needs of Bacterial Species. *mBio* 9. https://doi.org/10.1128/*mBio*.01541-18

Goemans, C.V., Collet, J.-F., 2019. Stress-induced chaperones: a first line of defense against the powerful oxidant hypochlorous acid. *F1000 Research* 8, 1678. https://doi.org/10.12688/f1000research.19517.1

Goemans, C.V., Vertommen, D., Agrebi, R., Collet, J.-F., 2018a. CnoX Is a Chaperedoxin: A Holdase that Protects Its Substrates from Irreversible Oxidation. *Molecular Cell* 70, 614-627.e7. https://doi.org/10.1016/j.molcel.2018.04.002

Goodfellow, M., Kämpfer, P., Busse, H.-J., Trujillo, M.E., Suzuki, K., Ludwig, W., Whitman, W.B. (Eds.), 2012. Bergey's Manual® of Systematic Bacteriology. Springer New York, New York, NY. https://doi.org/10.1007/978-0-387-68233-4

Goren, M.B., Brokl, M.C.O., 1978. Some Observations on Mycobacterial Acid-Fastness. *American Review of Respiratory Disease* 1. https://doi.org/10.1164/arrd.1978.118.1.151

Goude, R., Roberts, D.M., Parish, T., 2015. Electroporation of Mycobacteria, in: Parish, T., Roberts, D.M. (Eds.), Mycobacteria Protocols, Methods in Molecular Biology. Springer New York, New York, NY, pp. 117–130. https://doi.org/10.1007/978-1-4939-2450-9_7

Goyal, K., Qamra, R., Mande, S.C., 2006. Multiple Gene Duplication and Rapid Evolution in the groEL Gene: Functional Implications. *Journal of Molecular Evolution* 63(6), 781-787. https://doi.org/10.1007/s00239-006-0037-7

Graumann, J., Lilie, H., Tang, X., Tucker, K.A., Hoffmann, J.H., Vijayalakshmi, J., Saper, M., Bardwell, J.C.A., Jakob, U., 2001. Activation of the Redox-Regulated Molecular Chaperone Hsp33—A Two-Step Mechanism. *Structure* 9, 377–387. https://doi.org/10.1016/S0969-2126(01)00599-8

Gray, M.J., Wholey, W.-Y., Jakob, U., 2013. Bacterial Responses to Reactive Chlorine Species. *Annual Review of Microbiology* 67, 141–160. https://doi.org/10.1146/annurev-micro-102912-142520

Gray, M.J., Wholey, W.-Y., Wagner, N.O., Cremers, C.M., Mueller-Schickert, A., Hock, N.T., Krieger, A.G., Smith, E.M., Bender, R.A., Bardwell, J.C.A., Jakob, U., 2014. Polyphosphate Is a Primordial Chaperone. *Molecular Cell* 53, 689–699. https://doi.org/10.1016/j.molcel.2014.01.012

Gundlach, J., Winter, J., 2014. Evolution of *Escherichia coli* for maximum HOCl resistance through constitutive expression of the OxyR regulon. *Microbiology* 160, 1690–1704. https://doi.org/10.1099/mic.0.074815-0

Harnagel, A., Lopez Quezada, L., Park, S.W., Baranowski, C., Kieser, K., Jiang, X., Roberts, J., Vaubourgeix, J., Yang, A., Nelson, B., Fay, A., Rubin, E., Ehrt, S., Nathan, C., Lupoli, T.J., 2021. Nonredundant functions of *Mycobacterium tuberculosis* chaperones promote survival under stress. *Molecular Microbiology* 115, 272–289. https://doi.org/10.1111/mmi.14615

Hartl, F.U., Hayer-Hartl, M., 2002. Molecular Chaperones in the Cytosol: from Nascent Chain to Folded Protein. *Science* 295, 1852–1858. https://doi.org/10.1126/science.1068408

Hartman, D.J., Surin, B.P., Dixon, N.E., Hoogenraad, N.J., Høj, P.B., 1993. Substoichiometric amounts of the molecular chaperones GroEL and GroES prevent thermal denaturation and aggregation of mammalian mitochondrial malate dehydrogenase in vitro. *Proceedings of the National Academy of Sciences*, 90(6), 2276-2280. https://doi.org/10.1073/pnas.90.6.2276

Hasday, J.D., Thompson, C., Singh, I.S., 2014. Fever, Immunity, and Molecular Adaptations, in: Terjung, R. (Ed.), Comprehensive Physiology. John Wiley & Sons, Inc., Hoboken, NJ, USA, pp. 109–148. https://doi.org/10.1002/cphy.c130019

Hassan, H.M., Fridovich, I., 1979. Intracellular production of superoxide radical and of hydrogen peroxide by redox active compounds. *Archives of Biochemistry and Biophysics* 196, 385–395. https://doi.org/10.1016/0003-9861(79)90289-3

Henderson, B., Fares, M.A., Lund, P.A., 2013. Chaperonin 60: a paradoxical, evolutionarily conserved protein family with multiple moonlighting functions: Moonlighting chaperonin 60. *Biological Reviews* 88, 955–987. https://doi.org/10.1111/brv.12037

Hett, E.C., Rubin, E.J., 2008. Bacterial Growth and Cell Division: a Mycobacterial Perspective. *Microbiology and Molecular Biology Reviews* 72, 126–156. https://doi.org/10.1128/MMBR.00028-07

Hoffmann, J.H., Linke, K., Graf, P.C., Lilie, H., Jakob, U., 2004. Identification of a redox-regulated chaperone network. *EMBO Journal* 23, 160–168. https://doi.org/10.1038/sj.emboj.7600016

Hogan, A.B., Jewell, B.L., Sherrard-Smith, E., Vesga, J.F., Watson, O.J., Whittaker, C., Hamlet, A., Smith, J.A., Winskill, P., Verity, R., Baguelin, M., Lees, J.A., Whittles, L.K., Ainslie, K.E.C., Bhatt, S., Boonyasiri, A., Brazeau, N.F., Cattarino, L., Cooper, L.V., Coupland, H., Cuomo-Dannenburg, G., Dighe, A., Djaafara, B.A., Donnelly, C.A., Eaton, J.W., van Elsland, S.L., FitzJohn, R.G., Fu, H., Gaythorpe, K.A.M., Green, W., Haw, D.J., Hayes, S., Hinsley, W., Imai, N., Laydon, D.J., Mangal, T.D., Mellan, T.A., Mishra, S., Nedjati-

Gilani, G., Parag, K.V., Thompson, H.A., Unwin, H.J.T., Vollmer, M.A.C., Walters, C.E., Wang, H., Wang, Y., Xi, X., Ferguson, N.M., Okell, L.C., Churcher, T.S., Arinaminpathy, N., Ghani, A.C., Walker, P.G.T., Hallett, T.B., 2020. Potential impact of the COVID-19 pandemic on HIV, tuberculosis, and malaria in low-income and middle-income countries: a modelling study. *The Lancet Global Health* 8, e1132–e1141. https://doi.org/10.1016/S2214-109X(20)30288-6

Holmgren, A., 1995. Thioredoxin structure and mechanism: conformational changes on oxidation of the active-site sulfhydryls to a disulfide. *Structure* 3, 239–243. https://doi.org/10.1016/S0969-2126(01)00153-8

Holmgren, A., 1985. THIOREDOXIN. *Annual Review of Biochemistry* 54, 237–271. https://doi.org/10.1146/annurev.bi.54.070185.001321

Holmgren, A., 1979. Thioredoxin catalyzes the reduction of insulin disulfides by dithiothreitol and dihydrolipoamide. *Journal of Biological Chemistry* 254, 9627–9632. https://doi.org/10.1016/S0021-9258(19)83562-7

Holmgren, A., Söderberg, B.O., Eklund, H., Brändén, C.I., 1975. Three-dimensional structure of *Escherichia coli* thioredoxin-S2 to 2.8 A resolution. *Proceedings of the National Academy of Sciences*. 72, 2305–2309. https://doi.org/10.1073/pnas.72.6.2305

Hu, Y., Henderson, B., Lund, P.A., Tormay, P., Ahmed, M.T., Gurcha, S.S., Besra, G.S., Coates, A.R.M., 2008. A *Mycobacterium tuberculosis* Mutant Lacking the *groEL* Homologue *cpn60.1* Is Viable but Fails To Induce an Inflammatory Response in Animal Models of Infection. *Infection and Immunity* 76, 12. https://doi.org/10.1128/iai.01078-07

Huff, J., Czyz, A., Landick, R., Niederweis, M., 2010. Taking phage integration to the next level as a genetic tool for mycobacteria. *Gene* 468, 8–19. https://doi.org/10.1016/j.gene.2010.07.012

Inoue, H., Nojima, H., Okayama, H., 1990. High efficiency transformation of *Escherichia coli* with plasmids. *Gene* 96, 23–28. https://doi.org/10.1016/0378-1119(90)90336-P

Jakob, U., Muse, W., Eser, M., Bardwell, J.C.A., 1999. Chaperone Activity with a Redox Switch. *Cell* 96, 341–352. https://doi.org/10.1016/S0092-8674(00)80547-4

Judd, J.A., Canestrari, J., Clark, R., Joseph, A., Lapierre, P., Lasek-Nesselquist, E., Mir, M., Palumbo, M., Smith, C., Stone, M., Upadhyay, A., Wirth, S.E., Dedrick, R.M., Meier, C.G., Russell, D.A., Dills, A., Dove, E., Kester, J., Wolf, I.D., Zhu, J., Rubin, E.R., Fortune, S., Hatfull, G.F., Gray, T.A., Wade, J.T., Derbyshire, K.M., 2021. A Mycobacterial Systems Resource for the Research Community. *mBio* 12. https://doi.org/10.1128/*mBio*.02401-20

Khabibullina, N.F., Kutuzova, D.M., Burmistrova, I.A., Lyadova, I.V., 2022. The Biological and Clinical Aspects of a Latent Tuberculosis Infection. TropicalMed 7, 48. https://doi.org/10.3390/tropicalmed7030048

Khor, H.K., Fisher, M.T., Schöneich, C., 2004. Potential Role of Methionine Sulfoxide in the Inactivation of the Chaperone GroEL by Hypochlorous Acid (HOCl) and Peroxynitrite (ONOO–). *Journal of Biological Chemistry* 279, 19486–19493. https://doi.org/10.1074/jbc.M310045200

Kim, C.-J., Kim, N.-H., Song, K.-H., Choe, P.G., Kim, E.S., Park, S.W., Kim, H.-B., Kim, N.-J., Kim, E.-C., Park, W.B., Oh, M., 2013. Differentiating rapid- and slow-growing mycobacteria by difference in time to growth detection in liquid media. *Diagnostic Microbiology and Infectious Disease* 75, 73–76. https://doi.org/10.1016/j.diagmicrobio.2012.09.019

Kinsella, R.L., Zhu, D.X., Harrison, G.A., Mayer Bridwell, A.E., Prusa, J., Chavez, S.M., Stallings, C.L., 2021. Perspectives and Advances in the Understanding of Tuberculosis. *Annual Review of Pathology: Mechanisms of Disease* 16, 377–408. https://doi.org/10.1146/annurev-pathol-042120-032916

Kirakosyan, G., Bagramyan, K., Trchounian, A., 2004. Redox sensing by *Escherichia coli*: effects of dithiothreitol, a redox reagent reducing disulphides, on bacterial growth. *Biochemical and Biophysical Research Communications* 325, 803–806. https://doi.org/10.1016/j.bbrc.2004.10.119

Kohanski, M.A., Dwyer, D.J., Hayete, B., Lawrence, C.A., Collins, J.J., 2007. A Common Mechanism of Cellular Death Induced by Bactericidal Antibiotics. *Cell* 130, 797–810. https://doi.org/10.1016/j.cell.2007.06.049

Kolbe, K., Bell, A.C., Prosser, G.A., Assmann, M., Yang, H.-J., Forbes, H.E., Gallucci, S., Mayer-Barber, K.D., Boshoff, H.I., Barry III, C.E., 2020. Development and Optimization of Chromosomally-Integrated

Fluorescent *Mycobacterium tuberculosis* Reporter Constructs. *Frontiers in Microbiology* 11, 591866. https://doi.org/10.3389/fmicb.2020.591866

Kong, T.H., Coates, A.R., Butcher, P.D., Hickman, C.J., Shinnick, T.M., 1993. *Mycobacterium tuberculosis* expresses two chaperonin-60 homologs. *Proceedings of the National Academy of Sciences*. 90, 2608–2612. https://doi.org/10.1073/pnas.90.7.2608

Laemmli, U.K., 1970. Cleavage of Structural Proteins during the Assembly of the Head of Bacteriophage T4. *Nature* 227, 680–685. https://doi.org/10.1038/227680a0

LeBel, M., 1988. Ciprofloxacin: Chemistry, Mechanism of Action, Resistance, Antimicrobial Spectrum, Pharmacokinetics, Clinical Trials, and Adverse Reactions. *Pharmacotherapy: The Journal of Human Pharmacology and Drug Therapy* 8, 3–30. https://doi.org/10.1002/j.1875-9114.1988.tb04058.x

Lee, S.H., 2016. Tuberculosis Infection and Latent Tuberculosis. *Tuberculosis and Respiratory Disease* 79, 201. https://doi.org/10.4046/trd.2016.79.4.201

Lee, W.L., Gold, B., Darby, C., Brot, N., Jiang, X., de Carvalho, L.P.S., Wellner, D., St. John, G., Jacobs Jr, W.R., Nathan, C., 2009. *Mycobacterium tuberculosis* expresses methionine sulphoxide reductases A and B that protect from killing by nitrite and hypochlorite. *Molecular Microbiology* 71, 583–593. https://doi.org/10.1111/j.1365-2958.2008.06548.x

Leemans, J.C., Juffermans, N.P., Florquin, S., van Rooijen, N., Vervoordeldonk, M.J., Verbon, A., van Deventer, S.J.H., van der Poll, T., 2001. Depletion of Alveolar Macrophages Exerts Protective Effects in Pulmonary Tuberculosis in Mice. *Journal of Immunology* 166, 4604–4611. https://doi.org/10.4049/jimmunol.166.7.4604

Lin, J., Wilson, M.A., 2011. *Escherichia coli* Thioredoxin-like Protein YbbN Contains an Atypical Tetratricopeptide Repeat Motif and Is a Negative Regulator of GroEL. *Journal of Biological Chemistry* 286, 19459–19469. https://doi.org/10.1074/jbc.M111.238741

Lin, K., O'Brien, K.M., Trujillo, C., Wang, R., Wallach, J.B., Schnappinger, D., Ehrt, S., 2016. *Mycobacterium tuberculosis* Thioredoxin Reductase Is Essential for Thiol Redox Homeostasis but Plays a Minor Role in Antioxidant Defense. *PLoS Pathogens* 12, e1005675. https://doi.org/10.1371/journal.ppat.1005675

Linley, E., Denyer, S.P., McDonnell, G., Simons, C., Maillard, J.-Y., 2012. Use of hydrogen peroxide as a biocide: new consideration of its mechanisms of biocidal action. *Journal of Antimicrobial Chemotherapy* 67, 1589–1596. https://doi.org/10.1093/jac/dks129

Liu, W., Xie, Y., Ma, J., Luo, X., Nie, P., Zuo, Z., Lahrmann, U., Zhao, Q., Zheng, Y., Zhao, Y., Xue, Y., Ren, J., 2015. IBS: an illustrator for the presentation and visualisation of biological sequences. *Bioinformatics* 31(20):3359-3361. https://doi.org/10.1093/bioinformatics/btv362

Livak, K.J., Schmittgen, T.D., 2001. Analysis of Relative Gene Expression Data Using Real-Time Quantitative PCR and the 2−ΔΔCT Method. *Methods* 25, 402–408. https://doi.org/10.1006/meth.2001.1262

Lory, S., 2014. The Family Mycobacteriaceae, in: Rosenberg, E., DeLong, E.F., Lory, S., Stackebrandt, E., Thompson, F. (Eds.), The Prokaryotes. Springer Berlin Heidelberg, Berlin, Heidelberg, pp. 571–575. https://doi.org/10.1007/978-3-642-30138-4_339

Lovewell, R.R., Baer, C.E., Mishra, B.B., Smith, C.M., Sassetti, C.M., 2021. Granulocytes act as a niche for *Mycobacterium tuberculosis* growth. *Mucosal Immunology* 14, 229–241. https://doi.org/10.1038/s41385-020-0300-z

Lu, S., Wang, J., Chitsaz, F., Derbyshire, M.K., Geer, R.C., Gonzales, N.R., Gwadz, M., Hurwitz, D.I., Marchler, G.H., Song, J.S., Thanki, N., Yamashita, R.A., Yang, M., Zhang, D., Zheng, C., Lanczycki, C.J., Marchler-Bauer, A., 2020. CDD/SPARCLE: the conserved domain database in 2020. *Nucleic Acids Research* 48, D265–D268. https://doi.org/10.1093/nar/gkz991

Lupoli, T.J., Vaubourgeix, J., Burns-Huang, K., Gold, B., 2018. Targeting the Proteostasis Network for Mycobacterial Drug Discovery. *ACS Infectious Diseases* 21. https://doi.org/10.1021/acsinfecdis.7b00231

MacMicking, J.D., Taylor, G.A., McKinney, J.D., 2003. Immune Control of Tuberculosis by IFN-γ-Inducible LRG-47. *Science* 302, 654–659. https://doi.org/10.1126/science.1088063

Main, E.R.G., Xiong, Y., Cocco, M.J., D'Andrea, L., Regan, L., 2003. Design of Stable α-Helical Arrays from an Idealized TPR Motif. *Structure* 11, 497–508. https://doi.org/10.1016/S0969-2126(03)00076-5

Marchler-Bauer, A., Anderson, J.B., Derbyshire, M.K., DeWeese-Scott, C., Gonzales, N.R., Gwadz, M., Hao, L., He, S., Hurwitz, D.I., Jackson, J.D., Ke, Z., Krylov, D., Lanczycki, C.J., Liebert, C.A., Liu, C., Lu, F., Lu, S., Marchler, G.H., Mullokandov, M., Song, J.S., Thanki, N., Yamashita, R.A., Yin, J.J., Zhang, D., Bryant, S.H., 2007. CDD: a conserved domain database for interactive domain family analysis. *Nucleic Acids Research* 35, D237–D240. https://doi.org/10.1093/nar/gkl951

Martin, J.L., 1995. Thioredoxin —a fold for all reasons. *Structure* 3, 245–250. https://doi.org/10.1016/S0969-2126(01)00154-X

Martin, J.L., Bardwell, J.C.A., Kuriyan, J., 1993. Crystal structure of the DsbA protein required for disulphide bond formation in vivo. *Nature* 365, 464–468. https://doi.org/10.1038/365464a0

Martínez, M.C., Andriantsitohaina, R., 2009. Reactive Nitrogen Species: Molecular Mechanisms and Potential Significance in Health and Disease. *Antioxidants & Redox Signaling* 11, 669–702. https://doi.org/10.1089/ars.2007.1993

Master, S.S., Springer, B., Sander, P., Boettger, E.C., Deretic, V., Timmins, G.S., 2002. Oxidative stress response genes in *Mycobacterium tuberculosis*: role of ahpC in resistance to peroxynitrite and stage-specific survival in macrophages. *Microbiology* 148, 3139–3144. https://doi.org/10.1099/00221287-148-10-3139

McBee, M.E., Chionh, Y.H., Sharaf, M.L., Ho, P., Cai, M.W.L., Dedon, P.C., 2017. Production of Superoxide in Bacteria Is Stress- and Cell State-Dependent: A Gating-Optimized Flow Cytometry Method that Minimizes ROS Measurement Artifacts with Fluorescent Dyes. *Frontiers in Microbiology* 8. https://doi.org/10.3389/fmicb.2017.00459

McNeil, M.B., Cook, G.M., 2019. Utilization of CRISPR Interference To Validate MmpL3 as a Drug Target in *Mycobacterium tuberculosis*. *Antimicrobial Agents and Chemotherapy* 63. https://doi.org/10.1128/AAC.00629-19

Meireles, D., Yokomizo, C.H., Netto, L.E.S., 2020. Investigation on the requirements for YbbN/CnoX displaying thiol-disulfide oxidoreductase and chaperone activities (preprint). *Biochemistry*. https://doi.org/10.1101/2020.04.09.034579

Melkani, G.C., McNamara, C., Zardeneta, G., Mendoza, J.A., 2004. Hydrogen peroxide induces the dissociation of GroEL into monomers that can facilitate the reactivation of oxidatively inactivated rhodanese. *The International Journal of Biochemistry & Cell Biology* 36, 505–518. https://doi.org/10.1016/j.biocel.2003.08.012

Mendler, K., Chen, H., Parks, D.H., Lobb, B., Hug, L.A., Doxey, A.C., 2019. AnnoTree: visualization and exploration of a functionally annotated microbial tree of life. *Nucleic Acids Research* 47, 4442–4448. https://doi.org/10.1093/nar/gkz246

Migliori, G.B., Tiberi, S., Zumla, A., Petersen, E., Chakaya, J.M., Wejse, C., Muñoz Torrico, M., Duarte, R., Alffenaar, J.W., Schaaf, H.S., Marais, B.J., Cirillo, D.M., Alagna, R., Rendon, A., Pontali, E., Piubello, A., Figueroa, J., Ferlazzo, G., García-Basteiro, A., Centis, R., Visca, D., D'Ambrosio, L., Sotgiu, G., Arkub, T.A., Akkerman, O.W., Aleksa, A., Belilovski, E., Bernal, E., Blanc, F.-X., Boeree, M., Borisov, S., Bruchfeld, J., Cadiñanos Loidi, J., Caminero, J.A., Carvalho, A.C., Cebrian Gallardo, J.J., Charalampos, Danila, E., Davies Forsman, L., Denholm, J., Dheda, K., Diel, R., Diktanas, S., Dobler, C., Enwerem, M., Esposito, S., Escobar Salinas, N., Filippov, A., Formenti, B., García García, J.M., Goletti, D., Gomez Rosso, R., Gualano, G., Isaakidis, P., Kaluzhenina, A., Koirala, S., Kuksa, L., Kunst, H., Li, Y., Magis-Escurra, C., Manfrin, V., Manga, S., Manika, K., Marchese, V., Martínez Robles, E., Maryandyshev, A., Matteelli, A., Mariani, A., Mazza-Stalder, J., Mello, F., Mendoza, L., Mesi, A., Miliauskas, S., Mustafa Hamdan, H., Ndjeka, N., Nieto Marcos, M., Ottenhoff, T.H.M., Palmero, D.J., Palmieri, F., Papavasileiou, A., Payen, M.C., Pontarelli, A., Pretti Dalcolmo, M., Quirós Fernandez, S., Romero, R., Rossato Silva, D., Santos, A.P., Seaworth, B., Sinitsyn, M., Skrahina, A., Solovic, I., Spanevello, A., Tadolini, M., Torres, C., Udwadia, Z., van den Boom, M., Volchenkov, G.V., Yedilbayev, A., Zaleskis, R., Zellweger, J.P., 2020. MDR/XDR-TB management of patients and contacts: Challenges facing the new decade. The 2020 clinical update by the Global Tuberculosis Network. *International Journal of Infectious Diseases* 92, S15–S25. https://doi.org/10.1016/j.ijid.2020.01.042

Minato, Y., Gohl, D.M., Thiede, J.M., Chacón, J.M., Harcombe, W.R., Maruyama, F., Baughn, A.D., 2019. Genomewide Assessment of *Mycobacterium tuberculosis* Conditionally Essential Metabolic Pathways. *mSystems*, 4(4). https://doi.org/10.1128/msystems.00070-19

Müller, A., Langklotz, S., Lupilova, N., Kuhlmann, K., Bandow, J.E., Leichert, L.I.O., 2014. Activation of RidA chaperone function by N-chlorination. *Nature Communications* 5, 5804. https://doi.org/10.1038/ncomms6804

Nauseef, W.M., 2019. The phagocyte NOX2 NADPH oxidase in microbial killing and cell signaling. Current *Opinion in Immunology* 60, 130–140. https://doi.org/10.1016/j.coi.2019.05.006

Needleman, S.B., Wunsch, C.D., 1970. A General Method Applicable to the Search for Similarities in the Amino Acid Sequence of Two Proteins. *Journal of Molecular Biology*, 48(3), 443-453. https://doi.org/10.1016/0022-2836(70)90057-4

Newton, G.L., Arnold, K., Price, M.S., Sherrill, C., Delcardayre, S.B., Aharonowitz, Y., Cohen, G., Davies, J., Fahey, R.C., Davis, C., 1996. Distribution of thiols in microorganisms: mycothiol is a major thiol in most actinomycetes. *Journal of Bacteriology* 178, 1990–1995. https://doi.org/10.1128/jb.178.7.1990-1995.1996

Newton, G.L., Buchmeier, N., Fahey, R.C., 2008. Biosynthesis and Functions of Mycothiol, the Unique Protective Thiol of Actinobacteria. *Microbiology and Molecular Biology Reviews* 72, 471–494. https://doi.org/10.1128/MMBR.00008-08

Ng, V.H., Cox, J.S., Sousa, A.O., MacMicking, J.D., McKinney, J.D., 2004. Role of KatG catalase-peroxidase in mycobacterial pathogenesis: countering the phagocyte oxidative burst: Role of catalase in mycobacterial pathogenesis. *Molecular Microbiology* 52, 1291–1302. https://doi.org/10.1111/j.1365-2958.2004.04078.x

Ofer, N., Wishkautzan, M., Meijler, M., Wang, Y., Speer, A., Niederweis, M., Gur, E., 2012. Ectoine Biosynthesis in *Mycobacterium smegmatis*. *Applied and Environmental Microbiology* 78, 7483–7486. https://doi.org/10.1128/AEM.01318-12

Ojha, A., Anand, M., Bhatt, A., Kremer, L., Jacobs, W.R., Hatfull, G.F., 2005. GroEL1: A Dedicated Chaperone Involved in Mycolic Acid Biosynthesis during Biofilm Formation in Mycobacteria. *Cell*. https://doi.org/10.1016/j.cell.2005.09.012

Orgeur, M., Brosch, R., 2018. Evolution of virulence in the *Mycobacterium tuberculosis* complex. *Current Opinion in Microbiology* 41, 68–75. https://doi.org/10.1016/j.mib.2017.11.021

Orme, I.M., 2014. A new unifying theory of the pathogenesis of tuberculosis. *Tuberculosis* 94, 8–14. https://doi.org/10.1016/j.tube.2013.07.004

Pagán, A.J., Ramakrishnan, L., 2015. Immunity and Immunopathology in the Tuberculous Granuloma. *Cold Spring Harbour Perspectives in Medicine* 5, a018499. https://doi.org/10.1101/cshperspect.a018499

Parsell, D.A., Kowal, A.S., Singer, M.A., Lindquist, S., 1994. Protein disaggregation mediated by heat-shock protein Hspl04. *Nature* 372, 475–478. https://doi.org/10.1038/372475a0

Paul, B.D., Snyder, S.H., 2010. The unusual amino acid L-ergothioneine is a physiologic cytoprotectant. *Cell Death & Differentiation* 17, 1134–1140. https://doi.org/10.1038/cdd.2009.163

Pereira, A.C., Ramos, B., Reis, A.C., Cunha, M.V., 2020. Non-Tuberculous Mycobacteria: Molecular and Physiological Bases of Virulence and Adaptation to Ecological Niches. *Microorganisms* 8, 1380. https://doi.org/10.3390/microorganisms8091380

Perveen, S., Kumari, D., Singh, K., Sharma, R., 2022. Tuberculosis drug discovery: Progression and future interventions in the wake of emerging resistance. *European Journal of Medicinal Chemistry* 229, 114066. https://doi.org/10.1016/j.ejmech.2021.114066

Pettersen, E.F., Goddard, T.D., Huang, C.C., Meng, E.C., Couch, G.S., Croll, T.I., Morris, J.H., Ferrin, T.E., 2021. UCSF CHIMERAX : Structure visualization for researchers, educators, and developers. *Protein Science* 30, 70–82. https://doi.org/10.1002/pro.3943

Piacenza, L., Trujillo, M., Radi, R., 2019. Reactive species and pathogen antioxidant networks during phagocytosis. *Journal of Experimental Medicine* 216, 501–516. https://doi.org/10.1084/jem.20181886

Piccaro, G., Pietraforte, D., Giannoni, F., Mustazzolu, A., Fattorini, L., 2014. Rifampin Induces Hydroxyl Radical Formation in *Mycobacterium tuberculosis*. *Antimicrobial Agents and Chemotherapy* 58, 7527–7533. https://doi.org/10.1128/AAC.03169-14

Pierpaoli, E.V., Sandmeier, E., Baici, A., 1997. The Power Stroke of the DnaK/DnaJ/GrpE Molecular Chaperone System. *Journal of Molecular Biology* 269(5), 757-768. https://doi.org/10.1006/jmbi.1997.1072

Primm, T.P., Lucero, C.A., Falkinham, J.O., 2004. Health Impacts of Environmental Mycobacteria. *Clinical Microbiologyl Reviews* 17, 98–106. https://doi.org/10.1128/CMR.17.1.98-106.2004

Radi, R., 2013. Protein Tyrosine Nitration: Biochemical Mechanisms and Structural Basis of Functional Effects. *Accounts of Chemical Research.* 46, 550–559. https://doi.org/10.1021/ar300234c

Rahman, I., Gilmour, P.S., Jimenez, L.A., Biswas, S.K., Antonicelli, F., Aruoma, O.I., 2003. Ergothioneine inhibits oxidative stress- and TNF-α-induced NF-κB activation and interleukin-8 release in alveolar epithelial cells. *Biochemical and Biophysical Research Communications* 302, 860–864. https://doi.org/10.1016/S0006-291X(03)00224-9

Rahman, S.A., Singh, Y., Kohli, S., Ahmad, J., Ehtesham, N.Z., Tyagi, A.K., Hasnain, S.E., 2014. Comparative Analyses of Nonpathogenic, Opportunistic, and Totally Pathogenic Mycobacteria Reveal Genomic and Biochemical Variabilities and Highlight the Survival Attributes of *Mycobacterium tuberculosis*. *mBio* 5, e02020-14. https://doi.org/10.1128/*mBio*.02020-14

Raju, R.M., Unnikrishnan, M., Rubin, D.H.F., Krishnamoorthy, V., Kandror, O., Akopian, T.N., Goldberg, A.L., Rubin, E.J., 2012. *Mycobacterium tuberculosis* ClpP1 and ClpP2 Function Together in Protein Degradation and Are Required for Viability in vitro and During Infection. *PLoS Pathogens* 8, e1002511. https://doi.org/10.1371/journal.ppat.1002511

Ramakrishnan, L., 2012. Revisiting the role of the granuloma in tuberculosis. *Nature Reviews Immunology* 12, 352–366. https://doi.org/10.1038/nri3211

Ramakrishnan, L., Federspiel, N.A., Falkow, S., 2000. Granuloma-Specific Expression of Mycobacterium Virulence Proteins from the Glycine-Rich PE-PGRS Family. 288, 1436–1439. https://doi.org/10.1126/science.288.5470.1436

Rankine-Wilson, L.I., Shapira, T., Sao Emani, C., Av-Gay, Y., 2021. From infection niche to therapeutic target: the intracellular lifestyle of *Mycobacterium tuberculosis*. *Microbiology* 167. https://doi.org/10.1099/mic.0.001041

Rao, T., Lund, P.A., 2010. Differential expression of the multiple chaperonins of *Mycobacterium smegmatis*: Chaperonin expression in *Mycobacterium smegmatis*. *FEMS Microbiology Letters* 310, 24–31. https://doi.org/10.1111/j.1574-6968.2010.02039.x

Ravesloot-Chávez, M.M., Van Dis, E., Stanley, S.A., 2021. The Innate Immune Response to *Mycobacterium tuberculosis* Infection. *Annual Review in Immunology.* 39, 611–637. https://doi.org/10.1146/annurev-immunol-093019-010426

Rawat, M., Johnson, C., Cadiz, V., Av-Gay, Y., 2007. Comparative analysis of mutants in the mycothiol biosynthesis pathway in *Mycobacterium smegmatis*. *Biochemical and Biophysical Research Communications* 363, 71–76. https://doi.org/10.1016/j.bbrc.2007.08.142

Rawat, M., Newton, G.L., Ko, M., Martinez, G.J., Fahey, R.C., Av-Gay, Y., 2002. Mycothiol-Deficient *Mycobacterium smegmatis* Mutants Are Hypersensitive to Alkylating Agents, Free Radicals, and Antibiotics. *Antimicrobial Agents and Chemotherapy* 46, 3348–3355. https://doi.org/10.1128/AAC.46.11.3348-3355.2002

Receveur-Bréchot, V., Bourhis, J.-M., Uversky, V.N., Canard, B., Longhi, S., 2005. Assessing protein disorder and induced folding. *Proteins* 62, 24–45. https://doi.org/10.1002/prot.20750

Reichmann, D., Voth, W., Jakob, U., 2018. Maintaining a Healthy Proteome during Oxidative Stress. *Molecular Cell* 69, 203–213. https://doi.org/10.1016/j.molcel.2017.12.021

Robert, X., Gouet, P., 2014. Deciphering key features in protein structures with the new ENDscript server. *Nucleic Acids Research* 42, W320–W324. https://doi.org/10.1093/nar/gku316

Rock, J.M., Hopkins, F.F., Chavez, A., Diallo, M., Chase, M.R., Gerrick, E.R., Pritchard, J.R., Church, G.M., Rubin, E.J., Sassetti, C.M., Schnappinger, D., Fortune, S.M., 2017. Programmable transcriptional repression in mycobacteria using an orthogonal CRISPR interference platform. *Nature Microbiology* 2, 16274. https://doi.org/10.1038/nmicrobiol.2016.274

Rosen, H., Klebanoff, S.J., Wang, Y., Brot, N., Heinecke, J.W., Fu, X., 2009. Methionine oxidation contributes to bacterial killing by the myeloperoxidase system of neutrophils. *Proceedings of the National Academy of Sciences*. 106, 18686–18691. https://doi.org/10.1073/pnas.0909464106

Rosenzweig, R., Moradi, S., Zarrine-Afsar, A., Glover, J.R., Kay, L.E., 2013. Unraveling the Mechanism of Protein Disaggregation Through a ClpB-DnaK Interaction. *Science* 339, 1080–1083. https://doi.org/10.1126/science.1233066

Runyon, E.H., 1959. Anonymous Mycobacteria in Pulmonary Disease. *Medical Clinics of North America* 43, 273–290. https://doi.org/10.1016/S0025-7125(16)34193-1

Saelens, J.W., Viswanathan, G., Tobin, D.M., 2019. Mycobacterial Evolution Intersects With Host Tolerance. *Frontiers in Immunology* 10, 528. https://doi.org/10.3389/fimmu.2019.00528

Saini, V., Cumming, B.M., Guidry, L., Lamprecht, D.A., Adamson, J.H., Reddy, V.P., Chinta, K.C., Mazorodze, J.H., Glasgow, J.N., Richard-Greenblatt, M., Gomez-Velasco, A., Bach, H., Av-Gay, Y., Eoh, H., Rhee, K., Steyn, A.J.C., 2016. Ergothioneine Maintains Redox and Bioenergetic Homeostasis Essential for Drug Susceptibility and Virulence of *Mycobacterium tuberculosis*. *Cell Reports* 14, 572–585. https://doi.org/10.1016/j.celrep.2015.12.056

Sambrook, Russell, D.W., 2001. Molecular cloning: a laboratory manual, 4th ed. ed. Cold Spring Harbor Laboratory Press, Cold Spring Harbor, N.Y.

Santra, M., Farrell, D.W., Dill, K.A., 2017. Bacterial proteostasis balances energy and chaperone utilization efficiently. *Proceedings of the National Academy of Science* 114, E2654–E2661. https://doi.org/10.1073/pnas.1620646114

Sarkar, A., Ghosh, S., Shaw, R., Patra, M.M., Calcuttawala, F., Mukherjee, N., Das Gupta, S.K., 2020. *Mycobacterium tuberculosis* thymidylate synthase (ThyX) is a target for plumbagin, a natural product with antimycobacterial activity. *PLoS ONE* 15, e0228657. https://doi.org/10.1371/journal.pone.0228657

Sassetti, C.M., Boyd, D.H., Rubin, E.J., 2001. Comprehensive identification of conditionally essential genes in mycobacteria. *Proceedings of the National Academy of Sciences*. 98, 12712–12717. https://doi.org/10.1073/pnas.231275498

Schmittgen, T.D., Livak, K.J., 2008. Analyzing real-time PCR data by the comparative CT method. *Nature Protocols* 3, 1101–1108. https://doi.org/10.1038/nprot.2008.73

Schnappinger, D., Ehrt, S., 2014. Regulated Expression Systems for Mycobacteria and Their Applications. *Microbiology Spectrum.* https://doi.org/10.1128%2Fmicrobiolspec.MGM2-0018-2013

Schramm, F.D., Schroeder, K., Jonas, K., 2020. Protein aggregation in bacteria. *FEMS Microbiology Reviews* 44, 54–72. https://doi.org/10.1093/femsre/fuz026

Schröder, H., Langer, T., Hartl, F.U., Bukau, B., 1993. DnaK, DnaJ and GrpE form a cellular chaperone machinery capable of repairing heat-induced protein damage. *The EMBO Journal* 12, 4137–4144. https://doi.org/10.1002/j.1460-2075.1993.tb06097.x

Shastri, M.D., Shukla, S.D., Chong, W.C., Dua, K., Peterson, G.M., Patel, R.P., Hansbro, P.M., Eri, R., O'Toole, R.F., 2018. Role of Oxidative Stress in the Pathology and Management of Human Tuberculosis. *Oxidative Medicine and Cellular Longevity* 2018, 1–10. https://doi.org/10.1155/2018/7695364

Shoeb, H.A., Bowman, B.U., Ottolenghi, A.C., Merola, A.J., 1985. Peroxidase-mediated oxidation of isoniazid. *Antimicrobial Agents and Chemotherapy* 27, 399–403. https://doi.org/10.1128/AAC.27.3.399

Sievers, F., Higgins, D.G., 2018. Clustal Omega for making accurate alignments of many protein sequences: Clustal Omega for Many Protein Sequences. *Protein Science* 27, 135–145. https://doi.org/10.1002/pro.3290

Singer-Sam, J., Tanguay, R.L., Riggs, A.O., 1989. Use of Chelex to improve the PCR signal from a small number of cells.

Singh, A.R., Strankman, A., Orkusyan, R., Purwantini, E., Rawat, M., 2016. Lack of mycothiol and ergothioneine induces different protective mechanisms in *Mycobacterium smegmatis*. *Biochemistry and Biophysics Reports* 8, 100–106. https://doi.org/10.1016/j.bbrep.2016.08.006

Singh, P., Cole, S.T., 2011. *Mycobacterium leprae*: genes, pseudogenes and genetic diversity. *Future Microbiology* 6, 57–71. https://doi.org/10.2217/fmb.10.153

Singh, V., Chibale, K., 2021. Strategies to Combat Multi-Drug Resistance in Tuberculosis. *Accounts in Chemical Research* 54, 2361–2376. https://doi.org/10.1021/acs.accounts.0c00878

Snapper, S.B., Melton, R.E., Mustafa, S., Kieser, T., Jr', W.R.J., 1990. Isolation and characterization of efficient plasmid transformation mutants of *Mycobacterium smegmatis*. *Molecular Microbiology*, 4(11), 1911-1919. https://doi.org/10.1111/j.1365-2958.1990.tb02040.x

Springer, B., Master, S., Sander, P., Zahrt, T., McFalone, M., Song, J., Papavinasasundaram, K.G., Colston, M.J., Boettger, E., Deretic, V., 2001. Silencing of Oxidative Stress Response in *Mycobacterium tuberculosis* : Expression Patterns of ahpC in Virulent and Avirulent Strains and Effect of *ahpC* Inactivation. *Infection and Immunity* 69, 5967–5973. https://doi.org/10.1128/IAI.69.10.5967-5973.2001

Stinear, T.P., Seemann, T., Pidot, S., Frigui, W., Reysset, G., Garnier, T., Meurice, G., Simon, D., Bouchier, C., Ma, L., Tichit, M., Porter, J.L., Ryan, J., Johnson, P.D.R., Davies, J.K., Jenkin, G.A., Small, P.L.C., Jones, L.M., Tekaia, F., Laval, F., Daffé, M., Parkhill, J., Cole, S.T., 2007. Reductive evolution and niche adaptation inferred from the genome of Mycobacterium ulcerans , the causative agent of Buruli ulcer. *Genome Research* 17, 192–200. https://doi.org/10.1101/gr.5942807

St-Pierre, F., Cui, L., Priest, D.G., Endy, D., Dodd, I.B., Shearwin, K.E., 2013. One-Step Cloning and Chromosomal Integration of DNA. *ACS Synthetic Biology* 2, 537–541. https://doi.org/10.1021/sb400021j

Sudnitsyna, M.V., Mymrikov, E.V., Seit-Nebi, A.S., Gusev, N.B., 2012. The Role of Intrinsically Disordered Regions in the Structure and Functioning of Small Heat Shock Proteins. *Current Protein and Peptide Science* 13(1), 76-85. https://doi.org/10.2174/138920312799277875

Sundersingh, J.A., J, R., Rajan, A., Shankar, V., 2020. Features of the biochemistry of *Mycobacterium smegmatis*, as a possible model for *Mycobacterium tuberculosis*. *Journal of Infection and Public Health* 13, 1255–1264. https://doi.org/10.1016/j.jiph.2020.06.023

Tahlan, K., Wilson, R., Kastrinsky, D.B., Arora, K., Nair, V., Fischer, E., Barnes, S.W., Walker, J.R., Alland, D., Barry, C.E., Boshoff, H.I., 2012. SQ109 Targets MmpL3, a Membrane Transporter of Trehalose Monomycolate Involved in Mycolic Acid Donation to the Cell Wall Core of *Mycobacterium tuberculosis*. *Antimicrobial Agents and Chemotherapy* 56, 1797–1809. https://doi.org/10.1128/AAC.05708-11

Tamura, K., Stecher, G., Kumar, S., 2021. MEGA11: Molecular Evolutionary Genetics Analysis Version 11. *Molecular Biology and Evolution* 38, 3022–3027. https://doi.org/10.1093/molbev/msab120

Teixeira, H.D., Schumacher, R.I., Meneghini, R., 1998. Lower intracellular hydrogen peroxide levels in cells overexpressing CuZn-superoxide dismutase. *Proceedings of the National Academy of Sciences*. 95, 7872–7875. https://doi.org/10.1073/pnas.95.14.7872

Tortoli, E., 2019. The Taxonomy of the Genus Mycobacterium, in: Nontuberculous Mycobacteria (NTM). *Elsevier*, pp. 1–10. https://doi.org/10.1016/B978-0-12-814692-7.00001-2

Ulrich, K., Jakob, U., 2019. The role of thiols in antioxidant systems. *Free Radical Biology and Medicine* 140, 14–27. https://doi.org/10.1016/j.freeradbiomed.2019.05.035

Unissa, A., Hanna, L.E., 2017. Molecular mechanisms of action, resistance, detection to the first-line anti tuberculosis drugs: Rifampicin and pyrazinamide in the post whole genome sequencing era. *Tuberculosis* 105, 96–107. https://doi.org/10.1016/j.tube.2017.04.008

Urbanowski, M.E., Ordonez, A.A., Ruiz-Bedoya, C.A., Jain, S.K., Bishai, W.R., 2020. Cavitary tuberculosis: the gateway of disease transmission. *The Lancet Infectious Diseases* 20, e117–e128. https://doi.org/10.1016/S1473-3099(20)30148-1

van der Lee, R., Buljan, M., Lang, B., Weatheritt, R.J., Daughdrill, G.W., Dunker, A.K., Fuxreiter, M., Gough, J., Gsponer, J., Jones, D.T., Kim, P.M., Kriwacki, R.W., Oldfield, C.J., Pappu, R.V., Tompa, P., Uversky,

V.N., Wright, P.E., Babu, M.M., 2014. Classification of Intrinsically Disordered Regions and Proteins. *Chemical Reviews* 114, 6589–6631. https://doi.org/10.1021/cr400525m

van Kessel, J.C., Hatfull, G.F., 2007. Recombineering in *Mycobacterium tuberculosis*. *Nature Methods* 4, 147–152. https://doi.org/10.1038/nmeth996

Vásquez-Vivar, J., Joseph, J., Karoui, H., Zhang, H., Miller, J., Martásek, P., 2000. EPR spin trapping of superoxide from nitric oxide synthase. *Analysis* 28, 487–492. https://doi.org/10.1051/analusis:2000280487

Via, L.E., Lin, P.L., Ray, S.M., Carrillo, J., Allen, S.S., Eum, S.Y., Taylor, K., Klein, E., Manjunatha, U., Gonzales, J., Lee, E.G., Park, S.K., Raleigh, J.A., Cho, S.N., McMurray, D.N., Flynn, J.L., Barry, C.E., 2008. Tuberculous Granulomas Are Hypoxic in Guinea Pigs, Rabbits, and Nonhuman Primates. *Infection and Immunity* 76, 2333–2340. https://doi.org/10.1128/IAI.01515-07

Vilchèze, C., 2020. Mycobacterial Cell Wall: A Source of Successful Targets for Old and New Drugs. *Applied Sciences* 10, 2278. https://doi.org/10.3390/app10072278

Vilchèze, C., Jacobs, W.R., 2019. The Isoniazid Paradigm of Killing, Resistance, and Persistence in *Mycobacterium tuberculosis*. *Journal of Molecular Biology* 431, 3450–3461. https://doi.org/10.1016/j.jmb.2019.02.016

Vincent, A.T., Nyongesa, S., Morneau, I., Reed, M.B., Tocheva, E.I., Veyrier, F.J., 2018. The Mycobacterial Cell Envelope: A Relict From the Past or the Result of Recent Evolution? *Frontiers in Microbiology* 9, 2341. https://doi.org/10.3389/fmicb.2018.02341

Wang, Y., Branicky, R., Noë, A., Hekimi, S., 2018. Superoxide dismutases: Dual roles in controlling ROS damage and regulating ROS signaling. *Journal of Cell Biology* 217, 1915–1928. https://doi.org/10.1083/jcb.201708007

Wei, J.-R., Krishnamoorthy, V., Murphy, K., Kim, J.-H., Schnappinger, D., Alber, T., Sassetti, C.M., Rhee, K.Y., Rubin, E.J., 2011. Depletion of antibiotic targets has widely varying effects on growth. *Proceedings of the National Academy of Sciences*. 108, 4176–4181. https://doi.org/10.1073/pnas.1018301108

Weibezahn, J., Tessarz, P., Schlieker, C., Zahn, R., Maglica, Z., Lee, S., Zentgraf, H., Weber-Ban, E.U., Dougan, D.A., Tsai, F.T.F., Mogk, A., Bukau, B., 2004. Thermotolerance Requires Refolding of Aggregated Proteins by Substrate Translocation through the Central Pore of ClpB. *Trends in Biochemical Sciences* 30, i. https://doi.org/10.1016/S0968-0004(05)00043-5

Wengenack, N.L., Jensen, M.P., Rusnak, F., Stern, M.K., 1999. *Mycobacterium tuberculosis*KatG Is a Peroxynitritase. *Biochemical and Biophysical Research Communications* 256, 485–487. https://doi.org/10.1006/bbrc.1999.0358

Williams, C.H., 1995. Mechanism and structure of thioredoxin reductase from *Escherichia coli*. *FASEB Journal*. 9, 1267–1276. https://doi.org/10.1096/fasebj.9.13.7557016

Winter, J., Ilbert, M., Graf, P.C.F., Özcelik, D., Jakob, U., 2008. Bleach Activates a Redox-Regulated Chaperone by Oxidative Protein Unfolding. *Cell* 135, 691–701. https://doi.org/10.1016/j.cell.2008.09.024

Winter, J., Linke, K., Jatzek, A., Jakob, U., 2005. Severe Oxidative Stress Causes Inactivation of DnaK and Activation of the Redox-Regulated Chaperone Hsp33. *Molecular Cell* 17, 381–392. https://doi.org/10.1016/j.molcel.2004.12.027

Winterbourn, C.C., 2008. Reconciling the chemistry and biology of reactive oxygen species. *Nature Chemical Biology* 4, 278–286. https://doi.org/10.1038/nchem*Bio*.85

Winterbourn, C.C., Kettle, A.J., 2013. Redox Reactions and Microbial Killing in the Neutrophil Phagosome. *Antioxidants & Redox Signaling* 18, 642–660. https://doi.org/10.1089/ars.2012.4827

Winterbourn, C.C., Kettle, A.J., Hampton, M.B., 2016. Reactive Oxygen Species and Neutrophil Function. *Annual Review of Biochemistry* 85, 765–792. https://doi.org/10.1146/annurev-biochem-060815-014442

Wolf, A.J., Linas, B., Trevejo-Nuñez, G.J., Kincaid, E., Tamura, T., Takatsu, K., Ernst, J.D., 2007. *Mycobacterium tuberculosis* Infects Dendritic Cells with High Frequency and Impairs Their Function In Vivo. *Journal of Immunology* 179, 2509–2519. https://doi.org/10.4049/jimmunol.179.4.2509

Wong, C.F., Shin, J., Subramanian Manimekalai, M.S., Saw, W.G., Yin, Z., Bhushan, S., Kumar, A., Ragunathan, P., Grüber, G., 2017. AhpC of the mycobacterial antioxidant defense system and its interaction with its reducing partner Thioredoxin-C. *Scientific Reports* 7, 5159. https://doi.org/10.1038/s41598-017-05354-5

Woodman, M.E., Savage, C.R., Arnold, W.K., Stevenson, B., 2016. Direct PCR of Intact Bacteria (Colony PCR). *Current Protocols in Microbiology* 42. https://doi.org/10.1002/cpmc.14

World Health Organization, 2021. Report of the 7th virtual end TB strategy summit for the highest TB burden countries and countries on the WHO global watchlist, 16–17 November 2021. World Health Organization, Geneva.

Xu, J., Zhang, Y., 2010. How significant is a protein structure similarity with TM-score = 0.5? *Bioinformatics* 26, 889–895. https://doi.org/10.1093/bioinformatics/btq066

Xu, Y., Schmitt, S., Tang, L., Jakob, U., Fitzgerald, M.C., 2010. Thermodynamic Analysis of a Molecular Chaperone Binding to Unfolded Protein Substrates. *Biochemistry* 49, 1346–1353. https://doi.org/10.1021/bi902010t

Zeng, S., Soetaert, K., Ravon, F., Vandeput, M., Bald, D., Kauffmann, J.-M., Mathys, V., Wattiez, R., Fontaine, V., 2019. Isoniazid Bactericidal Activity Involves Electron Transport Chain Perturbation. *Antimicrobial Agents and Chemotherapy* 63, e01841-18. https://doi.org/10.1128/AAC.01841-18

Zhang, H., Ishige, K., Kornberg, A., 2002. A polyphosphate kinase (PPK2) widely conserved in bacteria. *Proceedings of the National Academy of Sciences*. 99, 16678–16683. https://doi.org/10.1073/pnas.262655199

Zhang, Y., Skolnick, J., 2005. TM-align: a protein structure alignment algorithm based on the TM-score. *Nucleic Acids Research* 33, 2302–2309. https://doi.org/10.1093/nar/gki524

Zhang, Y., Yew, W.W., 2009. Mechanisms of drug resistance in *Mycobacterium tuberculosis* 11. *International Journal of Tuberculosis and Lung Disease* 2009, 13(11), 1320-1330. https://doi.org/10.1007/978-3-642-80166-2_3

Zhang, Z., Hillas, P.J., Ortiz de Montellano, P.R., 1999. Reduction of Peroxides and Dinitrobenzenes by*Mycobacterium tuberculosis*Thioredoxin and Thioredoxin Reductase. *Archives of Biochemistry and Biophysics* 363, 19–26. https://doi.org/10.1006/abbi.1998.1056

Zheng, W., Zhang, C., Li, Y., Pearce, R., Bell, E.W., Zhang, Y., 2021. Folding non-homologous proteins by coupling deep-learning contact maps with I-TASSER assembly simulations. Cell Reports Methods 1, 100014. https://doi.org/10.1016/j.crmeth.2021.100014

Appendix A: Chemicals and Reagents

Table A1 Bacterial strains, plasmids, chemicals and reagents used within this study.

Product Name	Source	Reference
Bacterial Strains		
***Escherichia coli* BW25113**	Dharmacon, GE Healthcare	OEC5042
Escherichia coli* BW25113 Δ*cnoX	Dharmacon, GE Healthcare	OEC4987
***Escherichia coli* Mach1**	ThermoFisher Scientific	C862003
***Escherichia coli* Top10**	ThermoFisher Scientific	C4040
***Escherichia coli* XJa (DE3) Autolysis**	Zymo Research	T5031
***Escherichia coli* XJb (DE3) Autolysis**	Zymo Research	T5051
Mycobacterium smegmatis mc^{2}155	Laboratory Stock	Snapper *et al.* 1990
Plasmids		
pE-FLP	Addgene	#45978
pGiles::P_{smyc}	C. E. Barry III	Kolbe *et al.* 2020
pJET1.2/Blunt	ThermoFisher Scientific	K1231
pJV53	Addgene	#26904
pLJR962	Addgene	#115162
pML2714	Addgene	#117498
pMSG360Zeo	Addgene	#27154
pQE-80L	Qiagen	V010777
pUC19 Giles Integrase	Addgene	#170049
Chemicals		
Acetic Acid	Merck	695092
Acid washed Glass Beads	Sigma-Aldrich	G4649
Ammonium Chloride (NH_4Cl)	Acros Organics	423285000
Calcium Chloride dihydrate ($CaCl_2•2H_2O$)	Saarchem Univar	SAAR1524920EM
Disodium Phosphate (Na_2HPO_4)	Alfa Aesar	13437
Dimethyl Sulfoxide (DMSO)	Sigma-Aldrich	D8418
DPBS (1 ×)	Gibco	14190-094
Ethanol	Merck	108543
Glycine	Sigma-Aldrich	SAAR2676600EM
Magnesium Chloride Hexahydrate ($MgCl_2•6H_2O$)	Merck	SAAR4123000EM

Magnesium Sulphate Heptahydrate ($MgSO_4•7H_2O$)	Merck	SAAR4124000EM
Manganese Chloride Tetrahydrate ($MnCl_2•4H_2O$)	Sigma-Aldrich	203734
Methanol	Merck	1424109
Monopotassium Phosphate (KH_2PO_4)	Acros Organics	205925000
Monosodium Phosphate (NaH_2PO_4)	Merck	SAAR5822680EM
(1,4-Piperazinediethanesulfonic acid) PIPES	Boehringer Mannheim	83676220-56
Potassium Chloride (KCl)	Merck	SAAR5042020EM
Potassium Dihydrogen Orthophosphate (KH_2PO_4)	Merck	SAAR5043600EM
Potassium Hydroxide (KOH)	Merck	SAAR5044400EM
Potassium Phosphate, dibasic (K_2HPO_4)	Sigma-Aldrich	795496-100G
Sodium Chloride (NaCl)	Merck	SAAR5822320FL
Sodium Hydroxide (NaOH)	Merck	SAAR5823180EM
Ultra-Pure Distilled Water	ThermoFisher Scientific	10977-035
UltraPure™ Tris	ThermoFisher Scientific	15504-020
Growth Media and Supplements		
Acetamide	Sigma-Aldrich	00160
Agar Bacteriological	Merck	HG000BX1.500
D-(+)- Glucose	Sigma-Aldrich	G7021
Glycerol	Merck	SAAR2676520LC
L-(+)- Arabinose	Sigma-Aldrich	A3256
Middlebrook 7H9 Broth	BD Difco	271310
Middlebrook 7H10 Agar	BD Difco	262710
Middlebrook 7H11 Agar	BD Difco	212203
Middlebrook Seven H11 Agar	BD Difco	283810
Resazurin Sodium Salt	Sigma-Aldrich	R7017
Sodium Chloride	Sigma-Aldrich	S7653
Sodium Succinate Dibasic Hexahydrate	Sigma-Aldrich	S2378
Tryptone Powder (Pancreatic Digest of Casein)	Merck	HG000BX4.250
Tween 80	Sigma-Aldrich	P8074
Ultra-Pure IPTG	ThermoFisher Scientific	R1161
Yeast Extract Powder	Merck	HG000BX6.500
Antibiotics & Antimicrobial Reagents		

Ampicillin Sodium Salt	VWR Life Science	0339
Anhydrotetracycline Hydrochloride	Sigma-Aldrich	37919
Ciprofloxacin	Alfa Aesar	J1970
Cumene Hydroperoxide	Aldrich	247502
Diamide	Sigma	D3648
DTT	ThermoFisher Scientific	R0861
Ethambutol	Alfa Aesar	J60695
Hydrogen Peroxide	Sigma-Aldrich	323381
Hygromycin B	Thermo	10687010
Hypochlorous Acid	Sigma Aldrich	425044
Isoniazid	Alfa Aesar	A10583
Kanamycin Sulphate	VWR Life Science	0408
Plumbagin	Sigma	P7262
Rifampicin	Alfa Aesar	13292-46-1
Zeocin	ThermoFisher Scientific	R25001
Kits		
CloneJET PCR Cloning Kit	ThermoFisher Scientific	K1231
Direct-zol™ RNA MiniPrep Plus	Zymo Research	R2071
E.Z.N.A. Plasmid DNA Mini Kit	Omega Bio-tek	D6942
GeneJET Genomic DNA Purification Kit	ThermoFisher Scientific	K0721
GeneJET PCR Purification Kit	ThermoFisher Scientific	K0701
GeneJET Plasmid MiniPrep Kit	ThermoFisher Scientific	K0502
Mix n Go! *E. coli* Transformation Kit	Zymo Research	T3001
RapidOut DNA Removal Kit	ThermoFisher Scientific	K2981
Silica Bead Gel Purification Kit	ThermoFisher Scientific	K0513
Apparatus & Equipment		
BeadBug 3 Microtube Homogenizer	Benchmark Scientific	D1030
Blue Light Transilluminator	IORodeo	IMG-04-03
GE ÄKTA FPLC	GE Healthcare (Cytiva)	ÄKTA FPLC
ChemiDoc XRS+	Bio-Rad	1708265SP
Fraction Collector 900	GE Healthcare (Cytiva)	Frac-900
Gene Pulser XCell	Bio-Rad	1652660

Jenway 6200 Spectrophotometer	Jenway	6200 Vis
Megafuge 1.0R	Heraeus	05718
Mini Gel Tank	ThermoFisher Scientific	A25977
MiniSpin Microfuge	Sigma-Aldrich	Z606235
Mini Sub Cell GT Horizontal Electrophoresis Chamber	Bio-Rad	1704487
MultiGene Mini PCR Thermal Cycler	Labnet International	Z739928
Nanodrop ND-1000 Spectrophotometer	ThermoFisher Scientific	ND-1000
PowerPac HC	Bio-Rad	1645052
QuantStudio™ 3 Real Time PCR System, 96 well, 0.2 mL	Applied Biosystems	A28567
SimpliAmp Thermal Cycler	Applied Biosystems	A24811
Spectramax M3	Molecular Devices	M3
Synergy Fluorimeter	BioTek	
SDS PAGE Mini Gel Tank System	ThermoFisher Scientific	A25977
VC-50 Vibra Cell Ultrasonic Processor	Sonics & Materials Inc	QDX-168-D20
RNA Extraction, cDNA Synthesis, qPCR		
DNase I	Zymo Research	E1011-A
LunaScript RT SuperMix Kit	New England Biolabs	E3010L
PowerUp SYBR Green Master Mix	ThermoFisher Scientific	100029283
SuperScript IV VILO	ThermoFisher Scientific	11766050
TRIzol™ Reagent	ThermoFisher Scientific, Invitrogen	15596026
TRI Reagent™ Solution	ThermoFisher Scientific	AM9738
TRI Reagent	Zymo Research	R2050-1-50
Restriction Enzymes & Buffers		
10 × Anza Buffer	ThermoFisher Scientific	IVGM2008
10 × FastDigest Buffer	ThermoFisher Scientific	K1991
Anza 5 BamHI	ThermoFisher Scientific	IVGN0056
Anza 10 DpnI	ThermoFisher Scientific	IVGN0106
Anza 12 XbaI	ThermoFisher Scientific	IVGN0126
Anza 16 HindIII	ThermoFisher Scientific	IVGN0166
Anza 17 KpnI	ThermoFisher Scientific	IVGN0176
Anza 22 SmaI	ThermoFisher Scientific	IVGN0226
Anza 23 PstI	ThermoFisher Scientific	IVGN0236

FD PaeI	ThermoFisher Scientific	FD0604
BsmBI V2	New England Biolabs	R0739S
SphI	Promega	R626A
Agarose Gels		
50 × TAE Electrophoresis Buffer	ThermoFisher Scientific	B49
Ethidium Bromide, 10 mg/mL	VWR Life Science	X328
GeneRuler 50 bp DNA Ladder	ThermoFisher Scientific	SM0371
GeneRuler 100 bp DNA Ladder	ThermoFisher Scientific	SM0241
GeneRuler 1 kb Plus DNA Ladder	ThermoFisher Scientific	SM1332
Low Range DNA Ladder	AmplIqon	A610241
TopVision Agarose Tablets	ThermoFisher Scientific	R2801
TriTrack Loading Dye (6 ×)	ThermoFisher Scientific	R1161
SDS-PAGE Gel Reagents		
β-Mercaptoethanol	Sigma-Aldrich	M6250
Bromophenol Blue	Associated Chemical Enterprises	115-39-9
Coomassie Brilliant Blue R-250	ThermoFisher Scientific	20278
PageRuler Prestained Protein Ladder	ThermoFisher Scientific	#26618
Sodium Lauryl Sulphate	Merck	SAAR5823610EM
SureCast™ Acrylamide Solution (40 %)	ThermoFisher Scientific	HC2040
SureCast™ Ammonium Persulphate (APS)	ThermoFisher Scientific	HC2005
SureCast™ Resolving Buffer	ThermoFisher Scientific	HC2212
SureCast™ Stacking Buffer	ThermoFisher Scientific	HC2112
SureCast™ TEMED	ThermoFisher Scientific	HC2006
Unstained Protein Marker	ThermoFisher Scientific	#26610
Protein Purification, Quantification and Assay Reagents		
Bradford Assay	ThermoFisher Scientific	23200
Coomassie Protein Assay Reagent	ThermoFisher Scientific	1856209
5,5'-Dithiobis-2-nitrobenzoic acid (DTNB)	Sigma-Aldrich	D8130
Diethylenetriaminepentaacetic acid	Sigma-Aldrich	D6518-5G
HisPur Ni-NTA Chromatography Catridge	Thermo Scientific	90098
Imidazole	Sigma-Aldrich	56750-100G
Insulin Solution Human	Sigma-Aldrich	I9278

L-Malate Dehydrogenase (MDH)	Sigma-Aldrich	LMDH-RO
Pierce BCA Kit	ThermoFisher Scientific	23225
Pierce Bovine Serum Albumin (BSA) Standard Ampules, 2 mg/mL	ThermoFisher Scientific	23209
Pierce Protease Inhibitor Mini Tablets, EDTA-free	ThermoFisher Scientific	A32955
Pierce Protein Concentrator PES, 10 K MWCO, 2-6 mL	ThermoFisher Scientific	88516
Phenylmethylsulphonyl Fluoride	Sigma-Aldrich	P7626-5G
SnakeSkin Dialysis Tubing, 10 K MWCO, 35 mm Dry	ThermoFisher Scientific	88245
Triton X-100	Sigma-Aldrich	T8787
PCR Reagents		
2 × Phusion Flash PCR Master Mix	ThermoFisher Scientific	F-548
Dimethyl Sulfoxide (100 %)	ThermoFisher Scientific	F-515
dNTP Solution Mix	New England Biolabs	N0447S
DreamTaq PCR Master Mix (2 ×)	ThermoFisher Scientific	K1071
KAPA Taq Ready Mix PCR Kit	Sigma-Aldrich	KK1006
KAPA Taq Ready Mix with Dye	Sigma-Aldrich	KK1024
Phusion High-Fidelity DNA Polymerase	ThermoFisher Scientific	F-530S
Resin Chelex 100 Molecular Grade 200-400 Mesh	Bio-Rad	1421253
Taq 2 × Master Mix	New England Biolabs	M0270L
Modification Enzymes		
Anza DNA End Repair Kit	ThermoFisher Scientific	IVGN2504
Anza T4 DNA Ligase (5 U/µL)	ThermoFisher Scientific	EL0012
Anza T4 DNA Master Mix	ThermoFisher Scientific	IVGN2104
Anza T4 PNK 5' Phosphorylation	ThermoFisher Scientific	IVGN230-4
Fast AP Thermosensitive Alkaline Phosphatase	ThermoFisher Scientific	EF0651
Instant Sticky-end Ligase Master Mix	New England Biolabs	M0370
RNase A	ThermoFisher Scientific	8003088
T4 DNA Ligase	Promega	M180A
Miscellaneous		
0.2 cm Gap Electroporation Cuvette	Thermo	P45050

Table A2 List of DNA fragments and their sequences ordered during the course of this project.

DNA Fragments	Sequence (5' to 3')[a]
***Ms*CnoX**	ATTCGAGCTC**GGTACC**TAAGGCAACAGCTATGACACGTCCGCGTCCGAGCATTGGTCCGGCACT GGCAGGCGCAGTTGATCTGAGCGCACTGAAACGTCCGGCAGCAAGCGGTGAAGCAGCACCGGCA CCTGGTGGTCCGAATGTTACCGAAGTGACCGAAGCAAATTTTGAAGCAGAAGTTCTGGTTCGTAG CGGTCAGGTTCCGGTTGTTGTTGTTCTGTGGTCACCGCGTAGTGATGCAAGCGCACAGCTGACCG AAACCTTTGCAGATCTGGCAAGCGCAGATGGTGGTAAATGGTCACTGGCAGCAGTTAATGTTGAT ACCACACCGCGTATTGCACAGATGTTTGGTATTCAGGCAGTTCCGACCGTTGTTGCATTAGCCGGT GGTCAGCCGATTGCAAGCTTTCAGGGTCCGCAGCCTCCGGAACAGCTGCGTCGTTGGGTTGATAG CCTGCTGGAAGCAACCGCAGGTAAACTGAGCGGTAGTGGTGAAGAAGCAGAACAGGTTGATCCT GCACTGGCACAGGCACGTGCACATCTGGATCAGGGTAATTTTGATGAAGCACTGAAAGCCTATGA AGCAATTCTGGAAGCACAGCCGAATCATCCGGAAGCAAAAGGTGCAGTTCGTCAGATTGGTTTTC TGCAGCGTGCCACCGCACAGCGTCCGGATGCAGTTGAAGTTGCAGATGCCGCACCGGATGATATT GAAGCAGCCTTTGCAGCAGCAGATGTTGAAATTCTGGCACAGCAGGTTAGCGCAGCATTTGATCG TCTGATTGCACTGATTAAACGTACAGCCGGTGATGATCGTACCAAAGTTCGTACACGCCTGATTG AACTGTTTGAGCTGTTTGATCCGGCAGATCCGGAAGTTATTGCAGGTCGTCGTAATCTGGCAAAT GCACTGTATACTAGTGATTATAAAGATGATGACGACAAATAA**TCTAGA**GTCGACCTGCAGGC
***Mt*CnoX**	ATTCGAGCTC**GGTACC**TAAGGCAACAGCTATGACCCGTCCGCGTCCGCCTCTGGGTCCTGCAATG GCAGGCGCAGTTGATCTGAGCGGTATTAAACAGCGTGCACAGCAGAATGCAGCAGCAAGCACCG ATGCAGATCGTGCACTGAGCACCCCGAGCGGTGTTACCGAAATTACCGAAGCAAATTTTGAAGAT GAAGTGATTGTGCGCAGTGATGAAGTTCCGGTTGTTGTGCTGCTGTGGTCACCGCGTAGCGAAGT TTGTGTTGATCTGCTGGATACCCTGAGCGGTCTGGCAGCAGCAGCCAAAGGTAAATGGTCACTGG CAAGCGTTAATGTTGATGTTGCACCGCGTGTTGCACAGATTTTTGGTGTTCAGGCAGTTCCGACCG TTGTTGCACTGGCAGCCGGTCAGCCGATTAGCAGCTTTCAGGGTCTGCAGCCTGCCGATCAGCTG AGCCGTTGGGTTGATAGCCTGCTGAGCGCAACCGCAGGTAAACTGAAAGGTGCAGCCAGCAGCG AAGAAAGCACCGAAGTTGATCCGGCAGTTGCACAGGCACGTCAGCAGCTGGAAGATGGTGATTT TGTTGCAGCACGTAAAAGCTATCAGGCAATTCTGGATGCAAATCCGGGTAGCGTTGAAGCAAAA GCAGCAATTCGTCAGATTGAATTTCTGATTCGTGCAACCGCACAGCGTCCGGATGCAGTTAGCGT TGCAGATAGCCTGAGTGATGATATTGATGCAGCATTTGCAGCAGCCGATGTTCAGGTTCTGAATC AGGATGTTAGCGCAGCCTTTGAACGTCTGATTGCACTGGTTCGTCGTACCAGCGGTGAAGAACGT ACCCGTGTTCGTACACGCCTGATTGAACTGTTTGAGCTGTTTGATCCTGCAGATCCGGAAGTTGTT GCAGGTCGTCGTAATCTGGCAAATGCACTGTATACTAGTGATTATAAAGATGATGACGACAAATA A**TCTAGA**GTCGACCTGCAGGC
***Ec*CnoX**	ATTCGAGCTC**GGTACC**TAAGGCAACAGCTATGAGCGTGGAAAACATTGTGAACATCAATGAAAG CAATCTGCAGCAGGTTCTGGAACAGAGCATGACCACACCGGTTCTGTTTTACTTTTGGAGCGAAC GTAGCCAGCATTGTCTGCAGCTGACCCCGATTCTGGAAAGCCTGGCAGCACAGTATAATGGTCAG TTTATTCTGGCAAAACTGGATTGTGATGCAGAGCAGATGATTGCAGCCCAGTTTGGTCTGCGTGC AATTCCGACCGTTTACCTGTTTCAGAATGGTCAGCCGGTTGATGGTTTTCAGGGTCCGCAGCCGG AAGAAGCAATTCGCGCACTGCTGGATAAAGTTCTGCCTCGTGAAGAAGAACTGAAAGCACAGCA GGCAATGCAGCTGATGCAAGAAAGCAATTATACCGATGCACTGCCGCTGCTGAAAGATGCATGG CAGCTGAGCAATCAGAATGGCGAAATTGGTCTGCTGCTGGCAGAAACCCTGATTGCACTGAATCG TAGCGAAGATGCAGAAGCAGTTCTGAAAACAATTCCGCTGCAGGATCAGGATACCCGTTATCAA GGTCTGGTTGCACAGATTGAACTGCTGAAACAAGCAGCAGATACACCGGAAATCCAGCAGCTGC AGCAGCAGGTAGCAGAAAATCCGGAAGATGCCGCACTGGCAACCCAGCTGGCACTGCAACTGCA TCAGGTTGGTCGTAATGAAGAAGCACTGGAACTGCTGTTTGGTCATCTGCGTAAAGATCTGACCG CAGCAGATGGTCAGACCCGTAAAACCTTTCAAGAAATTCTGGCAGCATTAGGCACCGGTGATGCA CTGGCCAGCAAATATCGTCGTCAGCTGTATGCACTGCTGTATACTAGTGATTATAAAGATGATGA CGACAAATAA**TCTAGA**GTCGACCTGCAGGC
[a] Where present, RE sites are bold, underlined	

Appendix B: Molecular Weight Markers

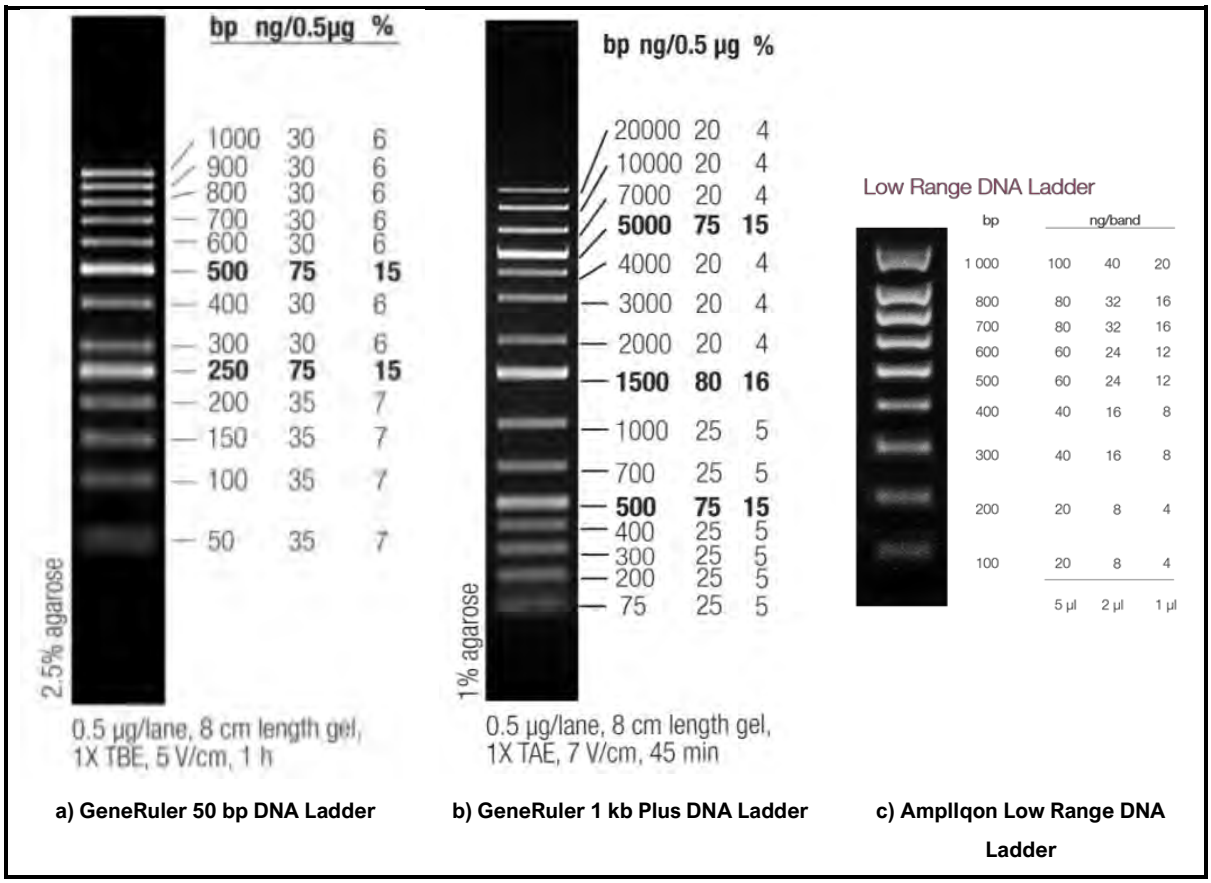

a) GeneRuler 50 bp DNA Ladder

b) GeneRuler 1 kb Plus DNA Ladder

c) AmpIIqon Low Range DNA Ladder

Figure B1.1 Molecular weight markers for DNA analysis used in this study.

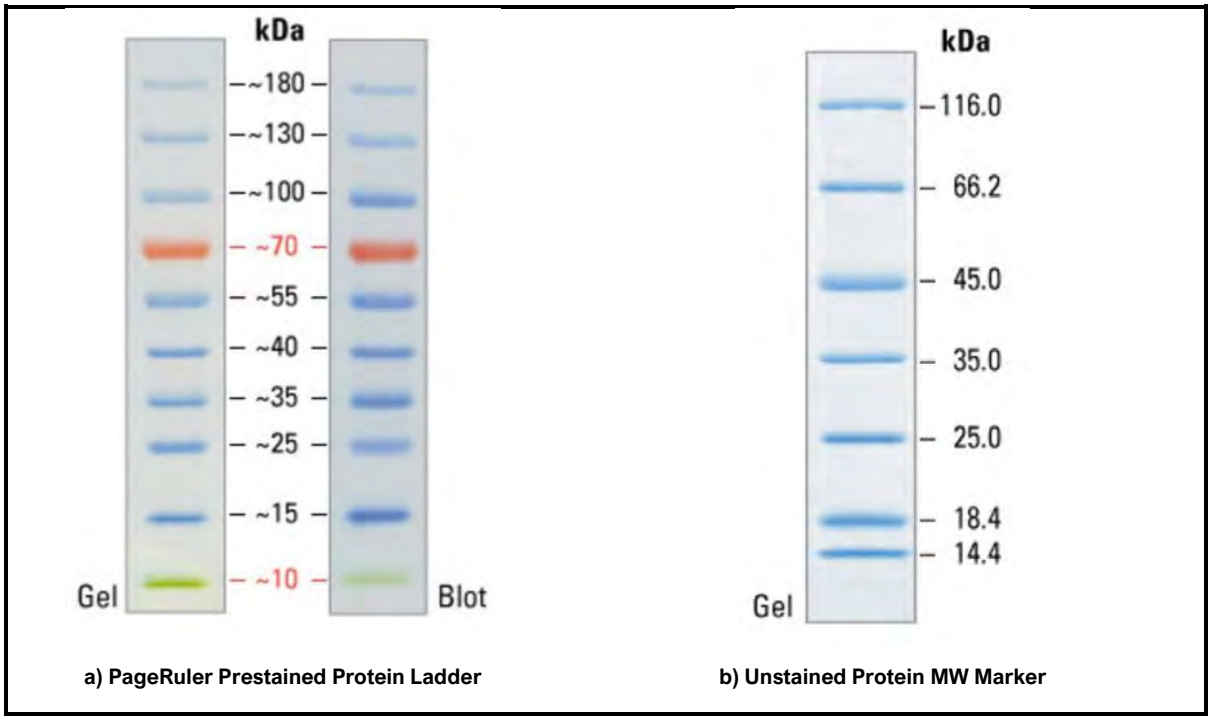

a) PageRuler Prestained Protein Ladder

b) Unstained Protein MW Marker

Figure B1.2 SDS PAGE molecular weight markers.

Appendix C: Plasmid Construction

C1: Construction of cloning vectors harbouring synthetic *cnoX* genes

DNA fragments harbouring the *E. coli cnoX* gene (934 bp) or its codon optimised homologs from Msm (970 bp) and Mtb (994 bp) (henceforth designated *EccnoX*, *MscnoX*, and *MtcnoX*, respectively) were purchased as synthetic GeneArt Strings DNA fragments from ThermoFisher Scientific. Once obtained, the DNA fragments were ligated into pJET1.2/Blunt (2974 bp) using the CloneJET PCR Cloning Kit (ThermoFisher Scientific), transformed into *E. coli* Mach1 competent cells, and plated on LA plates supplemented with ampicillin. Recombinant plasmids were isolated from two ampicillin-resistant transformants from each transformation reaction, followed by restriction with KpnI and XbaI. As shown in **Figure C1** (**Lanes 2-7**), two bands corresponding to the expected sizes of the linearised vector (~3000 bp) and cloned DNA inserts (~900 to 1000 bp) were identified following agarose gel electrophoresis analysis of each of the restricted plasmids. The cloned DNA inserts in the recombinant plasmids were sequenced to confirm that no errors were present in the synthesised DNA fragments.

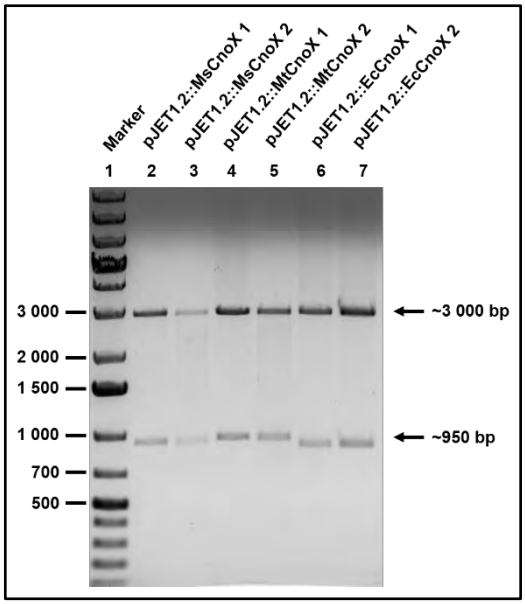

Figure C1.1 Agarose gel electrophoresis of recombinant pJET1.2 plasmids harbouring the *MscnoX*, *MtcnoX*, and *EccnoX* genes. Restriction endonuclease digests of the indicated plasmids were performed using KpnI and XbaI at 37 °C for 3 hr. The reactions were electrophoresed on a 0.8 % (w/v) agarose gel at 80 V for 50 min prior to visualisation under UV light. **Lane 1**: Molecular Weight Marker; **Lanes 2-3**: pJET1.2::*Ms*CnoX Clones 1 and 2; **Lanes 4-5**: pJET1.2::*Mt*CnoX Clones 1 and 2; **Lanes 6-7**: pJET1.2::*Ec*CnoX Clones 1 and 2. Black arrows indicate the sizes of the predicted PCR amplicons.

C2: Construction of and confirmation of recombinant expression vectors

For cloning into the pQE-80L expression vector, the *MscnoX*, *MtcnoX*, and *EccnoX* genes were amplified using the primer pairs MsCXFor/MsCXRev, MtCXFor/MtCXRev, and EcCXFor/EcCXRev, respectively, which introduced a BamHI restriction endonuclease site at the 5' end of each amplicon. Following PCR using Phusion DNA polymerase, the blunt-ended amplicons of 970, 994 and 934 bp (**Figure C2.1**, **Lanes 2-4**) were purified and treated with BamHI. The restricted amplicons were purified and ligated into the pQE-80L vector (~4700 bp) linearized with BamHI and SmaI (**Figure C2.1**, **Lane 6**) to generate pQE-80L::*Ms*CnoX, pQE-80L::*Mt*CnoX, and pQE-80L::*Ec*CnoX, respectively. The *MstrxC* gene was amplified using primer pair MsTrxCFor/MsTrxCRev and Msm mc^2155 genomic DNA as a template. The resulting 329 bp amplicon (**Figure C2.1**, **Lane 5**) was purified, restricted with BamHI and HindIII and ligated into pQE-80L linearised with the same enzymes (not shown) to generate pQE-80L::*Ms*TrxC.

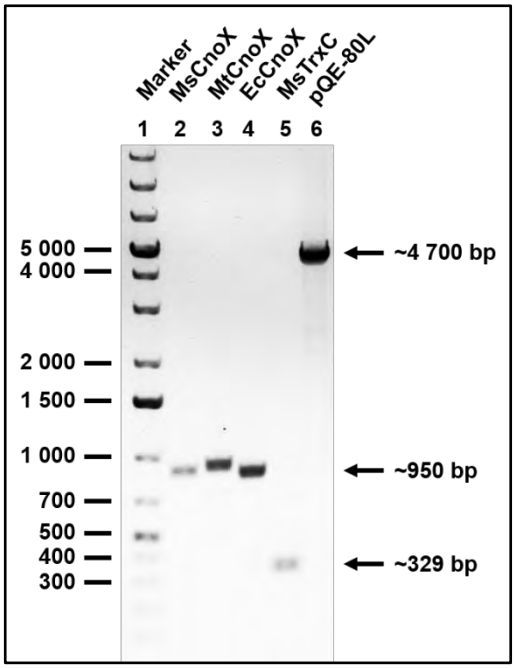

Figure C2.1 Agarose gel confirming the successful amplification of the *MscnoX*, *MtcnoX*, *EccnoX* and *MstrxC* genes for cloning into pQE-80L. The *cnoX* genes from Msm, Mtb and *E. coli* or *trxC* gene from Msm were amplified as described in the text. The pQE-80L expression vector was restricted with BamHI and SmaI. The PCR and restriction endonuclease reactions were electrophoresed on a 0.8 % (w/v) agarose gel at 80 V for 50 mins before visualisation under UV light. **Lane 1**: Molecular Weight Marker; **Lane 2**: PCR amplicon harbouring the *MscnoX* gene; **Lane 3**: PCR amplicon harbouring the *MtcnoX* gene; **Lane 4**: PCR amplicon harbouring the *EccnoX* gene; **Lane 5**: PCR amplicon harbouring the Msm *trxC* gene; **Lane 6**: pQE-80L restricted with BamHI and SmaI. Black arrows indicate the approximate sizes of DNA fragments.

The successful construction of the recombinant expression plasmids was confirmed by restriction endonuclease digestion with BamHI and HindIII (**Figure C2.2**). Restriction of pQE-80L::*Ms*CnoX, pQE-80L::*Mt*CnoX, pQE-80L::*Ec*CnoX and pQE-80L::*Ms*TrxC yielded two DNA fragments that corresponded to the size of the linearised vector (4700 bp; **Lanes 2-6**) and DNA fragments used for cloning each gene (**Lane 2:** 970 bp, **Lane 3:** 994 bp, **Lane 4:** 934 bp, and **Lane 5:** 329 bp). The sequence of the DNA inserts in the recombinant expression plasmids was sequenced to confirm that no errors had been introduced during PCR amplification. The plasmid maps of pQE-80L::*Ms*CnoX, pQE-80L::*Mt*CnoX, pQE-80L::*Ec*CnoX, and pQE-80L::*Ms*TrxC constructs can be seen in **Figure C2.3**.

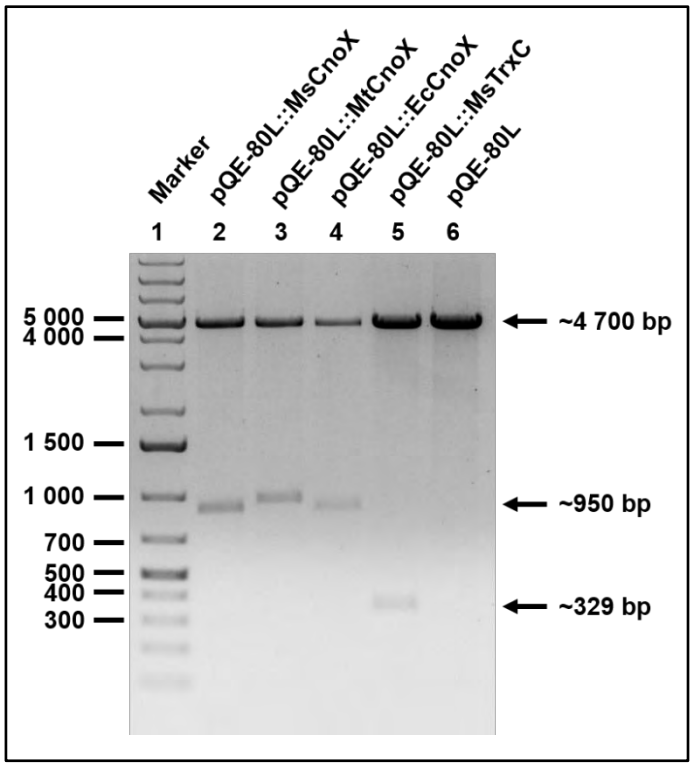

Figure C2.2 Agarose gel confirming the construction of recombinant pQE-80L expression vectors. pQE-80L and putative recombinant vectors harbouring the *MscnoX, MtcnoX, EccnoX* and *MstrxC* genes were analysed by restriction with the BamHI and HindIII restriction endonuclease at **37 f**or 3 hr. The reactions were electrophoresed on a 0.8 % (w/v) agarose gel at 80 V for 90 min before visualisation under UV light. The DNA samples used were as follows: **Lane 1**: Molecular Weight Marker; **Lanes 2**: pQE-80L::*Ms*CnoX; **Lane 3**: pQE-80L::*Mt*CnoX; **Lane 4**: pQE-80L::*Ec*CnoX; **Lane 5**: pQE-80L::*Ms*TrxC; **Lane 6**: pQE-80L. Black arrows indicate the approximate sizes of the linearised vector and DNA inserts.

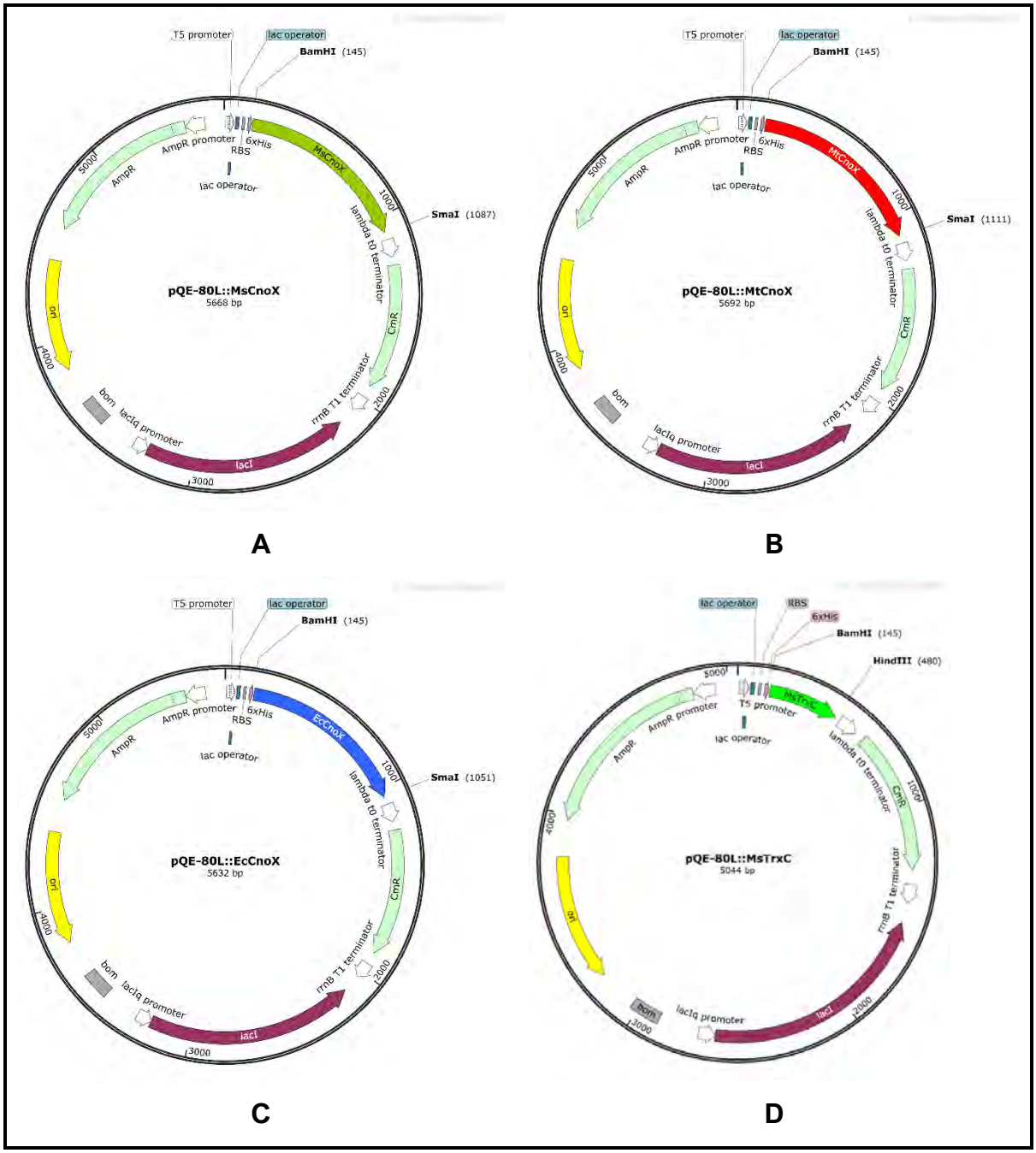

Figure C2.3 Complement constructs of A) pQE-80L::*Ms*CnoX, B) pQE-80L::*Mt*CnoX, C) pQE-80L::*Ec*CnoX, and D) pQE-80L::*Ms*TrxC maps. Indicating direction of replication, the inserted genes of interest (*MscnoX, MtcnoX, EccnoX,* and *MstrxC*, respectively**)**, and relevant restriction enzyme sites (BamHI, SmaI, and HindIII).

C3: Construction and confirmation of recombinant CRISPRi vectors

To generate CRISPRi vectors capable of silencing the expression of the *cnoX* gene in Msm, sgRNAs that target the non-template strand of the gene were designed. For this, we first identified all of the PAM sequences recognised by dCas9 on the non-template strand of the *cnoX* gene. As shown in **Figure C3.1**, a total of 18 PAM sequences were identified in the *MscnoX* gene. Three PAM sequences (5'-ATGGAAG-3', 5'-CAGGAAA-3' and 5'-CGAGGAT-3') with the greatest similarity to the canonical dCas9 PAM were selected for use in designing the sgRNA targeting sequences *cnoX*_sgRNA1, *cnoX*_sgRNA2 and *cnoX*_sgRNA3. The DNA sequences 21, 22 and 20 bp downstream of the three respective PAM sequences (**Figure C3.1**) were ordered as complementary oligonucleotides that were annealed and ligated into pLJR962 as BsmBI fragments using Golden Gate Cloning (see **Methods Section 2.12.1**, and **Figure C3.2**). A 22 bp DNA sequence encoding a sgRNA targeting sequence for the essential *mmpL3* gene was included as a positive control. The Golden Gate cloning reactions were subsequently introduced into chemically competent *E. coli* and transformants selected on LA/Kan plates.

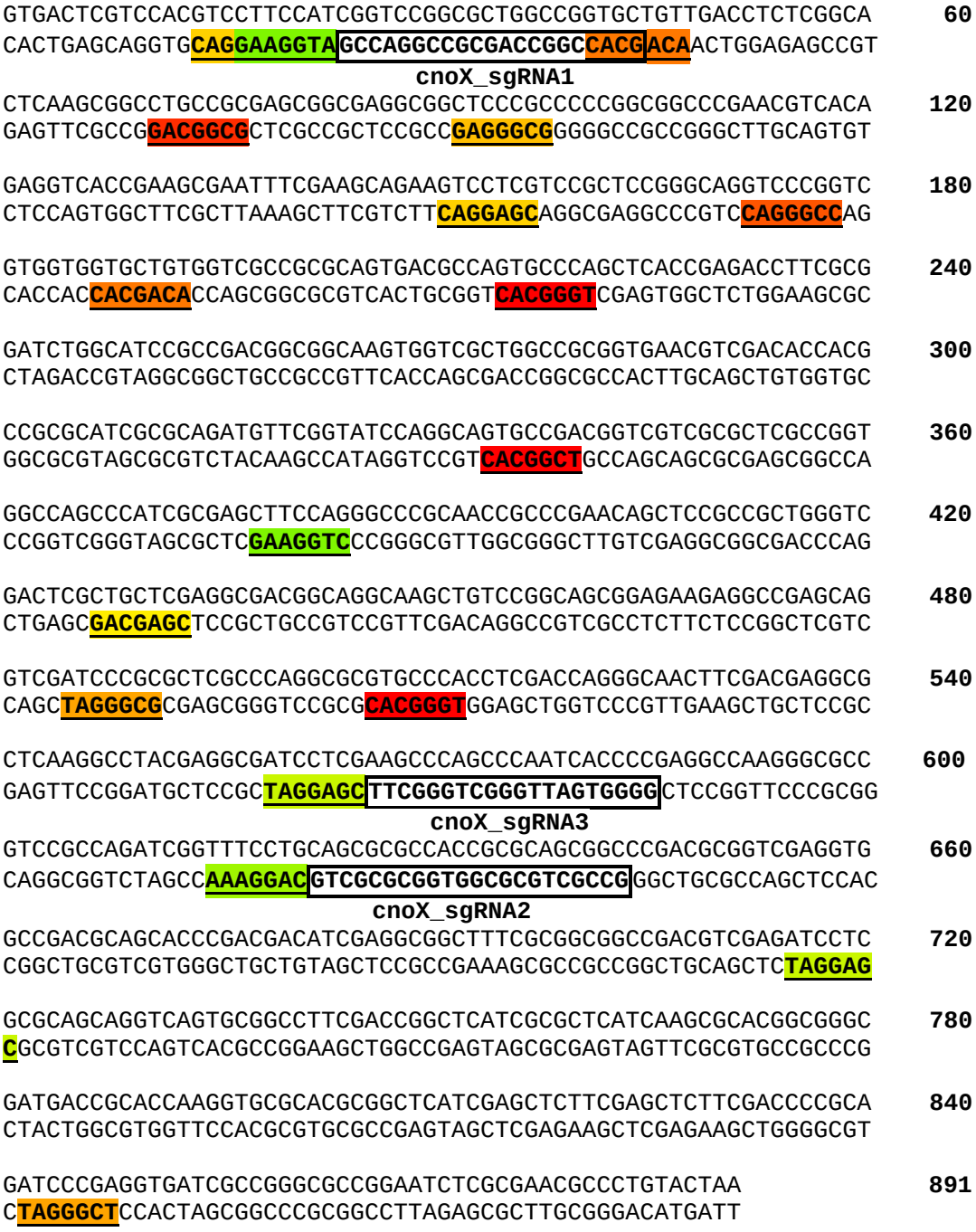

Figure C3.1 Location of dCas9 PAM sequence in the *MscnoX* gene. The sequence and location of PAM sequences recognized by the pLJR962-encoded dCas9 in mycobacterial species are underlined and their strength is indicated by colour, ranging from green (strong) to red (weak). The 3 PAM sequences used in this study with their corresponding sgRNA sequences (cnoX_sgRNA1, cnoX_sgRNA2 and cnoX_sgRNA3) are labelled and indicated by a box.

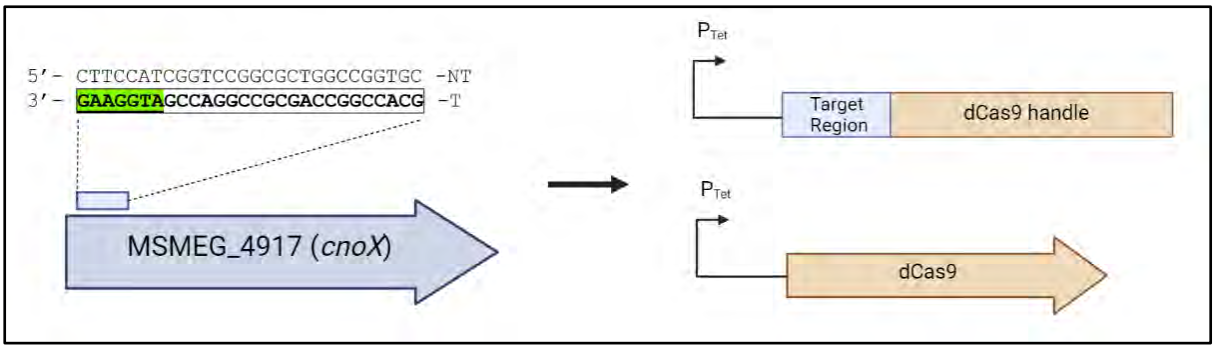

Figure C3.2 Schematic of CRISPRi targeting of the Msm *cnoX* gene. A) The sequence and relative location of the PAM and targeting sequence of *cnoX*_sgRNA1 used to generate the Msm *cnoX* KD1 mutant are indicated. **B)** The integrating pLJR962 plasmid expresses both the sgRNA together with the targeting region and dCas9 handle, as well as **C)** the $dCas9_{Sth1}$ from ATc-inducible promoters (P_{tet}).

The successful introduction of the sgRNAs into the pLJR962 plasmid was confirmed by colony PCR analysis of two Kan^R transformants from each ligation using a sgRNA-specific forward primer (cnoX_sgRNA_For1, 2 or 3) and a vector-specific reverse primer (pLJR-Seq-Rev). As shown in **Figure C3.3**, PCR products of the predicted size (~250 bp) were identified for each of the *cnoX*-specific (**Lanes 2-3**: *cnoX*-sgRNA1; **Lanes 4-5**: *cnoX*-sgRNA2; **Lanes 6-7:** *cnoX*_sgRNA3) and *mmpL3*-specific sgRNA targeting sequences (**Lanes 8-9:** *mmpL3* sgRNA 1) confirming the successful generation pLJR962::*cnoX* sgRNA1, pLJR962::*cnoX*_sgRNA2, pLJR962::*cnoX*_sgRNA3, and pLJR962::*mmpL3*_ sgRNA plasmids. Following the purification of the recombinant plasmids from positive clones, the presence and sequence of the sgRNA sequences were subsequently confirmed by Sanger sequencing (with pLJR-Seq-For and pLJR-Seq-Rev).

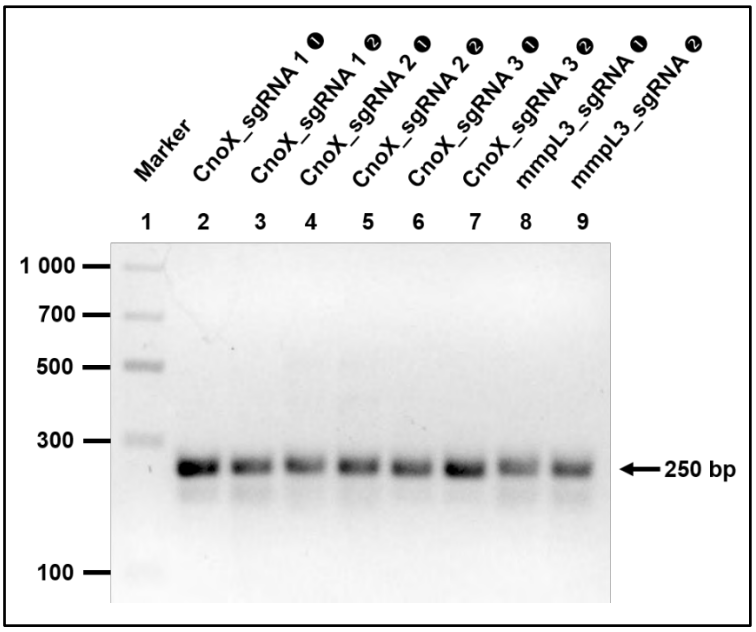

Figure C3.3 Confirmation of the successful cloning of the sgRNA oligonucleotides into pLJR962 by colony PCR. PCR amplification of the DNA inserts contained in pLJR962 was performed using cell lysates obtained from Kan^R transformants using forward primers specific for *cnoX*_sgRNA1 (**Lanes 2-3**), *cnoX*_sgRNA2 (**Lanes 4-5**), *cnoX*_sgRNA3 (**Lanes 6-7**) or *mmpL3*_sgRNA (**Lanes 8-9**) together with a vector-specific reverse primer, pLJR-Rev-Seq. The reaction products were subjected to electrophoresis on 0.8 % (w/v) agarose at 80 V for 45 mins and visualised under UV light. **Lane 1**: MW Marker, **Lanes 2-3**: Colony PCR products from pLJR962::*cnoX*_sgRNA1 clones 1 and 2; **Lanes 4-5**: Colony PCR products from pLJR962::*cnoX* _sgRNA2 clones 1 and 2; **Lanes 6-7**: Colony PCR products from pLJR962::*cnoX*_sgRNA3 clones 1 and 2; **Lanes 8-9**: Colony PCR products from pLJR962::*mmpL3*_sgRNA clones 1 and 2.

C4: Construction and confirmation of complementation vectors

To generate complementation vectors capable of restoring the growth phenotypes of the *cnoX* mutant strains, the *cnoX* gene from Msm was PCR amplified and cloned into the integrative vector, pGiles::P_{smyc}, under control of either the plasmid-borne, strong mycobacterial promoter (P_{smyc}) or its native promoter as described in the Materials and Methods (**Section 2.12.3**). As shown in **Figure C4.1**, PCR amplification of the *MscnoX* gene with the CnoX-CompX-SphI-For and CnoX-Comp-HindIII-Rev or CnoX-CompP-XbaI-For and Comp-HindIII-Rev primer pairs produced amplicons of the expected size (914 and 1139 bp, respectively; **Lanes 2 and 4**). The 914 bp PCR product was digested with SphI and HindIII and ligated into pGiles::P_{smyc} digested with the same enzymes (**Figure C4.1**, **Lane 3**) to generate pCnoX-CompX. The 1139 bp PCR product was digested with XbaI and HindIII and ligated into pGiles::P_{smyc} (**Figure C4.1**, **Lane 5**) digested with the same enzymes to generate pCnoX-CompP.

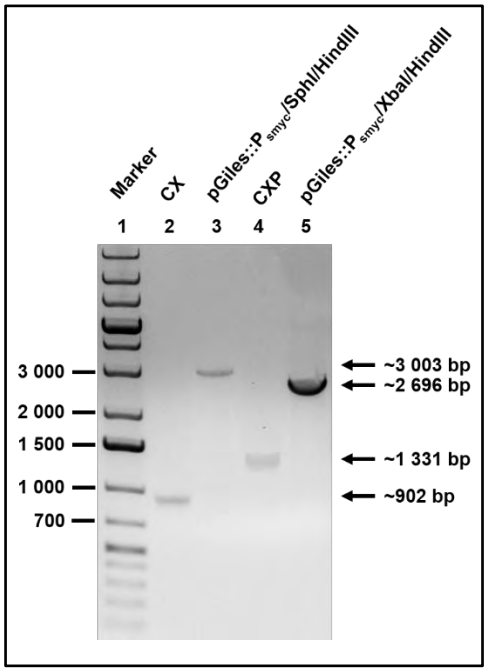

Figure C4.1 Agarose gel electrophoresis of PCR amplicons harbouring the *MscnoX* gene with (CompP) and without (CompX) and restricted pGiles::P_{smyc} plasmid. PCR reactions were performed using genomic DNA isolated from WT Msm using primers CnoX-CompX-SphI-For and Comp-HindIII-Rev (CompX fragment) and CnoX-CompP-XbaI-For and Comp-HindIII-Rev (CompP fragment). Plasmid pGiles::P_{smyc} was digested with the indicated restriction enzymes. The PCR reactions and digestion products were electrophoresed on a 0.8 % (w/v) agarose gel at 80 V for 50 mins. **Lane 1**: Molecular Weight Marker; **Lane 2**: *cnoX* gene amplicon; **Lane 3**: pGiles::P_{smyc} digested with SphI and HindIII; **Lane 4**: *cnoX* gene and its natural promoter amplicon; **Lane 5**: pGiles::P_{smyc} digested with XbaI and HindIII. Black arrows indicate the predicted sizes of DNA fragments.

Following restriction enzyme digestion and ligation into pGiles::P_{smyc}, the presence of *cnoX* with (CompP) or without (CompX) its native promoter in the recombinant plasmids was confirmed by restriction enzyme digestion with XbaI and HindIII or SphI and HindIII, respectively (**Figure C4.2**). For pCnoX-CompX, two bands of ~3000 bp and 900 bp were identified following restriction enzyme digestion with SphI and HindIII, confirming the presence of the correct DNA insert (**Figure C4.2**, **Lanes 2 and 3**). By contrast, a single band of ~3000 bp was identified when the parental pGiles::P_{smyc} was digested with the same enzymes (**Figure C4.2**, **Lane 4**). For pCnoX-CompP, two bands of ~2700 bp and 1300 bp were identified following restriction enzyme digestion with XbaI and HindIII, confirming the presence of the correct DNA insert (**Figure C4.2**, **Lanes 5 and 6**). Two bands of ~2700 bp and ~350 bp, corresponding to the linearized vector backbone and stuffer fragment, were identified when the parental pGiles::P_{smyc} vector was digested with the same enzymes (**Figure C4.2**, **Lane 7**). The plasmid maps of pCnoX-CompX and pCnoX-CompP constructs can be seen in **Figure C4.3**.

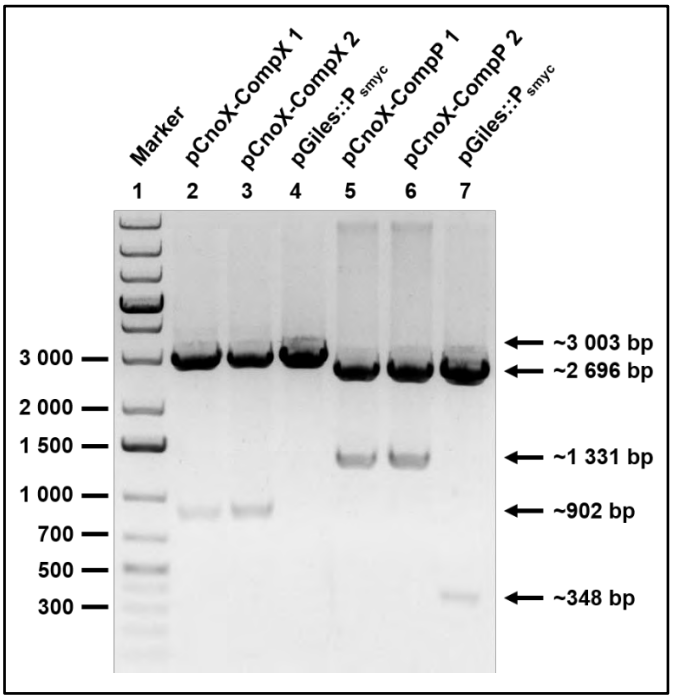

Figure C4.2 Agarose gel electrophoresis of restriction digests of *Ms*CnoX complementation plasmids. Two putative pCnoX-CompX or pCnoX-CompP plasmids were restricted with SphI and HindIII (**Lanes 2-4**) or XbaI and HindIII (**Lanes 5-7**). pGiles::P_{smyc} (**Lanes 4 and 7**) were included as controls. The products of the restriction enzyme digestion were electrophoresed on a 0.8 % (w/v) agarose gel at 80 V for 50 min. The DNA samples used in each lane were as follows: **Lane 1**: Molecular Weight Marker; **Lanes 2-3**: pCnoX-CompX; **Lane 4**: pGiles::P_{smyc}; **Lanes 5-6**: pCnoX-CompP; **Lane 7**: pGiles::P_{smyc} digested with XbaI and HindIII. Black arrows indicate the sizes of the predicted PCR amplicons.

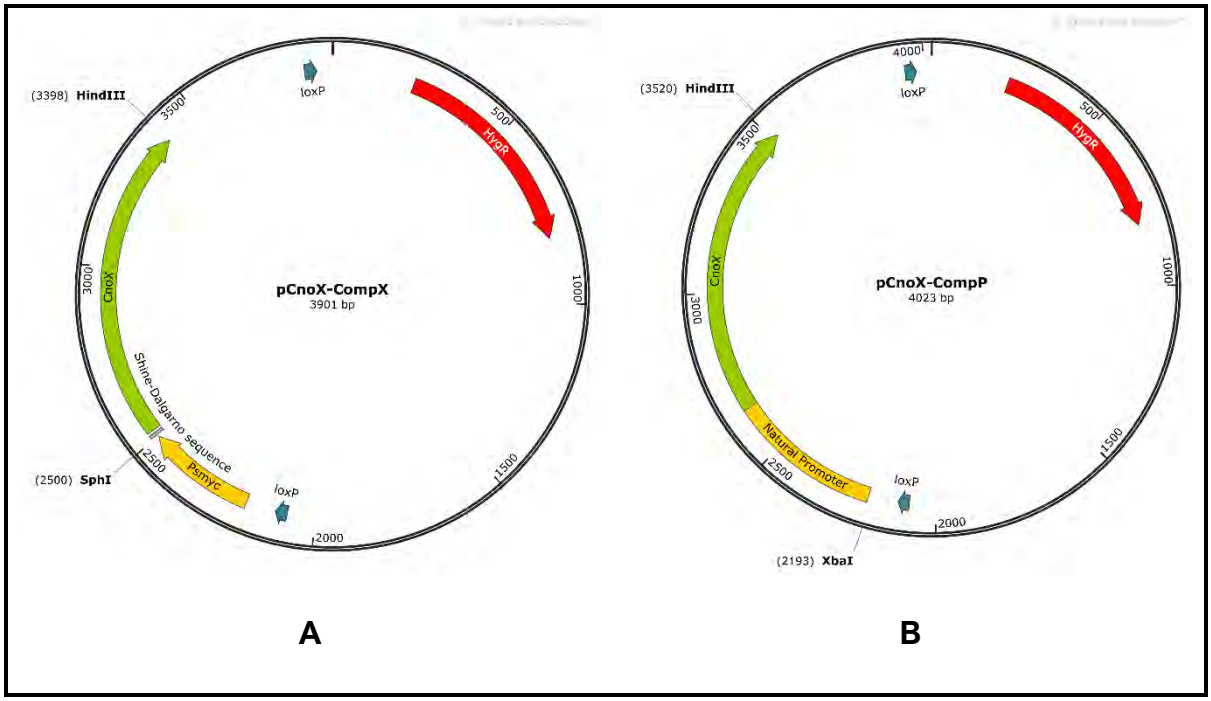

Figure C4.3 Complement constructs of A) pCnoX-CompX and B) pCnoX-CompP maps. Indicating the direction of replication, the inserted genes of interest (*cnoX* without its natural promoter, and with its natural promoter, respectively**)**, and relevant restriction enzyme sites (SphI, XbaI, and HindIII).

Appendix D: Supporting Experiments

D1: Examination of recombinant protein solubility

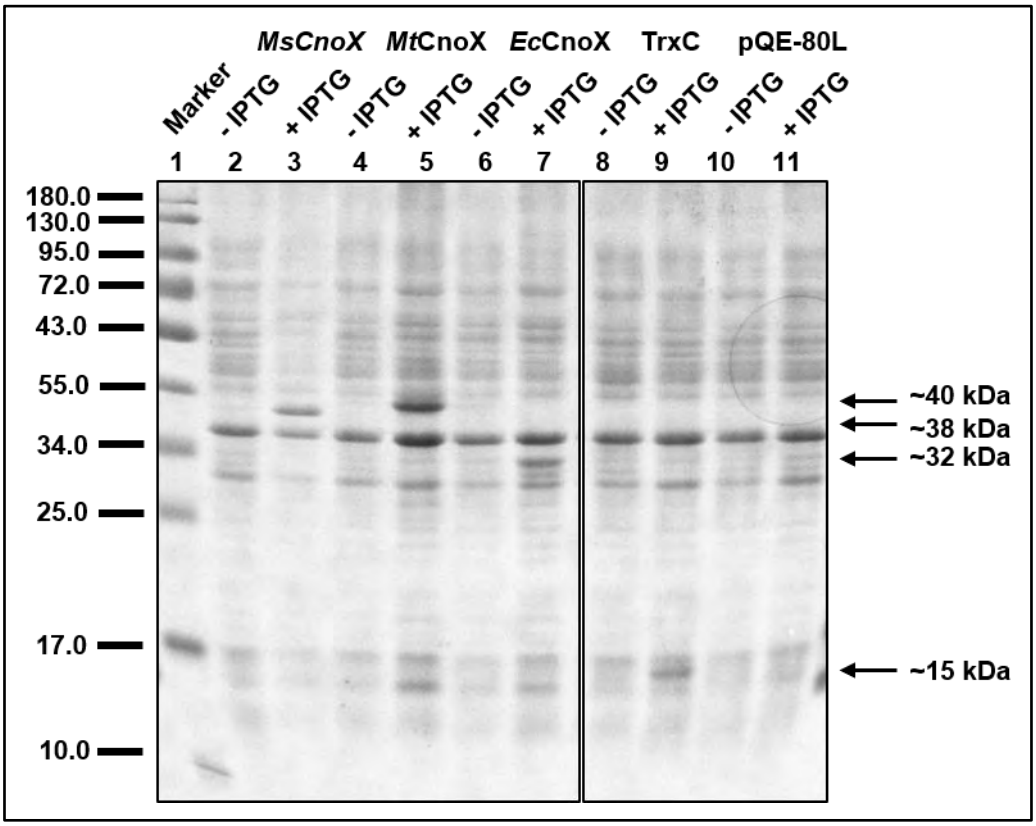

Figure D1.1 SDS-PAGE analysis of the insoluble fraction containing the expressed *Ms*CnoX, *Mt*CnoX, *Ec*CnoX, and *Ms*TrxC recombinant proteins. *E. coli* XJb cells were transformed with pQE-80L encoding the CnoX enzymes from *Msm*, *Mtb*, and *E. coli*, as well as pQE-80L encoding the *Msm* TrxC and pQE-80L parental vector alone were included as positive and negative controls, respectively. Faint bands of ~38, ~40, ~32 and ~15 kDa bands were observed in the insoluble fractions in the presence of 0.1 mM IPTG (+IPTG), but not in the absence of IPTG (-IPTG). No over-expressed proteins were observed in the cells transformed with the parental vector. The size of the molecular weight markers (kDa) is indicated. **Lane 1**: Molecular Weight Marker; **Lane 2:** uninduced pQE-80L::*Ms*CnoX culture; **Lane 3:** induced pQE-80L::*Ms*CnoX culture; **Lane 4:** uninduced pQE-80L::*Mt*CnoX culture; **Lane 5:** induced pQE-80L::*Mt*CnoX culture; **Lane 6:** uninduced pQE-80L::*Ec*CnoX culture; **Lane 7:** induced pQE-80L::*Ec*CnoX culture; **Lane 8:** uninduced pQE-80L::*Ms*TrxC culture; **Lane 9:** induced pQE-80L::*Ms*TrxC culture; **Lane 10:** uninduced pQE-80L vector only culture; **Lane 11:** induced pQE-80L vector only culture. Black arrows indicate insoluble forms of each protein.

D2: Examination of ATc Susceptibility

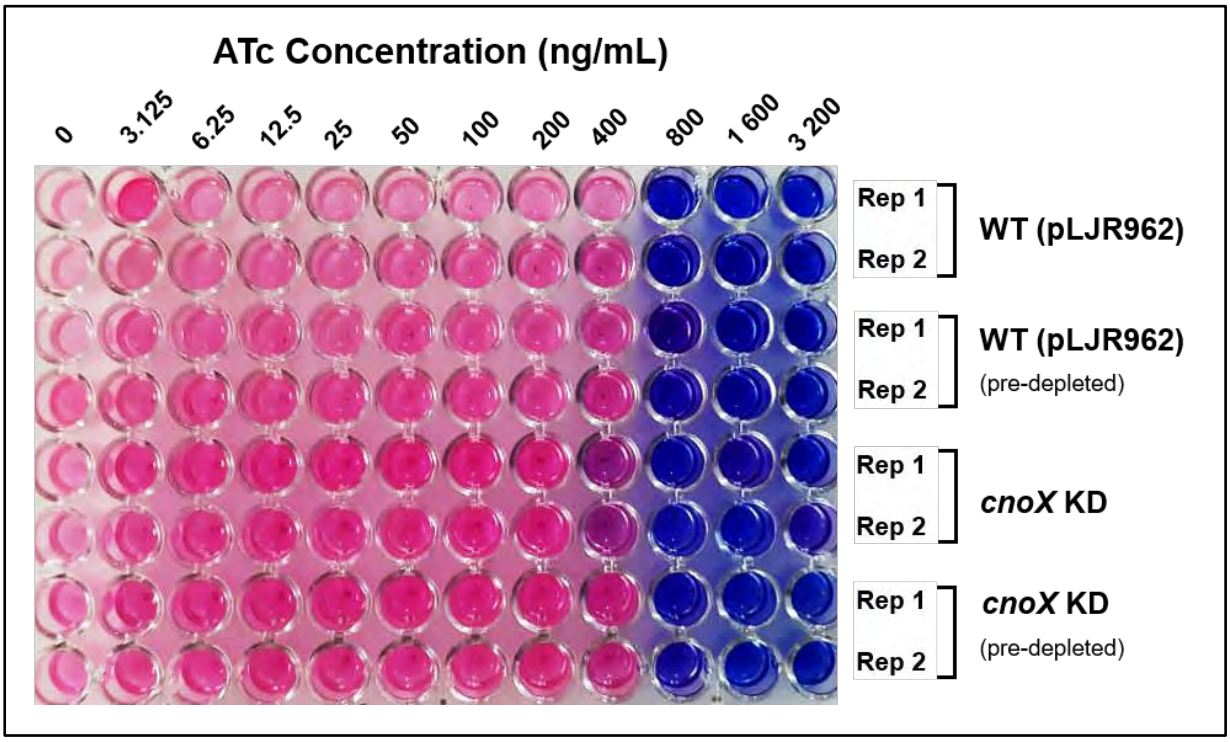

Figure D2.1 Relative growth of the Msm cnoX KD1 mutant and WT (pLJR962) control strain at varying concentrations of ATc. The Msm CRISPRi *cnoX* KD1 mutant and WT (pLJR962) control strains were cultured in the presence (200 ng/mL – pre-depleted) and absence (0 ng/mL) of ATc to mid-log phase, followed by dilution to a final OD_{600} of 0.002 in 7H9. ATc was added as a 2-fold dilution series. Resazurin was used to indicate bacterial growth, with a transition from a blue to a pink colour indicating active bacterial growth. A dark blue colour indicates the absence of growth.

Appendix E: Heterologous Complementation Analysis of *E. coli cnoX* Mutants

E1: Genotypic and phenotypic analysis of the *E. coli* cnoX mutant

To examine whether the mycobacterial CnoX enzymes could complement the growth phenotypes of an *E. coli* Δ*cnoX* mutant, the WT *E. coli* BW25113 and marked Δ*cnoX::*Kan^R mutant from Keio Collection (Baba *et al.*, 2006; Datsenko and Wanner, 2000) was purchased from Dharmacon. To confirm the genotypes of the WT and Δ*cnoX::*Kan^R strains, PCR was performed using the EC-CnoX-For and EC-CnoX-Rev primers. A PCR product of ~1300 bp was amplified from the WT strain (**Figure E1.1**), which corresponds with the predicted size of the full-length *cnoX* gene. A PCR product of ~1700 bp was, by contrast, obtained for the Δ*cnoX::*Kan^R mutant (**Figure E1.1**), which corresponds with the expected size of the marked *cnoX* gene harbouring the kanamycin-resistance cassette.

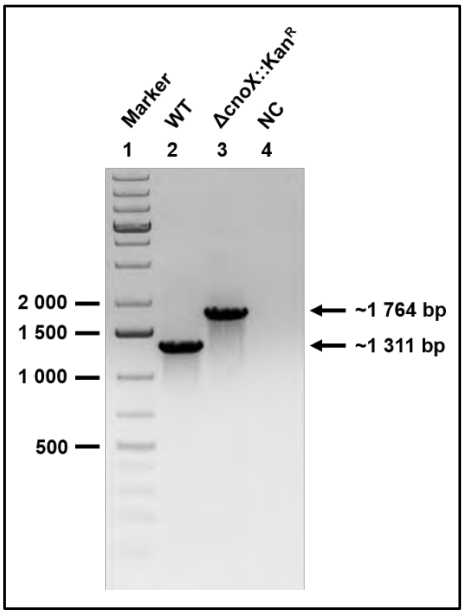

Figure E1.1 PCR confirmation of the genotype of the putative Msm *cnoX*::Kan^R mutant. PCR reactions were performed using genomic DNA isolated from WT or one putative Δ*cnoX*::Kan^R mutant using primers EC-CnoX-For and EC-CnoX-Rev. The products of the PCR reactions were electrophoresed on a 0.8 % (w/v) agarose gel at 80 V for 50 mins. The gDNA used as a template in the PCR reactions were as follows: **Lanes 2**: *E. coli* BW25113 WT gDNA, **Lanes 3**: *E. coli* BW25113 Δ*cnoX*::Kan^R gDNA, **Lane 4**: No DNA negative control. Black arrows indicate the sizes of the predicted PCR amplicons.

Following confirmation of the genotype of the marked Δ*cnoX::*Kan^R mutant, an unmarked *cnoX* mutant was generated via the introduction of pE-FLP into chemically competent *E. coli* BW25113 Δ*cnoX*::Kan^R cells. Following selection on LA plates supplemented with ampicillin and incubation at 30 °C, the genotypes of ampicillin-resistant transformants were determined by PCR using the EC-CnoX-For and EC-CnoX-Rev primers. As described above, amplicons of ~1300 and 1700 bp were obtained for the WT and marked Δ*cnoX::*Kan^R mutant (**Figure E1.2, Lanes 2 and 3**). The unmarked Δ*cnoX* mutant yielded an amplicon of ~550 bp (**Figure E1.2**), which corresponds to the predicted size of the *cnoX* gene following excision of the FRT-flanked kanamycin resistance cassette by FLP recombinase. The strain was cured of temperature-sensitive pE-FLP by streaking colonies on LA and incubating them at 37 °C, before subsequent experiments.

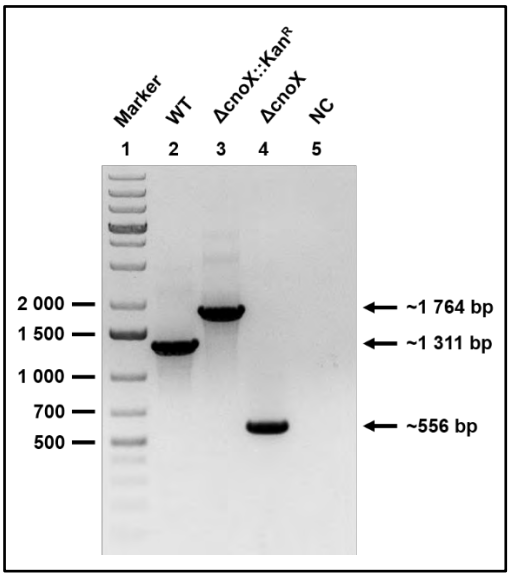

Figure E1.2 PCR confirmation of the genotype of the putative unmarked Δ*cnoX* mutant. PCR reactions were performed using genomic DNA isolated from WT, Δ*cnoX*::Kan^R, or putative Δ*cnoX* mutant using primers EC-CnoX-For and EC-CnoX-Rev. The products of the PCR reactions were electrophoresed on a 0.8 % (w/v) agarose gel at 80 V for 50 mins followed by visualisation under UV light. The gDNA used as a template in the PCR reactions were as follows: **Lanes 2**: *E. coli* BW25113 WT gDNA, **Lanes 3**: *E. coli* BW25113 Δ*cnoX::*Kan^R gDNA, **Lane 4**: *E. coli* BW25113 Δ*cnoX*; **Lane 5**: No DNA negative control. Black arrows indicate the sizes of the predicted PCR amplicons.

Following the generation of an unmarked *E. coli* BW25113 Δ*cnoX* strain, pQE-80L and its recombinant derivatives generated in **Section 3.1** (further expanded in **Appendix C1**) were transformed into chemically competent *E. coli* BW25113 Δ*cnoX* cells and plated on LA plates supplemented with ampicillin, generating the heterologous complement strains.

E2: Examination of NaOCl susceptibility of the *E. coli* BW25113 Δ*cnoX* mutant.

Previous research has established that an *E. coli cnoX* mutant, is hyper-susceptible to HOCl (Goemans *et al.*, 2018a). To examine the suitability of the mutant strain for conducting heterologous complementation analysis, the susceptibility for the *E. coli* WT and Δ*cnoX* mutant was compared. To this end, the survival of the strains following exposure to various concentrations of NaOCl (0, 200, 200 μM) was initially examined using a spotting assay. As shown in **Figure E2.1**, no significant differences between the survival of the *E. coli* BW25113 WT and Δ*cnoX* mutant strains was observed when exposed to these concentrations 37 °C for 20 min.

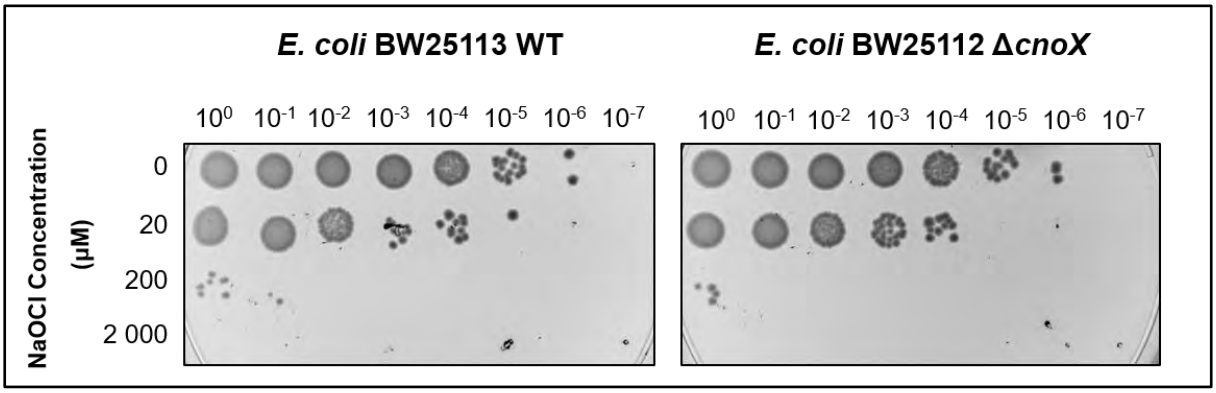

Figure E2.1 Survival of the *E. coli* BW25113 WT and Δ*cnoX* mutant strains following exposure to NaOCl. The indicated strains were grown in M9 MM at 37 °C to an OD_{600} of 0.4 and harvested by centrifugation. The cells were washed (1 ×) and resuspended in PBS containing the indicated concentration of NaOCl for 20 min at 37 °C. The NaOCl was quenched by the addition of methionine and the samples were serially diluted ten-fold and spotted onto LA plates. The plates were incubated at 37 °C for 16 h before imaging. These images are representative of three experimental replicates.

No significant difference in the size of the zones of inhibition was, furthermore, observed for the WT and unmarked Δ*cnoX* mutant strains following exposure to increasing concentrations of NaOCl using a disc-diffusion assay (**Figure E2.2**). The MIC of NaOCl for the two strains were also shown to be identical in both LB and M9 minimal medium (4 mM) when assayed using the broth microdilution method (data not shown), which is similar to previous findings in BW25113 where the MIC to NaOCl is 6 mM (Chen *et al.*, 2021).

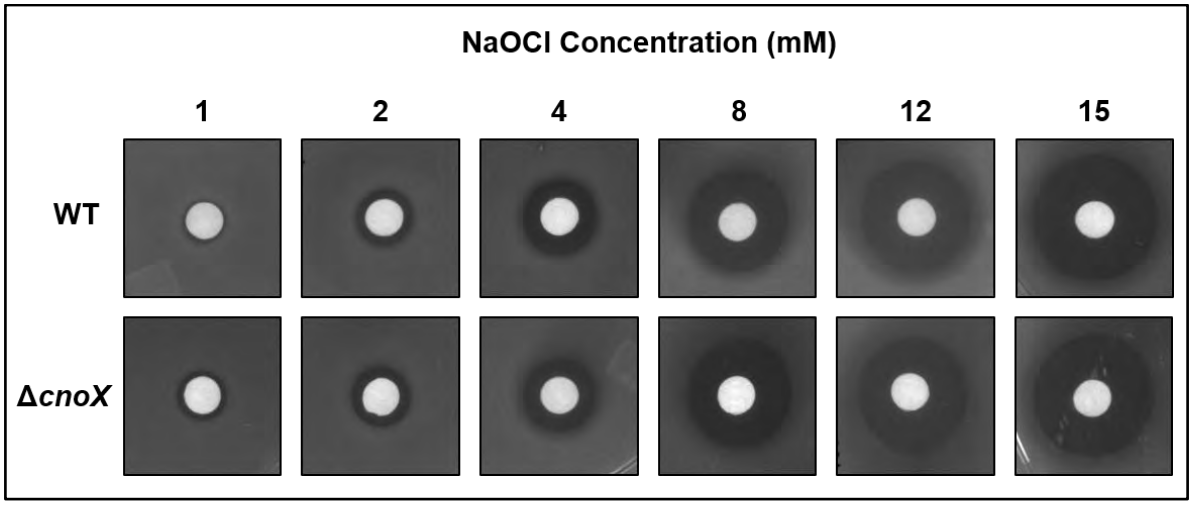

Figure E2.2 Susceptibility of the *E. coli* BW25113 Δ*cnoX* mutant following exposure to NaOCl. The indicated strains were cultured to an OD_{600} to mid-log phase, followed by dilution to a final OD_{600} of 0.025 in 1 % (w/v) molten agar to prepare agar overlay plates. Sodium hypochlorite (NaOCl) was aliquoted onto discs at the indicated concentrations and placed on the agar overlay plate. The zones of inhibition (ZOI) were measured after 24 h. These results are representative of six replicates.

Since no difference in the susceptibility of the WT and *cnoX* mutant was observed, further attempts at heterologous complementation were not pursued. The reason(s) for our inability to recapitulate the NaOCl-hyper susceptibility phenotype of the *cnoX* mutant reported by Goemans *et al.* (2018a) is not known. Our findings do, nevertheless, concur with the more recent findings of Meireles *et al.* (2020) who were also unable to reproduce the NaOCl-hyper susceptibility phenotype of the cnoX mutant in both the *E. coli* BW25113 and MG1655 genetic backgrounds.

Appendix F: Multiple Sequence Alignment of Mycobacterial CnoX Homologs

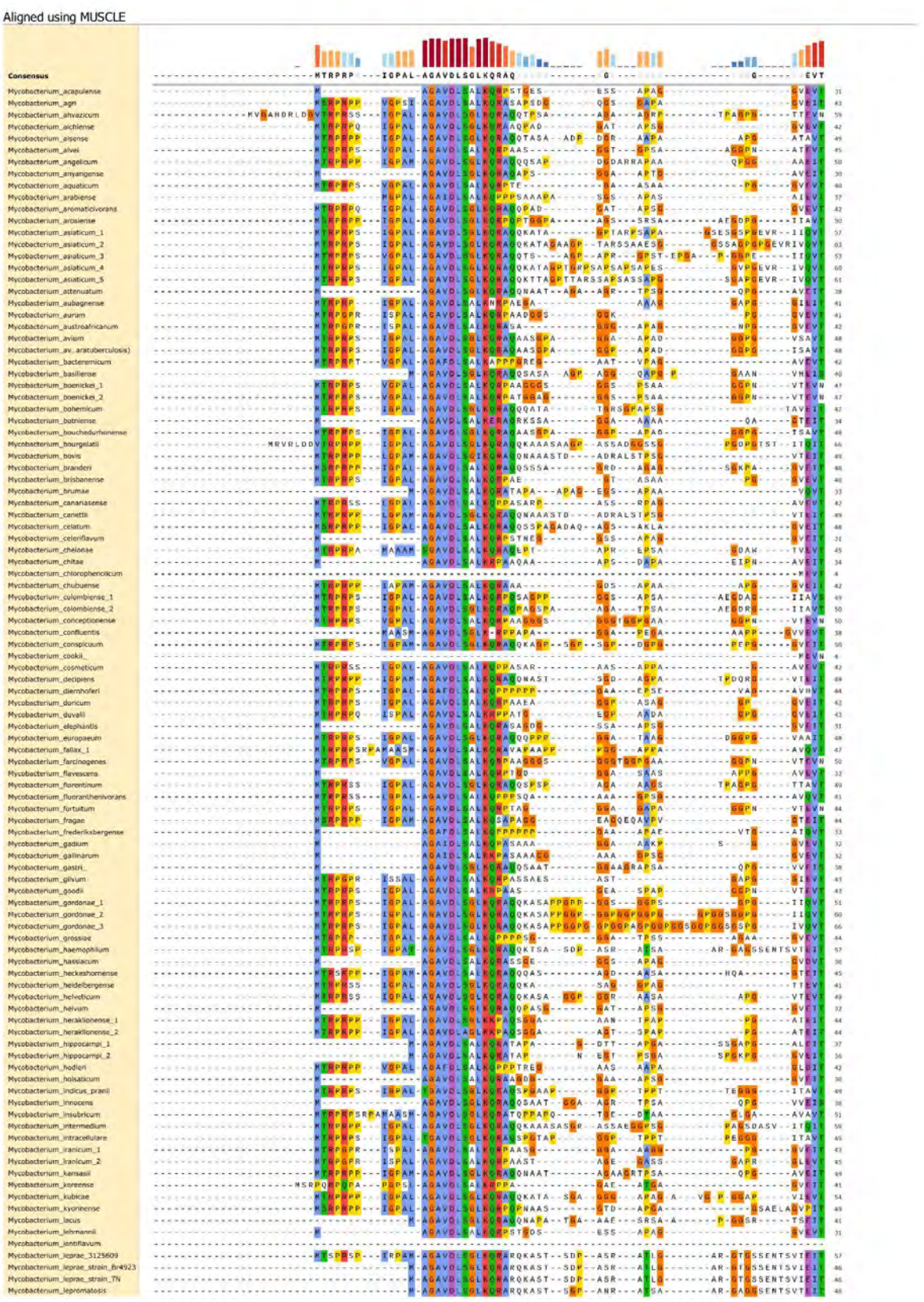

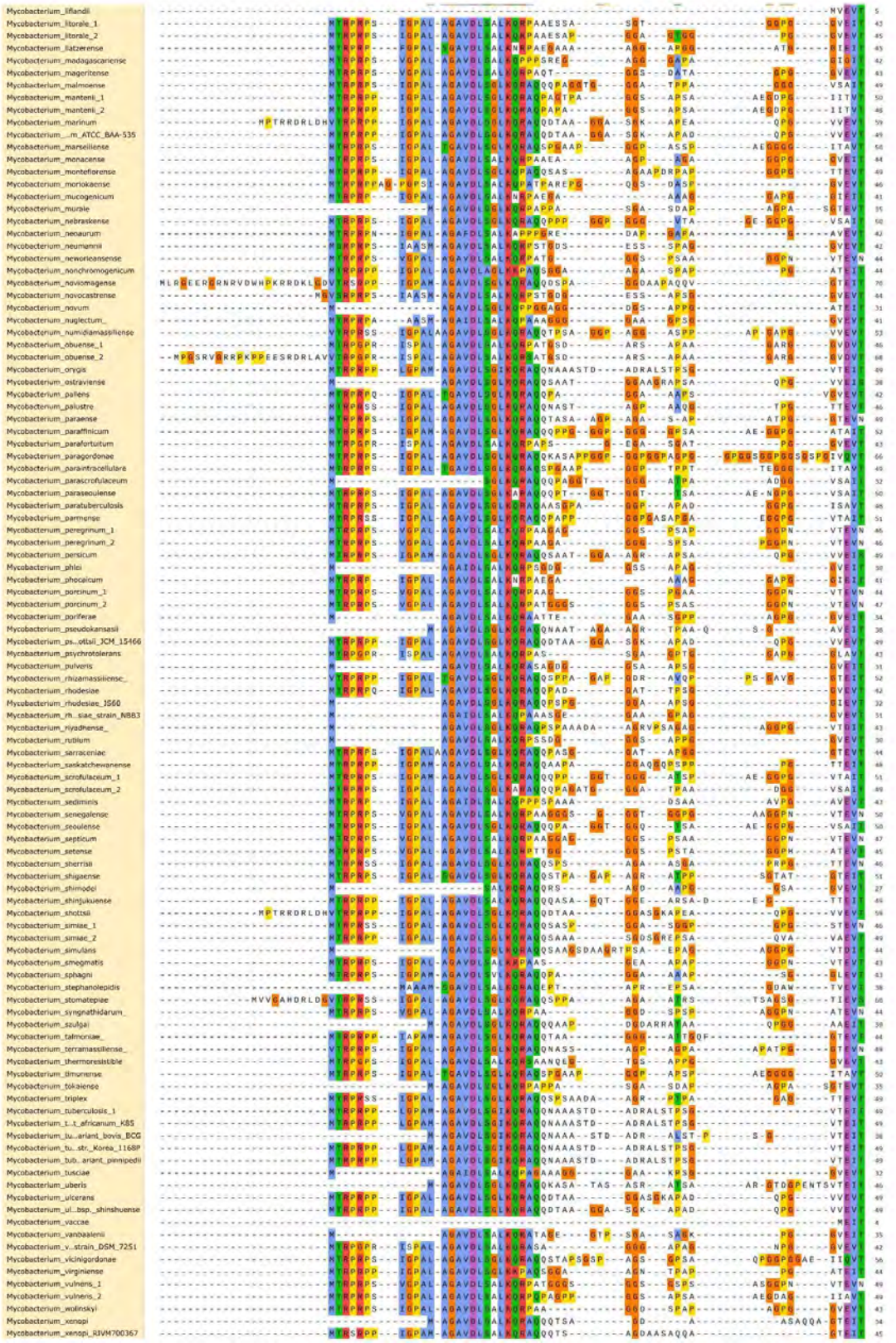
Mycobacterium_lifiandii
Mycobacterium_litorale_1
Mycobacterium_litorale_2
Mycobacterium_liflatzerense
Mycobacterium_madagascariense
Mycobacterium_mageritense
Mycobacterium_malmoense
Mycobacterium_mantenii_1
Mycobacterium_mantenii_2
Mycobacterium_marinum
Mycobacterium_...m_ATCC_BAA-535
Mycobacterium_marseillense
Mycobacterium_monacense
Mycobacterium_montefiorense
Mycobacterium_moriokaense
Mycobacterium_mucogenicum
Mycobacterium_murale
Mycobacterium_nebraskense
Mycobacterium_neoaurum
Mycobacterium_neumannii
Mycobacterium_neworleansense
Mycobacterium_nonchromogenicum
Mycobacterium_noviomagense
Mycobacterium_novocastrense
Mycobacterium_novum
Mycobacterium_nuglectum_
Mycobacterium_numidiamassiliense
Mycobacterium_obuense_1
Mycobacterium_obuense_2
Mycobacterium_orygis
Mycobacterium_ostraviense
Mycobacterium_pallens
Mycobacterium_palustre
Mycobacterium_paraense
Mycobacterium_paraffinicum
Mycobacterium_parafortuitum
Mycobacterium_paragordonae
Mycobacterium_paraintracellulare
Mycobacterium_parascrofulaceum
Mycobacterium_paraseoulense
Mycobacterium_paratuberculosis
Mycobacterium_parmense
Mycobacterium_peregrinum_1
Mycobacterium_peregrinum_2
Mycobacterium_persicum
Mycobacterium_phlei
Mycobacterium_phocaicum
Mycobacterium_porcinum_1
Mycobacterium_porcinum_2
Mycobacterium_poriferae
Mycobacterium_pseudokansasii
Mycobacterium_ps...ottii_JCM_15466
Mycobacterium_psychrotolerans
Mycobacterium_pulveris
Mycobacterium_rhizamassiliense_
Mycobacterium_rhodesiae
Mycobacterium_rhodesiae_JS60
Mycobacterium_rh...siae_strain_NBB3
Mycobacterium_riyadhense_
Mycobacterium_rutilum
Mycobacterium_sarraceniae
Mycobacterium_saskatchewanense
Mycobacterium_scrofulaceum_1
Mycobacterium_scrofulaceum_2
Mycobacterium_sediminis
Mycobacterium_senegalense
Mycobacterium_seoulense
Mycobacterium_septicum
Mycobacterium_setense
Mycobacterium_sherrisii
Mycobacterium_shigaense
Mycobacterium_shimodei
Mycobacterium_shinjukuense
Mycobacterium_shottsii
Mycobacterium_simiae_1
Mycobacterium_simiae_2
Mycobacterium_simulans
Mycobacterium_smegmatis
Mycobacterium_sphagni
Mycobacterium_stephanolepidis
Mycobacterium_stomatepiae
Mycobacterium_syngnathidarum_
Mycobacterium_szulgai
Mycobacterium_talmoniae_
Mycobacterium_terramassiliense_
Mycobacterium_thermoresistibile
Mycobacterium_timonense
Mycobacterium_tokaiense
Mycobacterium_triplex
Mycobacterium_tuberculosis_1
Mycobacterium_t...t_africanum_K85
Mycobacterium_tu...ariant_bovis_BCG
Mycobacterium_tu...str._Korea_1168P
Mycobacterium_tub...ariant_pinnipedii
Mycobacterium_tusciae
Mycobacterium_uberis
Mycobacterium_ulcerans
Mycobacterium_ul...bsp._shinshuense
Mycobacterium_vaccae
Mycobacterium_vandoalenii
Mycobacterium_v...strain_DSM_7251
Mycobacterium_vicinigordonae
Mycobacterium_virginiense
Mycobacterium_vulneris_1
Mycobacterium_vulneris_2
Mycobacterium_wolinskyi
Mycobacterium_xenopi
Mycobacterium_xenopi_RIVM700367

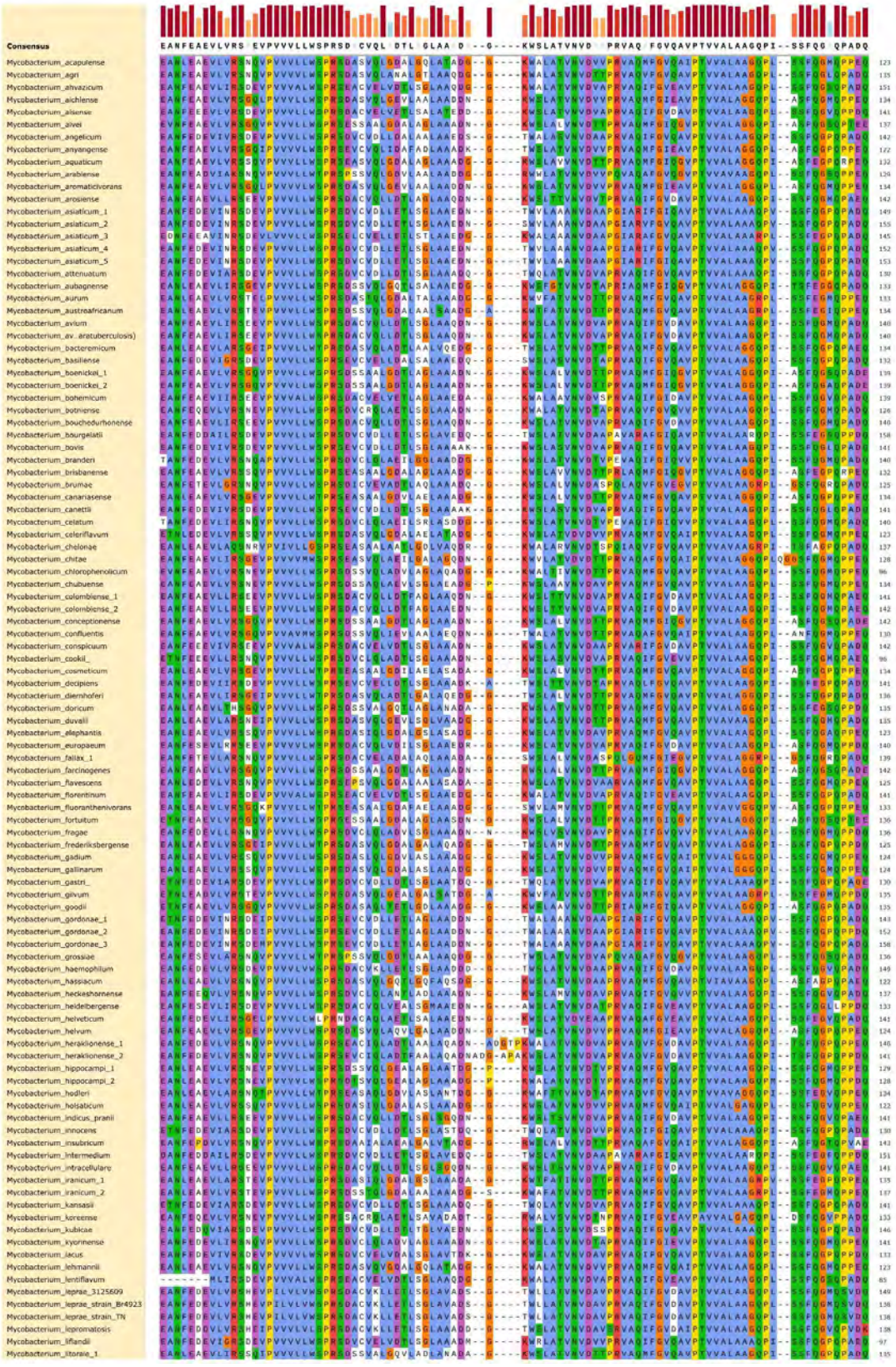
Consensus
Mycobacterium_acapulense
Mycobacterium_agri
Mycobacterium_ahvazicum
Mycobacterium_aichlense
Mycobacterium_alsense
Mycobacterium_alvei
Mycobacterium_angelicum
Mycobacterium_anyangense
Mycobacterium_aquaticum
Mycobacterium_arabiense
Mycobacterium_aromaticivorans
Mycobacterium_arosiense
Mycobacterium_asiaticum_1
Mycobacterium_asiaticum_2
Mycobacterium_asiaticum_3
Mycobacterium_asiaticum_4
Mycobacterium_asiaticum_5
Mycobacterium_attenuatum
Mycobacterium_aubagnense
Mycobacterium_aurum
Mycobacterium_austroafricanum
Mycobacterium_avium
Mycobacterium_av._aratuberculosis)
Mycobacterium_bacteremicum
Mycobacterium_basiliense
Mycobacterium_boenickei_1
Mycobacterium_boenickei_2
Mycobacterium_bohemicum
Mycobacterium_botniense
Mycobacterium_bouchedurhonense
Mycobacterium_bourgelatii
Mycobacterium_bovis
Mycobacterium_branderi
Mycobacterium_brisbanense
Mycobacterium_brumae
Mycobacterium_canariasense
Mycobacterium_canettii
Mycobacterium_celatum
Mycobacterium_celeriflavum
Mycobacterium_chelonae
Mycobacterium_chitae
Mycobacterium_chlorophenolicum
Mycobacterium_chubuense
Mycobacterium_colombiense_1
Mycobacterium_colombiense_2
Mycobacterium_conceptionense
Mycobacterium_confluentis
Mycobacterium_conspicuum
Mycobacterium_cookii_
Mycobacterium_cosmeticum
Mycobacterium_decipiens
Mycobacterium_diernhoferi
Mycobacterium_doricum
Mycobacterium_duvalii
Mycobacterium_elephantis
Mycobacterium_europaeum
Mycobacterium_fallax_1
Mycobacterium_farcinogenes
Mycobacterium_flavescens
Mycobacterium_florentinum
Mycobacterium_fluoranthenivorans
Mycobacterium_fortuitum
Mycobacterium_fragae
Mycobacterium_frederiksbergense
Mycobacterium_gadium
Mycobacterium_gallinarum
Mycobacterium_gastri_
Mycobacterium_gilvum
Mycobacterium_goodii
Mycobacterium_gordonae_i
Mycobacterium_gordonae_2
Mycobacterium_gordonae_3
Mycobacterium_grossiae
Mycobacterium_haemophilum
Mycobacterium_hassiacum
Mycobacterium_heckeshornense
Mycobacterium_heidelbergense
Mycobacterium_helveticum
Mycobacterium_helvum
Mycobacterium_heraklionense_1
Mycobacterium_heraklionense_2
Mycobacterium_hippocampi_1
Mycobacterium_hippocampi_2
Mycobacterium_hodleri
Mycobacterium_holsaticum
Mycobacterium_indicus_pranii
Mycobacterium_innocens
Mycobacterium_insubricum
Mycobacterium_intermedium
Mycobacterium_intracellulare
Mycobacterium_iranicum_1
Mycobacterium_iranicum_2
Mycobacterium_kansasii
Mycobacterium_koreense
Mycobacterium_kubicae
Mycobacterium_kyorinense
Mycobacterium_lacus
Mycobacterium_lehmannii
Mycobacterium_lentiflavum
Mycobacterium_leprae_3125609
Mycobacterium_leprae_strain_Br4923
Mycobacterium_leprae_strain_TN
Mycobacterium_lepromatosis
Mycobacterium_liflandii
Mycobacterium_litorale_1

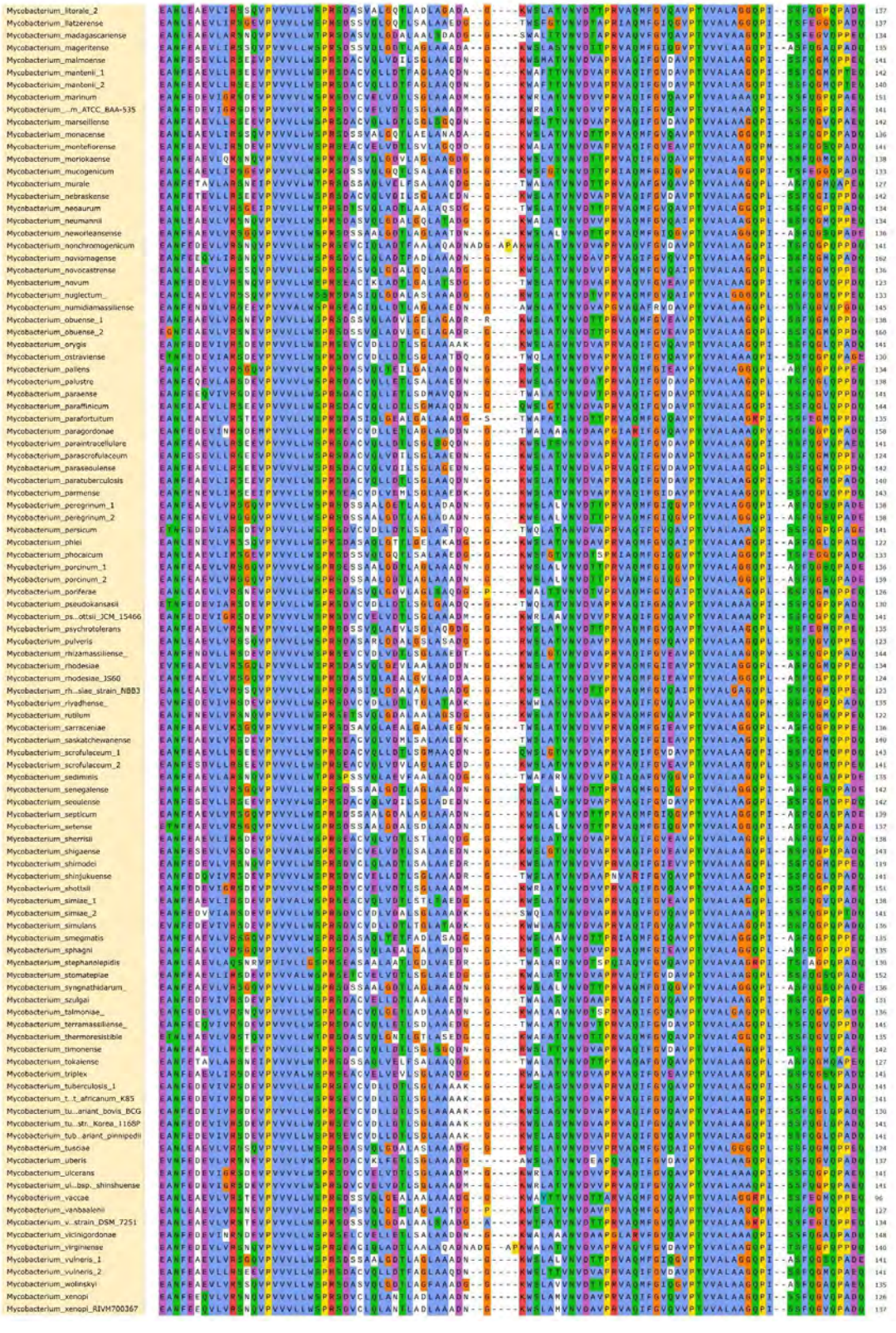
Mycobacterium_litorale_2
Mycobacterium_flatzerense
Mycobacterium_madagascariense
Mycobacterium_mageritense
Mycobacterium_malmoense
Mycobacterium_mantenii_1
Mycobacterium_mantenii_2
Mycobacterium_marinum
Mycobacterium_...m_ATCC_BAA-535
Mycobacterium_marseillense
Mycobacterium_monacense
Mycobacterium_montefiorense
Mycobacterium_moriokaense
Mycobacterium_mucogenicum
Mycobacterium_murale
Mycobacterium_nebraskense
Mycobacterium_neoaurum
Mycobacterium_neumannii
Mycobacterium_neworleansense
Mycobacterium_nonchromogenicum
Mycobacterium_noviomagense
Mycobacterium_novocastrense
Mycobacterium_novum
Mycobacterium_nuglectum_
Mycobacterium_numidiamassiliense
Mycobacterium_obuense_1
Mycobacterium_obuense_2
Mycobacterium_orygis
Mycobacterium_ostraviense
Mycobacterium_pallens
Mycobacterium_palustre
Mycobacterium_paraense
Mycobacterium_paraffinicum
Mycobacterium_parafortuitum
Mycobacterium_paragordonae
Mycobacterium_paraintracellulare
Mycobacterium_parascrofulaceum
Mycobacterium_parasaoulense
Mycobacterium_paratuberculosis
Mycobacterium_parmense
Mycobacterium_peregrinum_1
Mycobacterium_peregrinum_2
Mycobacterium_persicum
Mycobacterium_phlei
Mycobacterium_phocaicum
Mycobacterium_porcinum_1
Mycobacterium_porcinum_2
Mycobacterium_poriferae
Mycobacterium_pseudokansasii
Mycobacterium_ps...ottii_JCM_15466
Mycobacterium_psychrotolerans
Mycobacterium_pulveris
Mycobacterium_rhizamassiliense_
Mycobacterium_rhodesiae
Mycobacterium_rhodesiae_JS60
Mycobacterium_rh...siae_strain_NBB3
Mycobacterium_riyadhense_
Mycobacterium_rutilum
Mycobacterium_sarraceniae
Mycobacterium_saskatchewanense
Mycobacterium_scrofulaceum_1
Mycobacterium_scrofulaceum_2
Mycobacterium_sediminis
Mycobacterium_senegalense
Mycobacterium_seoulense
Mycobacterium_septicum
Mycobacterium_setense
Mycobacterium_sherrisii
Mycobacterium_shigaense
Mycobacterium_shimodei
Mycobacterium_shinjukuense
Mycobacterium_shottsii
Mycobacterium_simiae_1
Mycobacterium_simiae_2
Mycobacterium_simulans
Mycobacterium_smegmatis
Mycobacterium_sphagni
Mycobacterium_stephanolepidis
Mycobacterium_stomatepiae
Mycobacterium_syngnathidarum_
Mycobacterium_szulgai
Mycobacterium_talmoniae_
Mycobacterium_terramassiliense_
Mycobacterium_thermoresistibile
Mycobacterium_timonense
Mycobacterium_tokaiense
Mycobacterium_triplex
Mycobacterium_tuberculosis_1
Mycobacterium_t...t_africanum_K85
Mycobacterium_tu...ariant_bovis_BCG
Mycobacterium_tu...str._Korea_1168P
Mycobacterium_tub...ariant_pinnipedii
Mycobacterium_tusciae
Mycobacterium_uberis
Mycobacterium_ulcerans
Mycobacterium_ul...bsp._shinshuense
Mycobacterium_vaccae
Mycobacterium_vanbaalenii
Mycobacterium_v...strain_DSM_7251
Mycobacterium_vicinigordonae
Mycobacterium_virginiense
Mycobacterium_vulneris_1
Mycobacterium_vulneris_2
Mycobacterium_wolinskyi
Mycobacterium_xenopi
Mycobacterium_xenopi_RIVH700367

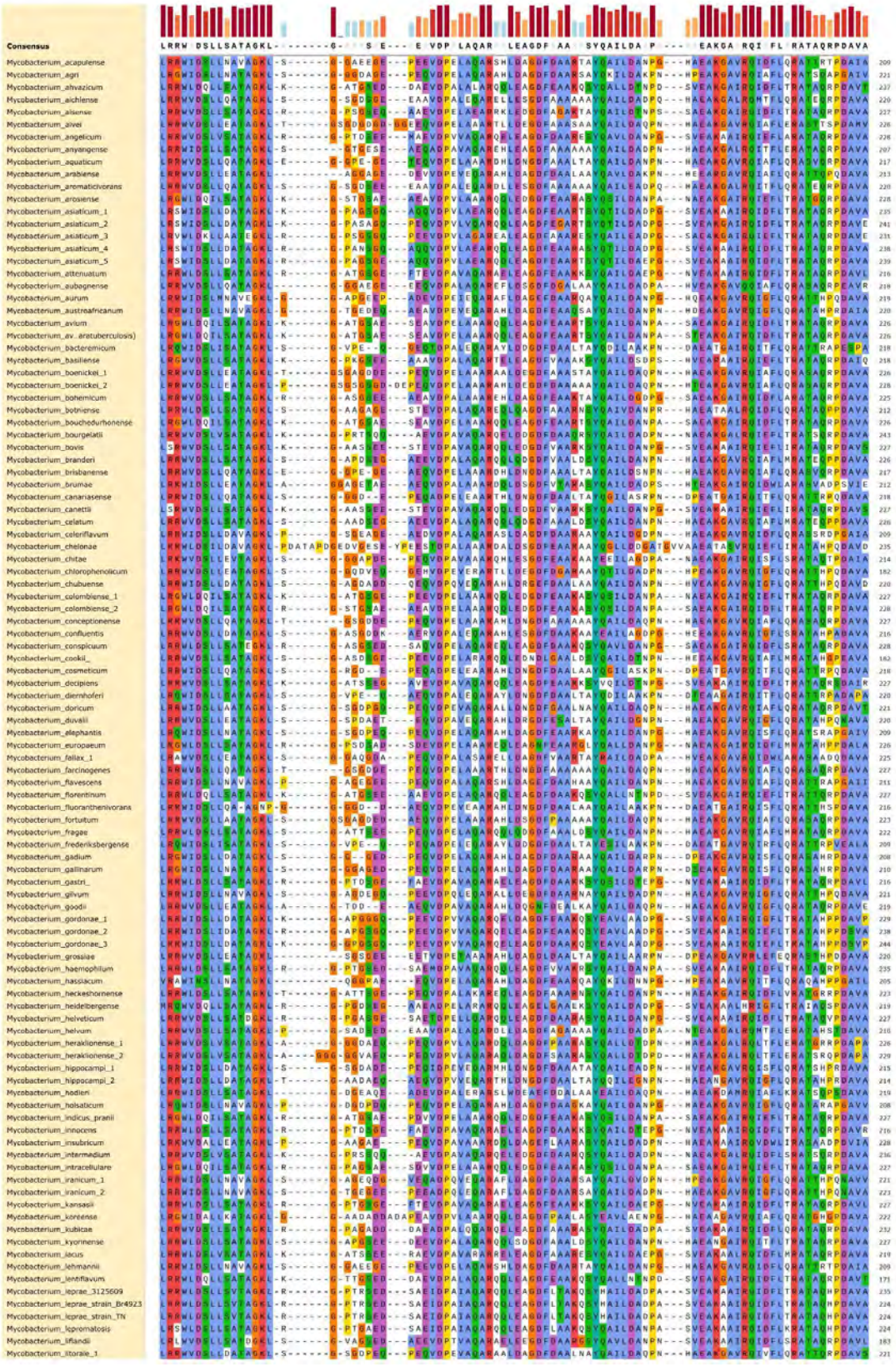
Consensus
Mycobacterium_acapulense
Mycobacterium_agri
Mycobacterium_ahvazicum
Mycobacterium_aichlense
Mycobacterium_alsense
Mycobacterium_aivei
Mycobacterium_angelicum
Mycobacterium_anyangense
Mycobacterium_aquaticum
Mycobacterium_arabiense
Mycobacterium_aromaticivorans
Mycobacterium_arosiense
Mycobacterium_asiaticum_1
Mycobacterium_asiaticum_2
Mycobacterium_asiaticum_3
Mycobacterium_asiaticum_4
Mycobacterium_asiaticum_5
Mycobacterium_attenuatum
Mycobacterium_aubagnense
Mycobacterium_aurum
Mycobacterium_austroafricanum
Mycobacterium_avium
Mycobacterium_av._aratuberculosis)
Mycobacterium_bacteremicum
Mycobacterium_basiliense
Mycobacterium_boenickei_1
Mycobacterium_boenickei_2
Mycobacterium_bohemicum
Mycobacterium_botniense
Mycobacterium_bouchedurhonense
Mycobacterium_bourgelatii
Mycobacterium_bovis
Mycobacterium_branderi
Mycobacterium_brisbanense
Mycobacterium_brumae
Mycobacterium_canariasense
Mycobacterium_canettii
Mycobacterium_celatum
Mycobacterium_celeriflavum
Mycobacterium_chelonae
Mycobacterium_chitae
Mycobacterium_chlorophenolicum
Mycobacterium_chubuense
Mycobacterium_colombiense_1
Mycobacterium_colombiense_2
Mycobacterium_conceptionense
Mycobacterium_confluentis
Mycobacterium_conspicuum
Mycobacterium_cookii_
Mycobacterium_cosmeticum
Mycobacterium_decipiens
Mycobacterium_diernhoferi
Mycobacterium_doricum
Mycobacterium_duvalii
Mycobacterium_elephantis
Mycobacterium_europaeum
Mycobacterium_fallax_1
Mycobacterium_farcinogenes
Mycobacterium_flavescens
Mycobacterium_florentinum
Mycobacterium_fluoranthenivorans
Mycobacterium_fortuitum
Mycobacterium_fragae
Mycobacterium_frederiksbergense
Mycobacterium_gadium
Mycobacterium_gallinarum
Mycobacterium_gastri_
Mycobacterium_gilvum
Mycobacterium_goodii
Mycobacterium_gordonae_1
Mycobacterium_gordonae_2
Mycobacterium_gordonae_3
Mycobacterium_grossiae
Mycobacterium_haemophilum
Mycobacterium_hassiacum
Mycobacterium_heckeshornense
Mycobacterium_heidelbergense
Mycobacterium_helveticum
Mycobacterium_helvum
Mycobacterium_heraklionense_1
Mycobacterium_heraklionense_2
Mycobacterium_hippocampi_1
Mycobacterium_hippocampi_2
Mycobacterium_hodleri
Mycobacterium_holsaticum
Mycobacterium_indicus_pranii
Mycobacterium_innocens
Mycobacterium_insubricum
Mycobacterium_intermedium
Mycobacterium_intracellulare
Mycobacterium_iranicum_1
Mycobacterium_iranicum_2
Mycobacterium_kansasii
Mycobacterium_koreense
Mycobacterium_kubicae
Mycobacterium_kyorinense
Mycobacterium_lacus
Mycobacterium_lehmannii
Mycobacterium_lentiflavum
Mycobacterium_leprae_3125609
Mycobacterium_leprae_strain_Br4923
Mycobacterium_leprae_strain_TN
Mycobacterium_lepromatosis
Mycobacterium_liflandii
Mycobacterium_litoralei_1

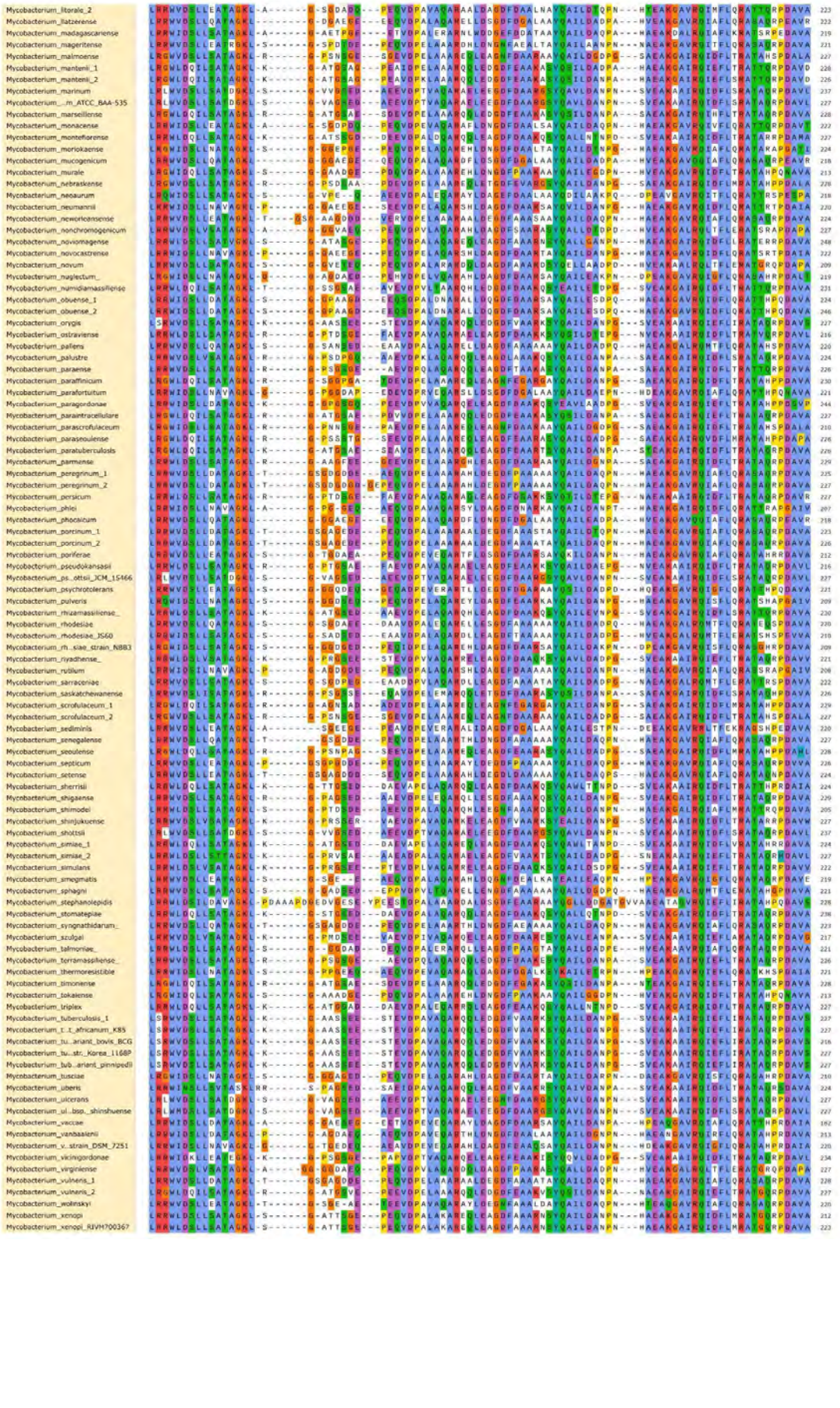
Mycobacterium_litorale_2
Mycobacterium_flatzerense
Mycobacterium_madagascariense
Mycobacterium_mageritense
Mycobacterium_malmoense
Mycobacterium_mantenii_1
Mycobacterium_mantenii_2
Mycobacterium_marinum
Mycobacterium_...m_ATCC_BAA-535
Mycobacterium_marseillense
Mycobacterium_monacense
Mycobacterium_montefiorense
Mycobacterium_moriokaense
Mycobacterium_mucogenicum
Mycobacterium_murale
Mycobacterium_nebraskense
Mycobacterium_neoaurum
Mycobacterium_neumannii
Mycobacterium_neworleansense
Mycobacterium_nonchromogenicum
Mycobacterium_noviomagense
Mycobacterium_novocastrense
Mycobacterium_novum
Mycobacterium_nuglectum_
Mycobacterium_numidiamassiliense
Mycobacterium_obuense_1
Mycobacterium_obuense_2
Mycobacterium_orygis
Mycobacterium_ostraviense
Mycobacterium_pallens
Mycobacterium_palustre
Mycobacterium_paraense
Mycobacterium_paraffinicum
Mycobacterium_parafortuitum
Mycobacterium_paragordonae
Mycobacterium_paraintracellulare
Mycobacterium_parascrofulaceum
Mycobacterium_paraseoulense
Mycobacterium_paratuberculosis
Mycobacterium_parmense
Mycobacterium_peregrinum_1
Mycobacterium_peregrinum_2
Mycobacterium_persicum
Mycobacterium_phlei
Mycobacterium_phocaicum
Mycobacterium_porcinum_1
Mycobacterium_porcinum_2
Mycobacterium_poriferae
Mycobacterium_pseudokansasii
Mycobacterium_ps...ottsii_JCM_15466
Mycobacterium_psychrotolerans
Mycobacterium_pulveris
Mycobacterium_rhizamassiliense_
Mycobacterium_rhodesiae
Mycobacterium_rhodesiae_JS60
Mycobacterium_rh...siae_strain_NBB3
Mycobacterium_riyadhense_
Mycobacterium_rutilum
Mycobacterium_sarraceniae
Mycobacterium_saskatchewanense
Mycobacterium_scrofulaceum_1
Mycobacterium_scrofulaceum_2
Mycobacterium_sediminis
Mycobacterium_senegalense
Mycobacterium_seoulense
Mycobacterium_septicum
Mycobacterium_setense
Mycobacterium_sherrisii
Mycobacterium_shigaense
Mycobacterium_shimodei
Mycobacterium_shinjukuense
Mycobacterium_shottsii
Mycobacterium_simiae_1
Mycobacterium_simiae_2
Mycobacterium_simulans
Mycobacterium_smegmatis
Mycobacterium_sphagni
Mycobacterium_stephanolepidis
Mycobacterium_stomatepiae
Mycobacterium_syngnathidarum_
Mycobacterium_szulgai
Mycobacterium_talmoniae_
Mycobacterium_terramassiliense_
Mycobacterium_thermoresistibile
Mycobacterium_timonense
Mycobacterium_tokaiense
Mycobacterium_triplex
Mycobacterium_tuberculosis_1
Mycobacterium_t...t_africanum_K85
Mycobacterium_tu...ariant_bovis_BCG
Mycobacterium_tu...str._Korea_1168P
Mycobacterium_tu...ariant_pinnipedii
Mycobacterium_tusciae
Mycobacterium_uberis
Mycobacterium_ulcerans
Mycobacterium_ul...bsp._shinshuense
Mycobacterium_vaccae
Mycobacterium_vanbaalenii
Mycobacterium_v...strain_DSM_7251
Mycobacterium_vicinigordonae
Mycobacterium_virginiense
Mycobacterium_vulneris_1
Mycobacterium_vulneris_2
Mycobacterium_wolinskyi
Mycobacterium_xenopi
Mycobacterium_xenopi_RIVH700367

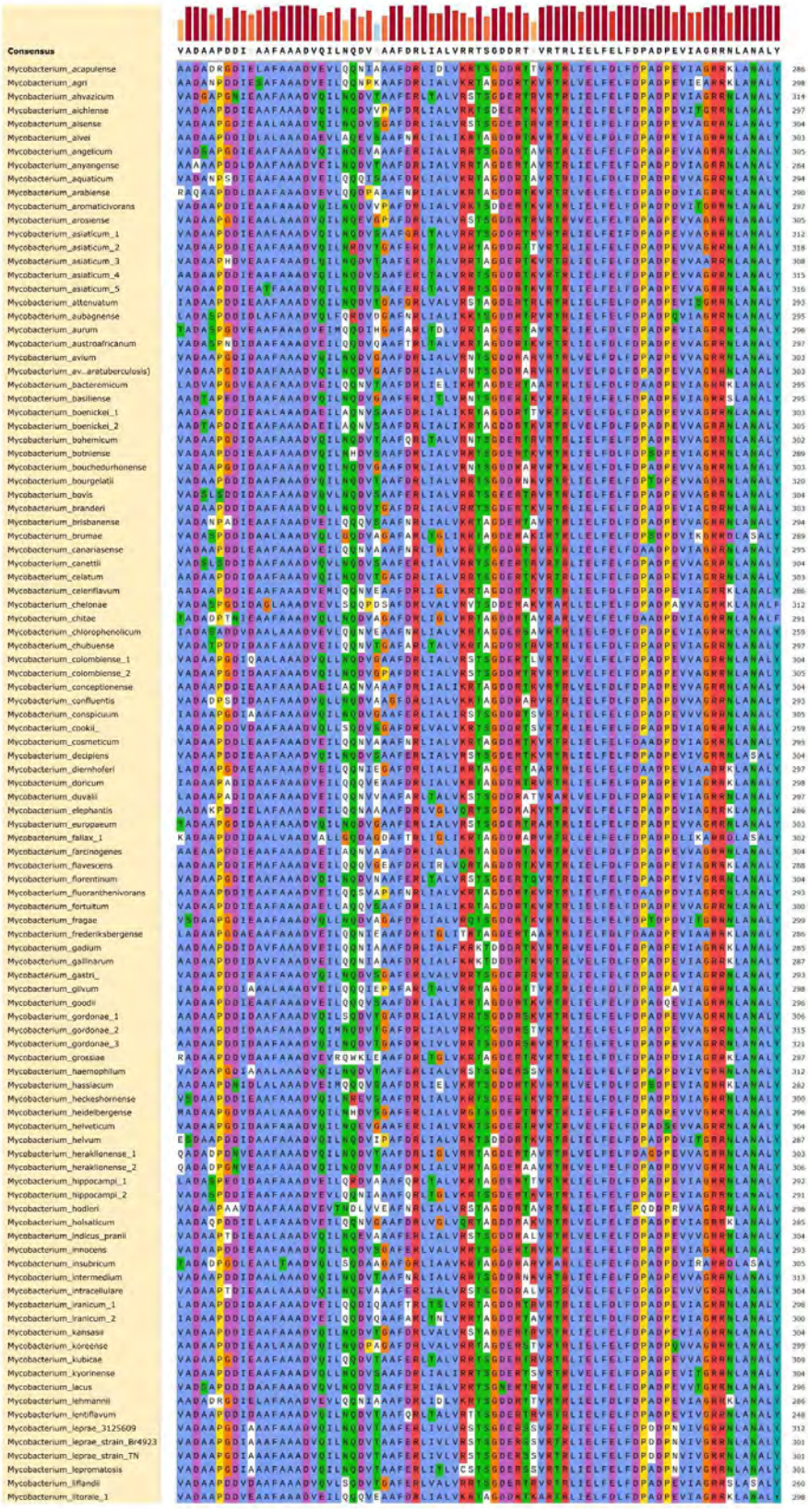
Consensus
VADAAPDDI AAFAAADVQILNQDV AAFDRLIALVRRTSGDDRT VRTRLIELFELFDPADPEVIAGRRNLANALY
Mycobacterium_acapulense
Mycobacterium_agri
Mycobacterium_ahvazicum
Mycobacterium_aichlense
Mycobacterium_aisense
Mycobacterium_alvei
Mycobacterium_angelicum
Mycobacterium_anyangense
Mycobacterium_aquaticum
Mycobacterium_arabiense
Mycobacterium_aromaticivorans
Mycobacterium_arosiense
Mycobacterium_asiaticum_1
Mycobacterium_asiaticum_2
Mycobacterium_asiaticum_3
Mycobacterium_asiaticum_4
Mycobacterium_asiaticum_5
Mycobacterium_attenuatum
Mycobacterium_aubagnense
Mycobacterium_aurum
Mycobacterium_austroafricanum
Mycobacterium_avium
Mycobacterium_av._aratubercolosis)
Mycobacterium_bacteremicum
Mycobacterium_basiliense
Mycobacterium_boenickei_1
Mycobacterium_boenickei_2
Mycobacterium_bohemicum
Mycobacterium_botniense
Mycobacterium_bouchedurhonense
Mycobacterium_bourgelatii
Mycobacterium_bovis
Mycobacterium_branderi
Mycobacterium_brisbanense
Mycobacterium_brumae
Mycobacterium_canariasense
Mycobacterium_canettii
Mycobacterium_celatum
Mycobacterium_celeriflavum
Mycobacterium_chelonae
Mycobacterium_chitae
Mycobacterium_chlorophenolicum
Mycobacterium_chubuense
Mycobacterium_colombiense_1
Mycobacterium_colombiense_2
Mycobacterium_conceptionense
Mycobacterium_confluentis
Mycobacterium_conspicuum
Mycobacterium_cookii_
Mycobacterium_cosmeticum
Mycobacterium_decipiens
Mycobacterium_diernhoferi
Mycobacterium_doricum
Mycobacterium_duvalii
Mycobacterium_elephantis
Mycobacterium_europaeum
Mycobacterium_fallax_1
Mycobacterium_farcinogenes
Mycobacterium_flavescens
Mycobacterium_florentinum
Mycobacterium_fluoranthenivorans
Mycobacterium_fortuitum
Mycobacterium_fragae
Mycobacterium_frederiksbergense
Mycobacterium_gadium
Mycobacterium_gallinarum
Mycobacterium_gastri_
Mycobacterium_gilvum
Mycobacterium_goodii
Mycobacterium_gordonae_1
Mycobacterium_gordonae_2
Mycobacterium_gordonae_3
Mycobacterium_grossiae
Mycobacterium_haemophilum
Mycobacterium_hassiacum
Mycobacterium_heckeshornense
Mycobacterium_heidelbergense
Mycobacterium_helveticum
Mycobacterium_helvum
Mycobacterium_heraklionense_1
Mycobacterium_heraklionense_2
Mycobacterium_hippocampi_1
Mycobacterium_hippocampi_2
Mycobacterium_hodleri
Mycobacterium_holsaticum
Mycobacterium_indicus_pranii
Mycobacterium_innocens
Mycobacterium_insubricum
Mycobacterium_intermedium
Mycobacterium_intracellulare
Mycobacterium_iranicum_1
Mycobacterium_iranicum_2
Mycobacterium_kansasii
Mycobacterium_koreense
Mycobacterium_kubicae
Mycobacterium_kyorinense
Mycobacterium_lacus
Mycobacterium_lehmannii
Mycobacterium_lentiflavum
Mycobacterium_leprae_3125609
Mycobacterium_leprae_strain_Br4923
Mycobacterium_leprae_strain_TN
Mycobacterium_lepromatosis
Mycobacterium_liflandii
Mycobacterium_litorale_1

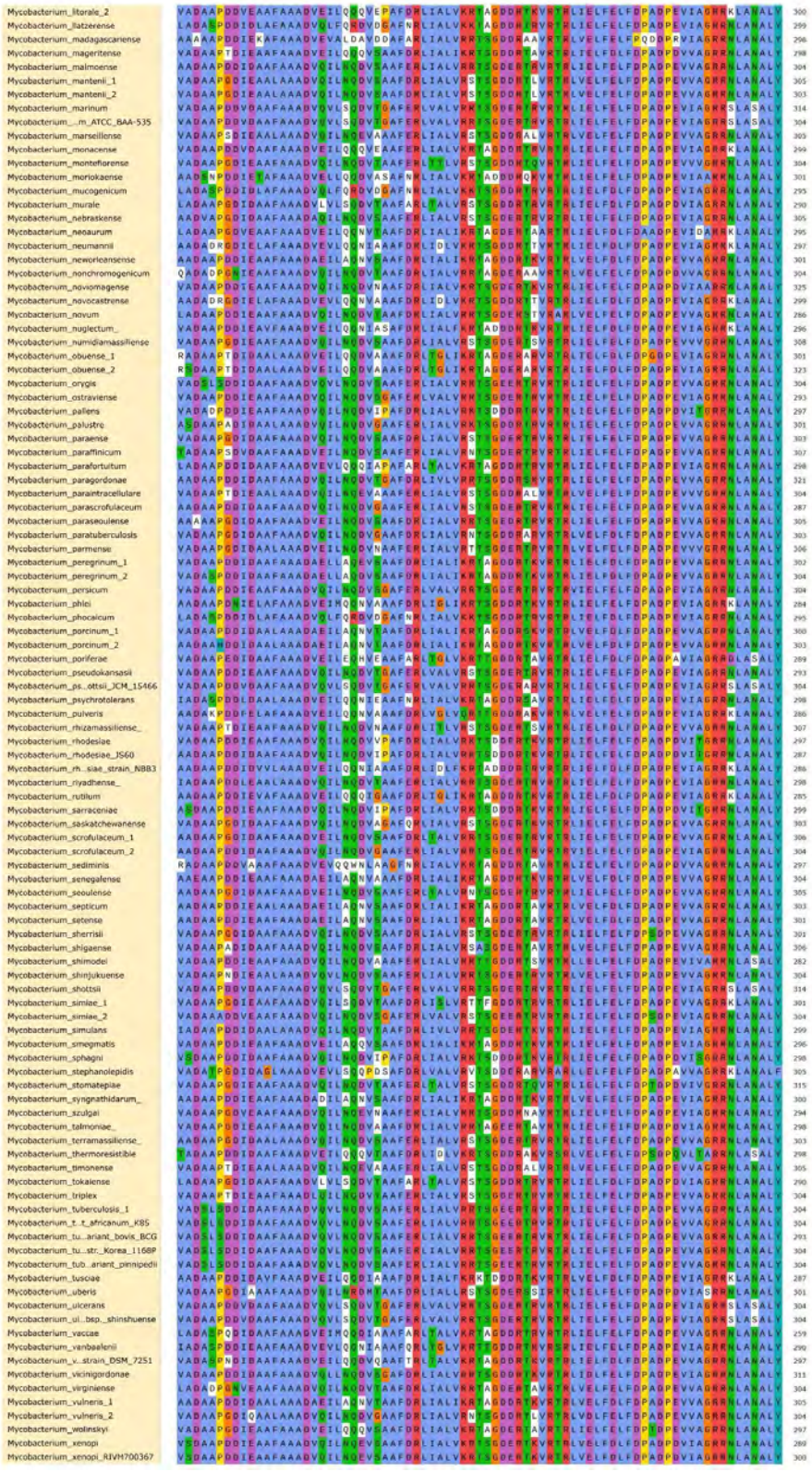
Mycobacterium_litorale_2
Mycobacterium_flatzerense
Mycobacterium_madagascariense
Mycobacterium_mageritense
Mycobacterium_malmoense
Mycobacterium_mantenii_1
Mycobacterium_mantenii_2
Mycobacterium_marinum
Mycobacterium_...m_ATCC_BAA-535
Mycobacterium_marseillense
Mycobacterium_monacense
Mycobacterium_montefiorense
Mycobacterium_moriokaense
Mycobacterium_mucogenicum
Mycobacterium_murale
Mycobacterium_nebraskense
Mycobacterium_neoaurum
Mycobacterium_neumannii
Mycobacterium_neworleansense
Mycobacterium_nonchromogenicum
Mycobacterium_noviomagense
Mycobacterium_novocastrense
Mycobacterium_novum
Mycobacterium_nuglectum_
Mycobacterium_numidiamassiliense
Mycobacterium_obuense_1
Mycobacterium_obuense_2
Mycobacterium_oryzae
Mycobacterium_ostraviense
Mycobacterium_pallens
Mycobacterium_palustre
Mycobacterium_paraense
Mycobacterium_paraffinicum
Mycobacterium_parafortuitum
Mycobacterium_paragordonae
Mycobacterium_paraintracellulare
Mycobacterium_parascrofulaceum
Mycobacterium_paraseoulense
Mycobacterium_paratuberculosis
Mycobacterium_parmense
Mycobacterium_peregrinum_1
Mycobacterium_peregrinum_2
Mycobacterium_persicum
Mycobacterium_phlei
Mycobacterium_phocaicum
Mycobacterium_porcinum_1
Mycobacterium_porcinum_2
Mycobacterium_poriferae
Mycobacterium_pseudokansasii
Mycobacterium_ps...ottsii_JCM_15466
Mycobacterium_psychrotolerans
Mycobacterium_pulveris
Mycobacterium_rhizamassiliense_
Mycobacterium_rhodesiae
Mycobacterium_rhodesiae_JS60
Mycobacterium_rh...siae_strain_NBB3
Mycobacterium_riyadhense_
Mycobacterium_rutilum
Mycobacterium_sarraceniae
Mycobacterium_saskatchewanense
Mycobacterium_scrofulaceum_1
Mycobacterium_scrofulaceum_2
Mycobacterium_sediminis
Mycobacterium_senegalense
Mycobacterium_seoulense
Mycobacterium_septicum
Mycobacterium_setense
Mycobacterium_sherrisii
Mycobacterium_shigaense
Mycobacterium_shimodei
Mycobacterium_shinjukuense
Mycobacterium_shottsii
Mycobacterium_simiae_1
Mycobacterium_simiae_2
Mycobacterium_simulans
Mycobacterium_smegmatis
Mycobacterium_sphagni
Mycobacterium_stephanolepidis
Mycobacterium_stomatepiae
Mycobacterium_syngnathidarum_
Mycobacterium_szulgai
Mycobacterium_talmoniae_
Mycobacterium_terramassiliense_
Mycobacterium_thermoresistibile
Mycobacterium_timonense
Mycobacterium_tokaiense
Mycobacterium_triplex
Mycobacterium_tuberculosis_1
Mycobacterium_t..r_africanum_K85
Mycobacterium_tu...ariant_bovis_BCG
Mycobacterium_tu...str._Korea_1168P
Mycobacterium_tub...ariant_pinnipedii
Mycobacterium_tusciae
Mycobacterium_uberis
Mycobacterium_ulcerans
Mycobacterium_ul...bsp._shinshuense
Mycobacterium_vaccae
Mycobacterium_vanbaalenii
Mycobacterium_v...strain_DSM_7251
Mycobacterium_vicinigordonae
Mycobacterium_virginiense
Mycobacterium_vulneris_1
Mycobacterium_vulneris_2
Mycobacterium_wolinskyi
Mycobacterium_xenopi
Mycobacterium_xenopi_RIVH700367